Analysis of single and coupled dielectric rib waveguides and discontinuities

Husain, M. N.

Award date:
1991

Awarding institution:
University of Bath

ANALYSIS OF SINGLE AND COUPLED DIELECTRIC RIB WAVEGUIDES AND DISCONTINUITIES

submitted by M.N. HUSAIN

for the degree of PhD

of the University of Bath

1991

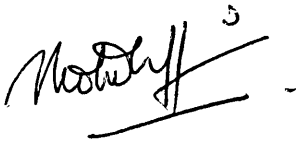

ProQuest LLC
789 East Eisenhower Parkway
P.O. Box 1346
Ann Arbor, MI 48106-1346

CONTENTS

SUMMARY

This thesis considers the theoretical analysis of the rib waveguide, a waveguiding structure most favoured for integrated optics and in millimetre waves. The work begins by considering the application of the Transverse Resonance Diffraction method (TRD) to the rib waveguide in the pure LSE/LSM polarizations. In solving the TRD problem, a variational method of order one, i.e. that assumes at the transverse step discontinuity a single function 'trial field', which takes into explicit account the singularities at the dielectric corners, is used. The formulation leads to a scalar dispersion equation and a simple transverse equivalent network. Theoretical results for discrete bound mode propagation constant are compared with the vector finite element method. The agreement is found to be excellent and, hence, LSE/LSM provide an accurate approximation. The investigation is completed by considering a full hybrid rigorous analysis of the structure.

The analysis of a single guide is extended to cover multiple coupled waveguides. The approach adopted to analyse this structure is to represent the uniform section of the coupled structure by its equivalent two-port network. In this way, the problem of multiple coupled guides is turned into a cascade of equivalent networks, which can be tackled by simple network method. The theory is applied to analyse directional couplers, three guide couplers, non symmetrical coupled waveguides and waveguide arrays.

In order to complete the characterization of the modal spectrum of the rib waveguide, the continuum portion of the spectrum is derived. The approach adopted uses an eigenfunction in a manner analogous to the bound mode description of the guided fields. Finally, with knowledge of the complete spectrum, the problem of abruptly terminated rib waveguide and discontinuities between two rib waveguides are addressed. To avoid excessive computational effort a number of simplifications are employed giving results which agree quite well with those of FEM analysis.

ACKNOWLEDGMENTS

I would like to thank Professor T. Rozzi for the knowledge, supervision and guidance he has provided during the course of this work. Thanks are also due to the University of Technology, Malaysia for the award of study leave and financial support. I also wish to express my thanks for the help I have received from my friends in the Wolfson Laboratory. Last but not least, I would like to thank my wife Khadijah, and my childrens Norhashimah, Noraishah, Norazlin, Nurulhuda and Nurfatiah for the encouragement they have given and also their patience throughout this work.

PUBLICATIONS ARISING FROM THIS WORK

1. 'Strongly coupled dielectric rib waveguides use of the 'transition function' and of edge discontinuities' , Proc. 19th. European Microwave Conference, London, 1989.
2. 'Variational analysis of the dielectric rib waveguide using the concept of 'transition function' and including edge singularities', I.E.E.E Trans. on Microwave Theory and Techniques, vol. MTT-39, Feb. 1991.
3. 'Rigorous analysis of multiple coupled rib waveguide', Submitted for publication to I.E.E.E Trans. on Microwave Theory and Techniques.

ABBREVIATIONS

TRD	Transverse Resonance Diffraction
LSE	Longitudinal-Section Electric
LSM	Longitudinal-Section Magnetic
FEM	Finite Element Method
FDM	Finite Difference Method
EDC	Effective Dielectric Constant
L.H.S	Left hand side
R.H.S	Right hand side
VFEM	Vectorial Finite Element Method
SVFDM	Semi-Vectorial Finite Difference Method

SYMBOLS

D,d – Asymmetrical slab heights

$\bar{d}$ – Intermediate slab height

h – y-directed wavenumber in film

σ – y-directed wavenumber in substrate

ρ – y-directed wavenumber in air

$\phi_{sh}(y)$ – Orthonormalised distribution of TE surface modes of an asymmetrical slab guide of height D

$\psi_{sh}(y)$ – Orthonormalised distribution of TE surface modes of an asymmetrical slab guide of height d

$\phi_h(y,\sigma)$ – Orthonormalised distribution of TE substrate modes of an asymmetrical slab guide of height D

$\psi_h(y,\sigma)$ – Orthonormalised distribution of TE substrate modes of an asymmetrical slab guide of height d

$\phi_{h\mu}(y,\rho)$ – Orthonormalised distribution of TE air modes of an asymmetrical slab guide of height D

$\psi_{h\mu}(y,\rho)$ – Orthonormalised distribution of TE air modes of an asymmetrical slab guide of height d

$\phi_{se}(y)$ – Orthonormalised distribution of TM surface modes of an asymmetrical slab guide of height D

$\psi_{se}(y)$ – Orthonormalised distribution of TM surface modes of an asymmetrical slab guide of height d

$\phi_e(y,\sigma)$ – Orthonormalised distribution of TM substrate modes of an asymmetrical slab guide of height D

$\psi_e(y,\sigma)$ – Orthonormalised distribution of TM substrate modes of an asymmetrical slab guide of height d

$\phi_{e\mu}(y,\rho)$ – Orthonormalised distribution of TM air modes of an asymmetrical slab guide of height D

$\psi_{e\mu}(y, \rho)$ – Orthonormalised distribution of TM air modes of an asymmetrical slab guide of height d

$\bar{U}_{sh}(y)$ – Orthonormalised distribution of TE surface modes of an intermediate slab guide

$\bar{U}_{se}(y)$ – Orthonormalised distribution of TM surface modes of an intermediate slab guide

H – Magnetic field

E – Electric field

π_h – Magnetic Hertzian vector potential

π_e – Electric Hertzian vector potential

β – Propagation constant

β_s – Propagation constant of discrete bound mode

β_o – Propagation constant of odd mode

β_e – Propagation constant of even mode

$\psi_h(x,y)$ – Magnetic scalar wave equation

$\psi_e(x,y)$ – Electric scalar wave equation

Z, Z_L, Z_R, Z_T – Impedances

Y, Y_L, Y_R, Y_T – Admittances

ω – Angular frequency

μ_0 – Permeability of free space

ε_0 – Permittivity of free space

ε_r – Relative permittivity

ε_{eh} – Effective dielectric constant (LSE)

ε_{ee} – Effective dielectric constant (LSM)

k_x – x-directed wavenumber

k_y – y-directed wavenumber

k_{ys} – y-directed wavenumber in film

q_{sh} – x-directed wave number of the discrete bound mode

in film (LSE)

q_{se} - x-directed wave number of the discrete bound mode in film (LSM)

q_h - x-directed wave number of the discrete bound mode in air (LSE)

q_e - x-directed wave number of the discrete bound mode in air (LSM)

p_h - x-directed wave number of the discrete bound mode in substrate (LSE)

p_e - x-directed wave number of the discrete bound mode in substrate (LSM)

$\tilde{Z},\tilde{Y},\tilde{U},\tilde{T}_R,\tilde{Z}_L$ - Integral operators

$Z_{(y,y')}$ - Kernel of integral operator $\tilde{Z}$

$Y_{(y,y')}$ - Kernel of integral operator $\tilde{Y}$

$U_{(y,y')}$ - Kernel of integral operator $\tilde{U}$

$T_{(y,y')}$ - Kernel of integral operator $\tilde{T}$

$g(y,y';\lambda)$, $G(r;k_{ts})$, $G(r;k_t)$ - Green functions

k_o - Free space wave number

L_t - Transfer length for maximum power transfer

L_{ct},L_{ot} - Coupling length for three guide coupler

$h_s(x,y)$ - Discrete mode function of the rib waveguide (LSE)

$e_s(x,y)$ - Discrete mode function of the rib waveguide (LSM)

$\Psi_I(x,y)$ - Discrete mode function of intermediate rib waveguide

$\tilde{Z}(k_t)$ - Complex impedance operator

$Z_v(k_t)$ - Total transverse impedance for v-th solution for a given value of k_t^2

Γ - Reflection coefficient

$|\tau|$ - Transmitted amplitude

$\psi_a(x,y;k_t)$ – Spectral distribution in air

$\psi_s(x,y)$ – Discrete mode function of the rib waveguide

$\psi_c(x,y;k_t)$ – Continuous mode function of the rib waveguide

$\psi_{cs}(x,y;k_t)$ – Spectral component of the continuum in film

$\psi_{c\sigma}(x,y;k_t)$ – Spectral component of the continuum in substrate

$\psi_{c\rho}(x,y;k_t)$ – Spectral component of the continuum in air

CHAPTER 1

GENERAL INTRODUCTION

The advancement of coherent optical fibre communication systems, in particular, the development of low loss single mode fibres with zero dispersion, rekindled the interest in practical integrated optics devices for the system components. The object of integrated optics is to maniaturise optical components such as beam splitters, modulators,switches,filters,multiplexers,samplers,sources and detectors, and finally to fabricate a complete optical circuit on a small chip similar to those in integrated circuit at lower frequencies. The advantages to be gained would include reduced size, improved device performance and mechanical stability. A good review and discussion on this subject can be found in the literature which has grown considerably since its conception in 1969, for example [1-4]. Generally, metal clad waveguides are too lossy at optical frequencies and dielectric or semiconductor materials must be used as optical signal carriers. The choice of material will depend upon the wavelength and the application, e.g for a fully integrated system a lasing material must be used. Semiconductor materials, in particular, III - V alloy semiconductors have the necessary properties to realize optical circuits and all the above mentioned devices. They have a major advantage over other materials such as LiNb O_3 in that optical sources in the wavelength used for optical fibre communications can also be fabricated in the same material [5]. In particular, the InGaAsP/InP system has been exploited to produce highly efficient light sources in the 1.3 to 1.6 μm region, and this is very important if a fully integrated system is to be achieved. Another advantage of semiconductors is that the refractive index profile and geometric shape of the waveguide may be very well defined and controlled. Furthermore, a large electro-optic effect in both GaAs and InP allows refractive index changes of the waveguide to be controlled externally. With the advancement of III - V semiconductor technology, primarily epitaxial growth, guides

with relatively low loss and low voltage operation have been demonstrated [6].

The most basic components of optical integrated circuit are single and coupled waveguides, and other optical devices may be realized from these components [7-10]. Two main kinds of waveguides are used in integrated optics; these are the planar and the strip guide. Strip guide is the most favoured form of optical channel, as the energy is confined in both transverse directions. This confinement is the most desired feature for the fabrication of all devices derived from single and coupled guides. The types of dielectric and semiconductor strip waveguides that have been proposed and used in integrated optics are shown in Fig. 1.1 . In each structure, waveguiding depends on the difference in the refractive indices of the waveguiding region and of the surrounding region, and the lateral confinement is provided by the geometrical shape of the waveguide. Slot guide [11], channel strip guide [12], and rib waveguide [13], have been successfully realized in III-V semiconductors using various fabrication techniques. Of the three types, rib waveguide is the most attractive form for implementation of integrated optics in III - V semiconductors, since its fabrication is simple and this allows greater versatility and flexibility in device design. The refractive index of the outer region can be controlled by controlling the rib height and this, in turn, allows control of the lateral confinement. Increasing the rib height increases the lateral confinement and, hence, bends with reasonably sharp angles can be fabricated. Furthermore, by growing an undoped InP layer and p^+InP layer as shown in Fig. 1.2, the optical energy in the guide can be controlled externally by the electrooptic effect. These are the necessary properties for modulation and switching of optical energy. All these features make rib guide structures the most attractive choices for integrated optics in III-V compound semiconductors.

The high unit cost of optical integrated circuit fabrication, inhibits a trial and error approach to design. Design needs to be optimised prior to the fabrication stage. In order to develop an accurate and efficient design algorithm for single and coupled waveguides

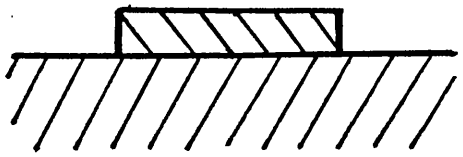

a) Raised Strip

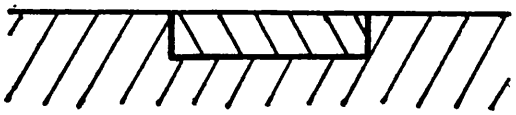

b) Embedded Strip

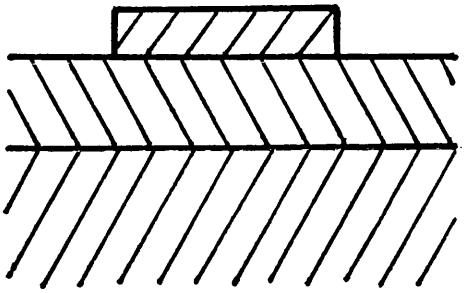

c) Strip-loaded guide

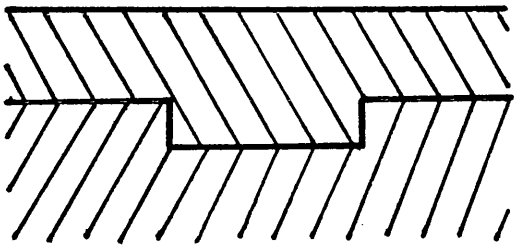

d) Embedded rib guide

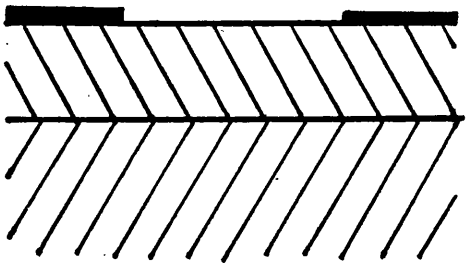

e) Slot guide

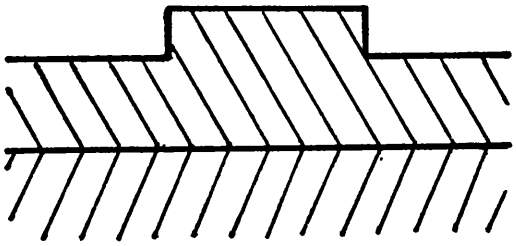

f) Rib guide

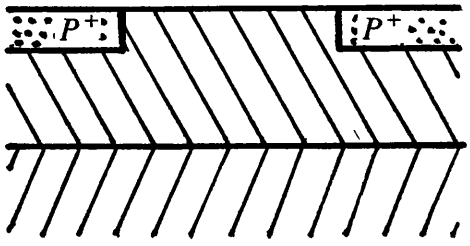

g) Channel stop strip guide

Fig. 1.1 Examples of open waveguides for millimetre waves and integrated optics.

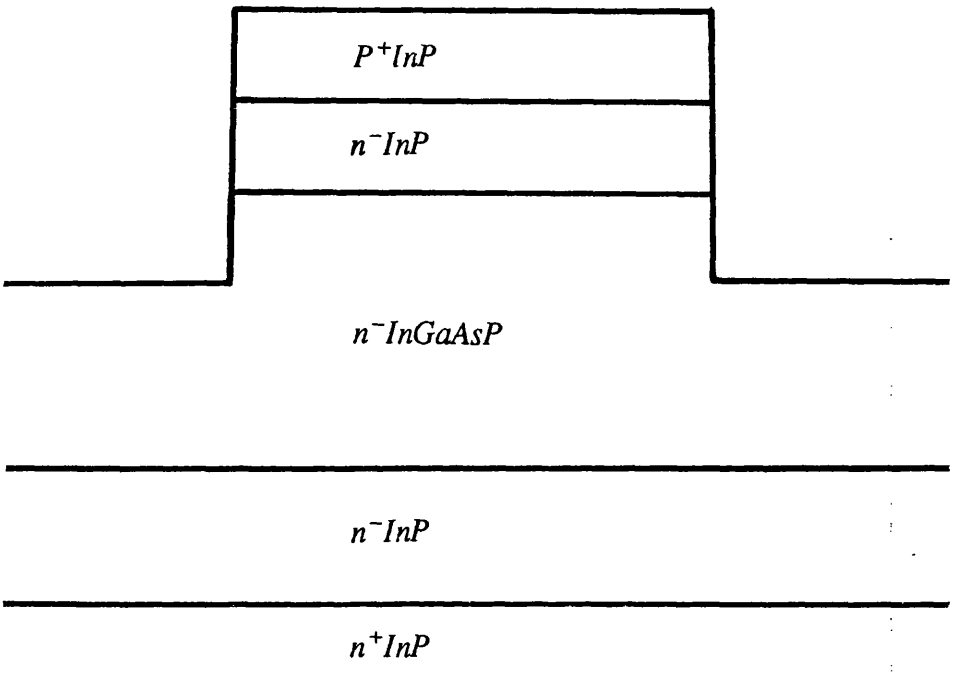

Fig. 1.2 A heterojunction rib guide suitable for electrooptic modulation.

as well as for devices constructed from these components, an accurate knowledge and understanding of the electrical properties such as the propagation constants and field distribution of the guide is needed. Being an open waveguide structure, rib guide has both discrete bound modes and continuous modes. Therefore, in addition to the bound modes, the continuum must also be obtained if practical components with waveguide discontinuities are to be analysed. Propagation of optical power in waveguide can be investigated by solving Maxwell's equations subject to the appropriate boundary conditions. However, the rib guide allows no accurate analytic solution due to the difficulty posed by the presence of corners, and approximate methods have to be employed. In view of the importance of rib guide in integrated optics, in recent years there has been great interest in the theoretical analysis of the discrete bound modes of such structures. A variety of methods have been proposed and many of them take advantage of the techniques originally developed for applications to discontinuity problems in microwaves. They range from very approximate methods like the Effective Dielectric Constant (EDC) method to very sophisticated numerical techniques like Finite Difference Method (FDM) or Finite Element Method (FEM). For some years, the EDC in various forms has been the accepted approximated method to study the waveguide in integrated optics. In spite of its simplicity and ease of implementation, it lacks the accuracy required and is not usually applicable to all practical structures. In fact, the method breaks down when the surrounding region of the rib guide structure does not support a surface mode. This motivates the development of more accurate analyses such as the Transverse Resonance and Network approach using mode matching, the variational approach, FDM and FEM approach. FDM/FEM being a purely numerical method has the potential of giving very accurate results but it is very expensive in computer time. Furthermore, due to the computation complexity its extension to more complicated structures, such as multiple coupled guide seems correspondingly difficult. Transverse Resonance method with direct mode matching is also computationally complex as they involve mode matching with a partially discrete and partially

continuous spectrum. Moreover, direct mode matching does not take account of the true diffraction field at the discontinuity interface and suffers from slow convergence to the solution and requires many modes to accurately model the field. Therefore, it is desirable to avail a method of modelling which takes account all the physical properties of structure to accelerate convergence and offers flexibility for analysing more complex structures. The motivation behind the present work is to develop an accurate Transverse Resonance Diffraction (TRD) variational analysis of order one, i.e. that assumes at the transverse step discontinuity a single function "trial field". The formulation leads to a simple transverse equivalent network representation that is easy to use and allows modification for extension to more complex structures. The use of a single trial field function avoids the use of matrices and, hence, the numerical complexity of the solution can be reduced substantially. The success of this approach ,however, is dependent on the careful choice of the trial field function where the choice is critical for an accurate solution.

In chapter two, is given the basic background theory necessary for the development of the rigorous analysis outlined in detail in latter chapters. In order to put the present work in proper context, this chapter begins with a review of the existing methods of analysis of the rib waveguide structure. This is followed by an overview of the complete modal spectrum of a multilayer asymmetrical slab guide, as an example of an open waveguide structure. The chapter ends with a discussion of the Hertzian vector potential and an overview of the Transverse Resonance Diffraction method as used in the thesis.

In chapter three, is treated a rigorous analysis of the rib waveguide in the pure LSE and LSM polarizations. The problem is seen as one of diffraction by a transverse step discontinuity, whereupon transverse resonance is employed to derive the propagation constant. In solving the TRD problem, a variational formulation of Rayleigh - Ritz type with a single trial function at the transverse step discontinuity is used. This consists, in fact, of the surface mode of a multilayer slab waveguide of height intermediate between

those of the inner and surrounding slabs, including dielectric edge singularities, which we call "transition function". With this choice of trial field, a scalar dispersion equation and a simple two-port transverse equivalent network are derived. The accuracy of the technique is checked by comparisons with other methods of analysis. In particular the vector Finite Element method [14], which is considered very accurate, is taken as the bench mark for comparison in this work. The accuracy is found to be excellent even near cut-off where other approximate methods tend to fail or give less accurate results. In order to justify a solution with a single term trial field, the TRD problem is also solved using the Ritz-Galerkin variational formulation with a set of expanding functions.

In chapter four, a full hybrid rigorous analysis of the rib waveguide is given, where all the six field components are taken in to account in the formulation of the TRD problem. The results obtained for the LSE and LSM like modes closely resemble those of the pure LSE and LSM modes respectively. This seems to suggest that although the bound field of the rib waveguide is recognised as being hybrid in nature, at optical frequencies the hybrid content is minor for small aspect ratio, so that the field can be conveniently represented by a five field approximation. Cross polarization, however, could be excited in radiation problems [15].

In chapter five, coupled rib waveguides are analysed theoretically. This is done by modifying the approach adopted in chapter three for a single guide. The uniform guide, which is the basic building block of the coupled structure, is represented by its equivalent 'T' or 'π' network. In this way, multiple coupled guides such as three guide couplers and rib waveguide arrays can be treated directly by solving a cascade of equivalent circuits, which is easily effected by simple network methods. The theory is applied to analyse directional couplers, three guide couplers, non symmetrical coupled waveguides and waveguide arrays. The results of the simulations are compared with those of FDM/FEM [16] where possible and found to be in excellent agreement.

In chapter six, the complete spectrum of an open rib waveguide in the pure LSE/LSM polarization is presented. First, the question of normalisation of the discrete spectrum, developed in chapter three, is discussed. After obtaining the normalisation constant of the bound-mode, we construct the orthonormalised continuum of an open rib waveguide structure. The treatment adopted in this work uses an eigenfunction in a manner analogous to the bound mode description of the guided fields.

In order to demonstrate the validity of the complete mode spectrum constructed in chapter six, its application to discontinuity problems in integrated optics is discussed in chapter seven. In this chapter we address the problem of abruptly terminated rib waveguides and analyse different types of discontinuities between two rib waveguides, such as horizontal misalingment, change of rib width and change of rib height. These are the basic step discontinuity problems often encountered in integrated optics and, by extending this type of approach, it may be possible to analyse a wide variety of structures, in rib guide, such as tapers, bends, y-junctions, gratings and filters. For example, the problem of single step change in rib height can be extended to the problem of a periodic change of rib height such as in gratings or optical filters by using network methods similar to those developed in chapter five.

In the final chapter, general conclusions and the contribution of this work to the analysis of open waveguide structure with non separable cross section and the discontinuity problems in integrated optics are summarised.

REFERENCES

[1] H.F Taylor and A. Yariv, "Guided wave optics", Proc. I.E.E.E., vol. 62, No. 8, Aug. 1974, pp. 1044-1060.

[2] Special issue on Integrated Optics : I.E.E.E. Trans. on Microwave Theory and Techniques, vol. MTT-23, No. 1, Jan. 1975.

[3] D. Marcuse, (Ed.) " Integrated Optics " , I.E.E.E. Press, N.Y., 1973.

[4] T. Tamir, (Ed.) " Integrated Optics : Topics in Applied Physics ", Springer-Verlag, vol. 7, 1975, Berlin.

[5] A.P. Agrawal and N.K. Dutta, " Long-wavelength semiconductor lasers ", Van Nostrand Reinhold Company, N.Y., 1986.

[6] R.G. Walker and R.C. Goodfellow, " Attenuation measurements on MOCVD-grown GaAs/GaAlAs optical waveguides ", Electron. Lett., vol. 19, No, 15, 1983, pp. 590-592.

[7] J.C. Campbell, F.A. Blum and D.W. Shaw, "GaAs Electrooptic channel waveguide modulator ", Appl. Phys. Lett., vol. 26, June 1975, pp. 640-642.

[8] F.J. Leonberger and C.O. Bozler, " GaAs directional coupler switch with stepped $\delta\beta$ reversal ", Appl. Phys. Lett., vol. 31, Aug. 1977, pp. 223-226.

[9] F.J. Leonberger, J.P. Donelly and C.O. Bozler, " Wavelength dependence of GaAs directional couplers and electrooptic switches ", Appl. Optics, vol. 17, No.14, 15 July 1978, pp. 2250-2254.

[10] R.C. Alferness and R.V. Schmidth, " Tunable optical waveguide directional coupler filter ", Appl. Phys. Lett., vol. 33, No. 2, July 1978, pp. 161-163.

[11] Y. Yamamoto, T. Kamiya and H. Yanai, " Propagation Characteristics of partially

metal clad optical guide: Metal clad optical stripline ", Appl. Optics, vol. 14, Feb. 1975, pp. 322-326.

[12] F.J. Leonberger, J.P. Donnelly and C.O. Bozler, " Low loss GaAs$p^+n_n^+$ three dimensional optical waveguides ", Appl. Phys. Lett., vol. 28, May 1976, pp. 616-619.

[13] B. Buchmann and A.J.N. Houghton, " Optical Y-Junctions and S-bends formed by preferentially Etched single mode rib waveguides in InP ", Electron. Lett., No. 18, 1982, pp. 850-852.

[14] B.M.A. Rahman and J.B. Davies, " Vector H finite element solution of GaAs/GaAlAs rib waveguides ", I.E.E. Proc., vol. 132, Pt. J, DEc. 1985, pp. 349-353.

[15] S.T. Peng and A.A. Oliner, "Guidence and leakage properties of a class of open dielectric waveguides: Part 1 and 2 "I.E.E.E Trans. Microwave Theory and Technique, vol. MTT-29, pp. 843-869, Sept. 1981.

[16] M.J. Robertson, S. Ritchie and P. Dayan, " Semiconductor waveguides: Analysis of optical propagation in single rib structures and directional couplers ", I.E.E. Proc., vol. 132, Pt. J, No. 6, Dec. 1985, pp. 336-342.

CHAPTER 2

BACKGROUND THEORY AND INTRODUCTION TO TRANSVERSE RESONANCE DIFFRACTION METHOD

2.1 INTRODUCTION

The purpose of this chapter is to introduce the necessary background material and the method of analysis used in this work to compute the propagation characteristics of rib waveguides. Before this is done it is appropriate to give a brief review of the existing methods of analysis of the open rib waveguide structure. In the discussion, we will evaluate their accuracy and the computational complexity they involve. This is followed by a brief overview of the method for obtaining the complete mode spectrum of an asymmetrical slab waveguide, a main component required in the contruction of the potential functions used to derive the electromagnetic fields of the rib waveguide. Finally, an overview of the Transverse Resonance Techniques (TRD) method, as used in the present work, is given. This discussion is intended to give a clear picture and understanding of the steps involved in the development of the analysis presented in chapters three and four.

2.2 A REVIEW OF THE EXISTING ANALYSES OF RIB WAVEGUIDE

The need for an accurate knowledge of the electrical parameters of rib waveguides for the design of transmission channels and devices motivated the development of several methods of analysis and some of these are reviewed in this section. This review is not intended to present a complete survey, but only to give an outline of the techniques involved behind the solution of the problem and to highlight the merit and shortcoming of the various methods.

A solution of the electromagnetic problem must satisfy Maxwell's equations and the boundary conditions under which the solution is sought. In many cases, practical waveguide structures for integrated optics or millimetre waves happen to be arbitrarily shaped, which is due either to design preference or to the actual manufacturing process. As a result, the boundary conditions become more complicated and the analytical solution of Maxwell's equations become correspondingly complex. In fact, even for relatively simple dielectric rib waveguides and other dielectric strip guides, such as shown in Fig. 1.1, no exact analytic solution is known. However, for this class of waveguides, the solution can be approached by using purely numerical methods, where no prior knowledge of the actual form of the field is assumed and an iterative process is used or semi - analytic methods, where knowledge of the field solution and algebraic manipulations, are used to reduce the equations prior to computation.

2.21 NUMERICAL METHODS

Finite difference and finite elements methods have been widely used to analyse dielectric waveguides operating at optical and millimetric frequencies. The finite difference method in various form, that is, the scalar FDM [1,2], the semi - vectorial FDM [3,4], and the finite element method [5,6] has been applied to rib waveguide structures. In these methods, the waveguide cross-section over which the field solution is sought is divided in to a large number of elements that form a mesh. The field at each mesh point is expressed in terms of the field values of the mesh points that surround it. The unknown field in each element is represented by a suitable function (polynomial) and by imposing continuity on all interfaces between the different elements, the field values at other mesh points are found. By employing a variational expression for Maxwell's equations, an eigenvalue matrix equation is obtained and solved using standard matrix methods. An initial guess is made as to the propagation constant and to each field value and a new estimate is found for each iteration until satisfactory convergence is obtained. The use of a variational formulation in the finite difference

method is optional but it is a necessary step in the finite element method. In fact, it is the variational approach that makes the finite difference and the finite element technique very closely related [7]. The method has the potential of giving very accurate results. A vector $\vec{H}$ - field formulation [8] considers truly hybrid modes without approximation, results from this method are accurate and are taken as bench mark to check the accuracy of the present analysis. However, the accuracy of the finite difference/element technique depends upon the mesh size and the function used to derive the elemental fields from the mesh point values. As mesh size is reduced, accuracy increases but this in turn increases required computation time and hence reduces speed. In order to apply this technique to open waveguide structures, the infinite domain is reduced to a finite one by artificially closing the structure with a conducting plane so that it is effectively boxed. The box is made large enough to contain all regions in which the field is significant so as not to perturb the waveguide fields. Such consideration increases the size of the domain and hence the required computation time. In order to alleviate this problem some researchers have introduced the infinite elements method [5]. In view of the above fundamental assumption, this technique only true for bound modes and "never" for radiation modes. A troublesome problem with the vector finite element method is the existence of spurious numerical modes which are generated by the numerical technique and do not represent physical modes of the waveguide. In [8] the spurious solutions problem is dealt with by using a penalty function and by taking only divergence free solutions as physical modes. The need to check whether a solution satisfies $\nabla \times H = 0$ obviously increases the computational time and effort.

2.22 SEMI - ANALYTIC METHODS

2.221 MODE MATCHING TECHNIQUES AND NETWORK APPROACH

The mode matching technique is one of the oldest and simplest technique used for the solution of the discontinuity problems. This technique, which has proved successful in

closed waveguide problems, has been used by various researchers to analyze composite guide structures such as rib waveguide [9,10,11,12]. In this method the guide is divided into several uniform regions. In each region, the field is expanded in terms of an orthogonal modal set, which, in general, is constituted by the mode functions of the uniform region, with each set satisfying the required boundary conditions. Equating the field components at all continuous boundaries yields linear equations in the unknown mode amplitudes that can be solved using standard matrix techniques. The equations are only exact when a complete set of modes is taken in each region. For numerical computation these sets have to be truncated to a finite size and, to maintain reasonable accuracy, a large number of modes has to be taken into consideration, which means large matrices may have to be inverted by the computer, resulting in slow speed and ill - conditioning.

Although mode matching is a more analytical technique than the purely numerical approaches previously mentioned, nevertheless it still requires large computer resources, if accuracy is required. In the case of open structures such as rib waveguide, direct mode matching involves discrete as well as a continuous spectrum. Also direct mode matching does not take explicitly account of the true diffraction field at the transverse discontinuous interfaces and, consequently, suffers from slow convergence, particularly as a continuum is involved. This problem is not too serious when the field at the transverse discontinuity is regular, but it is more serious if the field at the transverse discontinuity is singular.

The ways mode matching is applied by different researchers to analyze composite open structure differ widely. The methods differ in the way they deal with the infinite extent of the waveguide cross-section and in the way they improve the accuracy or efficiency by combining two or more numerical methods in the solution. In solving the former problem, some researchers [9,10] set artificially bounds to the structure in order to discretize the continuous spectrum. Clearly, this approach is an approximate one which

turns the open guide problem in to a closed one. The solution involves reflected waves travelling inwards from the boundary and this in contrast with the properties of the open case that does only involve outgoing waves. It was pointed out by V.V. Shevkenko [13] that, however far away the boundaries are set, continuous modes always "feel" the presence of the boundary and hence the accuracy of this approximation is debatable.

Other researchers [11], consider the open structure and formulate a variational expression for impedance or admittance in terms of the unknown field at the discontinuous interface. Trial fields are used to expand the unknown field and the equivalent impedance of the surrounding region is calculated using a variational technique such as Rayleigh Ritz or the moment method. The use of variational formulation and moment method to supplement the mode matching technique improves the accuracy of matching the fields along the transverse discontinuous interface. This approach results in an equivalent circuit in the transverse direction, where the contribution from the continuous spectrum is represented as a lumped impedance or admittance and guided modes under the rib are represented by transmission lines. The key to a successful application of this technique is the choice of the trial field and with a proper choice an accurate results can be obtained. However, in the case of rib waveguide the choice of trial function is very limited and a suitable polynomial is hard to find.

In [12] a slightly different approach was adopted where the continuous spectrum is discretized by appropriate basis functions and a transmission line representation of the continuous spectrum is obtained. The rib guide structure is represented by a transmission line network connected through an ideal transformer modelling the step discontinuity. Although this approach gives accurate results for TE polarization where the field is regular, its accuracy for TM polarization have not been demonstrated, as direct mode matching does not take account of the true diffraction field at the step and suffers from well- known drawbacks. Furthermore, the application of the method to the analysis of cascades of step discontinuities, such as multiple coupled guides, seem to require a lot of

computation if interaction via the propagating continuous spectrum between non adjacent discontinuities is taken to account. Therefore, a method of modelling which takes account of the interaction via the propagating continuous spectrum between non adjacent discontinuities is highly desirable if computation effort and computer time is to be reduced.

In all the methods discussed above, transverse resonance is employed to derive the propagation constant β of the structure.

2.222 EFFECTIVE DIELECTRIC CONSTANT METHOD (EDC)

The first semi - analytic treatment of dielectric guides was presented by Marcatili. His pioneering work [14] concerns the study of the rectangular fibre and his analysis gives closed - form expression which are simple to use. This analysis begins with the assumption that modes in the structure are guided strongly with little field penetration in to the cladding regions and no field penetration in to the corner regions of the structure. Beside this approximation his analysis also neglected the necessary dependence between k_x and k_y , the wavenumber in the x and y direction respectively, and hence the analysis only works well for modes well above cut - off.

A more accurate analysis which may be considered as an improvement to the Marcatili's analysis is known as the Effective Dielectric Constant method. The technique was first introduced by Knox and Toulios [15] in their analysis of image line. Since then EDC technique has been used by other researcher and formulated in various forms to analyze dielectric waveguide in integrated optics [16,17]. The approach is to divide the waveguide cross section in to several laterally piecewise uniform regions and to replace each one of them by a single homogenous region of effective dielectric constant ε_{eff} calculated by letting the x - dimension of each uniform region approach infinity. In this way, the original structure is transformed into a layer of dielectric slab waveguides of dielectric constant ε_{eff} from which the field solution of the original structure may be

obtained. Clearly in this analysis the discontinuities at the boundaries between successive lateral regions are ignored, an approximation only valid under small step assumption. In spite of its simplicity, ease of implementation and little computational effort required, the results obtained by this method are not accurate enough for some practical configuration. In the case of rib waveguide structure, the method breaks down when there are no guided modes and hence there is no effective index in the outer region. Furthermore, the technique gives practical results only when the rib and outer regions support single mode propagation which avoids ambiguity in selecting the effective dielectric constant of the guide in each region. In the example worked out in chapter three it will be shown that the method gives very accurate results only when the outer region is well above cutoff and the step discontinuity is small, so that the contribution of the continuum is insignificant. A good discussion on the drawback of this method was given by Oliner et - al [9].

2.223 INTEGRAL EQUATION APPROACH

A mathematical formulation which has been increasingly gaining favour for solving field problem in composite structures is the integral equation approach where the Maxwell's equations are represented in their integral form. In this formulation, the field problem is represented by the Green function and the source function that they act upon. Integral equations can be solved by a variety of methods such as moment methods. Usually, the integral equations are variational in some quantity, for instance, in this case, the propagation constant β, and this property may be utilized to simplify the solution. Hence, a variational formulation that is stationary about the correct solution may be adopted to minimize the error of field modelling. This property is very useful particularly when the field is known only approximately. The accuracy and the efficiency of the method are dependent upon the ability to determine the correct Green's operators and the proper choice of trial functions. The approach of determining the Green's function as described above is known as the space domain approach. The

advantage of this approach is that there is no restriction on the choice of trial functions and, therefore, we have greater flexibility in choosing the optimum trial function. For instance, we may used to construct a trial field function that incorporates all a 'priori' known physical features of the solution, such as singularities at corners and so improve the efficiency of the solution.

For some waveguide structures the formulation of the Green's operators may be obtained in the Fourier domain, that is, the transformation of the integral equations in to the spectral domain [18]. In order to successfully apply this approach the transverse cross section of the guide must be uniform so that same Fourier transform hold in all regions of interest. However, this is not the case in non planar structures such as the rib waveguide and, hence, the spectral domain approach is not directly applicable in this situation. Furthermore, the spectral domain method requires a trial function which is Fourier transformable and this, in turn, restricts the choice of optimum trial functions, as a function constructed for sake of an efficient representation of the field may not always be Fourier transformable.

2.3 COMPLETE SPECTRUM OF AN ASYMMETRICAL MULTILAYER SLAB GUIDE

The cross section of an open rib waveguide under consideration in this work is shown in Fig. 2.1 . Indeed, if the rib height were very small and could be ignored, the rib waveguide would reduce to an asymmetrical three layer slab waveguide. The treatment of the slab guide problem is well known and documented and can be found in text books such as [19,20,21]. The methods for determining the mode spectrum range from a straightforward field matching at each dielectric interface to the more elegant approach based on a consideration of the singularities of the Green's function and the spectrum of second order differential operators. The latter method is powerful, since not only it yields mode functions which are automatically normalised but also it can be extended to

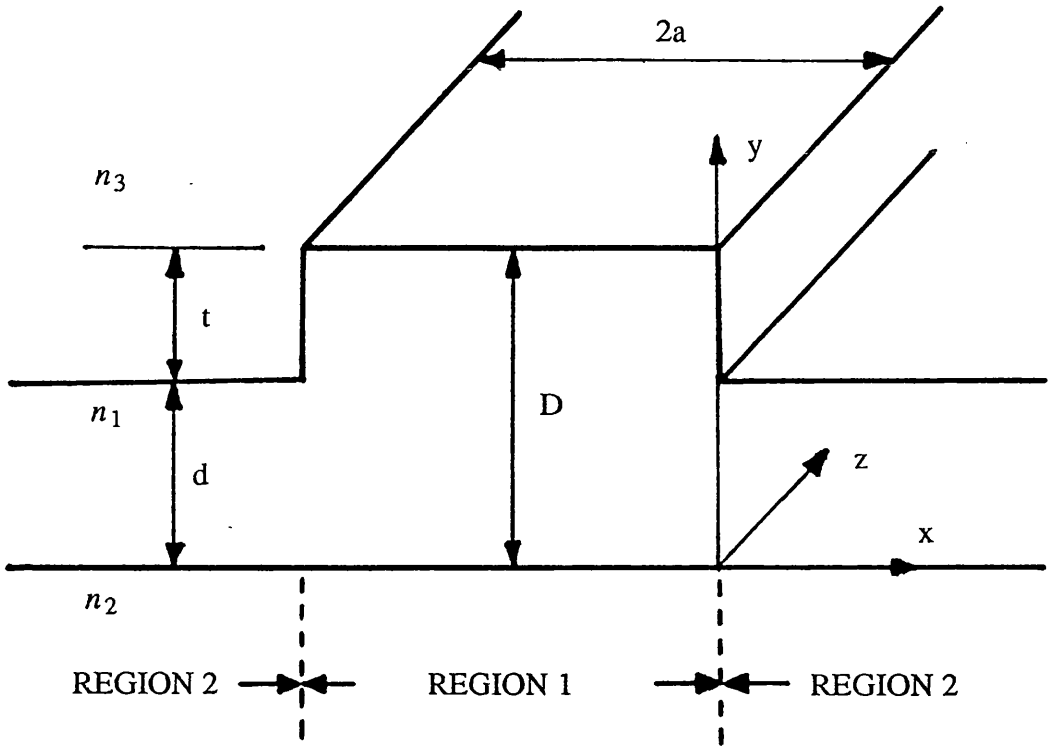

Fig. 2.1 Rib guide cross section.

the multilayer situation with ease and economy of effort. Our interest here is for the latter method and it is the intention of this section to retrace the procedure involved in this method of analysis. There are two reasons for including this discussion. Firstly, a method of analysis which is very closely related to the latter method will be employed in chapter six to study the mode completeness of rib waveguide structure. Hence, a good understanding of the approach is essential in order to follow the development of the analysis presented in that chapter. Secondly, the latter method serves as an example of the application of transverse resonance technique, the very concept we employ in order to determine dispersion characteristics of rib waveguide in the rigorous analysis developed in chapters three and four. The reader who is familiar with this approach and the transverse resonance technique can skip this section without loss of continuity. This section is organised in to three parts. Section 2.31 describes the relationship between characteristic Green's function for the Sturm - Liouville differential operator and eigenvalue solutions. This is followed with the construction of Green's function given in section 2.32 . The application of the method and transverse resonance technique to determine orthonormalised TE mode function for asymmetrical three layer slab guide is outlined in section 2.33 .

2.31 RELATIONSHIP BETWEEN CHARACTERISTICS GREEN'S FUNCTION FOR STURM - LIOUVILLE DIFFERENTIAL OPERATOR AND EIGENVALUE SOLUTIONS

A good discussion on this subject is given in a text book such as [21] and a clear treatment of the mathematical foundation of the process can be found in [22]. Therefore, only a brief outline of the procedure involved will be given.

The general Sturm - Liouville differential operator L may be written as,

$$L\,\phi(y) = \left[\frac{d}{dy}\,(p(y)\,\frac{d}{dy}) - q(y) + \lambda\, w(y) \right] \phi(y) \tag{2.1}$$

subject to the boundary conditions

$$\left[p\,\frac{d}{dy} + \alpha_{1,2} \right] \phi(y_{1,2}) = 0 \tag{2.2}$$

The characteristic Green's function $g(y,y';\lambda)$ for the Sturm - Liouville problem (2.1) is defined by

$$L\,g(y,y';\lambda) = -\delta(y-y') \quad ; y_1 < y' < y_2 \tag{2.3}$$

and equation (2.2) becomes,

$$\left[p\,\frac{d}{dy} + \alpha_{1,2} \right] g(y,y';\lambda) = 0 \quad ; y = y_{1,2} \tag{2.4}$$

As will be shown later, the parameter λ in equation (2.3) is arbitrary but so restricted as to assure a unique solution.

For the planar dielectric region, the network model of the characteristic Green's function problem is the non uniform transmission line shown in Fig. 2.2 . The network is excited at $y = y'$ by a unit current source $i(y') = \delta(y-y')$. With reference to the figure, the transmission line equations for voltage and current are written as,

$$-\frac{d}{dy}\,V(y,y') = j\,k_y(y)\,Z(y)\,I(y,y') \tag{2.5a}$$

$$-\frac{d}{dy}\,I(y,y') = j\,k_y(y)\,Y(y)\,V(y,y') - \delta(y-y') \tag{2.5b}$$

For a TE mode the impedance Z(y) is given by $Z(y) = \dfrac{1}{Y(y)} = \dfrac{\omega\mu_0}{k_y(y)}$, where $k_y(y)$ is the propagation constant. The corresponding second order differential equation for $V(y,y')$ is derived from the two coupled first - order differential equations (2.5), and is given by

$$\left[\frac{d}{dy}\left(\frac{1}{\mu'(y)} \frac{d}{dy} \right) + \varepsilon'(y)\, k_o^2 - \frac{\beta^2}{\mu'(y)} \right] V(y,y') = -j\,\omega\,\mu_0\,\delta(y-y') \tag{2.6}$$

where $k_o^2 = \omega^2 \mu_0 \varepsilon_0$, $\mu' = \dfrac{\mu(y)}{\mu_0}$ and $\varepsilon'(y) = \dfrac{\varepsilon(y)}{\varepsilon_0}$

Upon comparing equations (2.1) and (2.6), the equivalence of the two equations is observed with the identifications:

$$p(y) = w(y) = \frac{1}{\mu'(y)} \quad ; q(y) = -\varepsilon'(y)\, k_o^2$$

$$\beta^2 = -\lambda \quad ; \; V(y,y') = j\,\omega\,\mu_0\, g(y,y';\lambda) \tag{2.7}$$

The equivalence of the boundary conditions of equation (2.4) are obtained from equations (2.5a) and (2.7), given by

$$\frac{I}{V} = \frac{j\,p\,\dfrac{d}{dy} g(y,y')}{\omega\,\mu_0\, g(y,y';\lambda)} \tag{2.8}$$

Rewriting (2.8) in terms of the terminating admittances $\overrightarrow{Y}_T$ and $\overleftarrow{Y}_T$ at y_1 and y_2, we have

$$\overleftarrow{Y}_T = -\frac{I(y,y')}{V(y,y')} = j\,\frac{\alpha_1}{\omega\mu_0}$$

$$\overrightarrow{Y}_T = \frac{I(y,y')}{V(y,y')} = -j\,\frac{\alpha_2}{\omega\mu_0} \tag{2.9}$$

Next, we need to consider the behaviour of g and its first derivative in the vicinity of the source at $y = y'$. From the network in Fig. 2.2, it is readily shown that V is continuous across the current generator and I is discontinuous giving,

$$\lim_{\delta \to 0} \left[V(y,y'+\delta) - V(y,y'-\delta) \right] = 0 \tag{2.10a}$$

$$\lim_{\delta \to 0} \left[I(y,y'+\delta) - I(y,y'-\delta) \right] = 1 \tag{2.10b}$$

Consequently, the corresponding conditions on $g(y,y';\lambda)$ are

$$\lim_{\delta \to 0} \left[g(y,y' + \delta; \lambda) - g(y,y' - \delta; \lambda) \right] = 0 \tag{2.10c}$$

$$\lim_{\delta \to 0} \left[p(y) \frac{d}{dy} g(y,y' + \delta; \lambda) - p(y) \frac{d}{dy} g(y,y' - \delta; \lambda) \right] = -1 \tag{2.10d}$$

For a fixed $\alpha_{1,2}$ and $y_{1,2}$ the voltage response $g(y,y'; \lambda)$ of the network shown in Fig. 2.2 will be finite and well defined unless the choice of parameter λ is such that a resonance can exist. At resonances $\lambda = \lambda_n$, the voltage response will be infinite and there is no unique solution of the network problem. If λ in equation (2.3) is regarded as a general complex parameter, then $g(y,y'; \lambda)$ is a regular function of λ in the complex λ plane except at points $\lambda = \lambda_n$. Since the resonant condition $\lambda = \lambda_n$ implies the persistence of a response in the absence of the source, the functional form of the resonant solution satisfies the homogenous equation (2.1). Therefore, information regarding the desired eigensolutions of equation (2.1) is contained in the singularities of the characteristic Green's function $g(y,y'; \lambda)$, and consequently, the problem of determining a complete set of eigenfunctions is directly related to the complete investigation of the singularities of $g(y,y'; \lambda)$ in the complex λ plane.

In order to give a clear picture of the situation, let us consider briefly the relationship between $g(y,y'; \lambda)$ and the solution $\phi_n(y)$ of the homogeneous equation (2.1). Rewriting (2.1), we have

$$\left[\frac{d}{dy} \left(p(y) \frac{d}{dy} \right) - q(y) \right] \phi_n(y) = -\lambda_n w(y) \phi_n(y) \tag{2.11}$$

To relate the complete eigenmode set $\phi_n(y)$ to the Green's function $g(y,y'; \lambda)$, the function $g(y,y'; \lambda)$is written as an expansion in terms of $\phi_n(y)$ given by,

$$g(y,y'; \lambda) = \sum_n g_n(y'; \lambda) \phi_n(y) \quad ; y_1 < y < y_2 \tag{2.12}$$

where

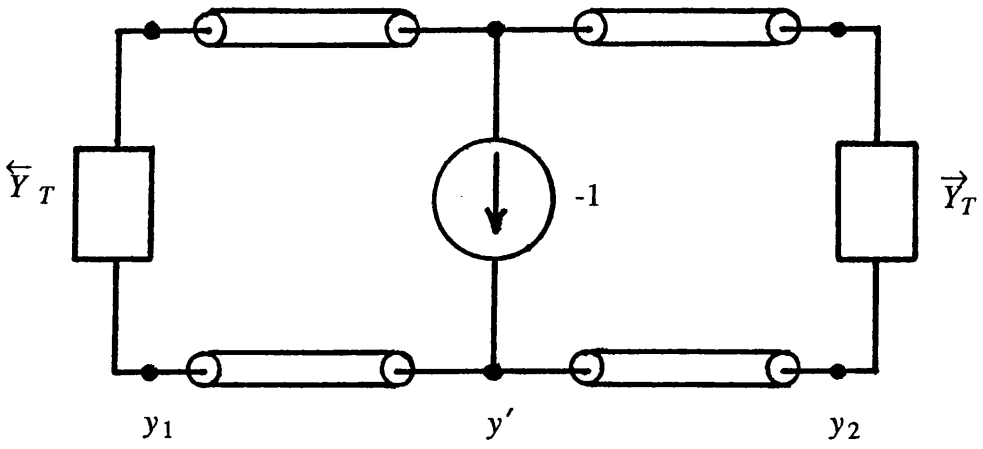

Fig. 2.2 Non-uniform transmission line excited with a unit current generator.

$$g_n(y';\lambda) = \int_{y_1}^{y_2} g(y,y';\lambda)\, w(y)\, \phi_n(y)\, dy \tag{2.13}$$

Substituting (2.12) in to (2.3), gives

$$L \sum_n g_n(y';\lambda)\, \phi_n(y) = -\delta(y-y') \tag{2.14}$$

Adding $\lambda\, w(y)\, \phi_n(y)$ to the R.H.S. and L.H.S. of (2.11), we have

$$L\, \phi_n(y) = (\lambda - \lambda_n)\, w(y)\, \phi_n(y) \tag{2.15}$$

Now substituting (2.15) in to (2.14) gives

$$\sum_n g_n(y';\lambda)\, (\lambda-\lambda_n)\, w(y)\, \phi_n(y) = -\delta(y-y') \tag{2.16}$$

Multiplying both sides of (2.16) by ϕ_n, integrating w.r.t. y and using the orthogonality of ϕ_n gives

$$g_n(y';\lambda)\, (\lambda-\lambda_n) = -\phi_n(y')$$

$$g_n(y';\lambda) = -\frac{\phi_n(y')}{(\lambda-\lambda_n)} \tag{2.17}$$

Hence, (2.12) becomes

$$g(y,y';\lambda) = -\sum_n \frac{\phi_n(y)\, \phi_n(y')}{(\lambda-\lambda_n)} \tag{2.18}$$

Equation (2.18) highlights the existence of simple poles in the complex λ plane at the eigenvalues λ_n corresponding to the eigenfunctions ϕ_n. If (2.18) is integrated in the complex λ plane about a contour C enclosing all the singularities of $g(y,y';\lambda)$, then by application of Cauchy's theorem we obtain

$$-\frac{1}{j\,2\pi}\oint_c g(y,y';\lambda)\, d\lambda = -\sum_n \phi_n(y)\, \phi_n(y') \left(-\frac{1}{j\,2\pi}\right)\oint_c \frac{1}{\lambda-\lambda_n}\, d\lambda$$

$$= \sum_n \phi_n(y)\, \phi_n(y') = \frac{\delta(y-y')}{w(y)} \tag{2.19}$$

Hence,

$$\frac{\delta(y-y')}{w(y)} = -\frac{1}{j2\pi}\oint_c g(y,y';\lambda)\,d\lambda \qquad (2.20)$$

Equation (2.20) is the well - known relationship between the Green's function of the wave equation and the delta function.

Having established the relationship between characteristic Green's function and the eigenvalue solutions of equation (2.3) we shall now proceed with the development for $g(y,y';\lambda)$ in order to completely describe the problem.

2.32 CONSTRUCTION OF GREEN'S FUNCTION

The Green's function $g(y,y';\lambda)$ can be constructed from two solutions of the homogenous equations (2.3) namely, $\overleftarrow{V}(y)$ and $\overrightarrow{V}(y)$ satisfying the required boundary conditions at y_1 and y_2 respectively, given by

$$L\overleftarrow{V}(y)=0 \quad ; \left(p\frac{d}{dy}+\alpha_1\right)\overleftarrow{V}(y)=0 \quad at\ y=y_1 \qquad (2.21a)$$

$$L\overrightarrow{V}(y)=0 \quad ; \left(p\frac{d}{dy}+\alpha_2\right)\overrightarrow{V}(y)=0 \quad at\ y=y_2 \qquad (2.21b)$$

The appropriate form of solution for $g(y,y';\lambda)$ which satisfies the homogenous equation (2.3) for $y \neq y'$ and the continuity condition at $y=y'$ given by (2.10c) is

$$\begin{aligned} g(y,y';\lambda) &= A\overleftarrow{V}(y)\overrightarrow{V}(y') \quad ; y<y' \\ &= A\overleftarrow{V}(y')\overrightarrow{V}(y) \quad ; y>y' \end{aligned} \qquad (2.22)$$

The constant A in (2.22) is chosen to satisfy the jump condition (2.10d) at $y=y'$. Substituting (2.22) in to (2.10d) gives

$$Ap\left[\overleftarrow{V}(y')\frac{d}{dy}\overrightarrow{V}(y)-\overrightarrow{V}(y')\frac{d}{dy}\overleftarrow{V}(y)\right]=-1$$

Hence,

$$g(y,y';\lambda) = \frac{\overleftarrow{V}(y_<)\overrightarrow{V}(y_>)}{-p\,W(\overleftarrow{V}, \overrightarrow{V})} \tag{2.23}$$

where,

$y_< = y \quad$ for $y < y'$

$\quad = y' \quad$ for $y > y'$

$y_> = y \quad$ for $y > y'$

$\quad = y' \quad$ for $y < y'$

and $W(\overleftarrow{V}, \overrightarrow{V}) = \overleftarrow{V}\,\frac{d\overrightarrow{V}}{dy} - \overrightarrow{V}\,\frac{d\overleftarrow{V}}{dy}$

, is the Wronskian determinant of $\overleftarrow{V}$, $\overrightarrow{V}$

In order to investigate the properties of the Wronskian determinant, equations (2.21a) and (2.21b) are multiplied by $\overleftarrow{V}$ and $\overrightarrow{V}$, respectively, and subtracting the resulting equations, we obtain

$$\overleftarrow{V}\,\frac{d}{dy}p\,\frac{d}{dy}\overrightarrow{V} - \overrightarrow{V}\,\frac{d}{dy}p\,\frac{d}{dy}\overleftarrow{V} = \frac{d}{dy}(p\,W(\overleftarrow{V}, \overrightarrow{V})) = 0 \tag{2.24}$$

Equation (2.24) shows that $p\,W(\overleftarrow{V}, \overrightarrow{V})$ is independent of y and can be evaluated at any convenient point y_0 in the interval $y_1 < y < y_2$.

Normalising V(y) such that $V(y_0) = 1$, we have

$$\overrightarrow{V}(y,y_0) = \frac{\overrightarrow{V}(y)}{V(y_0)} \quad ; \overleftarrow{V}(y,y_0) = \frac{\overleftarrow{V}(y)}{V(y_0)}$$

and recalling equations (2.8) and (2.9), the Green's function (2.23) can be written as

$$g(y,y';\lambda) = \frac{\overleftarrow{V}(y_<,y_0)\overrightarrow{V}(y_>,y_0)}{j\omega\mu_0 \overleftrightarrow{Y}(y_0)} \tag{2.25}$$

where $\overleftrightarrow{Y}(y_0)$ is the total admittance seen looking to the left and right of y_0.

From the above considerations, it can be seen that the poles of $g(y,y';\lambda)$ in the complex λ-plane occurring at $\lambda = \lambda_n$ coincide with the vanishing of the total admittance of the

equivalent network model i.e with the resonances of the equivalent network. If the singularities of $g(y,y';\lambda)$ are simple poles situated at the zeros λ_n of $\overleftrightarrow{Y}(y_0)$, then in order to evaluate the integral (2.20), the function $\overleftrightarrow{Y}(y_0)$ is expanded as a Taylor series in the neighbourhood of a zero, given by

$$\overleftrightarrow{Y}(y_0;\lambda) = \overleftrightarrow{Y}(y_0,\lambda_n) + (\lambda-\lambda_n)\frac{\partial}{\partial\lambda_n}\overleftrightarrow{Y}(y_0,\lambda_n) + ...$$

Substituting the series expansion into (2.20), we obtain the delta - function representation for the TE mode problem, namely

$$\begin{aligned}
\mu'(y)\,\delta(y-y') &= -\frac{1}{j2\pi}\oint_c g(y,y';\lambda)\,d\lambda = \sum_n \phi_n(y)\,\phi_n(y') \\
&= -\frac{1}{j2\pi}\oint_c \frac{\overleftarrow{V}(y_<,y_0;\lambda)\,\overleftarrow{V}(y_>,y_0;\lambda)}{j\omega\mu_0\,\overleftrightarrow{Y}(y_0;\lambda)}\,d\lambda \\
&= \sum_n \frac{\overleftarrow{V}(y_<,y_0;\lambda_n)\,\overleftarrow{V}(y_>,y_0;\lambda_n)}{-j\omega\mu_0\,\frac{\partial}{\partial\lambda_n}\overleftrightarrow{Y}(y_0;\lambda_n)}\,\frac{1}{j2\pi}\oint_c \frac{d\lambda}{\lambda-\lambda_n} \\
&= \sum_n \frac{\overleftarrow{V}(y,y_0;\lambda_n)\,\overrightarrow{V}(y',y_0;\lambda_n)}{\omega\mu_0\,\frac{\partial}{\partial\lambda_n}\overleftrightarrow{B}(y_0;\lambda_n)} \qquad ;\ \overleftrightarrow{Y} = j\overleftrightarrow{B}
\end{aligned}$$

Hence, the normalized mode functions $\phi_n(y)$ are given by,

$$\phi_n(y) = \frac{1}{\left[\omega\mu_0\ \frac{\partial}{\partial\lambda}\overleftrightarrow{B}(y_0;\lambda)\Big|_{\lambda=\lambda_n}\right]^{\frac{1}{2}}}\overleftarrow{V}(y,y_0;\lambda_n) \tag{2.26}$$

The above discussion applies to closed waveguides system where the dimensions of y_1 and y_2 are finite so that the equivalent network resonances at $\lambda=\lambda_n$, characterize simple pole singularities of $g(y,y';\lambda)$. In the case of open waveguides, where one or both of the dimensions becomes infinite, the discrete resonances may coalesce in to a continuous spectrum; where now $g(y,y';\lambda)$ possesses a branch - point singularity, giving rise to the necessity of introducing a branch-cut in the complex λ-plane to ensure uniqueness of $g(y,y';\lambda)$. This situation is best explained by considering an example. Let us consider

the configuration shown in Fig. 2.3, comprising two dielectrics semi infinite in y. In fact, this situation represents the limiting case of an asymmetrical slab guide with zero film thickness. The characteristic Green's function is

$$g(y,y';\lambda) = \frac{\overleftarrow{V}_\beta(y_<)\,\overrightarrow{V}_\beta(y_>)}{j\,\omega\,\mu_0\,\overleftrightarrow{Y}(0)}$$

where $\beta = 1$ and $\beta = 2$ correspond to $-\infty < y,y' < 0$ and $0 < y,y' < \infty$, respectively.

The voltage distributions are given by,

$$\overleftarrow{V}_1(y) = e^{i\sigma y} \quad , \; \sigma^2 = \rho^2(\sigma) = \varepsilon_2 k_o^2 + \lambda = \hat{\lambda} + (\varepsilon_2 - 1)k_o^2 \quad ; \; \mathrm{Im}\,\sigma < 0$$

$$\overrightarrow{V}_2(y) = e^{-j\rho y} \quad , \; \rho^2 = k_o^2 + \lambda = \hat{\lambda} \quad ; \; \mathrm{Im}\,\rho < 0$$

$$\overrightarrow{V}_1(y) = \cos(\sigma y) - j\,\frac{\rho}{\sigma}\sin(\sigma y)$$

$$\overleftarrow{V}_2(y) = \cos(\rho y) + j\,\frac{\sigma}{\rho}\sin(\rho y)$$

$$j\,\omega\,\mu_0\,\overleftrightarrow{Y}(0) = j\,(\sigma + \rho)$$

In order to examine the behaviour of $g(y,y';\lambda)$, the dependence of $g(y,y';\lambda)$ upon the wavenumbers σ andρ must be considered. Since $g(y,y';\lambda)$ is not an even function of either σ or ρ, branch points exist in the complex λ-plane at $\lambda = -k_o^2$ (i.e $\hat{\lambda} = 0$) and $\lambda = -\varepsilon_2 k_o^2$ (i.e. $\hat{\lambda} = -(\varepsilon_2 - 1)k_o^2$)

Now, define

$$\hat{\lambda} = \left|\hat{\lambda}\right| e^{j\theta}$$

$$\sqrt{\hat{\lambda}} = \left|\sqrt{\hat{\lambda}}\right| e^{j\frac{\theta}{2}}$$

Imposing the convergence requirement $\mathrm{Im}\sqrt{\hat{\lambda}} < 0$, restricts θ to the range $0 > arg\,(\hat{\lambda} + (\varepsilon_2 - 1)k_o^2) > -2\,\pi$.

In order to ensure uniqueness of $g(y,y';\lambda)$, a branch cut must be introduced running from $\hat{\lambda} = -(\varepsilon_2 - 1)k_o^2$ to infinity along the positive real axis. Now, if this problem is

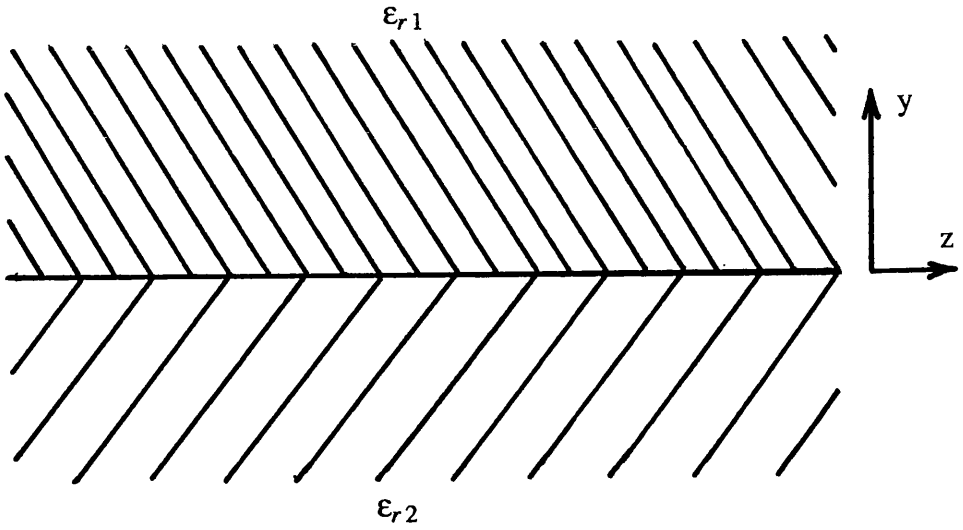

Fig. 2.3 Two dielectric layers infinite in y.

generalised to the case of an open asymmetrical slab waveguide, then, in addition to the branch cut singularities, we have simple pole singularities occurring at $\hat{\lambda}=\rho_n^2$, corresponding to the resonances of the equivalent network. Therefore, the appropriate contour of integration of the Green's function in the complex λ-plane is drawn in Fig. 2.4 enclosing all the singularities of $g(y,y';\lambda)$ plus the branch cut. The contribution of the discrete poles can be extracted as before in equation (2.26). The contour integral about the branch cut I_{bc} can be evaluated as follows:

$$
\begin{aligned}
I_{bc} &= -\frac{1}{j2\pi}\int_{\infty e^{j2\pi}}^{0} g(y,y';\lambda)\,d\hat{\lambda} - \frac{1}{j2\pi}\int_{0}^{\infty e^{-j0}} g(y,y';\lambda)\,d\hat{\lambda} \\
&= -\frac{1}{j2\pi}\int_{0}^{\infty e^{-j0}} \left[g(y,y';\hat{\lambda}-k_o^2) - g(y,y';\hat{\lambda}e^{-j2\pi}-k_o^2) \right] d\hat{\lambda} \\
&= -\frac{1}{\pi}\,\mathrm{Im}\int_{0}^{\infty e^{-j0}} g(y,y';\hat{\lambda}-k_o^2)\,d\hat{\lambda} \\
&= -\frac{2}{\pi}\,\mathrm{Im}\int_{0}^{k_o\sqrt{(\varepsilon_2-1)}} \sigma\, g(y,y';\sigma^2-\varepsilon_2 k_o^2)\,d\sigma - \frac{2}{\pi}\,\mathrm{Im}\int_{0}^{\infty} \rho\, g(y,y';\rho^2-k_o^2)\,d\rho
\end{aligned}
$$

Substituting for g in equation (2.28) yields

$$
I_{bc} = \frac{2}{\pi}\int_{0}^{k_o\sqrt{\varepsilon_2-1}} \sigma\,\mathrm{Re}\,\frac{\overleftarrow{V}(y_<,y_0)\,\overrightarrow{V}(y_>,y_0)}{\omega\mu_0\overleftrightarrow{Y}(y_0;\sigma^2)}\,d\sigma + \frac{2}{\pi}\int_{0}^{\infty} \rho\,\mathrm{Re}\,\frac{\overleftarrow{V}(y_<,y_0)\,\overrightarrow{V}(y_>,y_0)}{\omega\mu_0\overleftrightarrow{Y}(y_0;\rho^2)}\,d\rho \tag{2.27}
$$

Hence, the contribution to the integral for the fields propagating in air as well as in substrate is given by,

$$
\frac{2}{\pi}\int_{0}^{\infty} \rho\,\mathrm{Re}\,\frac{\overleftarrow{V}(y_<,y_0)\,\overrightarrow{V}(y_>,y_0)}{\omega\mu_0\overleftrightarrow{Y}(y_0;\rho^2)}\,d\rho \equiv \int_{0}^{\infty} d\rho\,\phi(y,\rho)\,\phi(y',\rho) \tag{2.28}
$$

and for the fields propagating in the substrate and decaying in air is given by

$$
I_{bc} = \frac{2}{\pi}\int_{0}^{k_o\sqrt{\varepsilon_2-1}} \sigma\,\mathrm{Re}\,\frac{\overleftarrow{V}(y_<,y_0)\,\overrightarrow{V}(y_>,y_0)}{\omega\mu_0\overleftrightarrow{Y}(y_0;\sigma^2)}\,d\sigma \equiv \int_{0}^{k_o\sqrt{\varepsilon_2-1}} \phi(y,\sigma)\,\phi(y',\sigma)\,d\sigma \tag{2.29}
$$

Therefore, the integration of the Green's function about a contour C in Fig. 2.4 yields a

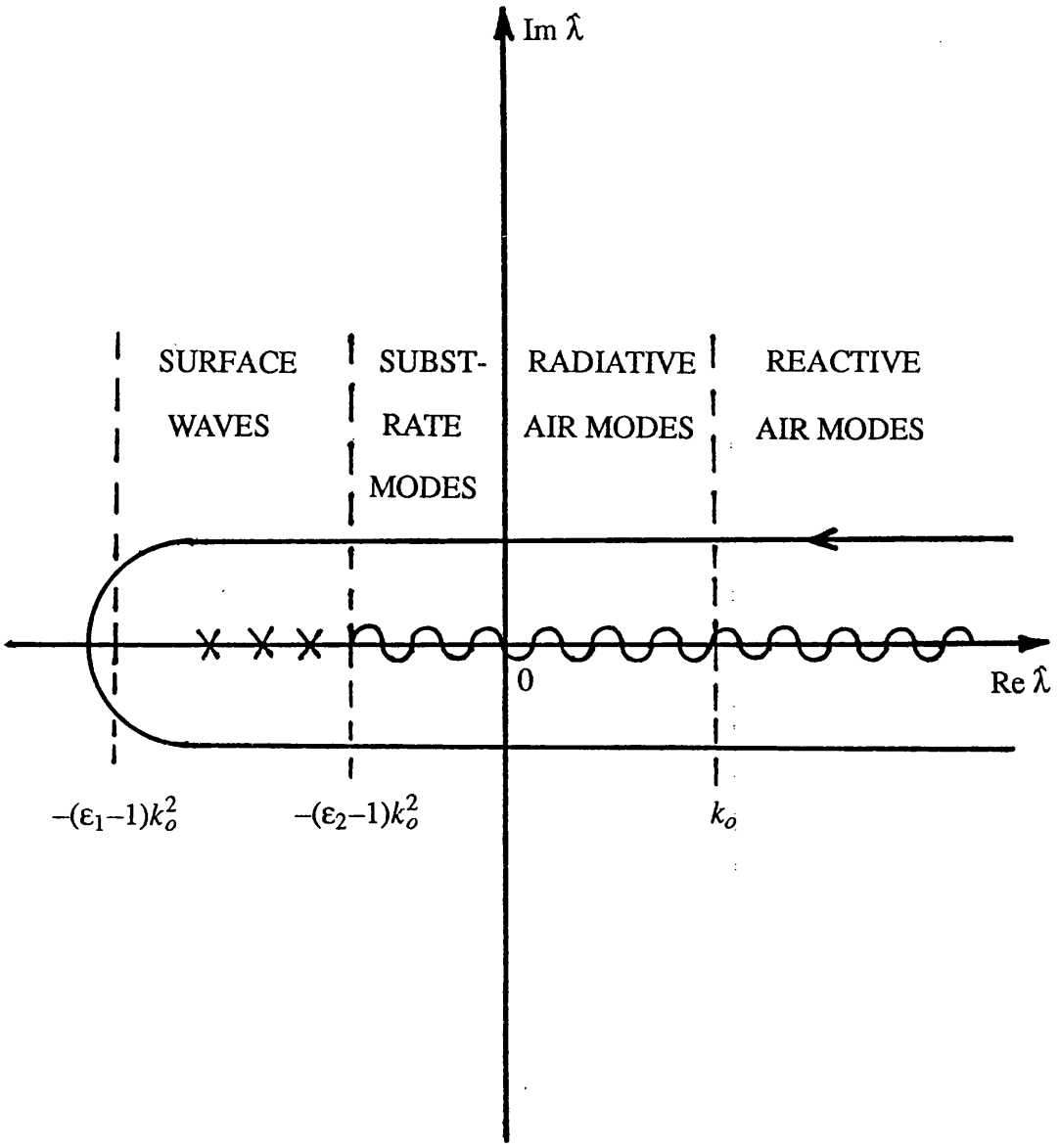

Fig. 2.4 Contour of integration and singularities in the complex $\hat{\lambda}$ - plane.

more general form of equation (2.19) given by

$$-\frac{1}{j2\pi}\oint_c g(y,y';\lambda)d\lambda = \frac{\delta(y-y')}{w(y)} = \sum_{n=1}^{N}\phi_n(y)\,\phi_n(y') + \int_0^{k_o\sqrt{\varepsilon_2-1}} d\sigma\,\phi(y,\sigma)\,\phi(y',\sigma)$$

$$+\int_0^{\infty} d\rho\,\phi(y,\rho)\,\phi(y',\rho) \qquad (2.30)$$

2.33 NORMALISED TE MODE FUNCTION FOR ASYMMETRICAL THREE LAYER SLAB WAVEGUIDE

The possible modes of an open asymmetrical slab guide for varying phase velocity β are shown diagramatically in Fig. 2.5, from [23]. The complete spectrum is constituted by three types of modes:

a) Surface modes shown in Fig. 2.5b - corresponding to fields decaying in the substrate as well as in air. They are discrete finite in number, and are given by the solutions of an eigenvalue equation in the range $n_2k_o < \beta < n_1k_o$

b) Substrate modes shown in Fig. 2.5c - corresponding to fields decaying in air but propagating in the substrate, $n_3k_o < \beta < n_2k_o$

c) Air modes shown in Fig. 2.5d - corresponding to fields propagating in air as well as in the substrate, $0 < \beta < n_3k_o$. As the transverse variation of an air mode gets more and more rapid, its propagation constant turns imaginary and it becomes a non propagating air mode. Such modes can be excited in the presence of sharp discontinuities and obstacles.

Modes shown in Fig. 2.5a, corresponding to $\beta > n_1k_o$, are not physically realizable and therefore not considered as modes of the guide. Hence, from (2.30), the completeness of the TE spectrum of the asymmetrical slab guide can be stated as;

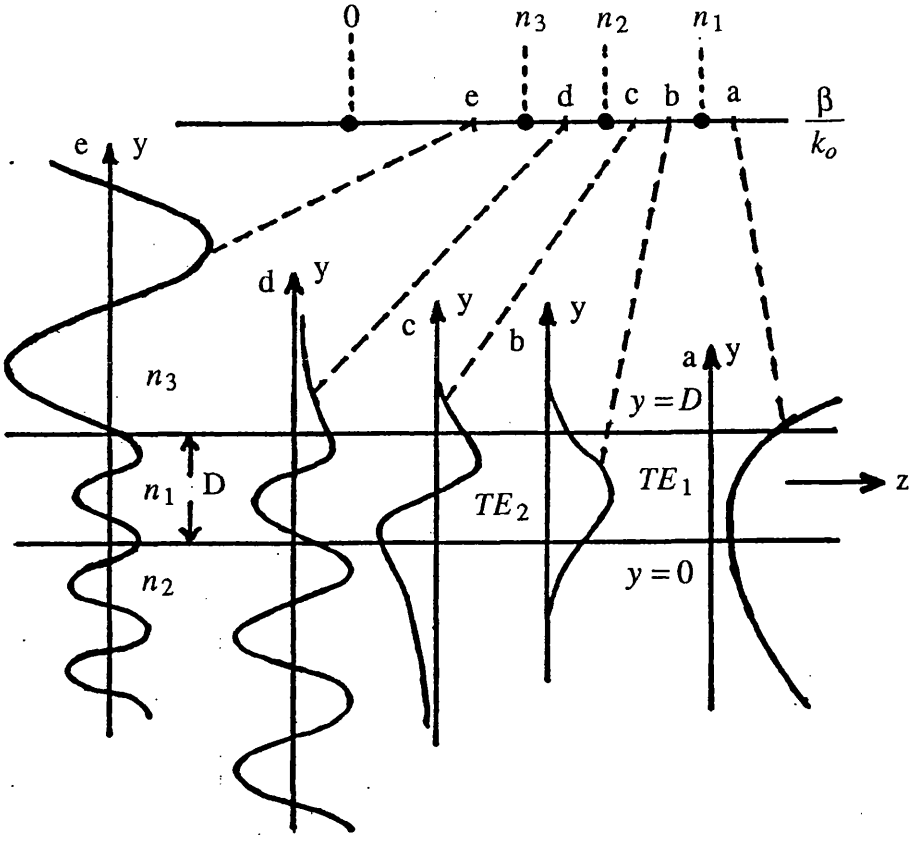

Fig. 2.5 The field distributions of an open asymmetric slab waveguide for different value of β.

$$\sum_{n=1}^{N} \phi_{hn}(y)\,\phi_{hn}(y') + \int_{o}^{k_o\sqrt{\varepsilon_2-1}} d\sigma\,\phi_h(y,\sigma)\,\phi_h(y',\sigma) + \int_{0}^{\infty} d\rho\,\phi_h(y,\rho)\,\phi_h(y',\rho) = \delta(y-y') \tag{2.31}$$

where $\phi_{hn}(y)$, $\phi_h(y,\sigma)$ and $\phi_h(y,\rho)$ denote the n - th surface mode, the substrate mode and air mode respectively. Their orthonormalisation is given below

$$\int_{-\infty}^{\infty} \phi_{hn}^2(y)\,dy = 1$$

$$\int_{-\infty}^{\infty} \phi_h(y,\rho)\,\phi_h(y,\rho')\,dy = \delta(\rho-\rho')$$

$$\int_{-\infty}^{\infty} \phi_h(y,\sigma)\,\phi_h(y,\sigma')\,dy = \delta(\sigma-\sigma') \tag{2.32}$$

The equivalent network model of the problem is shown in Fig. 2.6. The wavenumbers h, $\sigma = -jp$ and $\rho = -jq$ in the film, substrate and air regions respectively as follows

For the surface modes,

$$\beta^2 = \varepsilon_1 k_o^2 - h^2 = k_o^2 + q^2 = \varepsilon^2 k_o^2 + p^2 \tag{2.33}$$

For the substrate modes,

$$\beta^2 = \varepsilon_1 k_o^2 - h^2 = k_o^2 + q^2 = \varepsilon_2 k_o^2 - \sigma^2 \tag{2.34}$$

For the air modes,

$$\beta^2 = \varepsilon_1 k_o^2 - h^2 = k_o^2 - \rho^2 = \varepsilon_2 k_o^2 - \sigma^2 \tag{2.35}$$

Choosing any convenient point as a reference point, say $y = y_0$, we denote by $\vec{Y}(y_0)$ and $\overleftarrow{Y}(y_0)$ the admittance looking towards the positive and negative y axis. The total admittance of the cross section is then given by

$$\overleftrightarrow{Y}(y_0) = \overleftarrow{Y}(y_0) + \vec{Y}(y_0) \tag{2.36}$$

Equation (2.36) immediately gives the dispersion relation $\overleftrightarrow{Y} = 0$. The Green's function can be constructed from the voltage distribution at $y > y_0$ and $y < y_0$ denote by $\vec{V}(y,y_0)$ and $\overleftarrow{V}(y,y_0)$ respectively. Setting $\vec{V}(y_0)$ and $\overleftarrow{V}(y_0) = 1$, and if y and y_0 lie in the same

layer with propagation constant k_y, then from elementary transmission line equations $\overleftarrow{V}$ and $\overrightarrow{V}$ are defined as,

$$\overleftarrow{V}(y,y_0) = \cos(k_y(y-y_0)) + \frac{j\omega\mu_0}{k_y}\overleftarrow{Y}(y_0)\sin(k_y(y-y_0)) \qquad (2.37a)$$

$$\overrightarrow{V}(y,y_0) = \cos(k_y(y-y_0)) - \frac{j\omega\mu_0}{k_y}\overrightarrow{Y}(y_0)\sin(k_y(y-y_0)) \qquad (2.37b)$$

We are now in a position to apply the previous results to extract the normalised mode functions for the three types of modes.

Surface modes

The terminations of the equivalent network in Fig. 2.6 are purely reactive. The propagation constants in the different regions are given by equation (2.33) and the characteristic admittances in each region Y_{o1}, Y_{o2}, Y_{o3}, normalised to $\frac{1}{\omega\mu_0}$ are,

$$Y_{o1} = h \quad , Y_{o2} = -jp \quad , Y_{o3} = -jq$$

Choosing a reference point $y_0 = D$ for convenience, we have

$$\overrightarrow{Y}(D) = -jq$$

$$\overleftarrow{Y}(D) = jh\tan(hD - \bar{\phi}) \quad ; \tan(\bar{\phi}) = \frac{p}{h}$$

This immediately gives the dispersion relation (resonance condition),

$$\overleftrightarrow{Y}(D) = jh\tan(hD - \bar{\phi}) - jq = 0$$

Using (2.25) and (2.37) the field function $\phi_h(y)$ are obtained as

$$\phi_h(y) = A\, e^{-q(y-D)} \quad ; y \geq D$$

$$= A\frac{\cos(hy - \bar{\phi})}{\cos(hD - \bar{\phi})} \quad ; 0 \leq y \leq D$$

$$= A\frac{\cos(\bar{\phi})}{\cos(hD - \bar{\phi})}\, e^{py} \quad ; y \leq 0$$

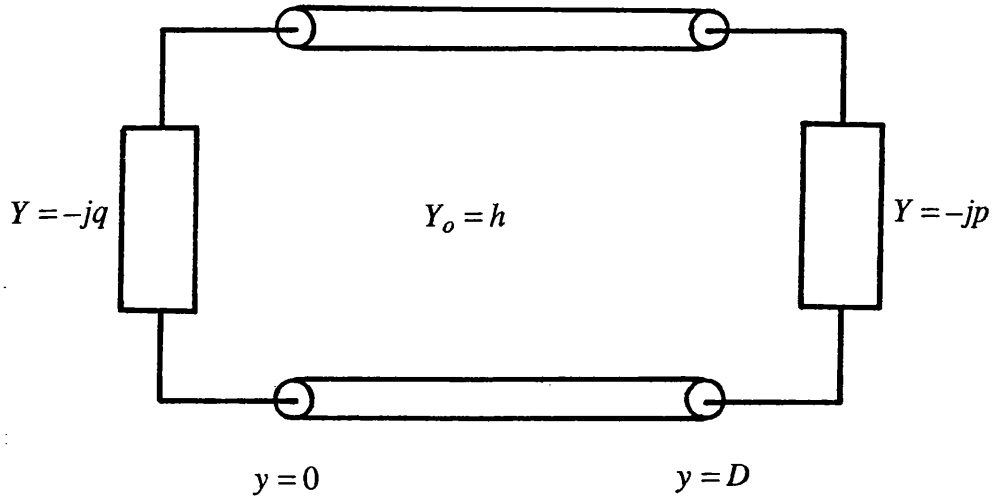

Fig. 2.6 Transverse Equivalent Network for determining surface modes and substrate modes.

where the normalization constant A is found according to (2.26) as

$$\frac{1}{A^2} = \partial_\lambda \left[h \tan(hD - \bar{\phi}) - q \right]$$

which yields

$$A = \left[\frac{2}{D + \frac{1}{p} + \frac{1}{q}} \right]^{\frac{1}{2}} \cos(hD - \bar{\phi})$$

Substrate modes

For the substrate mode, the termination on the substrate side in Fig. 2.6 is resistive while the termination on the air side remains reactive. The propagation constants in the different regions are given by equation (2.34) and the characteristic admittances in each region, normalised to $\frac{1}{\omega\mu_0}$ are,

$$Y_{o1} = h \quad , Y_{o2} = \sigma \quad , Y_{o3} = -jq$$

Referring the amplitude of the field to the top of the substrate, we choose a reference point $y_0 = 0$.

$$\overleftarrow{Y}(0) = \sigma$$

$$\overrightarrow{Y}(0) = jh \tan(\bar{\phi}_{sb}) \quad ; \quad \tan(\bar{\phi}_{sb}) = \frac{h \tan(hD) - q}{h + q \tan(hD)}$$

The total admittance at $y = 0$ is given by

$$\overleftrightarrow{Y}(0) = \sigma (1 + j\tan(\alpha_{sb}))$$

where we have introduced

$$\alpha_{sb} = \tan^{-1}\left(\frac{h}{\sigma} \tan(\bar{\phi}_{sb}) \right)$$

Using (2.25) and (2.37), we obtain the fields of the substrate mode as,

$$\phi_h(y,\sigma) = \sqrt{\frac{2}{\pi}}\, A_{sb} \cos(hD - \bar{\phi}_{sb})\, e^{-q(y-D)} \quad ; y \geq D$$

$$= \sqrt{\frac{2}{\pi}}\, A_{sb} \cos(hy - \bar{\phi}_{sb}) \quad ; 0 \leq y \leq D$$

$$= \sqrt{\frac{2}{\pi}} \cos(\sigma y - \alpha_{sb}) \quad ; y \leq 0$$

where

$$A_{sb} = \frac{\cos(\alpha_{sb})}{\cos(\bar{\phi}_{sb})} = \left[\frac{1}{\cos^2(\bar{\phi}_{sb}) + \frac{h^2}{\sigma^2} \sin^2(\bar{\phi}_{sb})} \right]$$

Air modes

The transverse equivalent circuit for deriving the air modes is shown in Fig. 2.7 where the termination at both ends are resistive. Since air modes are degenerate, we must consider their excitation located at $y \pm \infty$. In the case where equal or opposite excitations are applied at $y \pm \infty$ and the structure is symmetrical, then a magnetic or electric wall will occur at the plane of symmetry. To simplify the task of finding the fields in an asymmetric slab, it is convenient to locate the plane where a magnetic or electric wall falls when equal or opposite excitations are applied at $y \pm \infty$. This plane will then be used as a reference at which the two halves of the transverse equivalent network in Fig. 2.7 are effectively decoupled and the fields at the L.H.S. and R.H.S. of the reference plane can be found separately. It is readily shown by simple network theory that the necessary condition for the existence of a magnetic wall at y_0 in Fig. 2.7 is given by

$$\frac{\sin(2\bar{\phi}_e)}{\sin(2(hD - \bar{\phi}_e))} = \frac{\sigma}{\rho} \frac{\rho^2 - h^2}{\sigma^2 - h^2}$$

For the symmetrical guide we have $\rho = \sigma$, and the above expression reduces to

$$\bar{\phi}_e = \frac{hD}{2}$$

The propagation constants in the different regions are given by (2.35) and the

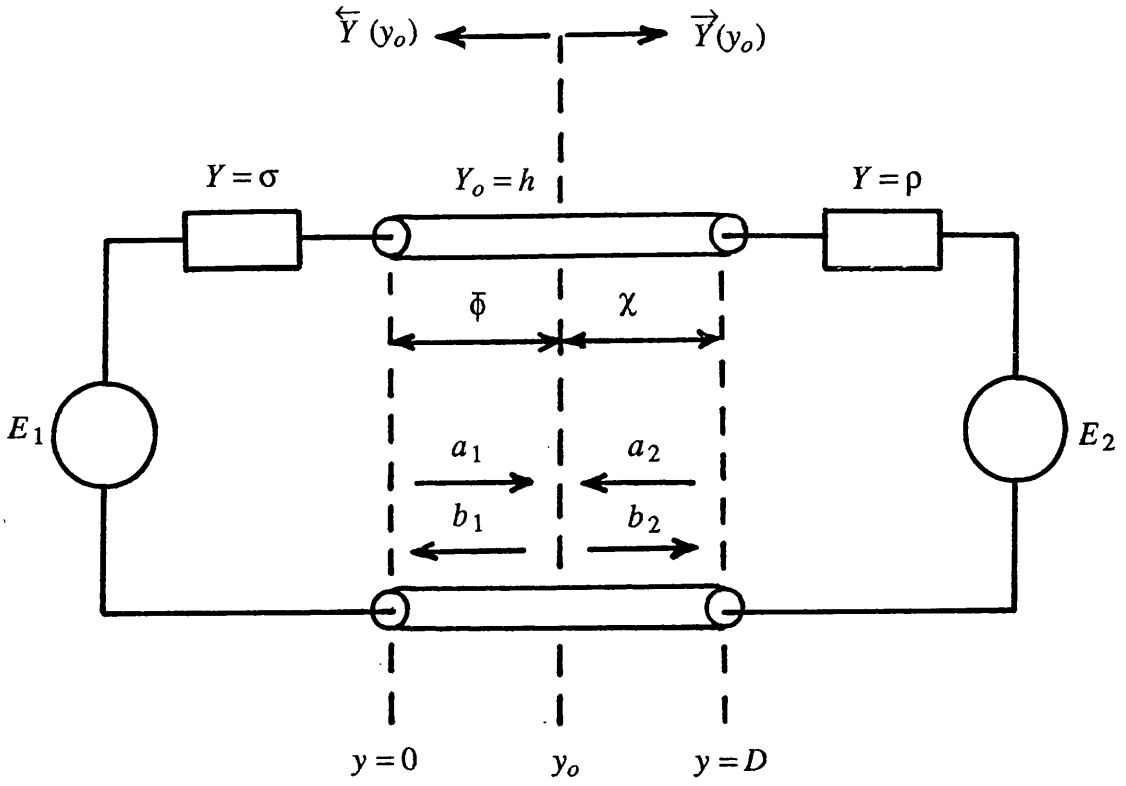

Fig. 2.7 Transverse Equivalent Network for deriving air modes.

characteristic admittances in each region Y_{o1}, Y_{o2}, Y_{o3}, normalised to $\frac{1}{\omega\mu_0}$, are

$$Y_{o1} = h \quad ; Y_{o2} = \sigma \quad ; Y_{o3} = \rho$$

Following the method outlined above and using (2.25) and (2.37) the following even air modes function are obtained,

$$\phi_{he}(y,\rho) = \sqrt{\frac{2}{\pi}}\, A_e \frac{\cos(hD - \bar{\phi}_e)}{\cos(\alpha_{De})} \cos(\rho(y+D) + \alpha_{De}) \quad ; y \geq D$$

$$= \sqrt{\frac{2}{\pi}}\, A_e \cos(hy - \bar{\phi}_e) \quad ; 0 \leq y \leq D$$

$$= \sqrt{\frac{2}{\pi}}\, A_e \frac{\cos(\bar{\phi}_e)}{\cos(\alpha_{0e})} \cos(\sigma y - \alpha_{0e}) \quad ; y \leq 0$$

where

$$\alpha_{De} = \tan^{-1}\left(\frac{h}{\rho}\tan(hD - \bar{\phi}_e)\right)$$

$$\alpha_{0e} = \tan^{-1}\left(\frac{h}{\sigma}\tan(\bar{\phi}_e)\right)$$

$$A_e = \left\{\frac{\sigma}{\rho}\left[\cos^2(\bar{\phi}_e) + \frac{h^2}{\sigma^2}\sin^2(\bar{\phi}_e)\right] + \cos^2(hD - \bar{\phi}_e) + \frac{h^2}{\rho^2}\sin^2(hD - \bar{\phi}_e)\right\}^{-\frac{1}{2}}$$

The odd air modes $\phi_{ho}(y,\rho)$ are obtained from the above formulae by replacing all cosine functions by sine and tangent by cotangent.

The TM spectrum of the asymmetrical slab waveguide can be found by following analogous procedure and are given in appendix 1.

2.4 TRANSVERSE RESONANCE DIFFRACTION METHOD - AS USED IN THE PRESENT WORK

The Transverse Resonance Diffraction method used in the present work is a space domain approach. In this approach, the problem is seen as one of diffraction by a

transverse step discontinuity, say at $x=0$ in Fig. 2.1, whereupon the transverse resonance condition discussed in section 2.3 is employed to derived the propagation constant β. The first rigorous TRD solution was presented in [24] to study image guide problem. Since then, it has been used to successfully analyse inset dielectric guide [25], microstrip [26] and finline [27]. A complete development of the TRD solution for the rib waveguide structure shown in Fig. 2.1 is given in chapter three using LSE and LSM mode approximation and in chapter four for the full rigorous solution. In order that the TRD formulation outlined in the next two chapters can be followed easily, it is useful at this stage to give an overview of the method. Before this is done it is appropriate to briefly introduce the Hertzian vector potential which is required to describe an electromagnetic fields distribution in the formulation of the field problem.

2.41 HERTZIAN VECTOR POTENTIAL

As already mentioned in the previous sections, direct solution of Maxwell's equations in the rib waveguide structure is extremely difficult and consequently, the field distributions need to be derived by means of indirect approach employing "Auxiliary Potential Functions". These functions are chosen to have the vector properties of either the electric or the magnetics fields, which are themselves solutions of Maxwell's equations.

From Maxwell's equations, the divergence equations and the constitutive relations, it is readily shown that in a source free and homogenous medium an electromagnetic field can be completely described by a superposition of electric and magnetic Hertzian vector potential [28], given by

$$\vec{H} = \left[j\,\omega\,\varepsilon\,\nabla\times\pi_e + k^2\,\pi_h + \nabla\,\nabla\cdot\pi_h \right] e^{-j\beta z} \tag{2.38a}$$

$$\vec{E} = \left[k^2\,\pi_e + \nabla\,\nabla\cdot\pi_e - j\,\omega\,\mu_0\,\nabla\times\pi_h \right] e^{-j\beta z} \tag{2.38b}$$

where the electric potential π_e and the magnetic potential π_h are solutions of Helmholtz

equation

$$\nabla^2 \pi + k^2 \pi = 0 \tag{2.39}$$

where $k^2 = \omega^2 \mu_0 \varepsilon_0$

The boundary conditions acting on π_e and π_h may be determined from those conditions acting on the electromagnetic field by expanding equations (2.38). For example, if the y - directed magnetic and electric potential functions are defined as $\pi_h = \psi_h(x,y)\vec{y}$ and $\pi_e = \psi_e(x,y)\vec{y}$ respectively, then from (2.38) a field representing them can be written as

$$\vec{E} = \begin{bmatrix} \omega \mu_0 \beta \\ 0 \\ -j \omega \mu_0 \partial_x \end{bmatrix} \psi_h(x,y) + \begin{bmatrix} \partial_x \partial_y \\ -(\partial_x^2 + \beta^2) \\ -j \beta \partial_y \end{bmatrix} \psi_e(x,y) \tag{2.40a}$$

and

$$\vec{H} = \begin{bmatrix} \partial_x \partial_y \\ -(\partial_x^2 + \beta^2) \\ -j \beta \partial_y \end{bmatrix} \psi_h(x,y) + \begin{bmatrix} -\omega \beta \\ 0 \\ j \omega \varepsilon \partial_x \end{bmatrix} \psi_e(x,y) \tag{2.40b}$$

The functions $\psi_e(x,y)$ and $\psi_h(x,y)$ are constructed from scalar wave equations subject to the appropriate boundary conditions of E_y and H_y respectively. If there are no additional conditions imposed on the remaining fields, "Longitudinal - Section Electric" (LSE) solutions described purely in terms of $\psi_h(x,y)$ and "Longitudinal - Section Magnetic" (LSM) solutions described purely in terms of $\psi_e(x,y)$ can exist independently. These are five field solutions with one of the y - directed field components absent. In general, equation (2.40) gives six field components and the field is hybrid. In some problems, particularly where the refractive index difference and aspect ratio are small and hybrid content is negligible, the electromagnetic field distributions may be accurately be approximated by pure LSE or LSM solutions. In the case of rib waveguide shown in Fig. 2.1, modes will require at least five field components, six to be exact. Consequently the problem will have to be formulated in terms of two coupled potentials.

2.42 AN OVERVIEW OF THE METHOD USED IN THE PRESENT ANALYSIS

An eigenvalue equation for the rib waveguide structure shown in Fig. 2.1 is sought for the guided field solutions which is propagated in the longitudinal direction with phase velocity β. The structure is viewed in terms of two basic building blocks where the constituents component are made up of uniform multilayer asymmetrical slab waveguides separated by the step discontinuities. A plane of symmetry is assumed about the y coordinate axis at $x = -a$ whereas no symmetry exist about the x coordinate axis. With this assumption, an electric wall or a magnetic wall can be placed at the plane of symmetry at $x = -a$ without disturbing the original field configuration and we are reduced to an even mode solution for the LSE or LSM approximations respectively. For hybrid solutions, an electric or magnetic wall at the plane of symmetry will give rise to LSE or LSM-like mode solution respectively. The cross section of the guide can be divided in to two uniform regions in the transverse x - direction namely region 1 $(-a < x < 0)$ and region 2 $(0 < x < \infty)$ separated by a step discontinuity. In this way, the field distribution of the rib waveguide structure can be conveniently expressed separately in the two regions. In region 1 and in region 2, the boundary conditions allows a field formulation in terms of a complete spectrum of the three layer asymmetric slab guides with thickness "D" and "d" respectively. Thus the field in each region will be of different form although for a guided modes the propagation constant β will be the same. Since the modal field can be derived from a knowledge of the transverse fields only, and the z - directed variation is common to both region, one proceeds by studying propagation in the transverse x or y direction. In the present work, the choice of direction of propagation in the x - direction is from point of view of convenience as we are dealing with only one discontinuous interface. Hence, continuity of the transverse fields is applied at the boundary between the two regions at $x = 0$.

The field components are derived from the y - directed magnetic potential (LSE - polarization) or electric potential (LSM - polarization) or superposition of the two

potentials (Hybrid - case) , defined separately for each region. The scalar functions $\psi_h(x,y)$ and $\psi_e(x,y)$ are chosen to have the dimensions of magnetic or electric field respectively in order to be consistent with the dimensionality of equation (2.40). In addition to this, $\psi_h(x,y)$ and $\psi_e(x,y)$ must satisfy the boundary condition of H_y and E_y. The choice of the spectral distribution for $\psi_h(x,y)$ and $\psi_e(x,y)$ will be discussed in chapters three and four.

By enforcing the continuity of the transverse field at the plane of discontinuity at $x = 0$, we obtain an integral equation of the form

$$Ax = f \tag{2.41}$$

where A is a linear integral operator, x is an unknown field and f is a source field. With propagation taken in the x - direction, a convenient field to retain as the unknown is the H_y for LSE polarization and E_y field for LSM polarization. The H_y field on the discontinuous plane $x = 0$ is regular and any suitable orthogonal polynomials may be used to model the field. However, our emphasis in this work is to find a trial field function where a single term expansion is sufficient to yield reasonably accurate and reliable results. The proper choice of the trial field function turns to be the modal solution of an asymmetric slab guide with height intermediate between those of the inner and outer regions. The E_y field on the other hand is singular at the 90 ° and 270 ° dielectric corners at $y = D$ and d respectively. The proper choice of the trial field function is now the modal solution of an intermediate slab modified to include the singular effect at the dielectric corners. Detailed discussion on the choice of the trial field function is given in chapter three. For the LSE polarization , with the transverse H_t field (i.e $H_t = H_y$) retained as the unknown and the transverse E_t field ($E_t = E_z$) as the source, the Green's operators take the dimension of impedance and equation (2.41) becomes in each region,

$$\tilde{Z}_L \cdot H_t = E_t \quad ; x \le 0 \tag{2.42a}$$

$$\tilde{Z}_R \cdot H_t = -E_t \quad ; x \geq 0 \tag{2.42b}$$

where L and R refer to the left and right of the interface and the minus sign is consistent with power flow away from the interface. The continuity of the transverse field at the interface gives

$$(\tilde{Z}_L + \tilde{Z}_R) \cdot H_t = 0 \tag{2.43}$$

By analogous development, it can be shown that the Green's operator for the LSM polarization take the dimension of admittance and continuity of the transverse field at the interface gives

$$(\tilde{Y}_L + \tilde{Y}_R) \cdot E_t = 0 \tag{2.44}$$

Equations (2.43) and (2.44) are statement of transverse resonance since zero source function excites a finite response. In the case of hybrid solution, the continuity of the transverse fields at the interface gives coupled equations of the type,

$$\begin{bmatrix} \tilde{Z}_L + \tilde{Z}_R & \tilde{T}_L - \tilde{T}_R \\ -(\tilde{U}_L - \tilde{U}_R) & \tilde{Y}_L + \tilde{Y}_R \end{bmatrix} \begin{bmatrix} H_t \\ E_t \end{bmatrix} = 0 \tag{2.45}$$

$\tilde{Z}$ and $\tilde{Y}$ are the integral operators of the pure LSE , LSM part of the field whereas $\tilde{T}$ and $\tilde{U}$ describe the hybrid part of the field. In order to solve for the propagation constant β the integral equations (2.43), (2.44) and (2.45) must be solved and a number of approximation techniques are available for this purpose such as Ritz variational procedure and moment methods [29,30]. In this work, however, we adopted a single trial field function to expand the field unknowns. In this way the integral equation reduces to a scalar equation which can be computed efficiently.

REFERENCES

[1] M.J. Robertson, S. Ritchie and P. Dayan, " Semiconductor waveguides: Analysis of optical propagation in single rib structures and directional couplers ", I.E.E. Proceeding, vol. 132, Pt. J, No. 6, pp. 336-342, Dec. 1985.

[2] T.M. Benson, J. Buus, " Optical guiding in III–V semiconductor Rib structures ", I.E.E Conf. Publ. 227, Cardiff, April 1983, pp. 17-20.

[3] M.S. Stern, " Semivectorial polarized finite difference method for optical waveguides with arbitrary index profile ", I.E.E Proc., vol. 135, Pt. J, No.1, Feb. 1989, pp. 56-63.

[4] M.S. Stern, " Semivectorial polarised $\tilde{H}$ field solutions for dielectric waveguides with arbitrary index profiles ", I.E.E Proc., vol. 135, Pt. J, No. 5, Oct. 1988, pp. 333-338.

[5] B.M.A. Rahman and J.B. Davies, " Finite element analysis of optical and microwave waveguide problems ", I.E.E.E Trans. Microwave Theory and Technique, vol. MTT-32, No. 1, pp. 20-28, Jan. 1984.

[6] N. Mabaya, P.E. Lagasse, P. Vandenbulcke, " Finite Element Analysis of Optical Waveguides ", I.E.E.E. Trans. Microwave Theory Techniques , vol. MTT-29, No. 6, June 1981, pp. 600-605.

[7] J.B. Davies, " Review of methods for numerical solution of the hollow - waveguide problem ", Proc. Inst. Elec. Eng., vol. 119, pp. 33-37, Jan. 1972.

[8] B.M.A. Rahman, J.B. Davies, " Vector H finite element solution of Ga As/Ga Al As rib waveguides ", I.E.E Proc., vol. 132, Pt. J, Dec. 1985, pp. 349-353.

[9] S.T. Peng and A.A. Oliner, "Guidence and leakage properties of a class of open dielectric waveguides: Part 1 and 2 "I.E.E.E Trans. Microwave Theory and Technique, vol. MTT-29, pp. 843-869, Sept. 1981.

[10] R. Mittra, Y.L. Hou and V. Jamnejad, " Analysis of open dielectric waveguides using mode matching technique and variational methods ", I.E.E.E. Trans. Microwave Theory and Technique, vol. MTT-28 , pp. 36-43, Jan. 1980.

[11] M. Koshiba and M. Suzuki, " Vectorial wave analysis od dielectric waveguides for optical integrated circuits using equivalent network approach", I.E.E.E. J. Lightwave Technology, vol. LT-4, pp. 656-664, June 1986.

[12] N. Dagli and C.G. Fonstad, " Analysis of rib dielectric waveguides ", I.E.E.E. J. Quantum Electronics, vol. QE-21, No. 4, pp. 315-321, April 1985.

[13] V.V. Shevchenko, " Continous Transitions in Open Waveguides ", Golem , 1971, ch. 1.

[14] E.A.J. Marcatili, " Dielectric rectangular waveguide ", Bell Syst. Tech. J., vol. 48, No. 9, pp. 2071-2102, Sept. 1969.

[15] M.R. Knox and P.P. Toulios, " Integrated circuits for the millimetre through optical frequency range ", Proceedings of the symposium on submillimetre waves. Polytechnic, N.Y., 1970, pp. 497-516.

[16] T. Rozzi, T. Itoh, L. Grun, " Two- dimensional analysis of the Ga As d.h. stripe geometry laser ", Radio Science, vol.2, No. 4, July - Aug. 1977, pp. 543-549.

[17] G.B. Hocker, W.K. Burns, " Mode dispersion in diffused channel waveguides by the effective index method ", Appl. Opt., vol. 16 , No. 1, Jan. 1977, pp. 113-118.

[18] T. Itoh, " Spectral Domain Immitance Approach for dispersion characteristics of generalized printed transmission lines ", I.E.E.E Trans. on Microwave Theory and Techniques, vol. MTT-28, No.7 , July 1980, pp. 733-736.

[19] D.Marcuse," Theory of Dielectric Optical Waveguides ", Academic Press, New York, 1972.

[20] N. Marcuvitz, L. Felsen, " Radiation and scattering of waves ", Englewood Cliffs, N.J., Prentice Hall, 1973, ch. 3, pp 278-282.

[21] T. Tamir, " Integrated Optics ", Springer Verlag, Berlin, 1979.

[22] B. Friedman, " Principles and Techniques of Applied Mathematics ", New York: Wiley, 1956, ch. 4 .

[23] A. Yariv, " Optical Electronics ", HRW international edition, 1985.

[24] J. Kot, T. Rozzi, " Rigorous modelling of single and coupled image and insular waveguide by TRD ", Proc. European Microwave Conference, Liege, Sept. 1984, pp. 424-429.

[25] T. Rozzi, S. Hedges, " Rigorous analysis and network modelling of the inset dielectric guide", I.E.E.E Trans. Microwave Theory and Techniqes, vol. MTT-35, pp. 823-834, Sept. 1987.

[26] C.J. Railton, T. Rozzi and J. Kot, " The efficient Calculation of High Order Shielded Microstrip Modes for use in Discontinuity Problems " , Proc. 16th. European Microwave Conference (Dublin), Sept. 1986, pp. 529-534.

[27] C.A. Olley and T. Rozzi, " Characterisation of Unilateral Finline Mode Spectrum Including Loss Analysis ", Proc. 16th. European Microwave Conference (Dublin), Sept. 1986, pp. 551-516.

[28] J.A. Stratton, " Electromagnetic Theory ", Mc Graw Hill, New York, 1941

[29] R.F. Harrington, " Matrix methods for field problems " , I.E.E.E. Proc., vol. 55, No. 2, Feb. 1967, pp 136-149.

[30] T.K. Sarkar, " A note on the variational method (Rayleight - Ritz) , Galerkin's method, and the method of least squares ", Radio Science, Vol. 18 , No. 6, Nov. - Dec. 1983, pp 1207-1224.

CHAPTER 3

LSE AND LSM ANALYSIS OF RIB WAVEGUIDE

3.1 INTRODUCTION

The aim of the work presented in this chapter is to develop a TRD analysis of rib waveguide in the pure LSE and LSM polarizations for use to compute the field solution of the discrete bound modes. The detailed formulation of the problem is derived by expanding fully the method outlined in chapter two. Numerical results are computed and compared with other method of analyses.

The cross sectional geometry of the rib waveguide under consideration is illustrated in Fig. 3.1 . The true modes of the structure are hybrid , however, it is believed that for rib structures with small aspect ratios $(D-d)/2a$ and small refractive indices differences LSE and LSM provide a very good approximation. The main field components of the LSE modes are E_x and H_y while those of the LSM modes are E_y and H_x. With a plane of symmetry is assumed at $x=-a$, the TRD solution of the problem may be subdivided in to four cases:

a) Even to x LSE modes with an electric wall at the plane of symmetry

b) Odd to x LSE modes with a magnetic wall at the plane of symmetry

c) Even to x LSM modes with a magnetic wall at the plane of symmetry

d) Odd to x LSM modes with an electric wall at the plane of symmetry

In the following we shall derive a TRD solution of the rib waveguide with modes having even symmetry with x; the analysis for odd modes can be treated by an analogous development. As the pure LSE and LSM polarizations considered only involve five field components, it is not possible to match the boundary conditions on all components with

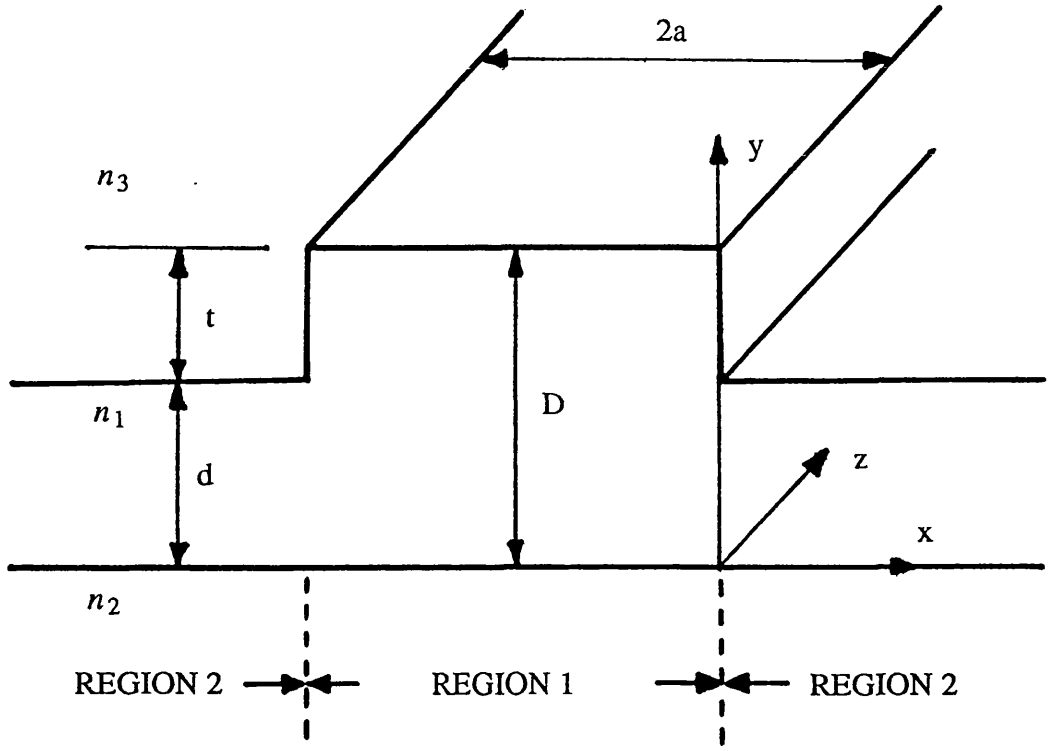

Fig. 3.1 Rib guide cross section.

zero E_y (in the LSE case) and zero H_y (in the LSM case). Clearly, this is an approximation, but it will be shown later the formulation to be a good one and to yield accurate results.

3.2 EVEN (to x) MODES LSE ANALYSIS

3.21 FIELD COMPONENTS FOR LSE MODES

For a LSE mode, with z- and time- dependence $e^{j(\omega t-\beta z)}$ suppressed, the electromagnetic field components may be expressed in terms of a y- directed potential $\psi_h(x,y)$ as,

$$E_x = \omega \mu_0 \beta \psi_h(x,y)\vec{y} \tag{3.1a}$$

$$E_y = 0 \tag{3.1b}$$

$$E_z = -j \omega \mu_0 \partial_x \psi_h(x,y)\vec{y} \tag{3.1c}$$

$$H_x = \partial_x \partial_y \psi_h(x,y)\vec{y} \tag{3.1d}$$

$$H_y = \left(\varepsilon_r k_o^2 + \partial_y^2 \right)\psi_h(x,y)\vec{y} \tag{3.1e}$$

$$H_z = -j \beta \partial_y \psi_h(x,y)\vec{y} \tag{3.1f}$$

Due to the symmetry of the structure, the fields need only be formulated over one half of the guide width. Since a y- directed potential is chosen to express the electromagnetic field distribution, the appropriate boundary conditions it must satisfy are those of the H_y field. With an electric wall placed at $x=-a$, we have maximum H_y there and the x-dependent variation of the y- directed magnetic fields can be represented with a cosine - like function. Thus , the y- directed Hertzian magnetic potential for region 1 is chosen in the form of a standing wave given by,

$$\psi_h(x,y) = \frac{1}{j\omega\mu_0}\left[\frac{1}{q_{sh}^2+\beta_s^2} V_s\,\phi_{sh}(y)\,\chi(x) + \int_0^{\infty} \frac{d\rho}{k_o^2-\rho^2} V(\rho)\,\phi_h(y,\rho)\,\chi(x,\rho)\right.$$

$$\left. + \int_0^{\nu} \frac{d\sigma}{\varepsilon_2 k_o^2-\sigma^2} V(\sigma)\,\phi_h(y,\sigma)\,\chi(x,\sigma)\right] \qquad (3.2a)$$

where,

$\phi_{sh}(y)$ - is the orthonormalised distribution of surface waves of an asymmetric slab guide.

$\phi_h(y,\rho)$ - is the orthonormalised distribution of air modes of an asymmetric slab guide with a continuous wavenumber $0 \le \rho < \infty$. Both, so called, "even" and "odd" air waves must be included in view of the lack of symmetry of the problem in the y direction. Where necessary, these will be distinguished by the notation $\phi_{h\mu}$; $\mu =$ even or odd .

$\phi_h(y,\sigma)$ - is the orthonormalised distribution of substrate modes of an asymmetric slab guide with wavenumber $0 < \sigma < \nu = k_o\sqrt{\varepsilon_2 - 1}$

The expression of this complete spectrum of the asymmetric slab guide used in the analysis is given in chapter 2. V_s, $V(\rho)$ and $V(\sigma)$ are modal amplitudes. As for each value of ρ , there are two contributions to the spectrum of air waves ($\mu =$ even and odd respectively), $V(\rho)$ and $\phi_h(y,\rho)$ stands for

$$\sum_{\mu=e,o} V_{h\mu}(\rho)\,\phi_{h\mu}(y,\rho)$$

The x - dependent terms have been fixed to be unity at $x = 0$ to ensure continuity across the interface, given by

$$\chi(x) = \frac{\cos(q_{sh}(x+a))}{\cos(q_{sh}a)}$$

$$\chi(x,\rho) = \frac{\cos(q(x+a))}{\cos(qa)}$$

$$\chi(x,\sigma) = \frac{\cos(p(x+a))}{\cos(pa)}$$

where the wavenumbers for a bound mode in x are given by

$$q_{sh}^2 + \beta_s^2 = \varepsilon_1 k_o^2 - k_{ys}^2 = \varepsilon_{eh} k_o^2$$
$$q^2 = k_o^2 - \beta_s^2 - \rho^2 = -\gamma^2$$
$$p^2 = \varepsilon_2 k_o^2 - \beta_s^2 - \sigma^2 = -\eta^2$$

k_{ys} is the y - directed wavenumber of the slab surface mode in the dielectric and ε_{eh} is the effective dielectric constant to the left of the interface plane.

In region 2, we choose a magnetic potential function using decaying waves in x rather than standing waves in order to ensure a bound mode in the x - direction. Here again, the x - dependent terms have been fixed to be unity at $x = 0$ to ensure continuity across the interface plane. The potential function has the form

$$\psi_h(x,y) = \frac{1}{j\omega\mu_0}\left[\frac{V_s'}{q_{sh}'^2 + \beta_s^2}\psi_{sh}(y)\, e^{-jq_{sh}'x} + \int_0^\infty \frac{d\rho}{k_o^2 - \rho^2} V'(\rho)\,\psi_h(y,\rho)\, e^{-jq'x} + \int_0^\nu \frac{d\sigma}{\varepsilon_2 k_o^2 - \sigma^2} V'(\sigma)\,\psi_h(y,\sigma)\, e^{-jp'x}\right] \qquad (3.2b)$$

where,

$\psi_{sh}(y)$,$\psi_h(y,\rho)$ and $\psi_h(y,\sigma)$ are the complete mode spectrum of the asymmetric slab guide with thickness equal to the outer layer "d".

V_s' , $V'(\rho)$ and $V'(\sigma)$ are the appropriate modal amplitudes. The wavenumbers for a bound mode in x are given by,

$$q_{sh}'^2 + \beta_s^2 = \varepsilon_1 k_o^2 - k_{ys}'^2 = \varepsilon_{eh}' k_o^2$$
$$q_{sh}'^2 = \varepsilon_{eh}' k_o^2 - \beta_s^2 = -\gamma_{sh}'^2$$
$$q'^2 = k_o^2 - \beta_s^2 - \rho^2 = -\gamma^2$$
$$p'^2 = \varepsilon_2 k_o^2 - \beta_s^2 - \sigma^2 = -\eta^2$$

For a bound mode q and p are pure imaginary and the only pole occurring in the integrand of equation (3.2a) and (3.2b) is for $\rho = k_o$. From equation (3.1e) the contribution of this term to H_y vanishes. Hence, $V(k_o) = 0$. The ρ integrals in (3.2a) and (3.2b) are taken as principal values. The remaining integrals over σ are regular. By substituting (3.2) in to (3.1) the electromagnetic field components at each side of the step may be derived.

3.22 FORMULATION OF INTEGRAL OPERATOR AND TRANSVERSE EQUIVALENT CIRCUIT

A suitable pair of transverse fields at the discontinuous interface $x = 0$ is constituted by E_z and H_y. At each side of the step, they are derived from (3.1) using the potential function (3.2). Substituting (3.2a) in to (3.1), the field components E_z and H_y in region 1 may be expressed as,

$$E_z(x,y) = \frac{q_{sh}}{q_{sh}^2 + \beta_s^2} V_s \, \phi_{sh}(y) \, \frac{\sin(q_{sh}(x+a))}{\cos(q_{sh}a)} + \sum_{\mu=e,o} \int_0^\infty \frac{d\rho}{k_o^2 - \rho^2} V_\mu(\rho) \, \phi_{h\mu}(y,\rho) \, q \, \frac{\sin(q(x+a))}{\cos(qa)} + \int_0^\nu \frac{d\sigma}{\varepsilon_2 k_o^2 - \sigma^2} V(\sigma) \, \phi_h(y,\sigma) \, p \, \frac{\sin(p(x+a))}{\cos(pa)} \tag{3.3a}$$

$$H_y(x,y) = \frac{1}{j\omega\mu_0} \left[V_s \, \phi_{sh}(y) \, \frac{\cos(q_{sh}(x+a))}{\cos(q_{sh}a)} + \sum_{\mu=e,o} \int_0^\infty d\rho \, V_\mu(\rho) \, \phi_{h\mu}(y,\rho) \, \frac{\cos(q(x+a))}{\cos(qa)} + \int_0^\nu d\sigma \, V(\sigma) \, \phi_h(y,\sigma) \, \frac{\cos(p(x+a))}{\cos(pa)} \right] \tag{3.3b}$$

Similarly, substituting (3.2b) in to (3.1), the field components E_z and H_y in region 2 may be expressed as

$$E_z(x,y) = j \left[\frac{q'_{sh}}{q'^2_{sh} + \beta^2} V'_s \psi_{sh}(y)\, e^{-jq'_{sh}x} + \sum_{\mu=e,o} \int_0^{\infty} \frac{d\rho}{k_o^2 - \rho^2} V'_\mu(\rho)\, \psi_{h\mu}(y,\rho)\, q'\, e^{-jq'x} \right.$$

$$\left. + \int_0^{v} \frac{d\sigma}{\varepsilon_2 k_o^2 - \sigma^2} V'(\sigma)\, \psi_h(y,\sigma)\, p'\, e^{-jq'x} \right] \qquad (3.4a)$$

$$H_y(x,y) = \frac{1}{j\omega\mu_0} \left[V'_s \psi_{sh}(y)\, e^{-jq'_{sh}x} + \sum_{\mu=e,o} \int_0^{\infty} d\rho\, V'_\mu(\rho)\, \psi_{h\mu}(y,\rho)\, e^{-jq'x} \right.$$

$$\left. + \int_0^{v} d\sigma\, V'(\sigma)\, \psi_h(y,\sigma)\, e^{-jq'x} \right] \qquad (3.4b)$$

Here it has been assumed that only one surface mode, $\phi_{sh}(y)$ and $\psi_{sh}(y)$ respectively, may be supported by the slab waveguide left and right of the step. At the discontinuous interface $x = 0$, the pair of transverse fields in (3.3) and (3.4) may be written as;

For region 1,

$$E_z(0,y) = \frac{q_{sh}}{q_{sh}^2 + \beta_s^2} \tan(q_{sh}a)\, V_s\, \phi_{sh}(y) + \sum_{\mu=e,o} \int_0^{\infty} \frac{d\rho}{k_o^2 - \rho^2} q \tan(qa)\, V_\mu(\rho)\, \phi_{h\mu}(y,\rho)$$

$$+ \int_0^{v} \frac{d\sigma}{\varepsilon_2 k_o^2 - \sigma^2} p \tan(pa)\, V(\sigma)\, \phi_h(y,\sigma) \qquad (3.5a)$$

$$H_y(0,y) = \frac{1}{j\omega\mu_0} \left[V_s\, \phi_{sh}(y) + \sum_{\mu=e,o} \int_0^{\infty} d\rho\, V_\mu(\rho)\, \phi_{h\mu}(y,\rho) \right.$$

$$\left. + \int_0^{v} d\sigma\, V(\sigma)\, \phi_h(y,\sigma) \right] \qquad (3.5b)$$

For region 2,

$$E_z(0,y) = j \left[\frac{q'_{sh}}{q'^2_{sh} + \beta^2} V'_s \psi_{sh}(y) + \sum_{\mu=e,o} \int_0^\infty \frac{d\rho}{k_o^2 - \rho^2} q' V'_\mu(\rho) \psi_{h\mu}(y,\rho) \right.$$

$$\left. + \int_0^v \frac{d\sigma}{\varepsilon_2 k_o^2 - \sigma^2} p' V'(\sigma) \psi_h(y,\sigma) \right] \tag{3.6a}$$

$$H_y(0,y) = \frac{1}{j\omega\mu_0} \left[V'_s \psi_{sh}(y) + \sum_{\mu=e,o} \int_0^\infty d\rho\, V'_\mu(\rho) \psi_{h\mu}(y,\rho) \right.$$

$$\left. + \int_0^v d\sigma\, V'(\sigma) \psi_h(y,\sigma) \right] \tag{3.6b}$$

Equation (3.5b) is multiplied through by $\phi_h(y)$, $\phi_h(y,\rho)$ and $\phi_h(y,\sigma)$ in turn, and integrated over y from $-\infty$ to ∞. By the orthogonality of the modal functions, expressions for V_s , $V_\mu(\rho)$ and $V(\sigma)$ are obtained, given by

$$V_s = j\omega\mu_0 \int_{-\infty}^{\infty} H_y(0,y)\, \phi_{sh}(y)\, dy \tag{3.7a}$$

$$V_\mu(\rho) = j\omega\mu_0 \int_{-\infty}^{\infty} H_y(0,y)\, \phi_{h\mu}(y,\rho)\, dy \tag{3.7b}$$

$$V(\sigma) = j\omega\mu_0 \int_{-\infty}^{\infty} H_y(0,y)\, \phi_h(y,\sigma)\, dy \tag{3.7c}$$

These expression are substituted in to equation (3.5a). After rearranging, this gives an integral equation of the type

$$E_z(0,y) = \tilde{Z}_L \cdot H_y(0,y) \tag{3.8}$$

where the kernel $Z_L(y,y')$ of the integral operator $\tilde{Z}_L$ is given by:

$$Z_L(y,y') = \frac{1}{j\omega\varepsilon_0}\left[-\frac{q_{sh}\tan(q_{sh}a)}{\varepsilon_{eh}}\,\phi_{sh}(y)\,\phi_{sh}(y') \right.$$

$$+ \sum_{\mu=e,o} \int_0^{\infty} \frac{d\rho}{1-\frac{\rho^2}{k_o^2}}\,\gamma\tanh(\gamma a)\,\phi_{h\mu}(y,\rho)\,\phi_{h\mu}(y',\rho)$$

$$\left. + \int_0^{\nu} \frac{d\sigma}{\varepsilon_2 - \frac{\sigma^2}{k_o^2}}\,\eta\tanh(\eta a)\,\phi_h(y,\sigma)\,\phi_h(y',\sigma) \right] \qquad (3.9)$$

Equation (3.8) gives the electric field at the interface due to all the magnetic field across the interface. Thus the impedance Green function looking in to the rib ($x = 0^-$) is given by equation (3.9).

Carrying out a process similar to that leading to equation (3.6), a relationship analogous to (3.7) and (3.8) at the R.H.S. of the step may be derived, namely,

$$V_s' = j\omega\mu_0 \int_{-\infty}^{\infty} H_y(0,y)\,\psi_{sh}(y)\,dy \qquad (3.10a)$$

$$V_\mu'(\rho) = j\omega\mu_0 \int_{-\infty}^{\infty} H_y(0,y)\,\psi_{h\mu}(y,\rho)\,dy \qquad (3.10b)$$

$$V'(\sigma) = j\omega\mu_0 \int_{-\infty}^{\infty} H_y(0,y)\,\psi_h(y,\sigma)\,dy \qquad (3.10c)$$

and

$$-E_z(0,y) = \tilde{Z}_R \cdot H_y(0,y) \qquad (3.11)$$

where the kernel $Z_R(y,y')$ of the integral operator $\tilde{Z}_R$ is given by the Green impedance function looking in to the outer region ($x = 0^+$), namely;

$$Z_R(y,y') = \frac{1}{j\omega\mu_0}\left[\frac{\gamma'_{sh}}{\varepsilon'_{eh}}\psi_{sh}(y)\,\psi_{sh}(y') + \sum_{\mu=e,o}\int_0^{\infty}\frac{d\rho}{1-\frac{\rho^2}{k_o^2}}\gamma\,\psi_{h\mu}(y,\rho)\,\psi_{h\mu}(y',\rho) + \int_0^{\nu}\frac{d\sigma}{\varepsilon_2-\frac{\sigma^2}{k_o^2}}\eta\,\psi_h(y,\sigma)\,\psi_h(y',\sigma)\right] \tag{3.12}$$

Here again equation (3.11) gives the electric field at the interface due to all the magnetic field across the interface. The signs of equations (3.8) and (3.11) are chosen so as to indicate that the operators have been formulated in each region for power flow away from the interface. The continuity of the fields has been built in (3.8) and (3.11). By adding them, we obtain the dispersion equation of the waveguide in the form of an integral equation

$$\tilde{Z}\cdot H_y(0,y) = 0 \tag{3.13}$$

where

$$\tilde{Z} = \tilde{Z}_L + \tilde{Z}_R$$

Equation (3.13) is a statement of transverse resonance since the zero source function excites a finite response. Before solving integral equation (3.13) rigorously, physical insight is gained by recasting it in a slightly different form. From this, one recovers a scalar transverse equivalent circuit for the surface mode under the rib in the form of transmission line with discontinuities as shown in Fig. 3.2 . Let us assume the solution $H(y) = H_y(0,y)$ of integral equation (3.13) to be known. Multiply this equation by H(y) and integrate over y from $-\infty$ to ∞ and divide through by

$$< \phi_{sh}(y)\,,\,H(y) >^2 = \left[\int_{-\infty}^{\infty}\phi_{sh}(y)\,H(y)\,dy\right]^2$$

giving

$$\frac{1}{j\omega\varepsilon_0}\left[-\frac{q_{sh}\tan(q_{sh}a)}{\varepsilon_{eh}}+\frac{\gamma'_{sh}<H(y),\psi_{sh}(y)>^2}{\varepsilon'_{eh}<H(y),\phi_{sh}(y)>^2}\right.$$

$$+\sum_{\mu=e,o}\int_0^{\infty}\frac{d\rho}{1-\frac{\rho^2}{k_o^2}}\gamma\left[\frac{\tanh(\gamma a)<H(y),\phi_{h\mu}(y,\rho)>^2+<H(y),\psi_{h\mu}(y,\rho)>^2}{<H(y),\phi_{sh}(y)>^2}\right]$$

$$\left.+\int_0^{\nu}\frac{d\sigma}{\varepsilon_2-\frac{\sigma^2}{k_o^2}}\eta\left[\frac{\tanh(\eta a)<H(y),\phi_h(y,\sigma)>^2+<H(y),\psi_h(y,\sigma)>^2}{<H(y),\phi_{sh}(y)>^2}\right]\right]$$

$$=0 \qquad (3.14)$$

Rearranging gives a scalar dispersion equation,

$$\frac{q_{sh}\tan(q_{sh}a)}{\varepsilon_{eh}}=Z_{sL}+Z_a+Z_{sb} \qquad (3.15)$$

and $Z_{sL}=\dfrac{n^2\gamma'_{sh}}{\varepsilon'_{eh}}$

Its transverse equivalent network interpretation is illustrated in Fig. 3.2 . In equation (3.15) and in Fig. 3.2 one recognizes four contributions , respectively, (all within a common factor $\dfrac{1}{j\omega\varepsilon_0}$)

a) The impedance of the surface wave under the rib. represented by a short - circuited transmission line of electrical length $q_{sh}a$ and characteristic impedance $\dfrac{q_{sh}}{\varepsilon_{eh}}$

b) The impedance of the air modes at both sides of the junction, as seen by the surface wave under the rib, given by

$$Z_a=\sum_{\mu=e,o}\int_0^{\infty}\frac{d\rho}{1-\frac{\rho^2}{k_o^2}}\gamma\left[\frac{\tanh(\gamma a)<H(y),\phi_{h\mu}(y,\rho)>^2+<H(y),\psi_{h\mu}(y,\rho)>^2}{<H(y),\phi_{sh}(y)>^2}\right] \qquad (3.16)$$

c) The impedance of the substrate modes at both sides of the junction, as seen by the

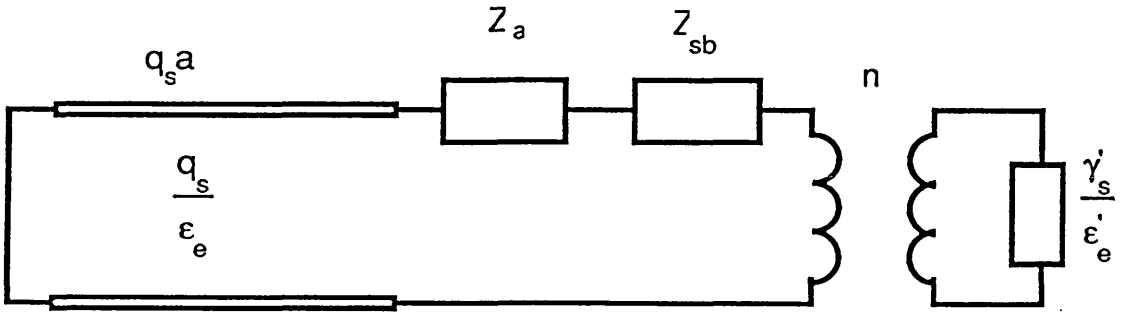

Fig. 3.2 Transverse Equivalent Circuit for LSE polarization.

surface wave under the rib, given by

$$Z_{sb} = \int_0^{\nu} \frac{d\sigma}{\varepsilon_2 - \frac{\sigma^2}{k_o^2}} \eta \left[\frac{\tanh(\eta a) < H(y) , \phi_h(y,\sigma) >^2 + < H(y) , \psi_h(y,\sigma) >^2}{< H(y) , \phi_{sh}(y) >^2} \right] \tag{3.17}$$

d) The contribution of the surface wave mode (if any) to the right of the junction, i.e. a load of impedance $\frac{\gamma'_{sh}}{j\omega\varepsilon_0 \varepsilon'_{eh}}$ with real γ'_{sh} for a bound mode in the x - direction. This load is seen by the surface wave mode under the rib through an ideal transformer

$$n = \frac{< H(y) , \psi_{sh}(y) >}{< H(y) , \phi_{sh}(y) >} = \frac{P'_{sh}}{P_{sh}} \tag{3.18}$$

If the outer region does not support surface wave modes then the transformer ratio n is equal to 0 and the total impedance seen by the surface wave mode under the rib is represented by Z_a and Z_{sb} only.

Equation (3.15) is quantitatively exact and enjoys variational properties. Although its accuracy depends on the actual knowledge of H(y), it is noted that H(y), being transverse to the dielectric wedge along the z - axis, is non - singular [1]. Hence, any reasonable assumption will lead to relatively good results.

If, at this point, the "small - step" approximation is made :

$\phi_{sh}(y) \approx \psi_{sh}(y) \approx H(y)$

then, by orthogonality, the contributions of air and substrate modes vanish, i.e. $Z_a = Z_{sb} = 0$ and $n = 1$ in equation (3.14) and we are reduced to the EDC calculation. It is worth remarking that even when the step is not small, so that $\phi_{sh}(y)$ and $\psi_{sh}(y)$ may differ from each other and from H(y), P_{sh} and P'_{sh} of (3.18) are both less than unity and their ratio is still fairly close to unity. This fact explains the remarkable accuracy of the EDC calculation in the LSE - case not too close to cutoff, where the continuous spectra can no longer be overlooked. The above observation is at the basis of a very accurate

first - order variational solution of the step problem to be discussed in the next section. From equation (3.15) and equivalent circuit in Fig. 3.2, the total impedance looking to the right of the step is given by

$$Z_T(\beta) = Z_s + Z_a + Z_{sb} \tag{3.19}$$

Writing (3.19) in full we have

$$Z_T(\beta) = \frac{\int_{-\infty}^{\infty}\int_{-\infty}^{\infty} Z(y,y')\,H(y)\,H(y')\,dy\,dy'}{\int_{-\infty}^{\infty}\int_{-\infty}^{\infty} H(y)\,H(y')\,\phi_{sh}(y)\,\phi_{sh}(y')\,dy\,dy'} \tag{3.20}$$

where,

$$\begin{aligned} Z(y,y') = {} & \frac{\psi_{sh}(y)\,\psi_{sh}(y')}{\varepsilon'_{eh}} \\ & + \sum_{\mu=e,o} \int_0^{\infty} \frac{d\rho}{1-\frac{\rho^2}{k_o^2}}\,\gamma\left[\tanh(\gamma a)\,\phi_{h\mu}(y,\rho)\,\phi_{h\mu}(y',\rho) + \psi_{h\mu}(y,\rho)\,\psi_{h\mu}(y',\rho)\right] \\ & + \int_0^{\nu} \frac{d\sigma}{\varepsilon_2 - \frac{\sigma^2}{k_o^2}}\,\eta\left[\tanh(\eta a)\,\phi_h(y,\sigma)\,\phi_h(y',\sigma) + \psi_h(y,\sigma)\,\psi_h(y',\sigma)\right] \end{aligned} \tag{3.21}$$

It is readily shown that the variational expression (3.20) is stationary with respect to arbitrary first order variations in H(y).

3.23 VARIATIONAL SOLUTION OF THE INTEGRAL EQUATION

3.231 FIRST ORDER SOLUTION

The expression for Z_T(i.e Z_s, Z_a and Z_{sb}) in equation (3.20) contains the unknown field H(y). The stationary nature of the expression means that if an approximate form of H(y) is known and substituted in to equation (3.20), a more accurate approximation for Z_T may be obtained. In choosing the trial functions for the unknown field, it is very

advantageous to be able to capture most of the solution with just one term, i.e a first order solution. The discussion in section 3.12 seems to suggest that a prudent choice for H(y) may consist in taking the surface mode of a slab waveguide. The choice is critical for the accuracy of the method, for instance, using just the surface mode right or left of the step is inaccurate because of its orthogonality to the continuum. In order to overcome this problem we choose to use the modal distribution, $\bar{U}_{sh}(y)$, of a slab waveguide whose height is intermediate between those of the slabs left and right of the step, that we call in the present work "transition function". For small steps, there would be little difference between the spectra of the three guides. The typical shape of the three fields is shown in Fig. 3.3. For larger steps, it seems intuitively reasonable that an intermediate waveguide with effective dielectric constant $\bar{\varepsilon}_{eh} \approx \sqrt{\varepsilon_{eh}\varepsilon'_{eh}}$ may provide a suitable "transition" between the two waveguides. More precisely, the "transition function", $\bar{U}_{sh}(y)$, overlaps the spectra of both slabs. We seek to optimize the modal overlapping with ϕ_{sh} and ψ_{sh} , where the latter exists, as the surface waves carry most of the power. Consequently, we choose $\bar{d}$ so as to minimize the error function:

$$\varepsilon(\bar{d}) = 2 - (P_{sh}^2 + P_{sh}'^2) > 0 \qquad (3.22)$$

As it turns out, $\bar{d}$ resulting from this condition is but little different from that corresponding to $\bar{\varepsilon}_{eh} \approx \sqrt{\varepsilon_{eh}\varepsilon'_{eh}}$. It is noted that, when no guidance is present in the outer slab, the criterion (3.22) breaks down. From this point onward we extrapolate for $\bar{d}$ as a function of d.

The evaluation of the overlapping integral P_{sh} and P'_{sh} between $\bar{U}_{sh}$ and the spectra at either side of the step is facilitated by the following result, which is proved in Appendix 2. This is a particular case of a much more general theorem for the calculation of the overlapping of two solutions of the wave equation. In particular we have

$$P_{sh} = \int_{-\infty}^{\infty} \bar{U}_{sh}\, \phi_{sh}\, dy = \frac{\varepsilon_r - 1}{\bar{\varepsilon}_{eh} - \varepsilon_{eh}} \int_{\bar{d}}^{D} \bar{U}_{sh}\, \phi_{sh}\, dy \qquad (3.23)$$

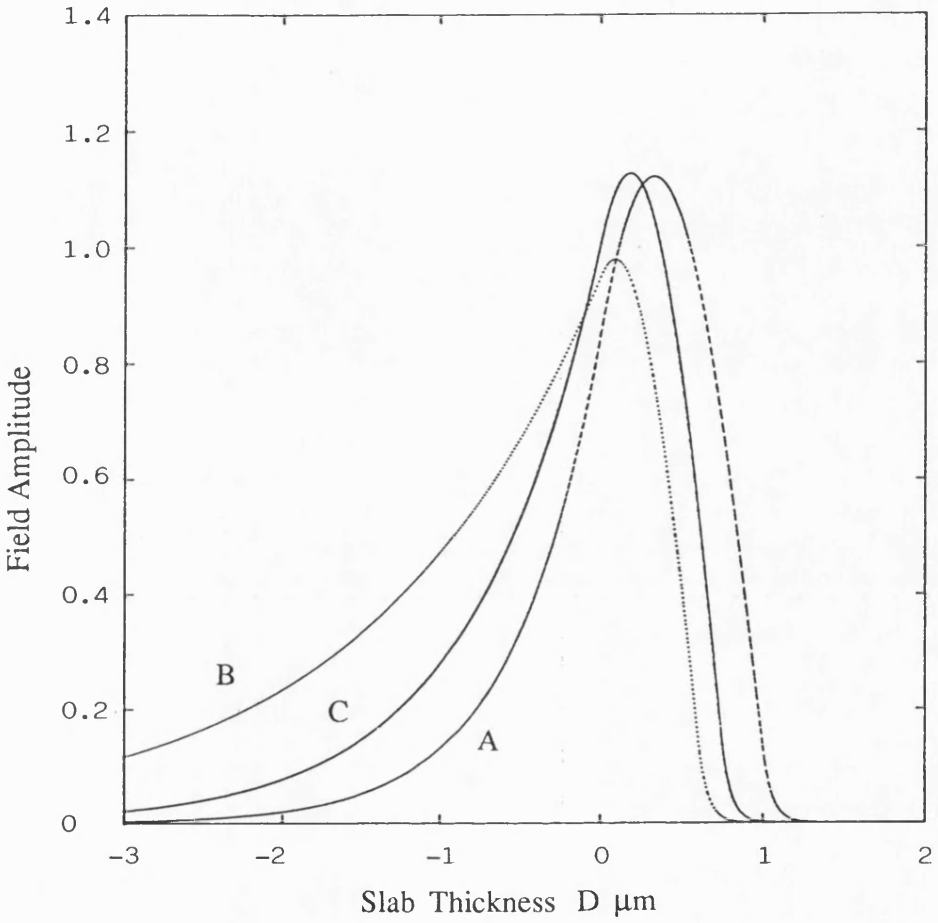

Fig. 3.3 Typical shape of the H_y component of the fundamental LSE mode for slab of height D (curve A), d (curve B), and $\bar{d}$ (curve C).

$$P'_{sh} = \int_{-\infty}^{\infty} \bar{U}_{sh}\, \psi_{sh}\, dy = \frac{\varepsilon_r - 1}{\varepsilon'_{eh} - \bar{\varepsilon}_{eh}} \int_{d}^{\bar{d}} \bar{U}_{sh}\, \psi_{sh}\, dy \tag{3.24}$$

and similarly for the remaining overlapping integrals with air and substrate modes. These overlapping integrals are given in Appendix 3.

The elements Z_a and Z_{sb} appearing in equation (3.20) may now be written as,

$$Z_a = \sum_{\mu=e,o} \int_0^{\infty} \frac{d\rho}{1 - \frac{\rho^2}{k_o^2}} \gamma \left[\tanh(\gamma a)\, P_{h\mu}{}^2(\rho) + P_{h\mu}{}'^2(\rho) \right] \tag{3.25}$$

$$Z_{sb} = \int_0^{v} \frac{d\sigma}{\varepsilon_2 - \frac{\sigma^2}{k_o^2}} \eta \left[\tanh(\eta a)\, P_h{}^2(\sigma) + P_h{}'^2(\sigma) \right] \tag{3.26}$$

The integral over the semi - infinite ρ - interval is more effectively performed in the complex θ - plane defined by the variable transformation,

$\rho = k_o \sin(\theta) \quad ; 0 \le \rho \le k_o$

$\rho = k_o \cosh(\theta'') \quad ; k_o \le \rho \le \infty$

along the path shown in Fig. 3.4. Using the above transformation, we have

$$\int_0^{\infty} \frac{d\rho}{1 - \frac{\rho^2}{k_o^2}} f(\rho) = k_o \left[\int_0^{\frac{\pi}{2}} \frac{d\theta}{\cos(\theta)} f(k_o \sin(\theta)) - \int_0^{\infty} \frac{d\theta''}{\sinh(\theta'')} f(k_o \cosh(\theta'')) \right]$$

where it is seen that the second integral decays exponentially for large θ''.

The modal propagation constant is solved by resonating the transverse equivalent network Fig. 3.2 such that

$$\frac{q_{sh} \tan(q_{sh} a)}{\varepsilon_{eh}} + Z_T = 0 \tag{3.27}$$

Numerical results are discussed in section 3.24 .

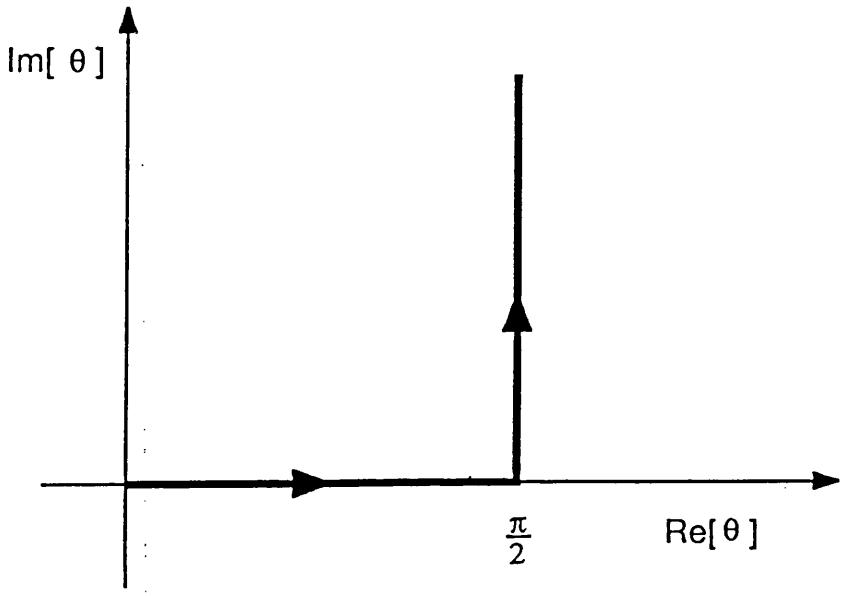

Fig. 3.4 Path of integration in the complex θ plane.

3.232 EXACT SOLUTION - THE APPLICATION OF RITZ - GALERKIN METHOD

To obtain the exact solution for Z_T , equation (3.20) may be solved by following the Ritz - Galerkin method used by Rozzi in [2]. The field unknown H(y) is expanded in terms of a suitable basis function $F_n(y)$

$$H(y) = \sum_{n=0}^{\infty} X_n F_n(y) \tag{3.28}$$

The function $F_n(y)$ form a complete set, are orthogonal over the interface and satisfy the interface boundary condition at $x = 0$. The choice of the $F_n(y)$ is discussed in the next section. Substituting equation (3.28) in to (3.20), gives rise to the matrix equation

$$\frac{1}{Z_T(\beta)} = \underline{P}^T \cdot \underline{\underline{Z}}^{-1} \cdot \underline{P} \tag{3.29}$$

The elements of the various matrices are given by

$$P_{hn} = \int_{-\infty}^{\infty} \phi_{sh}(y)\, F_n(y)\, dy \tag{3.30}$$

$$P_{hn\mu}(\rho) = \int_{-\infty}^{\infty} \phi_{h\mu}(y,\rho)\, F_n(y)\, dy \tag{3.31}$$

$$P_{hn}(\sigma) = \int_{-\infty}^{\infty} \phi_h(y,\sigma)\, F_n(y)\, dy \tag{3.32}$$

$$P'_{hn} = \int_{-\infty}^{\infty} \psi_{sh}(y)\, F_n(y)\, dy \tag{3.33}$$

$$P'_{hn\mu}(\rho) = \int_{-\infty}^{\infty} \psi_{h\mu}(y,\rho)\, F_n(y)\, dy \tag{3.34}$$

$$P'_{hn}(\sigma) = \int_{-\infty}^{\infty} \psi_h(y,\sigma)\, F_n(y)\, dy \tag{3.35}$$

and

$$Z_{mn} = \int_{-\infty}^{\infty} F_m(y)\, Z(y,y')\, F_n(y)\, dy\, dy'$$

$$= \frac{P'_{hm}\, P'_{hn}\, \gamma'_{sh}}{\varepsilon'_{eh}}$$

$$+ \sum_{\mu=e,o} \int_0^{\infty} \frac{d\rho}{1-\frac{\rho^2}{k_o^2}} \gamma \left[\tanh(\gamma a)\, P_{hm\mu}(\rho)\, P_{hn\mu}(\rho) + P'_{hm\mu}(\rho)\, P'_{hn\mu}(\rho) \right]$$

$$+ \int_0^{\nu} \frac{d\sigma}{\varepsilon_2 - \frac{\sigma^2}{k_o^2}} \eta \left[\tanh(\eta a)\, P_{hm}(\sigma)\, P_{hn}(\sigma) + P'_{hm}(\sigma)\, P'_{hn}(\sigma) \right] \qquad (3.36)$$

Having obtained $Z_T(\beta)$, the modal propagation constant β is solved by resonating the transverse equivalent circuit of Fig. 3.2 as in equation (3.27).

Alternatively, by substituting the expansion function (3.28) in to the integral equation (3.13) and integrating w.r.t. y from $-\infty$ to ∞, and then scalar multiplying with $F_n(y)$ and integrating w.r.t y from $-\infty$ to ∞, then, the unknown function H(y) becomes the N - dimensional vector X and the integral operator $\tilde{Z}$ becomes the $N \times N$ matrix. Hence,

$$\underline{\underline{Z}}(\beta) = \frac{1}{j\omega\varepsilon_0} \left[-\frac{q_{sh} \tan(q_{sh} a)}{\varepsilon_{eh}} P_{hn}\, P_{hn}^T + \frac{\gamma'_s}{\varepsilon'_{eh}} P'_{hn}\, P'^T_{hn} + Z_a + Z_{sb} \right] \qquad (3.37)$$

where

$$Z_a = \sum_{\mu=e,o} \int_0^{\infty} \frac{d\rho}{1-\frac{\rho^2}{k_o^2}} \gamma \left[\tanh(\gamma a)\, P_{hn\mu}(\rho)\, P^T_{hn\mu}(\rho) + P'_{hn\mu}(\rho)\, P'^T_{hn\mu}(\rho) \right] \qquad (3.38a)$$

$$Z_{sh} = \int_0^{\nu} \frac{d\sigma}{\varepsilon_2 - \frac{\sigma^2}{k_o^2}} \eta \left[\tanh(\eta a)\, P_{hn}(\sigma)\, P^T_{hn}(\sigma) + P'_{hn}(\sigma)\, P'^T_{hn}(\sigma) \right] \qquad (3.38b)$$

Consequently, the integral equation (3.13) becomes the matrix equation

$$\underline{\underline{Z}}(\beta) \cdot \underline{X} = 0 \qquad (3.39)$$

This matrix equation has a non - trivial solution when

$$\det\left[\underline{\underline{Z}}(\beta)\right]=0 \tag{3.40}$$

3.233 THE CHOICE OF BASIS FUNCTION

The success of the discretization process is dependent upon the choice of a suitable set of basis function. The Ritz - Galerkin procedure does not require an orthonormal basis and completeness is sufficient, but orthonormal bases are easier to handle. Morover, in order that the matrix equations (3.29) and (3.40) be solved they must be of a finite order, which requires that the expansion series (3.28) must be truncated at some point. For the truncation to introduce an acceptable error, the series in $F_n(y)$ must converge rapidly to a solution, which in turn requires that $F_n(y)$ closely approximates the expected field distribution across the interface.

The assumption that the unknown field H(y) is equal to the surface mode of the slab waveguide whose height is intermediate between the inner and outer region discussed in section 3.231 is reasonably good under a wide range of conditions. This approximation is extended to an exact solution by supplementing the intermediate surface mode with an appropriate set of functions. Using weight function $\overline{U}^2_{sh}(y)$, a set of polynomials, $f_n(y)$ is constructed such that,

$$\int_{-\infty}^{\infty} f_m(y)\,\overline{U}^2_{sh}(y)\,f_n(y)\,dy=\delta_{mn} \tag{3.41}$$

The zero order polynomial, $f_0(y)$, is chosen to be unity and the remaining polynomials are generated by the Gram- Schmidt orthogonalising procedure [3]. In this way, a set of function $F_n(y)$ defined by

$$F_n(y)=f_n(y)\,\overline{U}_{sh}(y) \tag{3.42}$$

is generated, with, $F_0(y)=\overline{U}_{sh}(y)$ and the higher order function orthogonal to $\overline{U}_{sh}(y)$. Discussion on the development of the basis function and the coefficient P_{nh}'s necessary for the evaluation of the matrix Z are given in Appendix 4.

3.24 NUMERICAL RESULTS

In order to demonstrate the application of the theory developed in the previous section and the effectiveness of the concept of transition function, we worked out numerical examples to investigate the propagation constant of a rib guide whose parameters are listed in Table 3.1 . The optical parameters of the waveguide chosen corresponds to that of semiconductor material made of III - V compounds. Beside demonstrating the applicability of the method in analyzing rib guides of semiconductor materials, the choice of these waveguides serves the purpose of comparison, as the same structures have been analyzed by several researchers [4,5,6,7] using the FDM/FEM method.

RIB GUIDE STRUCTURE	n_1	n_2	n_3	D μm	d μm	2a μm	λ μm
ST1	3.44	3.35	1.0	1.0	varying	3.0	1.15
ST2	3.44	3.40	1.0	1.0	varying	3.0	1.15
ST3	3.44	3.34	1.0	1.3	0.2	2.0	1.55
ST4	3.44	3.36	1.0	1.0	0.9	3.0	1.55
ST5	3.44	3.435	1.0	6.0	3.5	4.0	1.55
ST6	3.4406	3.4145	1.0	1.5	1.0	3.0	1.15

TABLE 3.1 : Parameters of the rib waveguide structures which have been analysed.

As a preliminary to the numerical exercise, the normalised dispersion relationship of TE modes of the slab guide for the optical parameters in Table 3.1 are shown in Fig. 3.5 . A plot of the intermediate slab thickness $\bar{d}$ as a function of the outer slab thickness d for constant inner slab thickness D calculated using the criterion discussed in section 3.131 are shown in Fig. 3.6 . Data from these two figures are used to determine the spectral distribution of the trial field function $\overline{U}_{sh}(y)$.

Using a single transition function as a trial field, we investigate the modal indices for structures 1 and 2 where the thickness of the inner region D is kept constant, while that of the outer region d is varied from 0.1 to 0.9μm. The outer regions of structure 1 and 2

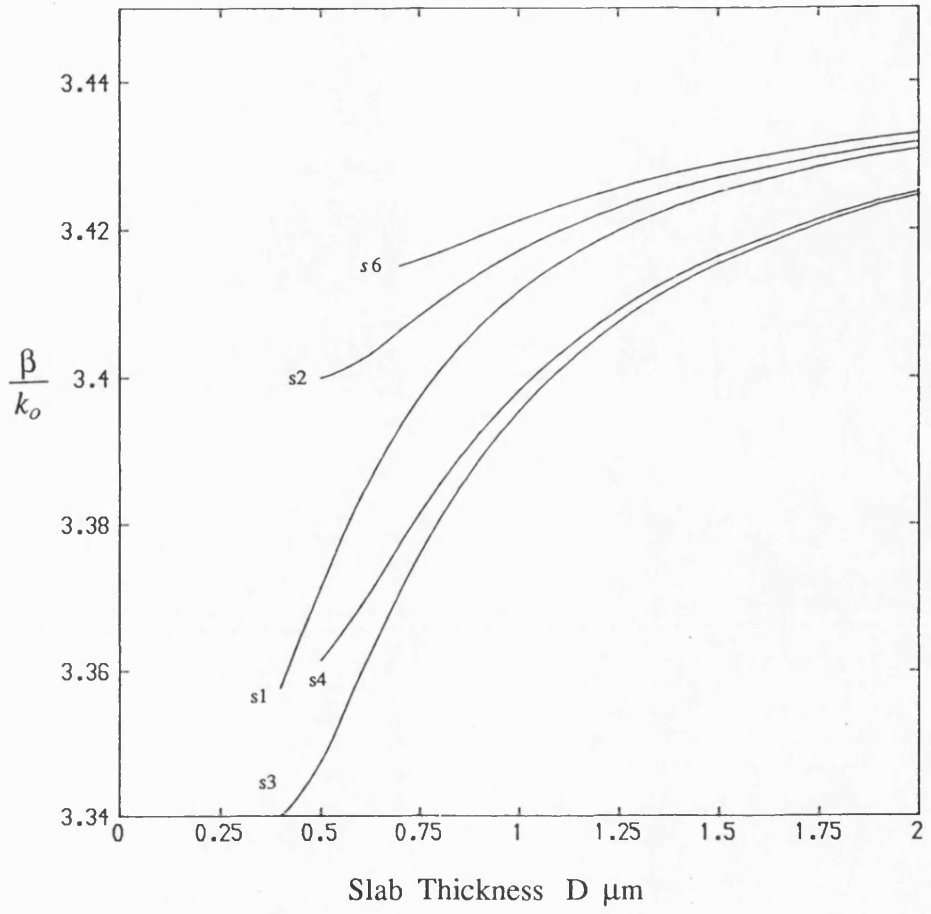

Fig. 3.5 Dispersion curves for fundamental TE modes of asymmetrical slab waveguides whose parameters shown in Table 3.1.

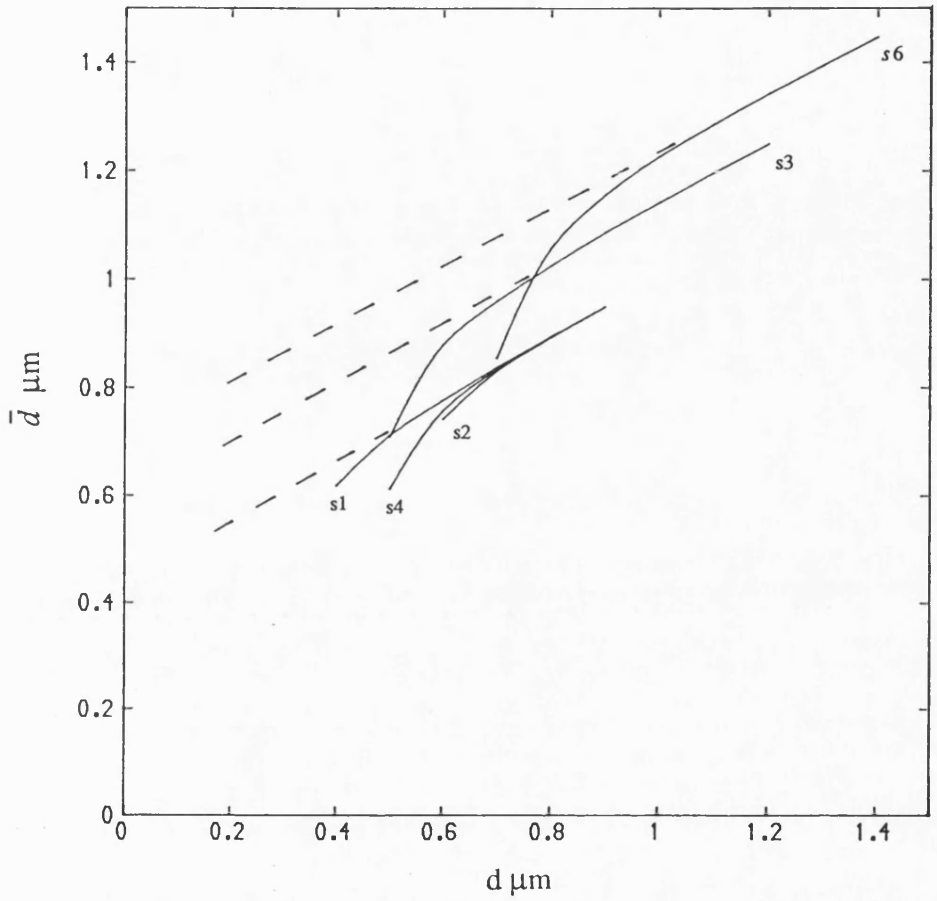

Fig. 3.6 Plot of intermediate slab height $\bar{d}$ as a function outer slab d for waveguides in Table 3.1.

——— According to eq. (3.22)

— — — Extrapolated value.

do not support guided modes when the thickness d is less than 0.4μm and 0.6μm respectively. These examples are chosen in order to demonstrate applicability and to judge the accuracy of analysis of rib guides with no guided modes in the outer region and of rib guides with guided modes in the inner and outer regions. Results of modal indices for structure 1 are shown in Table 3.2 .

d μm	EDC $\frac{\beta}{k_o}$	TRD WITHOUT CONTINUUM $\frac{\beta}{k_o}$	TRD WITH CONTINUUM $\frac{\beta}{k_o}$	FINITE ELEMENT [4] $\frac{\beta}{k_o}$
0.1	-	-	3.40633299	3.40693
0.2	-	-	3.40645318	3.40708
0.3	-	-	3.40671575	3.40725
0.4	3.40789032	3.40773878	3.40697658	3.40746
0.5	3.40809345	3.40807870	3.40727608	3.40770
0.6	3.40835953	3.40835496	3.40768495	3.40808
0.7	3.40869522	3.40869350	3.40816405	3.40856
0.8	3.40914440	3.40914510	3.40881849	3.40914
0.9	3.40983963	3.40984019	3.40972475	3.40970

TABLE 3.2 : Comparison of mode indices for structure ST1

Results obtained by standard EDC method, where applicable, are given in column 2. Results of the present analysis, but neglecting the effect of the continuum in the inner and outer regions are shown in column 3. It is noted that for the EDC approximation to be applicable as well as for neglecting the continuum there should be guided mode in the inner and outer regions. It can be seen that the propagation constant obtained from present method by completely neglecting the continuum is slightly different from that predicted by the EDC method as a consequence of the transformer ratio "n" being less than unity, due to the discontinuity. Column 4 reports the present results with continuum in both slabs taken in to account, valid for any value of d. These are compared with column 6 with those obtained in [4] by FDM analysis and the agreement are found to be excellent. Our results for structure 2 are compared with those of semi - vectorial FDM analysis [6] and those of vectorial FEM [7] in Fig. 3.7 . Differences, even for large steps

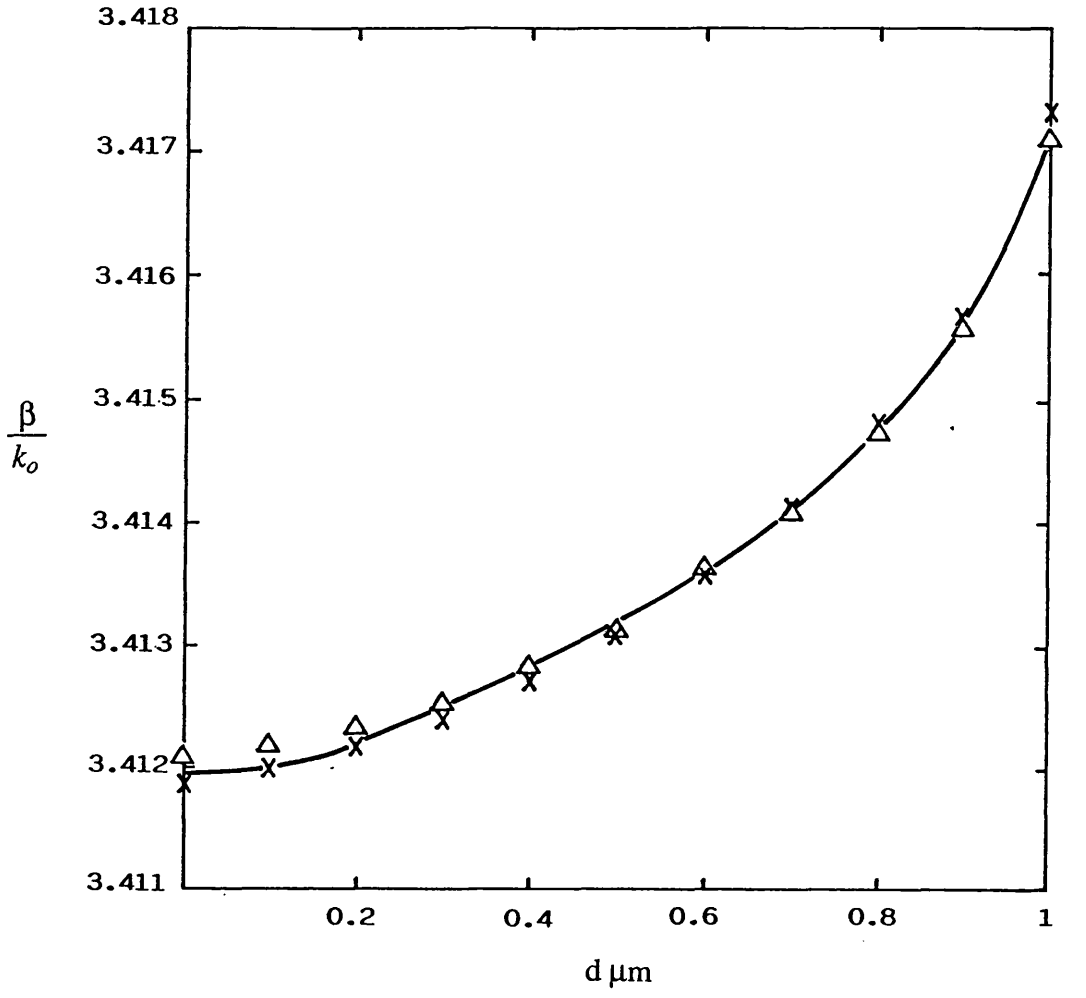

Fig. 3.7 Normalised propagation constant for the fundamental LSE mode as a function of outer slab height d for structure 2.

——— TRD analysis

Δ VFEM analysis (Ref. 7)

x SVFDM analysis (Ref. 6)

STRUC-TURE	MODAL INDICES	EDC	TRD	FDM FD(1) [5]	FD(2) [5]	[6]
ST3	$\frac{\beta}{k_o}$	3.39032237	3.3886900	3.3906177	3.3912917	3.3869266
	v	-	0.4832477	0.5025	0.5092	0.4655926
ST4	$\frac{\beta}{k_o}$	3.39547825	3.3953275	3.3951666	3.3954298	3.3954405
	v	-	0.4386987	0.4367	0.4400	0.4401
ST5	$\frac{\beta}{k_o}$	3.43732738	3.4368203	3.4368425	3.4368635	3.4368112
	v	-	0.3638981	0.3683	0.3725	0.3621

TABLE 3.3 : Comparison of modal indices for the LSE of structure ST3,ST4 and ST5

are seen to be minimal. Results on three additional guiding structures (structure 3, 4, and 5) are given in Table 3.3 and are found to be in excellent agreement with those of [5] and [6] obtained using FDM analysis.

In order to assess the accuracy of the intermediate slab function over the inner slab mode function chosen as the basis function, we investigate the propagation constant of structure 1 using both trial fields and the results are tabulated in Table 3.4 .

d	$v = \frac{(\frac{\beta}{k_o})^2 - n_2^2}{n_1^2 - n_2^2}$	
μm	INTERMEDIATE SLAB MODE FUNCTION	THICKER SLAB MODE FUNCTION
0.1	0.62282131	0.62219390
0.2	0.62416126	0.62234266
0.3	0.62708867	0.62261910
0.4	0.62999694	0.62281047
0.5	0.63333667	0.62339524
0.6	0.63789640	0.62501142
0.7	0.64324008	0.65078256
0.8	0.65054058	0.65525143
0.9	0.66065259	0.65787970

TABLE 3.4 : Comparison of modal indices of structure ST1 using different trial function.

It can be seen that the propagation constant value obtained using the inner slab mode function as the trial field is lower than that obtained using the intermediate slab function, particularly, when the the step is large. This confirms the assertion made in section 3.131, that using just the surface mode right or left of the step is inaccurate, because of its orthogonality to the continuum.

In order to assess the convergence of the solution, we investigate the propagation constant of structure 2 using the Ritz - Galerkin procedure and the basis functions developed in section 3.133. Results obtained for increasing order of the solution are

given in Table 3.5 . It can be observed that the general trend is $\frac{\beta}{k_o}$ converges very fast to a value correct to four decimal places. The fluctuation in the last digit may be due to rounding off errors in the numerical computation and is negligible. These results show that by taking an expansion of more than one term expansion, the change in the value of the propagation constant is only marginal. This confirms our belief that single term expansion represented by "transition function" is sufficient to yield results with good accuracy.

d	$\frac{\beta}{k_o}$			
	ORDER OF SOLUTION			
μm	$n=0$	$n=1$	$n=2$	$n=3$
0.1	3.411978	3.412206	3.412208	3.412205
0.2	3.412205	3.412344	3.412372	3.412390
0.3	3.412490	3.412521	3.412546	3.412585
0.4	3.412697	3.412744	3.412750	3.412764
0.5	3.412857	3.412935	3.412955	3.412957
0.6	3.413557	3.413580	3.413592	3.413595
0.7	3.414065	3.414086	3.414103	3.414140
0.8	3.414724	3.414733	3.414748	3.414768
0.9	3.415590	3.415592	3.415593	3.415596

TABLE 3.5 : Convergence of modal solution of structure ST2

In order to assess the contribution from the continuum on the results, we investigate the propagation constant with continuum represented by substrate modes only, substrate modes and air mode of outer region only and the complete continuum spectrum of both slabs. In this exercise, structure 2 is again taken as an example. Results are compared in Table 3.6 and the difference is found to be marginal. This shows that only the continuous spectra due to substrate modes contribute significantly to the field expansion. In fact, there is no significant difference between the results obtained by neglecting the air mode of the inner region and that obtained by considering the complete spectrum. This observation seem to suggest that we need only to include the substrates modes of

both slabs and the air modes of the outer slab in the field expansion to obtain results with good accuracy. It is also observed that when there are well guided modes in the inner and outer regions, the continuous spectrum contributes negligibly, especially if the step is small. In fact, by considering the continuous spectra due to the substrate modes only in the field expansion is enough to yield results with good accuracy.

d μm	$\frac{\beta}{k_o}$		
	AIR AND SUBSTRATE MODES BOTH REGIONS	NEGLECTING AIR MODES OF INNER REGION	NEGLECTING AIR MODES BOTH REGIONS
0.1	3.411978	3.411978	3.412188
0.2	3.412205	3.412215	3.412275
0.3	3.412490	3.412440	3.412405
0.4	3.412697	3.412670	3.412648
0.5	3.412857	3.412859	3.412855
0.6	3.413557	3.413633	3.413558
0.7	3.414065	3.414137	3.414066
0.8	3.414724	3.414763	3.414724
0.9	3.415590	3.415599	3.415590

TABLE 3.6 : Contribution of the continuum component on the accuracy of $\frac{\beta}{k_o}$

Fig. 3.8 gives a 3 - D plot of the H_y and E_x showing proper discontinuity on the side of the rib at $x = 0$.

3.3 EVEN (to x) MODES LSM ANALYSIS

The even LSM - modes (TM to y) of the rib waveguide in Fig. 3.1 are obtained by placing a magnetic wall on the plane of symmetry at $x = -a$. For a LSM mode, with z - and time - dependence $e^{j(\omega t - \beta z)}$ suppressed, the electromagnetic field components may be expressed in terms of a y - directed electric vector potential as,

$$E_x = \partial_x \, \partial_y \, \psi_e(x,y)\vec{y} \tag{3.43a}$$

$$E_y = (\varepsilon_r k_o^2 + \partial_y^2) \, \psi_e(x,y)\vec{y} \tag{3.43b}$$

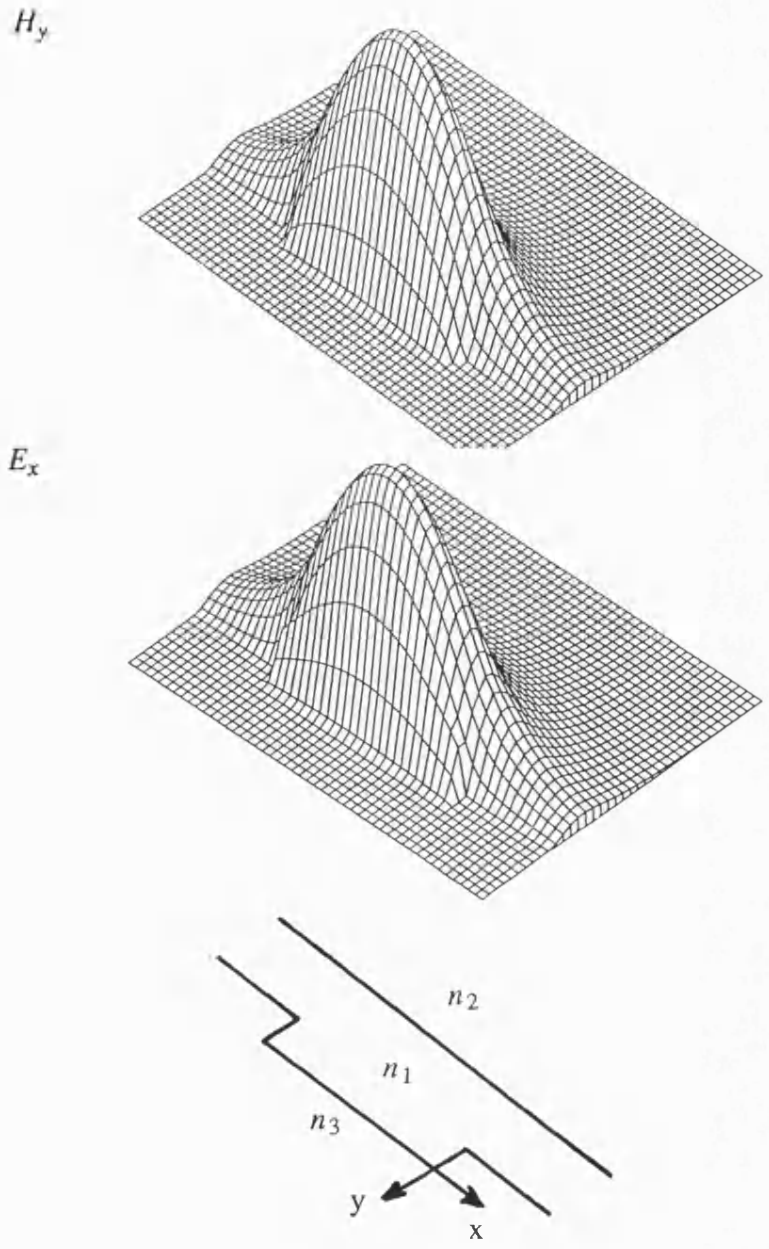

Fig. 3.8 H_y and E_x field components of the fundamental LSE mode plotted as the magnitude values over transverse guide section.

$$E_z = -j\,\beta\,\partial_y\,\psi_e(x,y)\,\vec{y} \tag{3.43c}$$

$$H_x = \omega\,\varepsilon_r\,\beta\,\psi_e(x,y)\,\vec{y} \tag{3.43)d}$$

$$H_y = 0 \tag{3.43e}$$

$$H_z = j\,\omega\,\varepsilon_r\,\partial_x\,\psi_e(x,y)\,\vec{y} \tag{3.43f}$$

With a magnetic wall at the plane of symmetry $x = -a$, we have maximum E_y there and consequently the x - dependent variation of the y - directed electric field can be represented by a cosine - like function. The y - directed Hertzian electric potential subjected to boundary condition for E_y for region 1 and 2 are chosen to be:

Region 1,

$$\psi_e(x,y) = \frac{1}{j\omega\varepsilon_0}\left[\frac{1}{q_{se}^2+\beta^2} I_s\,\phi_{se}(y)\,\chi_s(x) + \int_0^{\infty} \frac{d\rho}{k_o^2-\rho^2} I(\rho)\,\phi_e(y,\rho)\,\chi(x,\rho) + \int_0^{v} \frac{d\sigma}{\varepsilon_2 k_o^2-\sigma^2} I(\sigma)\phi_e(y,\sigma)\,\chi(x,\sigma)\right] \tag{3.44}$$

Region 2,

$$\psi_e(x,y) = \frac{1}{j\omega\varepsilon_0}\left[\frac{1}{q_{se}'^2+\beta^2} I_s'\,\psi_{se}(y)\,e^{-jq'_{se}x} + \int_0^{\infty} \frac{d\rho}{k_o^2-\rho^2} I'(\rho)\,\psi_e(y,\rho)\,e^{-jq'x} + \int_0^{v} \frac{d\sigma}{\varepsilon_2 k_o^2-\sigma^2} I'(\sigma)\,\psi_e(y,\sigma)\,e^{-jp'x}\right] \tag{3.45}$$

where the various functions and parameters are analogous to those defined under equations (3.2) and (3.3), but the expressions appropriate to TM modes, as given in Appendix 1, must be used.

3.31 FORMULATION OF INTEGRAL EQUATION AND TRANSVERSE EQUIVALENT NETWORK

By substituting equations (3.44) and (3.45) in to equation (3.43), the pair of fields

transverse to x, E_y and H_z, needed in the analysis, may be obtained. By a development analogous to that of section 3.12, we arrive at the integral equation for the unknown field E_y at the discontinuous interface $x = 0$, given by:

$$\tilde{Y} \cdot E_y(0,y) = 0 \tag{3.46}$$

where the kernel of the integral operators $\tilde{Y}$ is given by,

$$Y(y,y') = \frac{1}{j\omega\mu_0}\left[-\frac{q_{se}\tan(q_{se}a)}{\varepsilon_{ee}}\phi_{se}(y)\,\phi_{se}(y') + \frac{\gamma'_{se}}{\varepsilon'_{ee}}\psi_{se}(y)\,\psi_{se}(y') \right.$$

$$\left. + Y_a(y,y') + Y_{sb}(y,y') \right] \tag{3.47}$$

and,

$$Y_a(y,y') = \sum_{\mu=e,o}\int_0^{\infty} \frac{d\rho}{1-\frac{\rho^2}{k_o^2}}\gamma\left[\tanh(\gamma a)\,\phi_{e\mu}(y,\rho)\,\phi_{e\mu}(y',\rho) + \psi_{e\mu}(y,\rho)\,\psi_{e\mu}(y',\rho) \right] \tag{3.48}$$

$$Y_{sb}(y,y') = \int_0^{\nu} \frac{d\sigma}{\varepsilon_2 - \frac{\sigma^2}{k_o^2}}\eta\left[\tanh(\eta a)\,\phi_e(y,\sigma)\,\phi_e(y',\sigma) + \psi_e(y,\sigma)\,\psi_e(y',\sigma) \right] \tag{3.49}$$

Again, by a development similar to that of section 3.32, the following scalar dispersion equation is deduced:

$$\frac{q_{se}}{\varepsilon_{ee}}\tan(q_{se}a) = \frac{n^2\,\gamma'_{se}}{\varepsilon'_{ee}} + Y_a(y,y') + Y_{sb}(y,y') \tag{3.50}$$

Its equivalent network representation is illustrated in Fig. 3.9, which is the dual of Fig. 3.2 . In equation (3.50), $Y_a(y,y')$, $Y_{sb}(y,y')$ and n^2 are defined analogous to equations (3.16), (3.17) and (3.18) respectively, in terms now of the unknown transverse electric field at the interface $E_y(0,y) = E(y)$ and of the wavenumbers appropriate to the TM - case. It is noted, however, that unlike in the LSE - case, E fields transverse to a dielectric wedge are singular [1]. Hence, $y = d$ and $y = D$ are singular points, as further discussed in the next section, and the appropriate choice of E has more bearing on the accuracy of solution.

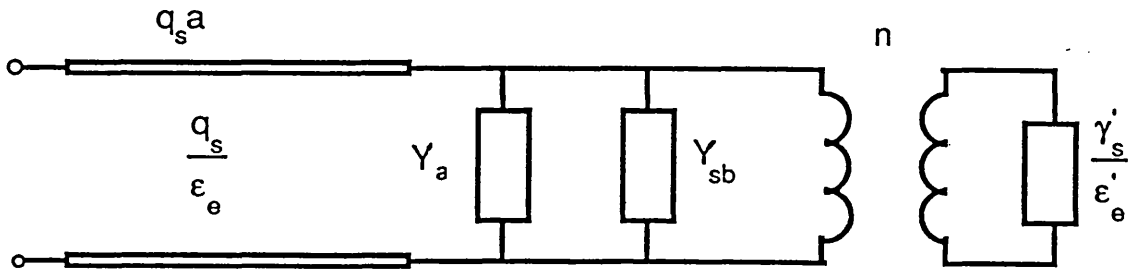

Fig. 3.9 Transverse Equivalent Circuit for LSM polarization.

The second feature about equation (3.50) is, in fact, its close resemblance to equation (3.15) which is dispersion equation for a TM line in x; whereas , according to a standard EDC procedure, the transmission line representing propagation in the x direction for a LSM - mode ought to be of the pure TE - type. This apparent incongruence is explained by noting that in the EDC approximation one applies the relationships between fields and potentials (3.43) to a separable potential of the type $f(y)e^{-jk_x x}$ in each region. Then, one has;

$$Y^{TE} = \frac{H_z}{E_y} = \frac{\omega \varepsilon_0 \varepsilon_r k_x}{\varepsilon_r k_o^2 - k_y^2} = \frac{\varepsilon_r k_x}{\omega \mu_0 \varepsilon_{ee}} \qquad (3.51)$$

Only if $k_y \approx 0$ or the identification $\varepsilon_r(y) \approx \varepsilon_{ee}$ can be made, is the characteristic admittance of a TE - wave recovered from equation (3.51). It is, therefore, fair to say that, whilst in the LSE - case, the EDC is the most basic level of approximation to the rigorous dispersion equation as obtained from Transverse Resonance Diffraction, in the LSM - case stronger approximations are required. It is consequently to be expected that the EDC approximation in the LSM - case be further removed from the accurate solution than in the LSE case.

3.32 VARIATIONAL SOLUTION OF THE INTEGRAL SOLUTION

3.321 FIRST ORDER VARIATIONAL SOLUTION FOR E_y AND USE OF EDGE SINGULARITIES

The integral equation (3.46) is solved rigorously by means of a first - order variational approach, taking account of the proper singularities of the transverse electric field at the dielectric corners $y = d$ and $y = D$ of Fig. 3.1 . It is well known that the transverse electric fields at a dielectric wedge of aperture θ between dielectrics ε_r and $\varepsilon_0 = 1$ are singular like r^{α}, where r is the distance from the wedge and α is in the range ($-1<\alpha<0$) is given by the lowest eigenvalue of the transcendental equation [1],

$$\sin(\alpha+1)\,\pi \pm \frac{\varepsilon_r-\varepsilon_0}{\varepsilon_r+\varepsilon_0}\sin(\alpha+1)\,(\theta-\pi)$$

For $\theta=\frac{\pi}{2}$ and $\theta=\frac{3\pi}{2}$ corresponding to corner $y=D$ and $y=d$ of Fig. 3.1 respectively, the order of the singularity is the same and is given by,

$$\alpha=\frac{2}{\pi}\cos^{-1}\left(\frac{1}{2}\frac{\varepsilon_r-\varepsilon_0}{\varepsilon_r+\varepsilon_0}\right)-1$$

ε_r	$\alpha=\frac{2}{\pi}\cos^{-1}\left(\frac{1}{2}\frac{\varepsilon_1-1}{\varepsilon_1+1}\right)-1$
1	0.0
2	-0.107
3	-0.161
5	-0.216
10	-0.268
11.8336	-0.277
20	-0.299
100	-0.326

TABLE 3.7 : Typical values of the order of the singularity near a dielectric wedge of aperture $\theta=\frac{\pi}{2}, \frac{3\pi}{2}$

Typical values of α are reported in Table 3.7 . For $10 < \varepsilon_r < 12$ which is the typical dielectric constant for the semiconductor used to fabricate rib guide at optical frequency, $\alpha \approx -0.28$, which is a non - negligible singularity. The typical shape of the true diffraction field at the interface $x=0$ is of the type shown qualitatively in Fig. 3.10 . Also, a finite jump takes place at the dielectric interfaces $y=0,D$, common to both sides of the step.

In order to obtain an accurate variational expression of the lowest possible order, all the above features ought to be built in to the trial field.

In view of the features discussed above, two forms of the trial field involving a "transition function" where the value of intermediate height $\bar{d}$ is determined as for the LSE case are used. The first was of the type of a product of a TM "transition function",

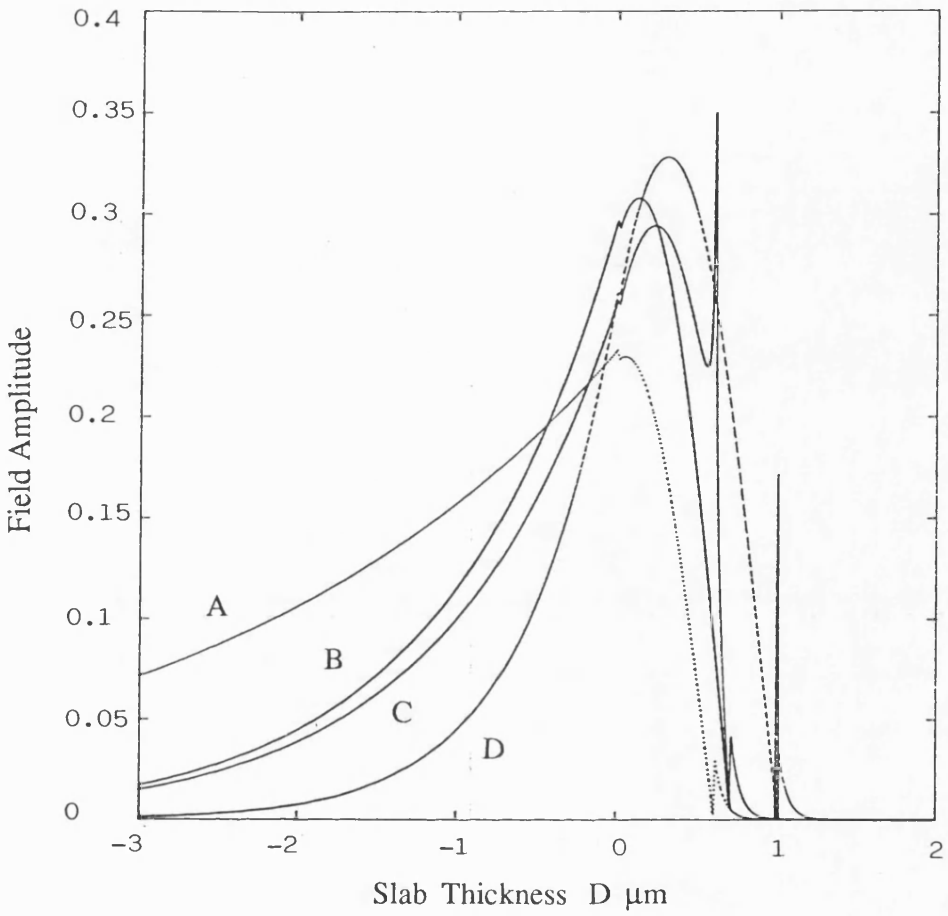

Fig. 3.10 E_y component of the fundamental LSM mode for slab of height d (curve A), $\bar{d}$ (curve B), D (curve D), compared with the trial field of the transition function (curve C).

$\frac{\bar{U}_{se}(y)}{\varepsilon_r(y)}$, times a term describing the singularity, namely,

$$E(y) = E_y(0,y) = \frac{\bar{U}_{se}(y)}{\varepsilon_r(y)} \left[1 + \frac{K}{|y-d|^{\alpha} |y-D|^{\alpha}} \right] \tag{3.52}$$

where K is a variational parameter that minimizes an appropriate functional (3.47).

Substituting equation (3.52) in to equation (3.47) gives,

$$Y = \frac{1}{j\omega\mu_0} \left[\frac{-q_{se} \tan(q_{se}a) P_{se}^2}{\varepsilon_{ee}} + \frac{\gamma'_{se} P'^2_{se}}{\varepsilon'_{ee}} + Y_a + Y_{sb} \right] \tag{3.53}$$

where

$$Y_a = \sum_{\mu=e,o} \int_0^{\infty} \frac{d\rho}{1 - \frac{\rho^2}{k_o^2}} \gamma \left[\tanh(\gamma a) P_{e\mu}^2(\rho) + P'^2_{e\mu}(\rho) \right]$$

$$Y_{sb} = \int_0^{\nu} \frac{d\sigma}{\varepsilon_2 - \frac{\sigma^2}{k_o^2}} \eta \left[\tanh(\eta a) P_e^2(\sigma) + P'^2_e(\sigma) \right]$$

In view of the relatively complicated nature of equation (3.52), the scalar products,

$$\begin{aligned}
P_{se} &= < \phi_{se}(y) , E(y) > \\
P'_{se} &= < \psi_{se}(y) , E(y) > \\
P_e(\sigma) &= < \phi_e(y,\sigma) , E(y) > \\
P'_e(\sigma) &= < \psi_e(y,\sigma) , E(y) > \\
P_{e\mu}(\rho) &= < \phi_{e\mu}(y,\rho) , E(y) > \\
P'_{e\mu}(\rho) &= < \psi_{e\mu}(y,\rho) , E(y) >
\end{aligned} \tag{3.54}$$

required in equation (3.53) need to be evaluated numerically. The choice of equation (3.52) as a trial field, however, produces accurate results, which are discussed in section 3.32 . In order to avoid the above inconvenience, also realizing that the effect of each singularity in this problem is well localized to a small neighbourhood of the singular corner itself, we used a second trial field given by,

$$
\begin{aligned}
E(y) &= \bar{A}\, e^{-\bar{q}(y-\bar{d})}\,(y-D)^{\alpha} && ; y \geq D \\
&= \frac{1}{\varepsilon_1}\,\bar{A}\, e^{-\bar{q}(y-\bar{d})}\,(D-y)^{\alpha} && ; \bar{d} \leq y \leq D \\
&= \frac{1}{\varepsilon_1}\,\bar{A}\cos(\bar{h}y-\bar{\phi}_b)\,(y-d)^{\alpha}\left[\frac{D-\bar{d}}{\bar{d}-d}\right]^{\alpha} && ; d \leq y \leq \bar{d} \\
&= \frac{1}{\varepsilon_1}\,\bar{A}\,\frac{\cos(\bar{h}y-\bar{\phi}_b)}{\cos(\bar{h}\bar{d}-\bar{\phi}_b)}\,(d-y)^{\alpha}\left[\frac{D-\bar{d}}{\bar{d}-d}\right]^{\alpha} && ; 0 \leq y \leq d \\
&= \frac{1}{\varepsilon_2}\,\bar{A}\,\frac{\cos(\bar{\phi}_b)}{\cos(\bar{h}\bar{d}-\bar{\phi}_b)}\,e^{\bar{p}y}\,d^{\alpha}\left[\frac{D-\bar{d}}{\bar{d}-d}\right]^{\alpha} && ; y \leq 0
\end{aligned}
\qquad (3.55)
$$

where

$$\tan(\bar{h}\bar{d}-\bar{\phi}_b) = \varepsilon_1\,\frac{\bar{q}}{\bar{h}}$$

$$\tan(\bar{\phi}_b) = \frac{\varepsilon_1\,\bar{q}}{\varepsilon_2\,\bar{h}}$$

We note, in fact, that the above form (3.55) takes account of each of the two singularities at $y = d,D$ one at a time and includes the dielectric jump at $y = 0$. Moreover, it is physically clear that no other discontinuity takes place between the two singularities at $y = d,D$. Hence, we assume a continuous function in this interval. For $y > D$, we include the effect of the singularity at $y = D$, whereas the dielectric constant is that of the "air region" above the rib. The shape of the trial field (3.55) is compared in Fig. 3.10 with those of the slab mode in the rib, that of the outer slab region and of the "transition function" $\frac{\bar{U}_{se}}{\varepsilon_r}(y)$ without inclusion of the singularities for a typical cross - section. From this figure, we note the non - negligible, but well localised, effects of the two singularities, whereas $\frac{\bar{U}_{se}}{\varepsilon_r}(y)$ is seen to have features intermediate between those of $\phi_{se}(y)$ and $\psi_{se}(y)$, according to the concept of "transition function".

The advantage of using equation (3.55) with respect to equation (3.52) lies in that the scalar products (3.54) can be cast analytically in terms of incomplete Gamma functions.

These are given in Appendix 5. These expressions can be evaluated numerically in rapidly converging series form. For large values of the argument, in fact, the series reduces to a single term. The analyticity of the "scalar products" results in far greater numerical efficiency of the second trial field, although the actual values of the propagation constants obtained in the two cases are very similar. This fact will be shown in the numerical exercise discussed in in the following section.

3.33 NUMERICAL RESULTS

In order to demonstrate the application of the theory developed in the previous section, we worked out numerical examples to investigate the propagation constant of a rib guide whose parameters are given in Table 3.1 . The LSM analysis is complicated by the presence of the singularities as discussed in the previous sections. A comparison between the results obtained in using the two trial fields discussed in the previous section for structure 2 and 6 is given in Table 3.8 and 3.9 respectively.

d	TRD WITH SINGULARITY		TRD WITHOUT SINGULARITY	FDM [6]	EDC
μm	$\frac{\beta}{k_o}$ (Eq. 3.52)	$\frac{\beta}{k_o}$ (Eq. 3.55)	$\frac{\beta}{k_o}$	$\frac{\beta}{k_o}$	$\frac{\beta}{k_o}$
0.1	3.41020	3.41021	3.41008	3.41060	-
0.2	3.41029	3.41024	3.41009	3.41073	-
0.3	3.41046	3.41026	3.41012	3.41092	-
0.4	3.41068	3.41077	3.41027	3.41117	-
0.5	3.41096	3.41122	3.41092	3.41150	-
0.6	3.41217	3.41182	3.41138	3.41190	3.41271
0.7	3.41247	3.41214	3.41148	3.41241	3.41293
0.8	3.41298	3.41285	3.41249	3.41303	3.41331
0.9	3.41380	3.41358	3.41378	3.41385	3.41394

TABLE 3.8 : Comparison of modal indices for the LSM of structure ST2

d μm	TRD WITH SINGULARITY $\frac{\beta}{k_o}$ (Eq. 3.52)	$\frac{\beta}{k_o}$ (Eq. 3.55)	TRD WITHOUT SINGULARITY $\frac{\beta}{k_o}$	EDC $\frac{\beta}{k_o}$
0.1	3.4230021	3.4230844	3.4229312	-
0.2	3.4230022	3.4231136	3.4229337	-
0.3	3.4230032	3.4233329	3.4229365	-
0.4	3.4230731	3.4234474	3.4229602	-
0.5	3.4232181	3.4235177	3.4230472	-
0.6	3.4234884	3.4237593	3.4231235	-
0.7	3.4239814	3.4239557	3.4231637	-
0.8	3.4251143	3.4243814	3.4231881	3.4256779
0.9	3.4251365	3.4244065	3.4232126	3.4258394
1.0	3.4253931	3.4247512	3.4234063	3.4260368
1.1	3.4257473	3.4252561	3.4239009	3.4262781
1.2	3.4262208	3.4257251	3.4250629	3.4265737
1.3	3.4267664	3.4265150	3.4264681	3.4269466
1.4	3.4274047	3.4272225	3.4273995	3.4274559

TABLE 3.9 : Comparison of modal indices for the LSM of structure ST6

Differences are seen to be minimal, but using the second form is considerably more economical in computing time. The accuracy of the method is validated by comparing with the results of [6] in Table 3.8, where differences are minimal. Fig. 3.11 shows the variation of normalised modal indices with rib width for the fundamental LSM mode for three different rib height. Fig. 3.12 shows the variation of normalised modal indices for the fundamental LSM mode with rib height for different rib widths. In Fig. 3.11 and 3.12 rib guide of structure 6 is taken as an example.

3.4 WAVEGUIDE LOSSES

In the previous analysis no mentioned was made on waveguide losses. The sources of loss in rib waveguide are twofold, consisting of bulk loss and corrugation on surfaces.

Bulk Losses

In a medium with finite conductivity σ, a conduction current $J = \sigma E$ will exist, resulting in energy loss. The loss characteristics can be expressed as a complex value of dielectric

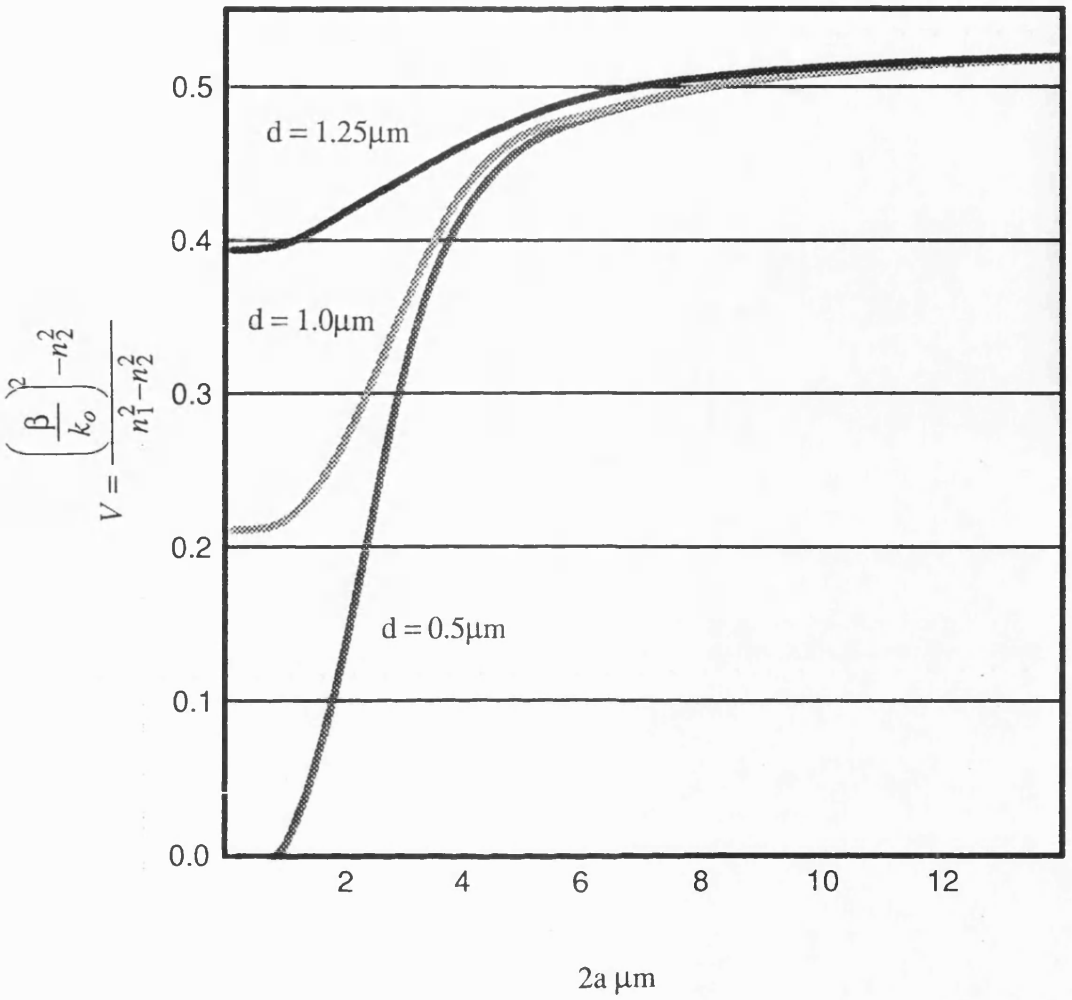

Fig. 3.11 Normalised propagation characteristics for LSM modes as a function of rib width for three different slab heights for structure 2.

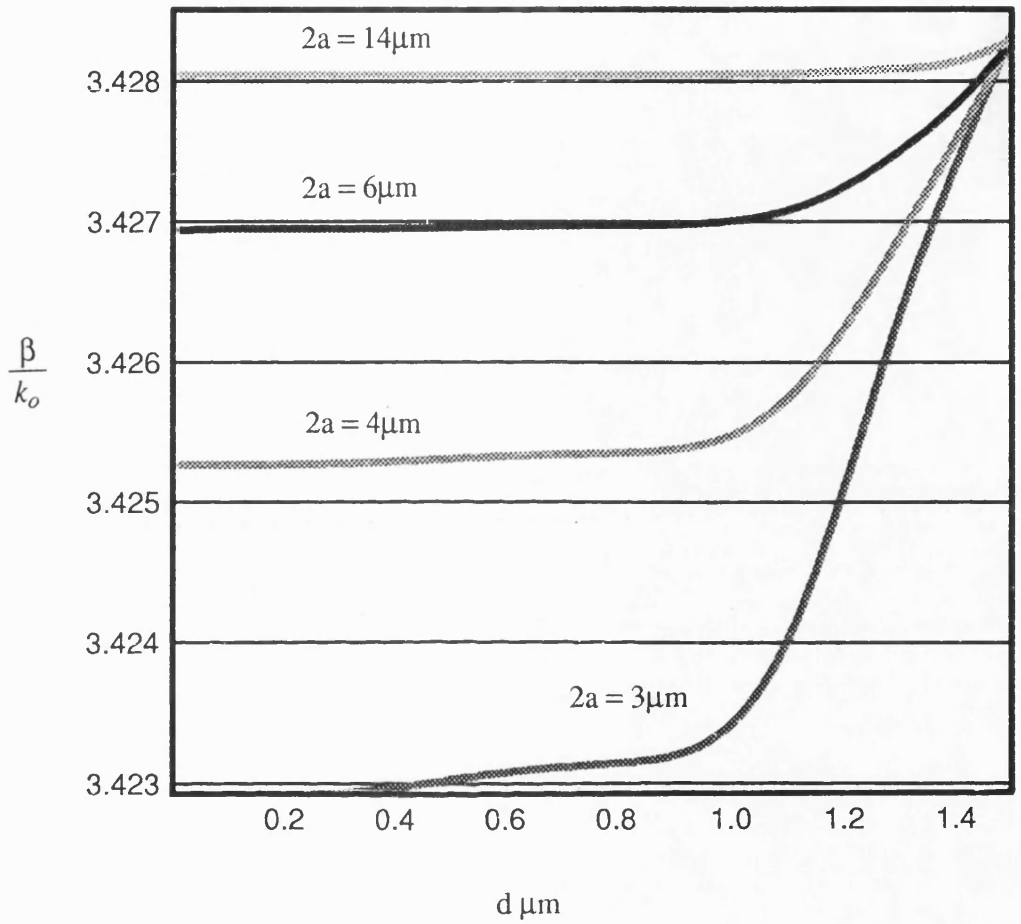

Fig. 3.12 Normalised propagation constant for the fundamental LSM mode as a function of rib height for different rib widths for structure 2.

constant given by

$$\tilde{\varepsilon} = \varepsilon(1 - j\tan\delta_l) = \varepsilon_0\varepsilon_r(1 - j\tan\delta_l)$$

This will correspond to a complex modal propagation constant γ such that

$$\gamma^2 = (\alpha + j\beta)^2 = k_x^2 + k_y^2 - \tilde{\varepsilon}k_o^2$$

$$= k_c^2 - \omega^2\mu_0\varepsilon(1 - j\tan\delta_l)$$

For small losses $\delta_l \ll 1$, $\alpha \ll \beta$ and

$$-\beta^2 - 2j\alpha\beta = k_c^2 - \omega^2\mu_0\varepsilon + j\omega^2\mu_0\varepsilon\tan\delta_l$$

so that

$$\alpha = \frac{k_o^2\varepsilon_r}{2\beta}\tan\delta_l$$

For GaAs/AlGaAs at 1.52μm the material absorption contribute < 0.04 dB/cm and, hence, there is no substantial difference to our results by considering real refractive index of the materials. However, for sufficiently high loss tangent, bulk losses can also couple LSE and LSM via the common E_x field component. In fact $J_x = \sigma E_x$ is a common induced source term. Hence, bulk loss is an additional coupling loss mechanisms.

Scattering losses

Propagation loss also results, however, from scattering by defects (such as photolithographics imperfections) and rib roughness. Corrugation on surfaces will results in loss due to coupling between LSE and LSM . This loss can be approximated with a simple theory based on Tien's result for scattering in slab waveguides [8].

$$\alpha = 4(k\sigma)^2 \frac{\dfrac{\cos^3\theta}{\sin\theta}}{W + \dfrac{2}{p}}$$

where k is the propagation constant in the guiding layer, σ is the surface roughness, θ the propagation angle in the guide and p the transverse decay constant in the cladding layers. The above expression has been used by [9] to check their experimental results for ion milled guides and the calculation suggests that approximately half of the propagation loss of 0.2 dB/cm at large rib width and small rib height is due to rib roughness. However, reduced scattering loss can be obtained with an improve fabrication process such as metalorganic chemical vapour deposition (MOCVD) and reactive ion etching (RIE) in BCl_3. Propagation losses as low as 0.15 dB/cm at 1.52μm have been achieved in single-mode GaAs/AlGaAs guides grown by organometallic vapor phase epitaxy (OMVPE) [10].

3.5 CONCLUSION

In this chapter, an approximate Transverse Resonance Diffraction solution of the rib waveguide in the pure LSE and LSM polarizations is derived. The problem is seen as one of diffraction by a transverse step discontinuity in the plane $x = 0$, and transverse resonance is employed to derived the propagation constant. In solving the TRD problem, a variational formulation of Rayleigh - Ritz and Ritz - Galerkin type are presented. In the Rayleigh - Ritz formulation we adopt a single trial field at the transverse step discontinuity which is the modal distribution of a slab of height intermediate between those of the inner and outer region, which we define "transition function". In the LSM case we include explicitly the proper singularity of the E_y - field at 90 ° and 270 ° dielectric corners. The "transition function" approximation leads to a scalar dispersion equation yielding results for the propagation constant which are of comparable accuracy with those obtained by purely numerical methods such as FDM/FEM. Also a single function trial field leads to a simple scalar transverse equivalent network representation of the waveguide and this feature is very useful, as it allows straightforward extension of the method to more complicated transverse cross-sections. The solution using Galerkin's approach shows very quick convergence. This is the result of the choice of trial field

function, where the first term in the expansion of H_y is already very close to the true field. Hence, we conclude that a single term "transition function" is a good choice of trial field function, that leads to a simple network representation of the waveguide and yields results of reliable accuracy.

REFERENCES

[1] J. Bach Andersen, U.V. Solodukhov, " Field behaviour near a dielectric wedge ", I.E.E.E Trans. on Antenna and Propagation, vol. AP-26, July 1978 , pp 598-602

[2] T. Rozzi, " Rigorous analysis of the step discontinuity in a planar dielectric weaveguide ", I.E.E.E Trans. on Microwave Theory and Techniques, vol. MTT-26, Oct. 1978, pp 738-746

[3] P.M. Morse, H. Feshback, " Methods of Theoretical Physics ", McGraw-Hill, 1953.

[4] T.M. Benson, J. Buus, " Optical guiding in III–V semiconductor Rib structures ", I.E.E Conf. Publ. 227, Cardiff, April 1983, pp 17-20

[5] M.J. Robertson, S. Ritchie and P. Dayan, " Semiconductor waveguides: Analysis of optical propagation in single rib structures and directional couplers ", I.E.E Proceeding, vol. 132, Pt. J, No. 6, Dec. 1985

[6] M.S. Stern, " Semivectorial polarised $\tilde{H}$ field solutions for dielectric waveguides with arbitrary index profiles ", I.E.E Proc., vol. 135, Pt. J, No. 5, Oct. 1988, pp 333-338

[7] B.M.A. Rahman, J.B. Davies, " Vector H finite element solution of Ga As/Ga Al As rib waveguides ", I.E.E Proc., vol. 132, Pt. J, Dec. 1985, pp 349-353

[8] P.K. Tien, Appl.Opt. No. 10, pp. 2395, 1971

[9] R.J. Deri, E. Kapon, L.M. Schiavone, " Scattering in low-loss GaAs/AlGaAs rib waveguides", Appl. Phys. Lett. Vol. 51, No.11, September 1987.

[10] M. Seto, A. Shahar, R.J. Deri, W.J. Tomlinson, A. Yi-Yan, " GaAs/AlGaAs single-mode optical waveguides with low propagation loss and strong optical confinement", Appl. Phys. Lett., Vol. 56, No. 11, 12 March 1990.

[11] I.S. Gradshteyn, I.M. Ryzhik, " Table of Integrals, series and products ", Academic Press, 1980

CHAPTER 4

RIGOROUS ANALYSIS OF RIB WAVEGUIDES

4.1 INTRODUCTION

An approximate analysis of the rib waveguide in the pure LSE and LSM polarizations was developed in chapter 3 and used to investigate its propagation characteristics. In that chapter it was stated that the true electromagnetic fields of the structure are hybrid. This is the consequence of the diffraction of the fields at the dielectric corners in the guide cross section. The aim of this chapter is to develop a complete rigorous analysis of rib waveguides taking into account the effect of LSE and LSM mode coupling at the dielectric corners. This is achieved by enforcing the continuity of all transverse field components across the discontinuous plane at $x = -a$, a boundary condition that is not possible to enforce with a zero E_y or H_y field in the approximate analysis. A consequence of this coupling is a hybrid mode solution where all six electromagnetic field components are present.

4.2 METHOD OF ANALYSIS AND FORMULATION OF INTEGRAL OPERATORS

The rib waveguide cross section under consideration is shown in Fig. 4.1 . The basic approach to the formulation of the problem was outlined in chapter two. We shall develop the formulation for the case where an electric wall is placed on the plane of symmetry, corresponding to a maximum of H_y and zero of E_y there. This is, in fact, the generalisation of the situation that leads to the even LSE five fields approximation presented in chapter three. Hence, this formulation is expected to yield a hybrid mode solution with even LSE - like mode behaviour. Likewise, by following analogous

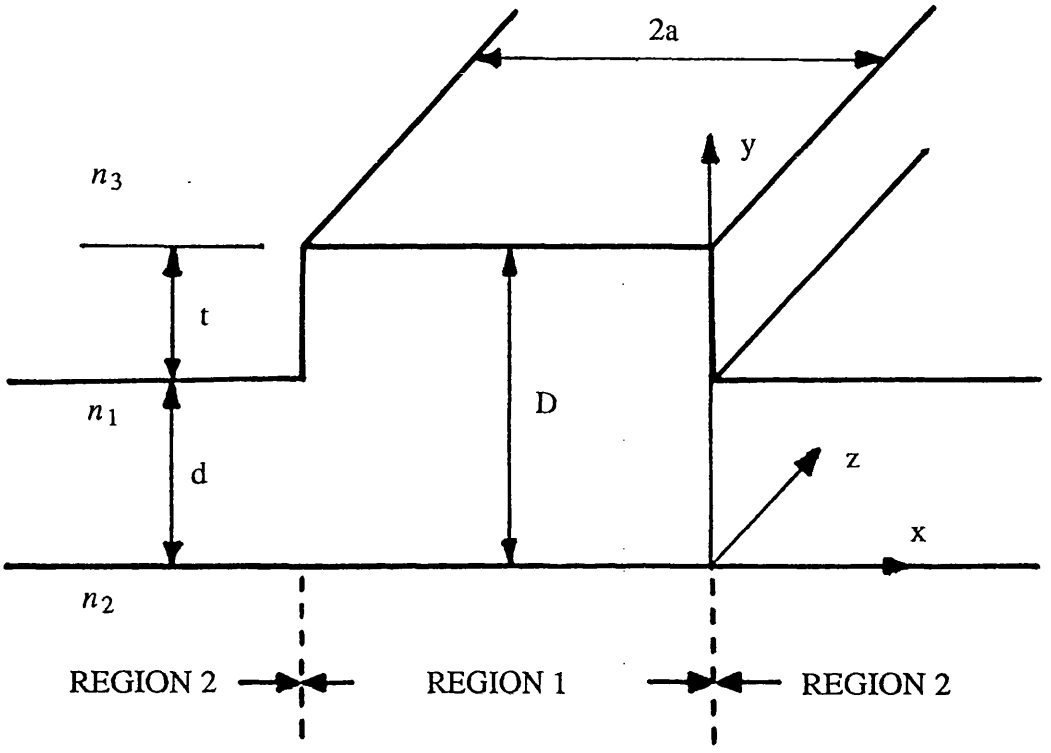

Fig. 4.1 Rib guide cross section.

procedure a formulation for the case with a magnetic wall placed at the plane of symmetry can be established and the analysis results in an even LSM - like hybrid mode solution.

In order to enforce the continuity condition on all four transverse field components across the discontinuous plane $x = 0$, the electromagnetic fields at each side of the discontinuous plane need to be described fully by six field components. These field components can be obtained from the superposition of z - directed LSE and LSM modes. This in turn requires at each side of the discontinuous plane, a pair of y - directed, vector potentials, one electric $\pi_e(x,y) = \psi_e(x,y)e^{-j\beta z}\vec{y}$ and one magnetic $\pi_h(x,y) = \psi_h(x,y)e^{-j\beta z}\vec{y}$, in order to derive the electromagnetic field components in terms of LSM and LSE modes, respectively. By referring to chapter two, the electromagnetic field components of the structure may be expressed as,

$$E_x = \partial_x \partial_y \psi_e(x,y) + \omega \mu_0 \beta \psi_h(x,y) \tag{4.1a}$$

$$E_y = (\varepsilon_r k_o^2 + \partial_y^2) \psi_e(x,y) \tag{4.1b}$$

$$E_z = -j \beta \partial_y \psi_e(x,y) - j \omega \mu_0 \partial_x \psi_h(x,y) \tag{4.1c}$$

$$H_x = -\omega \varepsilon_0 \varepsilon_r \beta \psi_e(x,y) + \partial_x \partial_y \psi_h(x,y) \tag{4.1d}$$

$$H_y = (\varepsilon_r k_o^2 + \partial_y^2) \psi_h(x,y) \tag{4.1e}$$

$$H_z = j \omega \varepsilon_0 \varepsilon_r \partial_x \psi_e(x,y) - j \beta \partial_y \psi_h(x,y) \tag{4.1f}$$

In (4.1) the time - and z - dependences $e^{j(\omega t - \beta z)}$ are assumed but suppressed. The scalar functions $\psi_e(x,y)$ and $\psi_h(x,y)$ are chosen at each side of the discontinuity plane so that they satisfy the correct boundary conditions for the field components and have dimensional consistency. Having obtained the expressions for the transverse to x field components, the continuity of the fields at the discontinuous interface between the two regions are enforced. This leads to a pair of coupled integral equations for the unknown fields E_y and H_y. Having obtained the integral equations, the condition for the transverse resonance is considered and the dispersion equation is derived. The dispersion equation is solved for the propagation constant β using methods similar to those adopted in the

approximate analysis of chapter three.

4.21 HYBRID FIELD COMPONENTS IN REGION 1

With an electric wall on the plane of symmetry $x = -a$, the x - dependent variation of the y - directed magnetic and electric fields can be represented with a cosine - and sine - like functions respectively. As discussed in chapter three, the potential functions $\psi_h(x,y)$ and $\psi_e(x,y)$ required to derive LSE and LSM field components are of the type given by:

$$\psi_h(x,y) = \frac{1}{j\omega\mu_0}\left[\frac{1}{q_{sh}^2+\beta^2} V_h\,\phi_h(y)\,\frac{\cos(q_{sh}(x+a))}{\cos(q_{sh}a)} + \sum_{\mu=e,o}\int_0^{\infty}\frac{d\rho}{k_o^2-\rho^2} V_{h\mu}(\rho)\,\phi_{h\mu}(y,\rho)\,\frac{\cos(q_h(x+a))}{\cos(q_h a)} + \int_0^{\nu}\frac{d\sigma}{\varepsilon_2 k_o^2-\sigma^2} V_h(\sigma)\,\phi_h(y,\sigma)\,\frac{\cos(p_h(x+a))}{\cos(p_h a)}\right] \tag{4.2a}$$

$$\psi_e(x,y) = \frac{1}{j\omega\varepsilon_0}\left[\frac{1}{q_{se}^2+\beta^2} I_e\,\phi_e(y)\,\frac{\sin(q_{se}(x+a))}{\sin(q_{se}a)} + \sum_{\mu=e,o}\int_0^{\infty}\frac{d\rho}{k_o^2-\rho^2} I_{e\mu}(\rho)\,\phi_{e\mu}(y,\rho)\,\frac{\sin(q_e(x+a))}{\sin(q_e a)} + \int_0^{\nu}\frac{d\sigma}{\varepsilon_2 k_o^2-\sigma^2} I_e(\sigma)\,\phi_e(y,\sigma)\,\frac{\sin(p_e(x+a))}{\sin(p_e a)}\right] \tag{4.2b}$$

All the wavenumbers and mode functions appearing in equation (4.2) are defined similar to those in chapter three. By substituting (4.2) in to (4.1), the field components transverse to x are found to be,

$$E_z(x,y) = \Bigg[\frac{1}{q_{sh}^2 + \beta^2} V_h\, \phi_h(y)\, q_{sh}\, \frac{\sin(q_{sh}(x+a))}{\cos(q_{sh}a)}$$

$$+ \sum_{\mu=e,o} \int_0^{\infty} \frac{d\rho}{k_o^2 - \rho^2} V_{h\mu}(\rho)\, q_h\, \phi_{h\mu}(y,\rho)\, \frac{\sin(q_h(x+a))}{\cos(q_h a)}$$

$$+ \int_0^{\nu} \frac{d\sigma}{\varepsilon_2 k_o^2 - \sigma^2} V_h(\sigma)\, p_h\, \phi_h(y,\sigma)\, \frac{\sin(p_h(x+a))}{\cos(p_h a)} \Bigg]$$

$$- \Bigg[\frac{\beta}{\omega\varepsilon_0} \Bigg[\frac{1}{q_{se}^2 + \beta^2} I_e\, \partial_y \phi_e(y)\, \frac{\sin(q_{se}(x+a))}{\sin(q_{se}a)}$$

$$+ \sum_{\mu=e,o} \int_0^{\infty} \frac{d\rho}{k_o^2 - \rho^2} I_{e\mu}(\rho)\, \partial_y \phi_{e\mu}(y,\rho)\, \frac{\sin(q_e(x+a))}{\sin(q_e a)}$$

$$+ \int_0^{\nu} \frac{d\sigma}{\varepsilon_2 k_o^2 - \sigma^2} I_e(\sigma)\, \partial_y \phi_e(y,\sigma)\, \frac{\sin(p_e(x+a))}{\sin(p_e a)} \Bigg] \Bigg]$$

$$= E_z^h + E_z^e \tag{4.3a}$$

$$E_y(x,y) = \frac{1}{j\omega\varepsilon_0} \Bigg[I_e\, \phi_e(y)\, \frac{\sin(q_{se}(x+a))}{\sin(q_{se}a)} + \int_0^{\nu} d\sigma\, I_e(\sigma)\, \phi_e(y,\sigma)\, \frac{\sin(p_e(x+a))}{\sin(p_e a)}$$

$$+ \sum_{\mu=e,o} \int_0^{\infty} d\rho\, I_{e\mu}(\rho)\, \phi_{e\mu}(y,\rho)\, \frac{\sin(q_e(x+a))}{\sin(q_e a)} \Bigg] \tag{4.3b}$$

$$H_y(x,y) = \frac{1}{j\omega\mu_0} \Bigg[V_h\, \phi_h(y)\, \frac{\cos(q_{sh}(x+a))}{\cos(q_{sh}a)} + \int_0^{\nu} d\sigma\, V_h(\sigma)\, \phi_h(y,\sigma)\, \frac{\cos(p_h(x+a))}{\cos(p_h a)}$$

$$+ \sum_{\mu=e,o} \int_0^{\infty} d\rho\, V_{h\mu}(\rho)\, \phi_{h\mu}(y,\rho)\, \frac{\cos(q_h(x+a))}{\cos(q_h a)} \Bigg] \tag{4.3c}$$

$$H_z(x,y) = \Bigg[\frac{1}{q_{se}^2 + \beta^2} I_e\, \phi_e(y)\, q_{se}\, \frac{\cos(q_{se}(x+a))}{\sin(q_{se}a)}$$

$$+ \sum_{\mu=e,o} \int_0^\infty \frac{d\rho}{k_o^2 - \rho^2} I_{e\mu}(\rho)\, q_e\, \phi_{e\mu}(y,\rho)\, \frac{\cos(q_e(x+a))}{\sin(q_e a)}$$

$$+ \int_0^\nu \frac{d\sigma}{\varepsilon_2 k_o^2 - \sigma^2} I_e(\sigma)\, p_e\, \phi_e(y,\sigma)\, \frac{\cos(p_e(x+a))}{\sin(p_e a)} \Bigg]$$

$$- \Bigg[\frac{\beta}{\omega\mu_0} \Bigg[\frac{1}{q_{sh}^2 + \beta^2} V_h\, \partial_y\, \phi_h(y)\, \frac{\cos(q_{sh}(x+a))}{\cos(q_{sh}a)}$$

$$+ \sum_{\mu=e,o} \int_0^\infty \frac{d\rho}{k_o^2 - \rho^2} V_{h\mu}(\rho)\, \partial_y\, \phi_{h\mu}(y,\rho)\, \frac{\cos(q_h(x+a))}{\cos(q_h a)}$$

$$+ \int_0^\nu \frac{d\sigma}{\varepsilon_2 k_o^2 - \sigma^2} V_h(\sigma)\, \partial_y\, \phi_h(y,\sigma)\, \frac{\cos(p_h(x+a))}{\cos(p_h a)} \Bigg] \Bigg]$$

$$= H_z^h + H_z^e \qquad (4.3d)$$

4.22 HYBRID FIELD COMPONENTS IN REGION 2

The potential functions for region 2 $\psi_h(x,y)$ and $\psi_e(x,y)$ are similar to those found in chapter three. The field components transverse to x for the LSE and LSM modes have already been derived in chapter three and are reproduced here as the superposition of the two polarizations according to equation (4.1) given by,

$$E_y(x,y) = \frac{1}{j\omega\varepsilon_0} \Bigg[I'_e\, \psi_e(y)\, e^{-jq'_{se}x} + \int_0^\nu d\sigma\, I'_e(\sigma)\, \psi_e(y,\sigma)\, e^{-jp'_e x}$$

$$+ \sum_{\mu=e,o} \int_0^\infty d\rho\, I'_{e\mu}(\rho)\, \psi_{e\mu}(y,\rho)\, e^{-jq'_e x} \Bigg] \qquad (4.4a)$$

$$E_z(x,y) = j \left[\frac{1}{q'^2_{sh} + \beta^2} V'_h \, \psi_h(y) \, q'_{sh} \, e^{-jq'_{sh}x} \right.$$

$$+ \sum_{\mu=e,o} \int_0^\infty \frac{d\rho}{k_o^2 - \rho^2} V'_{h\mu}(\rho) q'_h \, \psi_{h\mu}(y,\rho) \, e^{-jq'_h x}$$

$$\left. + \int_0^\nu \frac{d\sigma}{\varepsilon_2 k_o^2 - \sigma^2} V'_h(\sigma) \, p'_h \, \psi_h(y,\sigma) \, e^{-jp'_h x} \right]$$

$$- \left[\frac{\beta}{\omega\varepsilon_0} \left[\frac{1}{q'^2_{se} + \beta^2} I'_e \, \partial_y \, \psi_e(y) \, e^{-jq'_{se}x} \right. \right.$$

$$+ \sum_{\mu=e,o} \int_0^\infty \frac{d\rho}{k_o^2 - \rho^2} I'_{e\mu}(\rho) \, \partial_y \, \psi_{e\mu}(y,\rho) \, e^{-jq'_e x}$$

$$\left. \left. + \int_0^\nu \frac{d\sigma}{\varepsilon_2 k_o^2 - \sigma^2} I'_e(\sigma) \, \partial_y \, \psi_e(y,\sigma) \, e^{-jp'_e x} \right] \right]$$

$$= E_z^h + E_z^e \qquad (4.4b)$$

$$H_y(x,y) = \frac{1}{j\omega\mu_0} \left[V'_h \, \psi_h(y) \, e^{-jq'_{sh}x} + \int_0^\nu d\sigma \, V'_h(\sigma) \, \psi_h(y,\sigma) \, e^{-jp'_h x} \right.$$

$$\left. + \sum_{\mu=e,o} \int_0^\infty d\rho \, V'_{h\mu}(\rho) \psi_{h\mu}(y,\rho) \, e^{-jq'_h x} \right] \qquad (4.4c)$$

$$H_z(x,y) = -j \left[\frac{1}{q'^2_{se} + \beta^2} I'_e \, \psi_e(y) \, q'_{se} \, e^{-jq'_{se}x} + \int_0^\nu \frac{d\sigma}{\varepsilon_2 k_o^2 - \sigma^2} I'_e(\sigma) \, p'_e \, \psi_e(y,\sigma) \, e^{-jp'_e x} \right.$$

$$\left. + \sum_{\mu=e,o} \int_0^\infty \frac{d\rho}{k_o^2 - \rho^2} I'_{e\mu}(\rho) \, q'_e \, \psi_{e\mu}(y,\rho) \, e^{-jq'_e x} \right] -$$

$$-\left[\frac{\beta}{\omega\mu_0}\left[\frac{1}{q'^2_{sh}+\beta^2}V'_h\,\partial_y\,\psi_h(y)\,e^{-jq'_{sh}x}\right.\right.$$

$$+\sum_{\mu=e,o}\int_0^\infty \frac{d\rho}{k_o^2-\rho^2}V'_{h\mu}(\rho)\,\partial_y\,\psi_{h\mu}(y,\rho)\,e^{-jq'_h x}$$

$$\left.\left.+\int_0^\nu \frac{d\sigma}{\varepsilon_2 k_o^2-\sigma^2}V'_h(\sigma)\,\partial_y\,\psi_h(y,\sigma)\,e^{-jp'_h x}\right]\right]$$

$$=H_z^h+H_z^e \tag{4.4d}$$

4.23 FORMULATION OF THE INTEGRAL OPERATORS

In the previous sections expressions for the transverse field components in each region on either side of the discontinuous interface have been obtained. In order that the required integral operators can be determined, then two of the transverse field components must be written in terms of the other. Thus we seek in each region integral relationships of the type,

$$\begin{bmatrix} E_z(0,y) \\ -H_z(0,y)\end{bmatrix}=\begin{bmatrix} Z_L & T_L \\ -U_L & Y_L\end{bmatrix}\begin{bmatrix} H_y(0,y) \\ E_y(0,y)\end{bmatrix} \qquad : \text{for } x\le 0 \tag{4.5a}$$

$$\begin{bmatrix} -E_z(0,y) \\ H_z(0,y)\end{bmatrix}=\begin{bmatrix} Z_R & -T_R \\ U_R & Y_R\end{bmatrix}\begin{bmatrix} H_y(0,y) \\ E_y(0,y)\end{bmatrix} \qquad : \text{for } x\ge 0 \tag{4.5b}$$

where the various operators occurring in (4.5) are defined by

$$E_z^h(0,y)=\int_{-\infty}^{\infty} Z(y,y';x=x'=0)\,H_y(0,y')\,dy'$$

$$=\tilde{Z}\cdot H_y(0,y) \tag{4.6}$$

$$E_z^e(0,y) = \int_{-\infty}^{\infty} T(y,y';x=x'=0)\, E_y(0,y')\, dy'$$

$$= \tilde{T} \cdot E_y(0,y) \tag{4.7}$$

$$H_z^h(0,y) = \int_{-\infty}^{\infty} U(y,y';x=x'=0)\, H_y(0,y')\, dy'$$

$$= \tilde{U} \cdot H_y(0,y) \tag{4.8}$$

$$H_z^e(0,y) = \int_{-\infty}^{\infty} Y(y,y';x=x'=0)\, E_y(0,y')\, dy'$$

$$= \tilde{Y} \cdot E_y(0,y) \tag{4.9}$$

In (4.5), the signs are consistent with the power flow in to each region from the interface. The subscripts L and R refer to regions 1 and 2 respectively. $\tilde{Z}$ and $\tilde{Y}$ are the integral operators of the pure LSE and LSM parts of the fields respectively. $\tilde{T}$ and $\tilde{U}$ describe the hybrid part of the field. In order to determine their kernels for each region, we consider equations (4.3) and (4.4). From equations (4.3b) and (4.3c) and by using the orthogonality properties of the mode functions, expressions for V_h, $V_{h\mu}(\rho)$, $V_h(\sigma)$ and I_e, $I_{e\mu}(\rho)$, $I_e(\sigma)$ in terms of H_y and E_y are obtained that are given by,

$$I_e = j\,\omega\,\varepsilon_0 \int_{-\infty}^{\infty} E_y(0,y)\, \phi_e(y)\, dy \tag{4.10a}$$

$$I_{e\mu}(\rho) = j\,\omega\,\varepsilon_0 \int_{-\infty}^{\infty} E_y(0,y)\, \phi_{e\mu}(y,\rho)\, dy \tag{4.10b}$$

$$I_e(\sigma) = j\,\omega\,\varepsilon_0 \int_{-\infty}^{\infty} E_y(0,y)\, \phi_e(y,\sigma)\, dy \tag{4.10c}$$

$$V_h = j\,\omega\,\mu_0 \int_{-\infty}^{\infty} H_y(0,y)\, \phi_h(y)\, dy \tag{4.10d}$$

$$V_{h\mu}(\rho) = j\,\omega\,\varepsilon_0 \int_{-\infty}^{\infty} H_y(0,y)\, \phi_{h\mu}(y,\rho)\, dy \tag{4.10e}$$

$$V_h(\sigma) = j\,\omega\,\varepsilon_0 \int_{-\infty}^{\infty} H_y(0,y)\,\phi_h(y,\sigma)\,dy \tag{4.10f}$$

Similarly, from equations (4.4a) and (4.4c), by using the orthogonality properties of the mode functions we obtain,

$$I'_e = j\,\omega\,\varepsilon_0 \int_{-\infty}^{\infty} E_y(0,y)\,\psi_e(y)\,dy \tag{4.11a}$$

$$I'_{e\mu}(\rho) = j\,\omega\,\varepsilon_0 \int_{-\infty}^{\infty} E_y(0,y)\,\psi_{e\mu}(y,\rho)\,dy \tag{4.11b}$$

$$I'_e(\sigma) = j\,\omega\,\varepsilon_0 \int_{-\infty}^{\infty} E_y(0,y)\,\psi_e(y,\sigma)\,dy \tag{4.11c}$$

$$V'_h = j\,\omega\,\mu_0 \int_{-\infty}^{\infty} H_y(0,y)\,\psi_h(y)\,dy \tag{4.11d}$$

$$V'_{h\mu}(\rho) = j\,\omega\,\varepsilon_0 \int_{-\infty}^{\infty} H_y(0,y)\,\psi_{h\mu}(y,\rho)\,dy \tag{4.11e}$$

$$V'_h(\sigma) = j\,\omega\,\varepsilon_0 \int_{-\infty}^{\infty} H_y(0,y)\,\psi_h(y,\sigma)\,dy \tag{4.11f}$$

The explicit expansion of the integral operator of the pure LSE part of the fields $\tilde{Z}$ was already derived in earlier work and its kernel $Z(y,y')$ for both regions is reproduced here for ease of reference:

$$Z_L(y,y') = \frac{1}{j\omega\varepsilon_0}\left[-\frac{q_{sh}\tan(q_{sh}a)}{\varepsilon_{eh}}\,\phi_h(y)\,\phi_h(y') \right.$$

$$+ \sum_{\mu=e,o} \int_0^{\infty} \frac{d\rho}{1-\dfrac{\rho^2}{k_o^2}}\,\gamma_h \tanh(\gamma_h a)\,\phi_{h\mu}(y,\rho)\,\phi_{h\mu}(y',\rho)$$

$$\left. + \int_0^{\nu} \frac{d\sigma}{\varepsilon_2 - \dfrac{\sigma^2}{k_o^2}}\,\eta_h \tanh(\eta_h a)\,\phi_h(y,\sigma)\,\phi_h(y',\sigma) \right] \tag{4.12}$$

$$Z_R(y,y') = \frac{1}{j\omega\varepsilon_0}\left[\frac{\gamma'_{sh}}{\varepsilon'_{eh}}\psi_h(y)\,\psi_h(y') + \sum_{\mu=e,o}\int_0^{\infty}\frac{d\rho}{1-\frac{\rho^2}{k_o^2}}\gamma'_h\,\psi_{h\mu}(y,\rho)\,\psi_{h\mu}(y',\rho)\right.$$

$$\left. + \int_0^{v}\frac{d\sigma}{\varepsilon_2-\frac{\sigma^2}{k_o^2}}\eta'_h\,\psi_h(y,\sigma)\,\psi_h(y',\sigma)\right] \qquad (4.13)$$

From equations (4.3a) and (4.3d), the field E_z^e, H_z^h and H_z^e for region 1 at $x = 0$ are given by,

$$E_z^e(0,y) = -\frac{\beta}{\omega\varepsilon_o}\left[\frac{1}{q_{se}^2+\beta^2}I_e\,\partial_y\,\phi_e(y) + \sum_{\mu=e,o}\int_0^{\infty}\frac{d\rho}{k_o^2-\rho^2}I_{e\mu}(\rho)\,\partial_y\,\phi_{e\mu}(y,\rho)\right.$$

$$\left. + \int_0^{v}\frac{d\sigma}{\varepsilon_2 k_o^2-\sigma^2}I_e(\sigma)\,\partial_y\,\phi_e(y,\sigma)\right] \qquad (4.14)$$

$$H_z^h(0,y) = -\frac{\beta}{\omega\mu_o}\left[\frac{1}{q_{sh}^2+\beta^2}V_h\,\partial_y\,\phi_h(y) + \sum_{\mu=e,o}\int_0^{\infty}\frac{d\rho}{k_o^2-\rho^2}V_{h\mu}(\rho)\,\partial_y\,\phi_{h\mu}(y,\rho)\right.$$

$$\left. + \int_0^{v}\frac{d\sigma}{\varepsilon_2 k_o^2-\sigma^2}V_h(\sigma)\,\partial_y\,\phi_h(y,\sigma)\right] \qquad (4.15)$$

$$H_z^e(0,y) = \frac{q_{se}}{q_{se}^2+\beta^2}I_e\,cot(q_{se}a)\,\phi_e(y) + \sum_{\mu=e,o}\int_0^{\infty}\frac{d\rho}{k_o^2-\rho^2}I_{e\mu}(\rho)\,\phi_{e\mu}(y,\rho)\,\gamma_e\coth(\gamma_e a)$$

$$+ \int_0^{v}\frac{d\sigma}{\varepsilon_2 k_o^2-\sigma^2}I_e(\sigma)\,\phi_e(y,\sigma)\,\eta_e\coth(\eta_e a) \qquad (4.16)$$

By substituting (4.10a, 4.10b and 4.10c) in to equation (4.14) and equation (4.16) we recover equations (4.7) and (4.9) respectively with their kernels defined by,

$$T_L(y,y') = -j\frac{\beta}{k_o^2}\left[\frac{1}{\varepsilon_{ee}}\phi_e(y')\,\partial_y\,\phi_e(y) + \sum_{\mu=e,o}\int_0^{\infty}\frac{d\rho}{1-\frac{\rho^2}{k_o^2}}\phi_{e\mu}(y',\rho)\,\partial_y\,\phi_{e\mu}(y,\rho)\right.$$

$$\left. + \int_0^{\nu}\frac{d\sigma}{\varepsilon_2-\frac{\sigma^2}{k_o^2}}\phi_e(y',\sigma)\,\partial_y\,\phi_e(y,\sigma)\right] \qquad (4.17)$$

and

$$Y_L(y,y') = \frac{1}{j\omega\mu_0}\left[\frac{q_{se}\,cot(q_{se}a)}{\varepsilon_{ee}}\phi_e(y)\,\phi_e(y')\right.$$

$$+ \sum_{\mu=e,o}\int_0^{\infty}\frac{d\rho}{1-\frac{\rho^2}{k_o^2}}\gamma_e\coth(\gamma_e a)\,\phi_{e\mu}(y,\rho)\,\phi_{e\mu}(y',\rho)$$

$$\left. + \int_0^{\nu}\frac{d\sigma}{\varepsilon_2-\frac{\sigma^2}{k_o^2}}\eta_e\coth(\eta_e a)\,\phi_e(y,\sigma)\,\phi_e(y',\sigma)\right] \qquad (4.18)$$

Similarly substituting (4.10d, 4.10e and 4.10f) in to equation (4.15) we recover equation (4.8) with its kernel defined by,

$$U_L(y,y') = -j\frac{\beta}{k_o^2}\left[\frac{1}{\varepsilon_{eh}}\phi_h(y')\,\partial_y\,\phi_h(y) + \sum_{\mu=e,o}\int_0^{\infty}\frac{d\rho}{1-\frac{\rho^2}{k_o^2}}\phi_{h\mu}(y',\rho)\,\partial_y\,\phi_{h\mu}(y,\rho)\right.$$

$$\left. + \int_0^{\nu}\frac{d\sigma}{\varepsilon_2-\frac{\sigma^2}{k_o^2}}\phi_h(y',\sigma)\,\partial_y\,\phi_h(y,\sigma)\right] \qquad (4.19)$$

The explicit expression of Y, T and U for region 2 are found by analogous procedure. Upon substituting (4.11) in to (4.4) we obtain their kernels given by,

$$Y_R(y,y') = \frac{1}{j\omega\mu_0}\left[\frac{\gamma'_{se}}{\varepsilon'_{ee}}\psi_e(y)\,\psi_e(y') + \sum_{\mu=e,o}\int_0^{\infty}\frac{d\rho}{1-\frac{\rho^2}{k_o^2}}\gamma_e\,\psi_{e\mu}(y,\rho)\,\psi_{e\mu}(y',\rho)\right.$$

$$\left. + \int_0^{v}\frac{d\sigma}{\varepsilon_2-\frac{\sigma^2}{k_o^2}}\eta_e\,\psi_e(y,\sigma)\,\psi_e(y',\sigma)\right] \qquad (4.20)$$

$$T_R(y,y') = -j\frac{\beta}{k_o^2}\left[\frac{1}{\varepsilon'_{ee}}\psi_e(y')\,\partial_y\,\psi_e(y) + \sum_{\mu=e,o}\int_0^{\infty}\frac{d\rho}{1-\frac{\rho^2}{k_o^2}}\psi_{e\mu}(y',\rho)\,\partial_y\,\psi_{e\mu}(y,\rho)\right.$$

$$\left. + \int_0^{v}\frac{d\sigma}{\varepsilon_2-\frac{\sigma^2}{k_o^2}}\psi_e(y',\sigma)\,\partial_y\,\psi_e(y,\sigma)\right] \qquad (4.21)$$

$$U_R(y,y') = -j\frac{\beta}{k_o^2}\left[\frac{1}{\varepsilon'_{eh}}\psi_h(y')\,\partial_y\,\psi_h(y) + \sum_{\mu=e,o}\int_0^{\infty}\frac{d\rho}{1-\frac{\rho^2}{k_o^2}}\psi_{h\mu}(y',\rho)\,\partial_y\,\psi_{h\mu}(y,\rho)\right.$$

$$\left. + \int_0^{v}\frac{d\sigma}{\varepsilon_2-\frac{\sigma^2}{k_o^2}}\psi_h(y',\sigma)\,\partial_y\,\psi_h(y,\sigma)\right] \qquad (4.22)$$

It can be seen that T and U at either side of the discontinuity are functionally the same apart from the different modal functions and effective dielectric constant ε_e at each side.

4.3 DISPERSION EQUATION

Having derived the integral operator occurring in the coupled integral equation (4.5), we are now in a position to apply continuity of the transverse fields at the discontinuous interface $x = 0$.

Rewriting equation (4.5),

$$\begin{bmatrix} E_z(0,y) \\ -H_z(0,y) \end{bmatrix} = \begin{bmatrix} Z_L & T_L \\ -U_L & Y_L \end{bmatrix} \begin{bmatrix} H_y(0,y) \\ E_y(0,y) \end{bmatrix} \tag{4.5a}$$

$$\begin{bmatrix} -E_z(0,y) \\ H_z(0,y) \end{bmatrix} = \begin{bmatrix} Z_R & -T_R \\ U_R & Y_R \end{bmatrix} \begin{bmatrix} H_y(0,y) \\ E_y(0,y) \end{bmatrix} \tag{4.5b}$$

continuity of the transverse fields at the interface gives an integral equation in the unknowns $H_y(0,y)$, $E_y(0,y)$. By adding (4.5a and 4.5b), we obtain

$$\begin{bmatrix} Z & T \\ -U & Y \end{bmatrix} \begin{bmatrix} H_y(0,y) \\ E_y(0,y) \end{bmatrix} = 0 \tag{4.23}$$

where

$$Z = Z_L + Z_R$$

$$Y = Y_L + Y_R$$

$$T = T_L - T_R$$

$$U = U_L - U_R$$

It is noted in the continuity equation (4.23) that the off - diagonal terms, giving rise to the hybrid part of the field, contain the differences between the contributions left and right of the step at $x = 0$. Hence, they vanish rapidly for decreasing step height. Neglecting these terms altogether, the separate even LSE and odd LSM cases are recovered.

The integral equation (4.23) can be solved by Galerkin's method by expanding the unknown $H_y(y)$ and $E_y(y)$ in terms of two sets of suitable basis functions. This will transform the integral equation in to a matrix equation, from which the propagation constant β can be solved. The choice of a suitable finite expanding set was already discussed in chapter three and, in fact, for this particular problem none is readily available if the edge condition is to be satisfied. Satisfaction of the edge condition is of paramount important if rapid convergence of the solution is to be achieved without excessive computational effort. In order to reduce the computational effort by avoiding the use of large matrices, we employ here a single trial function in order to expand the

unknown fields. The choice of a suitable function was already discussed in the approximate analysis in chapter three and there it was shown that the transition functions, $\overline{U}_{sh}(y)$ and $\overline{U}_{se}(y)$ inclusive of the edge singularities provide an accurate trial functions to expand H_y and E_y respectively. Upon substituting $\overline{U}_{sh}(y)$ and $\overline{U}_{se}(y)$ for the fields in (4.23) we obtain,

$$Z = \frac{1}{j\omega\varepsilon_0}\left[-\frac{q_{sh}\tan(q_{sh}a)}{\varepsilon_{eh}} P_h^2 + \frac{\gamma'_{sh}}{\varepsilon'_{eh}} P_h'^2 \right.$$
$$+ \sum_{\mu=e,o} \int_0^{\infty} \frac{d\rho}{1-\frac{\rho^2}{k_o^2}} \gamma_h \left[\tanh(\gamma_h a)\, P_{h\mu}^2(\rho) + P_{h\mu}'^2(\rho) \right]$$
$$\left. + \int_0^{\nu} \frac{d\sigma}{\varepsilon_2 - \frac{\sigma^2}{k_o^2}} \eta_h \left[\tanh(\eta_h a)\, P_h^2(\sigma) + P_h'^2 \right] \right] \tag{4.24}$$

$$Y = \frac{1}{j\omega\mu_0}\left[\frac{q_{se}\cot(q_{se}a)}{\varepsilon_{ee}} P_e^2 + \frac{\gamma'_{se}}{\varepsilon'_{ee}} P_e'^2 \right.$$
$$+ \sum_{\mu=e,o} \int_0^{\infty} \frac{d\rho}{1-\frac{\rho^2}{k_o^2}} \gamma_e \left[\coth(\gamma_e a)\, P_{e\mu}^2(\rho) + P_{e\mu}'^2(\rho) \right]$$
$$\left. + \int_0^{\nu} \frac{d\sigma}{\varepsilon_2 - \frac{\sigma^2}{k_o^2}} \eta_e \left[\coth(\eta_e a)\, P_e^2(\sigma) + P_e'^2 \right] \right] \tag{4.25}$$

$$T = -j\frac{\beta}{k_o^2}\left[\frac{1}{\varepsilon_{ee}} P_e\, Q_{eh} - \frac{1}{\varepsilon'_{ee}} P'_e\, Q'_{eh} \right.$$
$$+ \sum_{\mu=e,o} \int_0^{\infty} \frac{d\rho}{1-\frac{\rho^2}{k_o^2}} \left[P_e(\rho)\, Q_{eh}(\rho) - P'_e(\rho)\, Q'_{eh}(\rho) \right]$$
$$\left. + \int_0^{\nu} \frac{d\sigma}{\varepsilon_2 - \frac{\sigma^2}{k_o^2}} \left[P_e(\sigma)\, Q_{eh} - P'_e(\sigma)\, Q'_{eh}(\sigma) \right] \right] \tag{4.26}$$

$$U = -j\frac{\beta}{k_o^2}\left[\frac{1}{\varepsilon_{eh}}P_h Q_{he} - \frac{1}{\varepsilon'_{eh}}P'_h Q'_{he}\right.$$

$$+\sum_{\mu=e,o}\int_0^{\infty}\frac{d\rho}{1-\frac{\rho^2}{k_o^2}}\left[P_h(\rho)\,Q_{he}(\rho) - P'_h(\rho)\,Q'_{he}(\rho)\right]$$

$$\left.+\int_0^{\nu}\frac{d\sigma}{\varepsilon_2-\frac{\sigma^2}{k_o^2}}\left[P_h(\sigma)\,Q_{he} - P'_h(\sigma)\,Q'_{eh}(\sigma)\right]\right] \qquad (4.27)$$

where, P_h's and P_e's are defined as before in chapter three, and Q's are given by

$$Q_{he} = <\bar{U}_{se}\,,\,\partial_y\,\phi_h> \qquad (4.28a)$$

$$Q'_{he} = <\bar{U}_{se}\,,\,\partial_y\,\psi_h> \qquad (4.28b)$$

$$Q_{eh} = <\bar{U}_{sh}\,,\,\partial_y\,\phi_e> \qquad (4.28c)$$

$$Q'_{eh} = <\bar{U}_{sh}\,,\,\partial_y\,\psi_h> \qquad (4.28d)$$

It is noted that equation (4.23) is, in fact, the dispersion relation for the hybrid bound modes of the rib waveguide. In order to solve for β we may derive the equivalent impedance representation $\underline{\underline{Z}}$ of the matrix in equation (4.23). The matrix $\underline{\underline{Z}}$ represent the total impedance looking to the left and right of the discontinuous interface. This matrix equation has a non trivial solution when $\det\left[\underline{\underline{Z}}\right] = 0$.

Although equation (4.23) is sufficient to solve for β, nevertheless, the formulation does not result in a scalar transverse equivalent circuit. In order to recover a scalar transverse equivalent circuit, it is convenient to reformulate the continuity equation prior to expanding the unknown fields. Considering the slab surface mode of region 2 (if any) and the continuous modes in both regions to be excited by the fundamental mode incident on the discontinous interface $x = 0$, then it is possible to isolate the fundamental mode terms from (4.23) and lump together all the other terms to give

$$-\frac{1}{\varepsilon_{eh}k_o^2}V_h\phi_h(y)q_{hs}\tan(q_{hs}a) + \frac{\beta}{\omega\varepsilon_0}\frac{1}{\varepsilon_{ee}k_o^2}I_e\partial_y\phi_e(y) = \tilde{Z}' + \tilde{T}' \qquad (4.29a)$$

$$-\frac{\beta}{\omega\mu_0}\frac{1}{\varepsilon_{eh}k_o^2}V_h\partial_y\phi_h(y)+\frac{1}{\varepsilon_{ee}k_o^2}I_e\phi_e(y)q_{es}\,cot(q_{es}a)=-\tilde{U}'+\tilde{Y}' \tag{4.29b}$$

where $\tilde{Z}'$, $\tilde{T}'$, $\tilde{U}'$ and $\tilde{Y}'$ are operators with contribution of the surface mode term for $x<0$ removed. Thus we seek for a relationship between voltages and currents at $x=0$ of the type

$$\begin{bmatrix} -I_h \\ V_e \end{bmatrix} = \underline{\underline{G}} \begin{bmatrix} V_h \\ -I_e \end{bmatrix} \tag{4.30}$$

The variational expressions for the elements of the matrix $\underline{\underline{G}}$ in (4.30) are derived from (4.29). Using (4.10a) and (4.10d) the quantities V_e and I_h are introduced to the left hand side of equation (4.29), which gives

$$\frac{V_h}{-I_h}\phi_h(y)\int_{-\infty}^{\infty}H_y\phi_h(y)dy+\frac{-I_e}{-I_h}\frac{j\beta}{\omega^2\varepsilon_0^2\varepsilon_{ee}Z_h}\partial_y\phi_e(y)\int_{-\infty}^{\infty}H_y\phi_h(y)dy=\tilde{Z}'+\tilde{T}' \tag{4.31a}$$

$$-\frac{V_h}{V_e}\frac{j\beta Z_e}{\omega^2\mu_0^2\varepsilon_{eh}}\partial_y\phi_h(y)\int_{-\infty}^{\infty}E_y\phi_e(y)+\frac{-I_e}{V_e}\phi_e(y)\int_{-\infty}^{\infty}E_y\phi_e(y)dy=-\tilde{U}'+\tilde{Y}' \tag{4.31b}$$

where,

$$Z_h=\frac{j\omega\mu_0 q_{hs}\tan(q_{hs}a)}{\varepsilon_{eh}k_o^2} \tag{4.32a}$$

$$Z_e=\frac{j\varepsilon_{ee}k_o^2\tan(q_{es}a)}{\omega\varepsilon_0 q_{es}} \tag{4.32b}$$

Now, equation (4.31a) is multiplied throught by H_y and (4.31b) by E_y and both equations are integrated over y. Expanding E_y and H_y using a single trial function $\overline{U}_{se}$ and $\overline{U}_{sh}$ respectively, gives

$$\frac{V_h}{-I_h}P_h^2+\frac{-I_e}{-I_h}S_eP_h=Z'+T' \tag{4.33a}$$

$$\frac{V_h}{V_e}S_hP_e+\frac{-I_e}{V_e}P_e^2=-U'+Y' \tag{4.33b}$$

where,

$$S_e = \frac{j\beta}{\omega^2 \varepsilon_0^2 \varepsilon_{ee} Z_h} Q_{eh}$$

$$S_h = \frac{-j\beta Z_e}{\omega^2 \mu_0^2 \varepsilon_{eh}} Q_{he}$$

The equivalent network model define by equation (4.30) is shown in Fig. 4.2 . The equivalent impedance representation of the network to the right of $x = 0$ may be derived from the $\underline{\underline{G}}$ matrix , given by

$$\begin{bmatrix} V_h \\ V_e \end{bmatrix} = \begin{bmatrix} Z_{11} & Z_{12} \\ Z_{21} & Z_{22} \end{bmatrix} \begin{bmatrix} -I_h \\ -I_e \end{bmatrix}$$

$$= \underline{\underline{\vec{Z}}} \cdot \begin{bmatrix} -I_h \\ -I_e \end{bmatrix} \qquad (4.34)$$

Looking to the left of $x = 0$, we may write the relationship between V and I given by

$$\begin{bmatrix} V_h \\ V_e \end{bmatrix} = \begin{bmatrix} Z_h & 0 \\ 0 & Z_e \end{bmatrix} \begin{bmatrix} I_h \\ I_e \end{bmatrix} \qquad (4.35)$$

Upon comparing equations (4.34) and (4.35), one obtains

$$\left[\underline{\underline{\overleftarrow{Z}}} + \underline{\underline{\vec{Z}}} \right] \left[\underline{I} \right] = 0$$

Non trivial solutions of the matrix equation yield the dispersion relation

$$\det \left[\underline{\underline{\leftrightarrow}} \right] = 0 \qquad (4.36)$$

4.4 NUMERICAL RESULTS

The theory developed in the previous section is used to investigate the dispersion characteristics of rib waveguide whose parameters are identical to those used in the approximate analysis. Fig. 4.3 and Fig. 4.4 show theoretical dispersion curves for formulation with an electric wall at the plane of symmetry $x = -a$. The dispersion curve for the pure LSE polarization is also shown in the figures. It can be seen that the results of the hybrid and pure LSE analysis overlap quite well. This shows that the hybrid content of the fields for the structure considered is very small. This observation is not

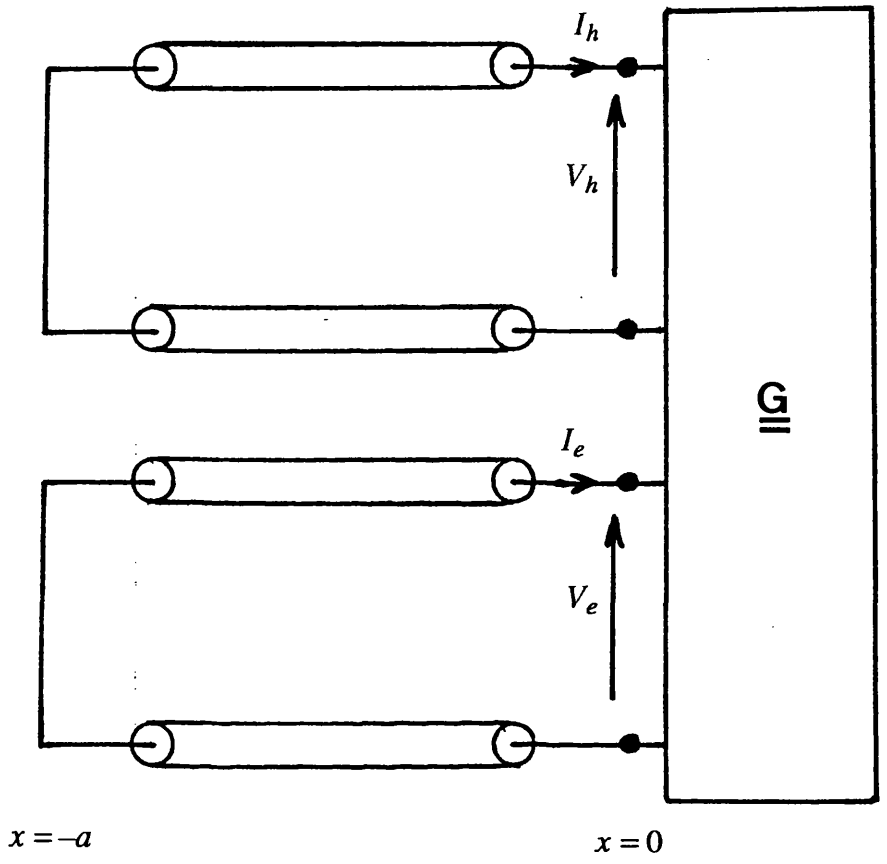

Fig. 4.2 Scalar transverse equivalent network.

surprising because it was shown in chapter three that the result of LSE approximation is already very accurate compared with the results of vector finite element method [1]. Hence, in this case the fields of the rib waveguide can be accurately represented by five field LSE polarization. Fig. 4.5 shows theoretical dispersion results with a magnetic wall placed at $x = -a$, along with results of the pure LSM polarization. Here too the hybrid content of the fields is small even for large step and, consequently, the electromagnetic field of the structure may be conviniently described by pure LSM polarization without significant error.

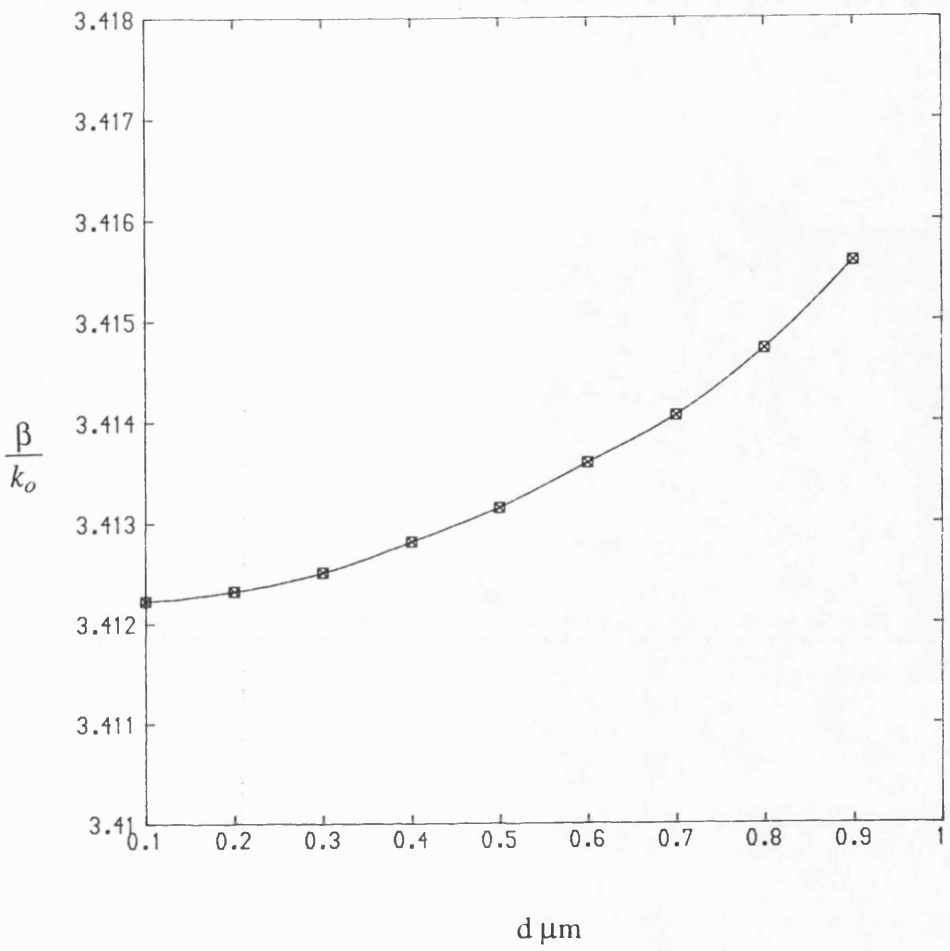

Fig. 4.3 Normalised propagation constant for the fundamental mode as a function of outer slab height d.

$n_1 = 3.44$, $n_2 = 3.40$, $n_3 = 1.0$, $\lambda = 1.15\mu m$, $2a = 3.0\mu m$, $D = 1.0\mu m$

× Hybrid Analysis

○ LSE Analysis

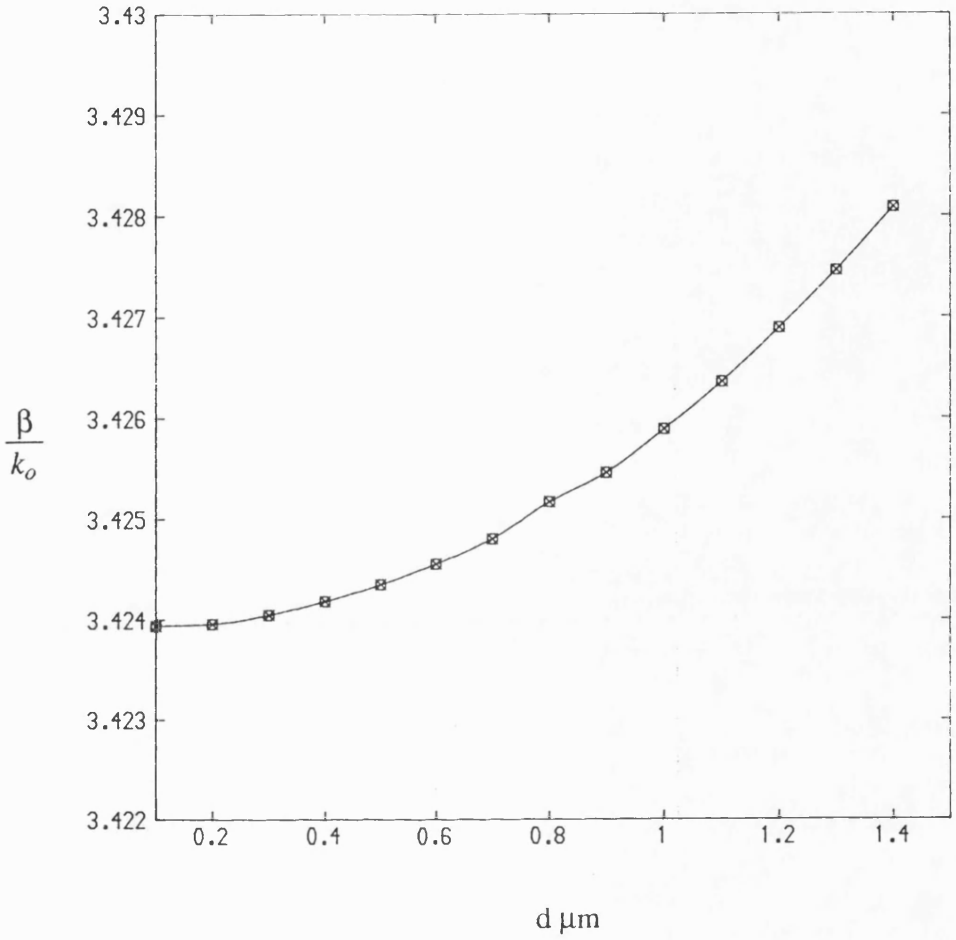

Fig. 4.4 Normalised propagation constant for the fundamental mode
as a function of outer slab height d.
$n_1 = 3.4406$, $n_2 = 3.4145$, $n_3 = 1.0$, $\lambda = 1.15\mu m$, $2a = 3.0\mu m$, $D = 1.5\mu m$

✘ Hybrid Analysis

○ LSE Analysis

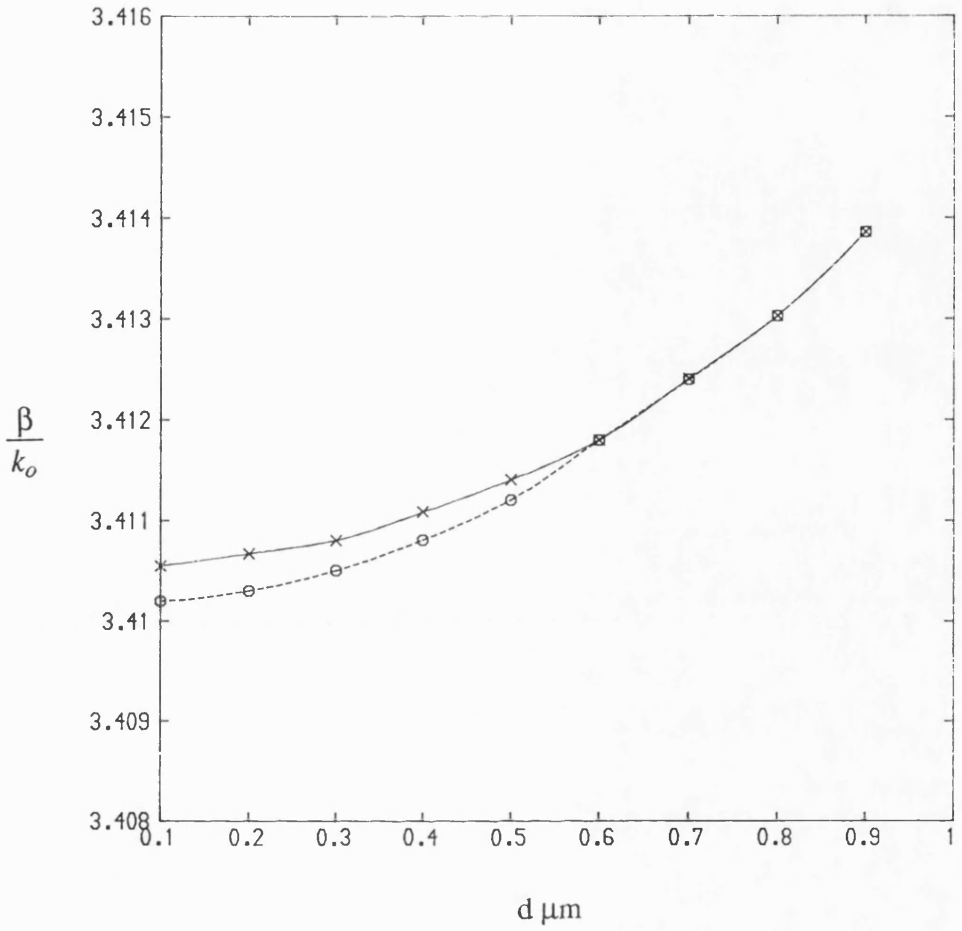

Fig. 4.5 Normalised propagation constant for the fundamental mode as a function of outer slab height d.

$n_1 = 3.44$, $n_2 = 3.40$, $n_3 = 1.0$, $\lambda = 1.15\mu m$, $2a = 3.0\mu m$, $D = 1.0\mu m$

x Hybrid Analysis

O LSM Analysis

REFERENCES

[1] B.M.A. Rahman, J.B. Davies, " Vector H finite element solution of Ga As/Ga Al As rib waveguides ", I.E.E Proc., vol. 132, Pt. J, Dec. 1985, pp 349-353.

CHAPTER 5

THEORETICAL STUDY OF COUPLED RIB WAVEGUIDES

5.1 INTRODUCTION

The electromagnetic field of a bound mode of a rib waveguide extends in to the region surrounding the rib. Thus, if two rib waveguides are placed in close proximity, energy couples from one waveguide to the other. Coupled structures play a very important role in the field of millimetre waves and integrated optics. Arrays of coupled dielectric antennas are interesting for millimetric applications. As already been mentioned in chapter 1, many optical devices may be realized using coupled rib guides. The feasibility of fabricating such devices using coupled guides has been demonstrated. Furthermore, the near field and propagation characteristics of laser arrays formed with coupled rib waveguides are already of great practical importance in integrated optics. As a consequence, accurate theoretical analyses of coupled structures are essential to the design of devices that meet specific requirements and criteria.

There are no truly exact analytical method available for the analysis of coupled rib waveguides. Approximate methods currently in use have mostly relied on either the EDC method [1,2], or coupled mode theory which is appropriate for weakly coupled systems [3]. The approach in [3] assumes the individual guide modes to be orthogonal in the coupled structure. An improved coupled mode theory [4,5] which removes the assumption is also available, but the approach is still an approximate one and it may not produce accurate results for practical structures. In fact, the EDC and the coupled mode theory fail to model the effects arising from leakage of energy via the substrate and the air regions, particularly in the millimetric case. These effects may also be significant at optical frequencies, particularly if the rib height is large where the interaction effects via the continuum cannot be neglected. For more accurate results, sophisticated numerical

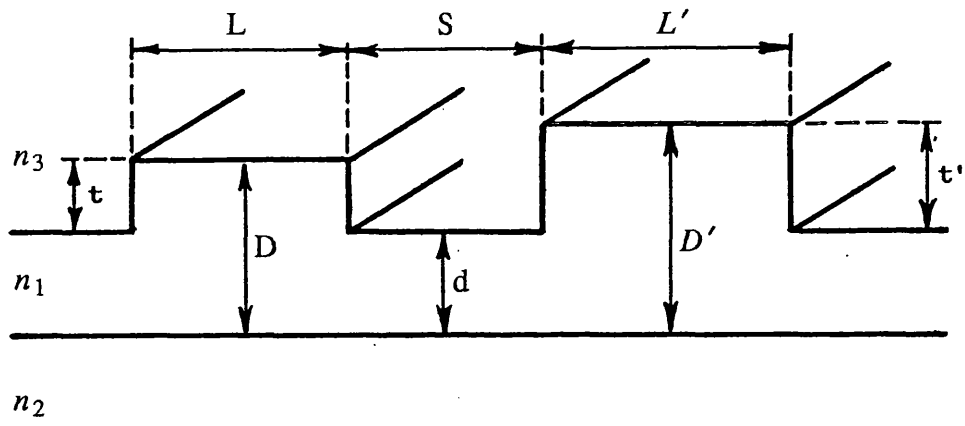

Fig. 5.1 Geometry of the coupled rib waveguides.

techniques such as Finite Element Method or Finite Difference Method are used [6]. The most important drawbacks of this approach, discussed in chapter 2, is the excessive computational effort needed for accurate results, as the area and hence the number of mesh points is doubled with respect to that needed to analyse a single guide. Moreover, FEM/FDM become extremely cumbersome for situations more complex than that of two identical closely coupled guides, as shown for instance in Fig. 5.1 . This is the typical problem we are addressing rigorously in this chapter. We develop a method of analysis of coupled rib waveguides in the pure LSE and LSM polarizations. The approach adopted in this work is consistent with that used in chapter 3 for a single guide. The analysis is followed by application to the case of the directional coupler, three guide coupler, closely spaced unequal guide and waveguide arrays. Wherever possible, results of the present method and of the FEM/FDM analysis are compared to demonstrate the effectiveness and the accuracy of the method. As will be shown, the method of analysis presented in this work yields accurate results with a computational effort only slightly greater than that needed to analyse a single guide according to chapter 3.

5.2 THEORETICAL APPROACH AND EQUIVALENT NETWORK

The cross sectional geometry of coupled rib waveguides under consideration is shown in Fig. 5.1 . In the framework of Transverse Resonance Diffraction (TRD), this configuration is seen as that of four cascaded step discontinuities in the transverse direction. Our aim is to derive a variational solution of the step problems that utilizes a single test function , the "transition function" developed in chapter 3, in order to expand the unknown interface field. Using a single test function at the interface yields a simple two port equivalent network representation of the coupled structure such as shown in Fig. 5.2 . Consequently, the analysis of the transverse cascade reduces to that of solving the two port network, which is easily effected by standard network technique.

In order to derive the variational expression for the parameters of the two port network

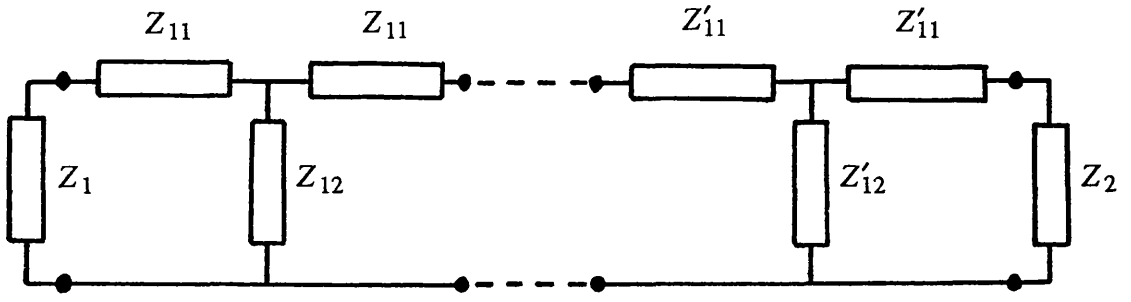

(a)

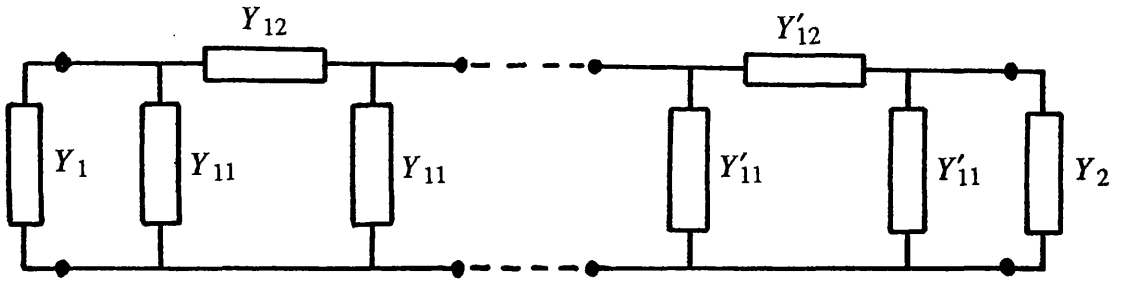

(b)

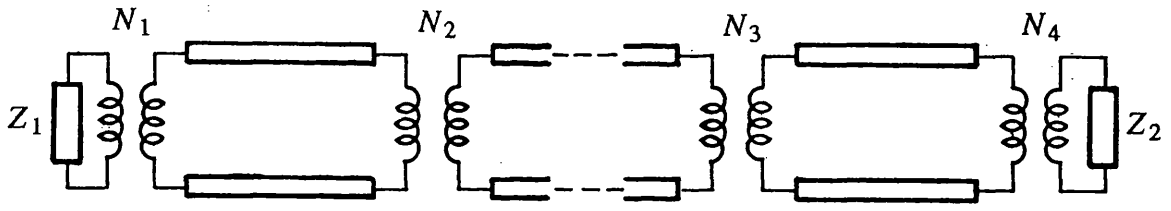

(c)

Fig. 5.2 Equivalent network representation of the coupled structure:
a) LSE case ; b) LSM case ; c) Neglecting interaction via continuous modes.

shown in Fig. 5.2, let consider the cross sectional geometry of Fig. 5.3 which represent the basic building component of the coupled structure in Fig. 5.1 . In this case, the analysis is complicated by the presence of the double step discontinuities at $x = 0$ and $x = L$. Considering the transverse propagation of LSE or LSM modes in such a structure, at each step discontinuity, continuous modes are excited and multiple reflections of these modes occur between the two steps. In applying standard Transverse Resonance to this situation, interaction via the continuous modes is ignored, i.e. a small step approximation is assumed. If this is done, then the uniform region and the step discontinuity can be represented by a transmission line and ideal transformer respectively. Interaction via the continuum between the steps at $x = 0$ and $x = L$ of Fig. 5.3 , however, is not representable by means of a finite number of transmission lines coupled at the discontinuities, as in a closed waveguides. Hence , in this work we adopt a "two-port" black-box representation of each region between two-successive steps. Its open-circuit impedance or short-circuit admittance parameters are obtained by placing a magnetic or electric wall at $x = 0$ and $x = L$ in turn. Under "open circuit" or "short circuit" conditions at $x = 0$ and $x = L$, integral operators are found relating the total E and H fields at various ports and then these are used to relate the total fields at each port to one another. This operator method was introduced by Rozzi in the treatment of cascaded longitudinal step discontinuities in slab waveguides [7]. In that approach a variational expression was derived and the field at each interface was developed in terms of a suitable set of expanding functions and multiport analysis was finally used to model the cascade. Although those concepts seem directly applicable to the present problem, numerical effectiveness in solving a transverse resonance equation would be limited by the size of the network matrix, containing integrals over the continuum in each element. Moreover, the interface fields in the longitudinal step discontinuities are complex and consequently a complex trial field is needed to accurately expand them. Hence, a solution based on Galerkin's method is more appropriate to that situation. By contrast, in the present problem, losslessness of the bound mode requires the interface fields at the

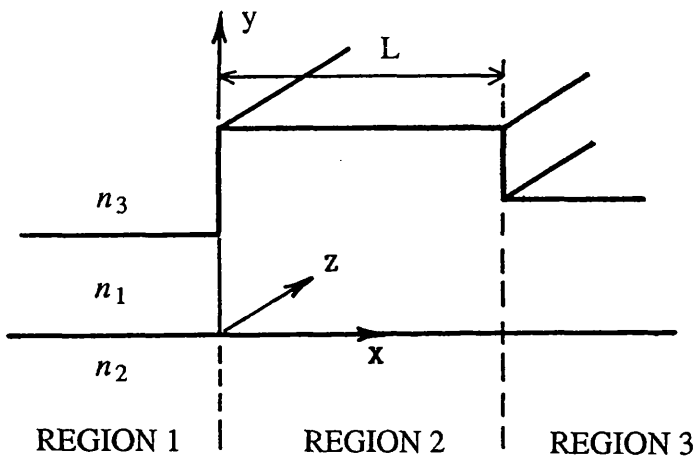

Fig. 5.3 Unit cell of the coupled structure showing double step discontinuity in the transverse x-direction.

transverse step discontinuities to be real. This suggests that the interface field be represented by a suitable real function. In this work, the interface field is approximated by a single "transition function", inclusive of the edge conditions in the LSM case as in chapter 3. As a consequence the numerical complexity of the problem is substantially reduced , avoiding the use of large matrices. Furthermore, as a five field model is considered, this formulation leads to an equivalent network model of the structure represented by a cascade of "T" or "π" two port networks as shown in Fig. 5.2.

5.21 LSE ANALYSIS

The derivation of variational expressions for the parameters of the network shown in Fig. 5.2 follows closely that given in chapter3. Consider the situation where slabs 1 and 3 of Fig. 5.3 are semi - infinite. The relationship between the transverse electric E (z - directed) and the transverse magnetic field H (y - directed) at $x = 0^-$ is given by,

$$E(0,y) = -\int_{-\infty}^{\infty} Z_1(y,y') \left[-H(0,y') \right] dy'$$

$$\equiv -\hat{Z}_1 \left[-H(0,y') \right] \tag{5.1}$$

where

$$Z_1(y,y') = -\left[z_{o1}\, \psi_{h1}(y)\, \psi_{h1}(y') + \sum_{\mu=e,o} \int_0^{\infty} d\rho\, z_{o1}(\rho)\, \psi_{h\mu 1}(y,\rho)\, \psi_{h\mu 1}(y',\rho) \right.$$

$$\left. + \int_0^{\nu} d\sigma\, z_{o1}(\sigma)\, \psi_{h1}(y,\sigma)\, \psi_{h1}(y'\sigma) \right] \tag{5.2}$$

$Z_1(y,y')$ is the Green's impedance function of the semi - infinite slab 1. $\psi_{h1}(y)$ is the modal field of the surface wave with characteristic impedance z_{o1}; $\psi_{h\mu 1}(y,\rho)$ and $\psi_{h1}(y,\sigma)$ represent the air and substrate mode with characteristic impedance $z_{o1}(\rho)$ and $z_{o1}(\sigma)$ respectively.

Similarly at $x = L$, we have

$$E(L,y) = \int_{-\infty}^{\infty} Z_3(y,y') \left[-H(L,y') \right] dy'$$

$$\equiv \hat{Z}_3 \left[-H(L,y') \right] \tag{5.3}$$

where

$$Z_3(y,y') = z_{o3}\, \psi_{h3}(y)\, \psi_{h3}(y') + \sum_{\mu=e,o} \int_0^{\infty} d\rho\, z_{o3}(\rho)\, \psi_{h\mu 3}(y,\rho)\, \psi_{h\mu 3}(y',\rho)$$

$$+ \int_0^{\nu} d\sigma\, z_{o3}(\sigma)\, \psi_{h3}(y,\sigma)\, \psi_{h3}(y',\sigma) \tag{5.4}$$

$Z_3(y,y')$ is the Green's impedance function of the semi - infinite slab 3. $\psi_{h3}(y)$ is the modal field of the surface wave with characteristic impedance z_{o3}; $\psi_{h\mu 3}(y,\rho)$ and $\psi_{h3}(y,\sigma)$ represent the air and substrate mode with characteristic impedance $z_{o3}(\rho)$ and $z_{o3}(\sigma)$ respectively. The characteristic impedance for air and substrate mode for slab 1 and 3 are the same given by

$$z_{o1}(\rho) = z_{o3}(\rho) = z_o(\rho)$$

$$z_{o1}(\sigma) = z_{o3}(\sigma) = z_o(\sigma)$$

$\hat{Z}_1$ and $\hat{Z}_3$ can be viewed as the driving - point impedance operators of the semi - infinite slab 1 and 3. In order to relate the total fields at $x = 0$ and $x = L$ a magnetic wall is placed at $x = 0$ and $x = L$ in turn and the relationship between the transverse E and transverse H field for each condition is derived. With a magnetic wall at $x = L$, the transverse electric field E(0,y) excited by magnetic field H(0,y) is given by

$$E(0,y) = \int_{-\infty}^{\infty} Z_{11}(y,y') \left[-H(0,y') \right] dy'$$

$$\equiv \hat{Z}_{11} \left[-H(0,y') \right] \tag{5.5}$$

where

$$Z_{11}(y,y') = z_{o2}\coth(\gamma_{sh2})\,\phi_{h2}(y)\,\phi_{h2}(y')$$

$$+\sum_{\mu=e,o}\int_0^\infty d\rho\, z_o(\rho)\coth(\gamma_h L)\,\phi_{h\mu 2}(y,\rho)\,\phi_{h\mu 2}(y',\rho)$$

$$+\int_0^\nu d\sigma\, z_o(\sigma)\coth(\eta_h L)\,\phi_{h2}(y,\sigma)\,\phi_{h2}(y',\sigma) \qquad (5.6)$$

Moreover, under the same boundary conditions, we have

$$E(L,y) = \int_{-\infty}^{\infty} Z_{21}(y,y')\left[-H(0,y')\right]dy'$$

$$\equiv \hat{Z}_{21}\left[-H(0,y)\right] \qquad (5.7)$$

where

$$Z_{21}(y,y') = z_{o2}\,cosech(\gamma_{sh2}L)\,\phi_{h2}(y)\,\phi_{h2}(y')$$

$$+\sum_{\mu=e,o}\int_0^\infty d\rho\, z_o(\rho)\,cosech(\gamma_h L)\,\phi_{h\mu 2}(y,\rho)\,\phi_{h\mu 2}(y',\rho)$$

$$+\int_0^\nu d\sigma\, z_o(\sigma)\,cosech(\eta_h L)\,\phi_{h2}(y,\sigma)\,\phi_{h2}(y',\sigma) \qquad (5.8)$$

When a magnetic wall is placed at $x = 0$, we have by symmetry

$$E(L,y) \equiv -\hat{Z}_{22}\left[-H(L,y)\right] \qquad (5.9)$$

and

$$E(0,y) \equiv \hat{Z}_{12}\left[-H(L,y)\right] \qquad (5.10)$$

where $\hat{Z}_{22} = -\hat{Z}_{11}$ and $\hat{Z}_{12} = -\hat{Z}_{21}$

Combining equations (5.5), (5.7), (5.9), and (5.10) we obtain a "two port" Green's open circuit impedance operator for the section $0 \le x \le L$ given by,

$$\begin{bmatrix} E(0,y) \\ E(L,y) \end{bmatrix} = \begin{bmatrix} \hat{Z}_{11} & -\hat{Z}_{21} \\ \hat{Z}_{21} & -\hat{Z}_{11} \end{bmatrix} \begin{bmatrix} -H(0,y) \\ -H(L,y) \end{bmatrix} \qquad (5.11)$$

In (5.2), (5.4), (5,6), and (5.8) we have implicitly assumed that just one surface wave (in

y) may be supported by the slab waveguide, and the various values of characteristic impedances are given by

$$z_{o1} = \frac{j\omega\mu_0\gamma_{sh1}}{\beta^2 - \gamma_{sh1}^2} \quad ; z_{o3} = \frac{j\omega\mu_0\gamma_{sh3}}{\beta^2 - \gamma_{sh3}^2} \quad ; z_{o2} = \frac{j\omega\mu_0\gamma_{sh2}}{\beta^2 - \gamma_{sh2}^2}$$

$$z_o(\rho) = \frac{j\omega\mu_0\gamma_h}{k_o^2 - \rho^2} \quad ; z_o(\sigma) = \frac{j\omega\mu_0\eta_h}{\varepsilon_2 k_o^2 - \sigma^2}$$

$$\varepsilon_{eh1}k_o^2 - \beta^2 = -\gamma_{sh1}^2 \quad ; \varepsilon_{eh2}k_o^2 - \beta^2 = -\gamma_{sh2}^2 \quad ; \varepsilon_{eh3}k_o^2 - \beta^2 = -\gamma_{sh3}^2$$

$$k_o^2 - \beta^2 - \rho^2 = -\gamma_h^2 \quad ; \varepsilon_2 k_o^2 - \beta^2 - \sigma^2 = -\eta_h^2 \quad ; \nu = k_o\sqrt{\varepsilon_2 - \varepsilon_3}$$

Having obtained the two port impedance operators for each uniform section of the waveguide as given by (5.11), we are now in a position to consider the cascade of steps in Fig. 5.1 . From (5.11) the relationship between the transverse fields at x_i and x_{i+1} can be written as,

$$\begin{bmatrix} E(x_i,y) \\ E(x_{i+1},y) \end{bmatrix} = \begin{bmatrix} \hat{Z}_{11}^{(i)} & -\hat{Z}_{21}^{(i)} \\ \hat{Z}_{21}^{(i)} & -\hat{Z}_{11}^{(i)} \end{bmatrix} \begin{bmatrix} -H(x_i,y) \\ -H(x_{i+1},y) \end{bmatrix} \tag{5.12}$$

If the continuity of the transverse fields is translated in to the continuity of voltages and currents at the interface plane x_i and the interface field is approximated by a scalar function, then the cascade of steps in Fig. 5.1 can be represented by an equivalent "T" network shown in Fig. 5.2a . In this formulation the interaction via the propagating air and substrate modes between non adjacent discontinuities is built in to the model, as $E(x_i,y)$ in (5.12) represents the total transverse field at x_i. If we disregard interaction via propagating continuum modes, then the equivalent network reduces to that of Fig. 5.2c . The application of this theory to the analysis of coupled and multiple coupled guides will be treated in section 5.3 .

5.22 LSM ANALYSIS

By placing an electric wall at $x = 0$ and $x = L$ in Fig. 5.3, and by development analogous to that of section 5.21 we obtained a "two - port" Green's short circuit admittance

operator for the length of the waveguide $0 \le x \le L$ given by,

$$\begin{bmatrix} -H(0,y) \\ -H(L,y) \end{bmatrix} = \begin{bmatrix} \hat{Y}_{11} & \hat{Y}_{12} \\ -\hat{Y}_{21} & -\hat{Y}_{22} \end{bmatrix} \begin{bmatrix} E(0,y) \\ E(L,y) \end{bmatrix} \tag{5.13}$$

where, $\hat{Y}_{12} = -\hat{Y}_{21}$ and $\hat{Y}_{22} = -\hat{Y}_{11}$

The various quantities occurring in (5.13) are dual to those occurring in (5.11) with

$$Y_{11}(y,y') = -\Big[y_{o2} \coth(\gamma_{se2} L)\, \phi_{e2}(y)\, \phi_{e2}(y') + \sum_{\mu=e,o} \int_0^\infty d\rho\, y_o(\rho) \coth(\gamma_e L)\, \phi_{e\mu 2}(y,\rho)\, \phi_{e\mu 2}(y',\rho) + \int_0^v d\sigma\, y_o(\sigma) \coth(\eta_e L)\, \phi_{e2}(y,\sigma)\, \phi_{e2}(y',\sigma) \Big] \tag{5.14}$$

and

$$Y_{21}(y,y') = -\Big[y_{o2}\, cosech(\gamma_{se2} L)\, \phi_{e2}(y)\, \phi_{e2}(y') + \sum_{\mu=e,o} \int_0^\infty d\rho\, y_o(\rho)\, cosech(\gamma_e L)\, \phi_{e\mu 2}(y,\rho)\, \phi_{e\mu 2}(y',\rho) + \int_0^v d\sigma\, y_o(\sigma)\, cosech(\eta_e L)\, \phi_{e2}(y,\sigma)\, \phi_{e2}(y',\sigma) \Big] \tag{5.15}$$

The driving point admittance operator of slab 1,3 is given by

$$Y_1(y,y') = y_{o1}\, \psi_{e1}(y)\, \psi_{e1}(y') + \sum_{\mu=e,o} \int_0^\infty d\rho\, y_o(\rho)\, \psi_{e\mu 1}(y,\rho)\, \psi_{e\mu 1}(y',\rho) + \int_0^v d\sigma\, y_o(\sigma)\, \psi_{e1}(y,\sigma)\, \psi_{e1}(y',\sigma) \tag{5.16}$$

and

$$Y_3(y,y') = y_{o3}\,\psi_{e3}(y)\,\psi_{e3}(y') + \sum_{\mu=e,o}\int_0^{\infty} d\rho\, y_o(\rho)\,\psi_{e\mu 3}(y,\rho)\,\psi_{e\mu 3}(y',\rho)$$

$$+\int_0^{\nu} d\sigma\, y_o(\sigma)\,\psi_{e3}(y,\sigma)\,\psi_{e3}(y',\sigma) \qquad (5.17)$$

In (5.14) to (5.17) the wavenumbers and modal function are those appropriate to the TM case. The various admittances occurring in (5.14) to (5.17) are given by

$$y_{o1} = \frac{j\omega\varepsilon_0\gamma_{se1}}{\beta^2-\gamma_{se1}^2} \quad ; y_{o3} = \frac{j\omega\varepsilon_0\gamma_{se3}}{\beta^2-\gamma_{se3}^2} \quad ; y_{o2} = \frac{j\omega\varepsilon_0\gamma_{se2}}{\beta^2-\gamma_{se2}^2}$$

$$y_o(\rho) = \frac{j\omega\varepsilon_0\gamma_e}{k_o^2-\rho^2} \quad ; y_o(\sigma) = \frac{j\omega\varepsilon_0\eta_e}{\varepsilon_2 k_o^2-\sigma^2}$$

and the wavenumbers are given by

$$\varepsilon_{ee1}k_o^2-\beta^2 = -\gamma_{se1}^2 \quad ; \varepsilon_{ee2}k_o^2-\beta^2 = -\gamma_{se2}^2 \quad ; \varepsilon_{ee3}k_o^2-\beta^2 = -\gamma_{se3}^2$$

$$k_o^2-\rho^2-\beta^2 = -\gamma_e^2 \quad ; \varepsilon_2 k_o^2-\sigma^2-\beta^2 = -\eta^2 \quad ; \nu = k_o\sqrt{(\varepsilon_2-\varepsilon_0)}$$

Using (5.13) and translating the continuity of the transverse fields at each port in to the continuity of voltages and currents and approximating the interface field by a scalar function we recover the equivalent network for the cascade of steps as shown in Fig. 5.2b . The application of the theory to the analysis of coupled structures will be discussed in section 5.3 .

5.3 NUMERICAL SOLUTION OF COUPLED RIB WAVEGUIDES

5.31 DIRECTIONAL COUPLERS

The cross sectional geometry of a straight rib waveguide directional coupler is shown in Fig. 5.4a . The two guides are identical. The field distribution of this structure shown in Fig. 5.4b comprises the even and odd modes propagating along the coupler with propagation constants β_e and β_o, respectively. Including time and z - dependence the even and odd mode amplitudes may be expressed as,

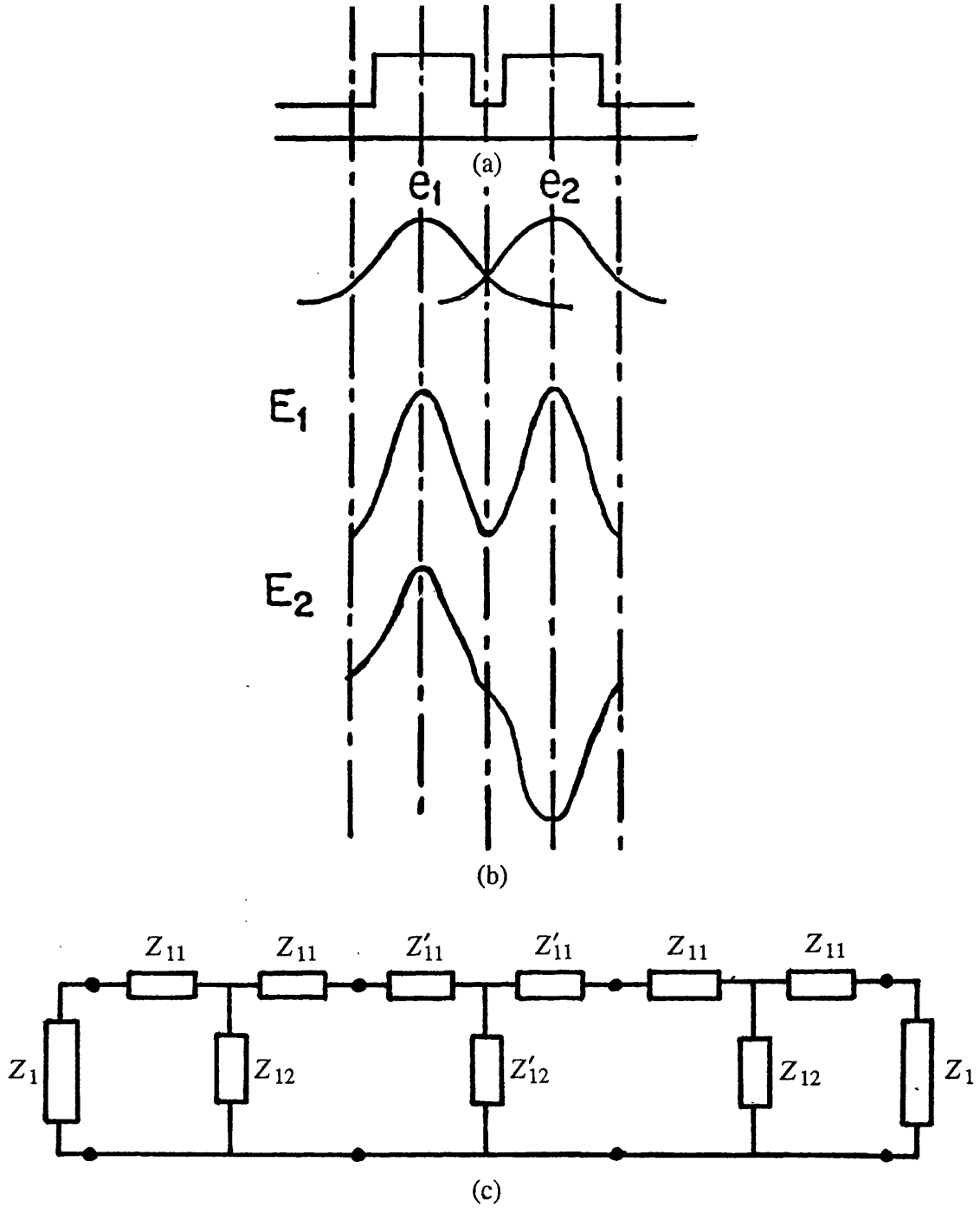

Fig. 5.4 a) Cross sectional geometry of straight rib waveguides directional coupler ; b) The even and odd field distribution of the structure ; c) Equivalent network modelling of the directional coupler.

For the even mode

$$E(z) \approx \cos(\omega t - \beta_e z)$$

For the odd mode

$$E(z) \approx \cos(\omega t - \beta_o z)$$

By linearity the response of the structure is given by the superposition of the even and odd mode responses. If the even and odd modes are excited with equal amplitudes, we have

For guide 1,

$$\begin{aligned} E_1(z) &= A\cos(\omega t - \beta_e z) + A\cos(\omega t - \beta_o z) \\ &= 2A\cos(\omega t - \frac{\beta_e+\beta_o}{2} z)\cos(\frac{\beta_e - \beta_o}{2} z) \\ &= 2A\cos(\omega t - \beta z)\cos(cz) \end{aligned}$$

For guide 2,

$$\begin{aligned} E_2(z) &= A\cos(\omega t - \beta_e z) - A\cos(\omega t - \beta_o z) \\ &= 2A\sin(\omega t - \frac{\beta_e+\beta_o}{2} z)\sin(-\frac{\beta_e-\beta_o}{2} z) \\ &= 2A\sin(\omega t - \beta z)\sin(-cz) \end{aligned}$$

Along the length of the coupler L_t, the relative phases of the two modes will reverse and at this point the mode fields reinforce each other in the opposite sense, accounting for the transfer of power between the two guides of the coupler. For this to occur,

$$\cos\left(\frac{\beta_e-\beta_o}{2} L_t\right) = 0$$

$$\frac{\beta_e-\beta_o}{2} L_t = \frac{n\pi}{2} \qquad ; n \text{ odd}$$

$$L_t = \frac{n\pi}{\beta_e-\beta_o} \tag{5.18}$$

where L_t is the transfer length for maximum power transfer.

If even and odd modes are not excited with equal amplitudes, then, when the two modes are out of phase, cancellation in one of the guides will not be complete. Hence, a small amount of power will be left which may contribute to the crosstalk. In this work emphasis is given to the determination of transfer lengths, a useful parameter required to characterize the coupler and the problems of crosstalk are not pursued further. Most practical structures are considered to be strongly coupled. For example, short transfer lengths are desired for small and fast switches. The key to evaluating the transfer length of a coupler is the calculation of β_e and β_o. Hence, an appropriate technique accurate for strongly coupled situation is highly desirable to determine the propagation constants. This is done using the theory developed in the previous section. The equivalent network modelling of the structure is shown in Fig. 5.4c . In this case, solving the coupled structure reduces to that of solving the equivalent network. This is achieved more effectively by cascade multiplication of the transfer matrices of the individual networks. The transfer matrix relates voltages and currents at the L.H.S ports to the R.H.S is given by

$$T = \begin{bmatrix} \hat{Z}_{11}\hat{Z}_{21}^{-1} & -\hat{Z}_{11}\hat{Z}_{22}\hat{Z}_{21} + \hat{Z}_{12}^{-1} \\ \hat{Z}_{21}^{-1} & \hat{Z}_{21}^{-1}\hat{Z}_{22} \end{bmatrix}$$

The z - directed propagation constants β_e and β_o of the even and odd modes respectively are determined from the transverse resonances condition applied at a chosen reference point. By using simple network theory and choosing reference point at $x = 0$, we obtained the scalar dispersion equation given by

$\hat{Z}_1 + \hat{Z}_{IN} = 0$; for *LSE polarization*

$\hat{Y}_1 + \hat{Y}_{IN} = 0$; for *LSM polarization*

where $\hat{Z}_{IN}$ and $\hat{Y}_{IN}$ is the input impedance and admittance respectively looking to the right of $x = 0$. Solving the dispersion equation yields the propagation constants β_e and

β_o.

RIB GUIDE STRUCTURE	n_1	n_2	n_3	D μm	d μm	L μm	S μm	λ μm
1	3.44	3.34	1.0	1.3	0.2	2.0	2.0	1.55
2	3.44	3.36	1.0	1.0	0.9	3.0	2.0	1.55
3	3.44	3.435	1.0	6.0	3.5	4.0	2.0	1.55

TABLE 5.1 : Parameters of the directional coupler which have been analysed.

In order to demonstrate the accuracy of the present technique, we consider first the directional couplers analysed by [6] using the Finite Difference Method. The parameters describing the directional couplers analysed in [6] are given in Table 5.1 . The results of the present analysis together with those of FDM and the EDC method are summarised in Table 5.2 . Simulations indicate that both present and FDM analysis results agree very well and prove the accuracy of the present method. The results of the EDC agree very well with the present and FDM analysis only for small rib height. This is not surprising for reasons already discussed in chapter 3 on single guides. As shown in Table 5.2, the present method does not produce the odd mode index for the third structure. This is because the odd mode for this structure is cutoff and the mode index is complex. This argument is justified by examining the index of the odd mode predicted by FDM analysis $\frac{\beta_o}{k_o}$ is less than the EDC of the outer slab $\sqrt{\varepsilon'_{eh}}$. The computer program used in the present analysis is developed to predict real mode index $\frac{\beta_o}{k_o}$ in the range $\sqrt{\varepsilon'_{eh}} < \frac{\beta_{e,o}}{k_o} < \sqrt{\varepsilon_{eh}}$. This is not a limitation of the method and if complex algebra is used in the computer program it should be able to yield a complex index for this mode. However, this problem is not pursued further as emphasis in this work is focussed on the determination of transfer length of coupled guides.

STRUCTURE	MODE INDICES	TRD USING Fig. 1a	TRD USING Fig. 1c	FDM [6]	EDC
ST1	$\frac{\beta_e}{k_o}$	3.388841027	3.388838939	3.391472377	3.390322424
	$\frac{\beta_o}{k_o}$	3.388841027	3.388838350	3.391470106	3.390322421
	$L_t\ (mm)$	-	1314.57	341.0	300000.0
ST2	$\frac{\beta_e}{k_o}$	3.395739365	3.395739353	3.396053426	3.395914969
	$\frac{\beta_o}{k_o}$	3.394802846	3.394802837	3.395097562	3.394954357
	$L_t\ (mm)$	0.827	0.827	0.811	0.807
ST3	$\frac{\beta_e}{k_o}$	3.436820329	3.436806957	3.437034755	3.437661171
	$\frac{\beta_o}{k_o}$	-	-	3.436459357	3.437072754
	$L_t\ (mm)$	-	-	1.347	1.317

TABLE 5.2 : Modal refractive indices of even and odd modes in directional coupler structures.

d μm	MODE INDICES	USING MODEL Fig. 1a	USING MODEL Fig. 1c	DIFFERENCE %
0.3	$\frac{\beta_e}{k_o}$	3.412597677	3.412595607	
	$\frac{\beta_o}{k_o}$	3.412551746	3.412549877	
	L_t (mm)	12.5272	12.5739	4.7
0.6	$\frac{\beta_e}{k_o}$	3.413685884	3.413685555	
	$\frac{\beta_o}{k_o}$	3.413535726	3.413535438	
	L_t (mm)	3.831	3.830	0.1
0.9	$\frac{\beta_e}{k_o}$	3.415891467	3.415891456	
	$\frac{\beta_o}{k_o}$	3.415203392	3.415203383	
	L_t (mm)	0.835666	0.835666	0.

TABLE 5.3 : Comparison of modal refractive indices of even and odd modes and transfer length of directional coupler structure for different outer slab height

In order to assess the effect of the propagating continuous modes on the transfer length of coupled guides at optical frequencies, we compare the results of the analysis using equivalent networks in Fig. 5.2a and Fig. 5.2c. The parameters of the structure examined in this exercise are $n_1 = 3.44$, $n_2 = 3.40$, $n_3 = 0$, $D = 1\mu m$, $W = 3\mu m$, $\lambda = 1.15\mu m$, $S = 2\mu m$ and d varying. The results of the simulations are summarised in Table 5.3. Simulations indicate that the effect of the propagating continuous modes on the transfer length is small even for well confined modes. This observation shows that at optical frequencies with $n_1 \gg n_3$, the interaction via the continuous modes is small and can be neglected. Hence, it is possible to obtain accurate results by considering interaction via the surface modes only and using the simpler equivalent network Fig. 5.2c .

Having established the accuracy of the technique, we are in a position to consider some

numerical results that can be utilized as design data. Two coupled structures namely ST4 and ST5 are considered and their parameters are shown in the figure. The variation of the modal indices of the even and odd modes as a function of the guide separation S is shown in Fig. 5.5 and Fig. 5.6 for structures ST4 and ST5 respectively. In the figure results of both polarizations LSE and LSM are shown. The even and odd mode indices are above and below the single guide index respectively. For small guides separation S i.e for strongly coupled system, the differences of even and odd modes indices from the single guide index are not equal and hence $\beta \neq \frac{\beta_e+\beta_o}{2}$. As the guide separation S increases both $\frac{\beta_e}{k_o}$ and $\frac{\beta_o}{k_o}$ appear to approach the single guide index and for sufficiently large S they become almost equally spaced from $\frac{\beta}{k_o}$. This behaviour is consistent with the prediction of coupled mode theory and β can be accurately predicted by $\beta = \frac{\beta_e+\beta_o}{2}$. This occurs when the coupling is loose. This observation shows that for a strongly coupled system, coupled mode theory is less than accurate and more rigorous analyses such as the present method should be used. The transfer lengths can be calculated using the data in Fig. 5.5 and Fig. 5.6 for structures ST4 and ST5 respectively. Plot of L_t vs S for structures ST4 and ST5 is shown in Fig. 5.7 and Fig. 5.8 respectively. The transfer length increases exponentially with increasing S. This shows that the coupling decreases exponentially as S is increased. This behaviour is direct consequence of the fact that fields decay exponentially outside the guides. Their decay constant may be predicted from the gradient of the plot of ln L_t vs S given in Fig. 5.9 and Fig. 5.10 for structures ST4 and ST5, respectively.

5.32 THREE GUIDE COUPLERS

A symmetrical three guide coupler composed of three identical rib waveguides in close proximity is shown in Fig. 5.11a . The individual waveguides are assumed to be single

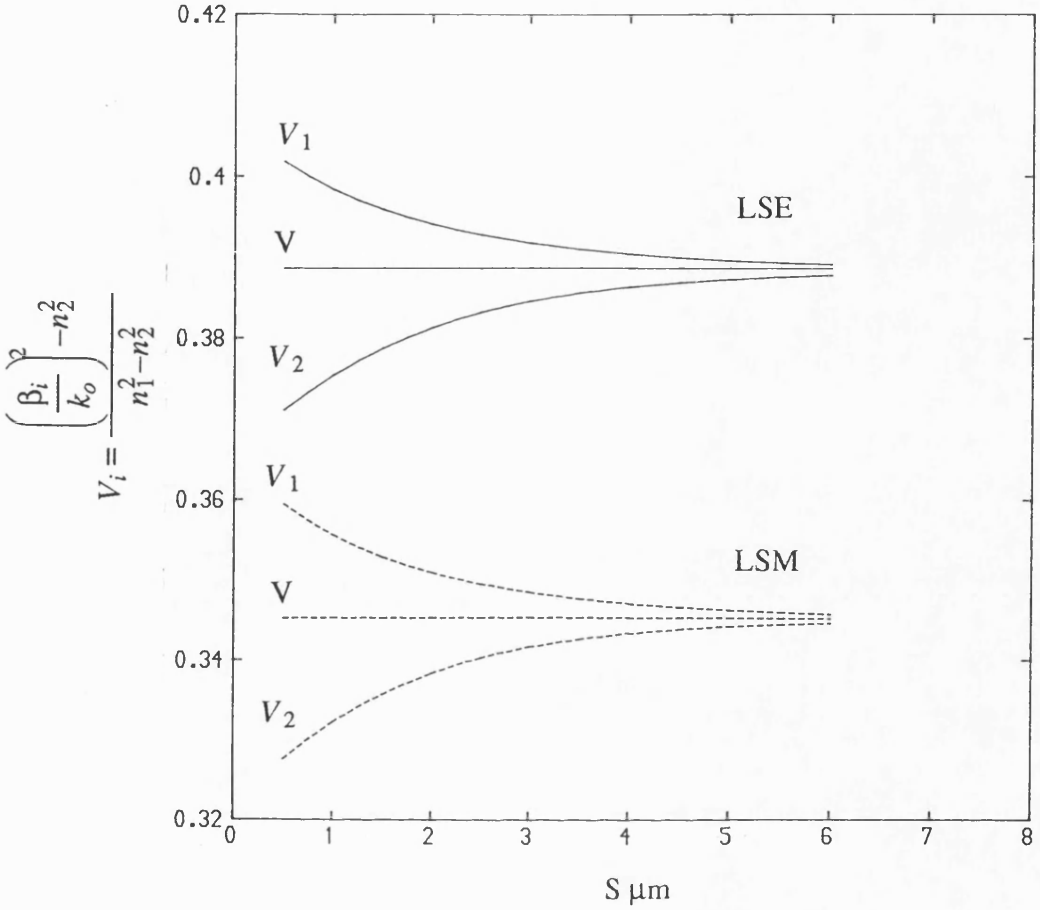

Fig. 5.5 Variation of the normalised modal indices of the even and odd modes as a function of the guide separation S for directional coupler.

V_1 - Even mode , V_2 - Odd mode , V - Mode of single guide

ST4: $n_1 = 3.44, n_2 = 3.40, n_3 = 1.0, D = 1\mu m$, $d = 0.9\mu m$, $L = 3\mu m$, $\lambda = 1.15\mu m$

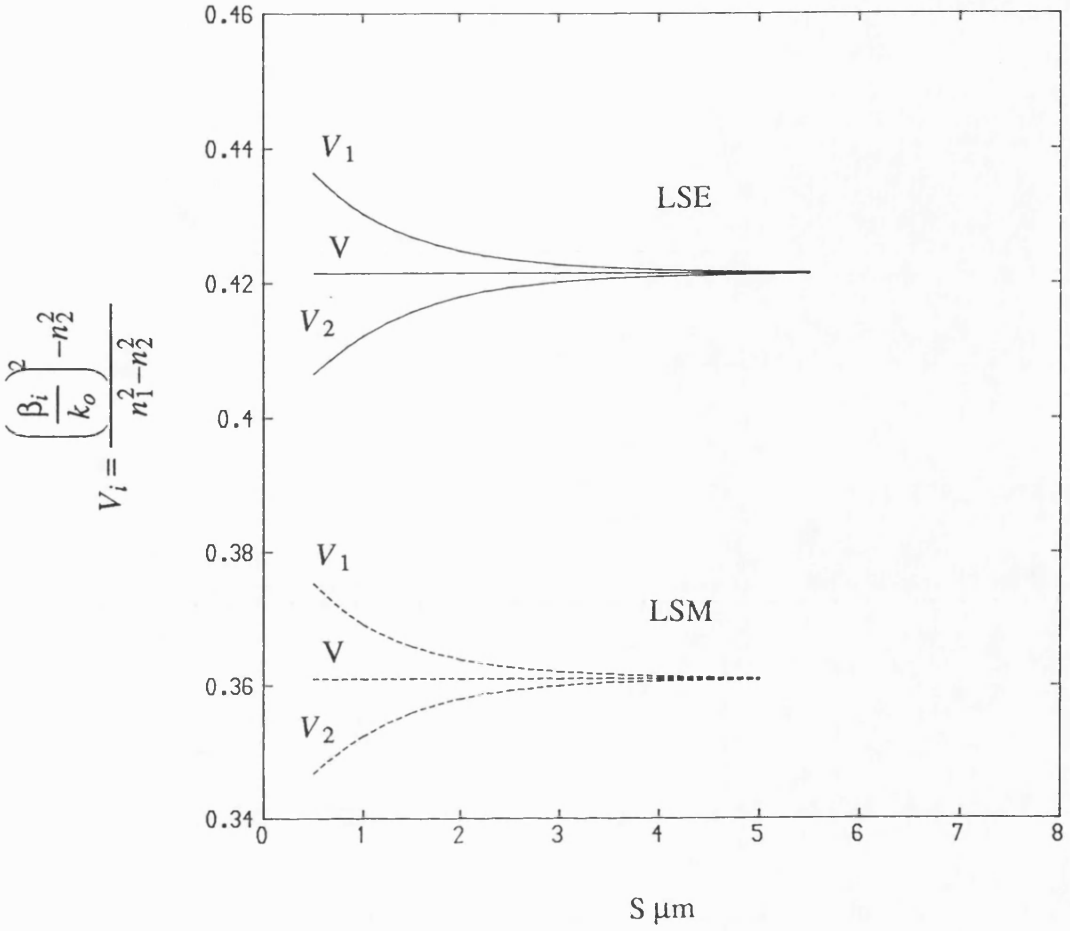

Fig. 5.6 Variation of the normalised modal indices of the even and odd modes as a function of the guide separation S for directional coupler.

V_1 - Even mode, V_2 - Odd mode, V - Mode of single guide

ST5: $n_1 = 3.44, n_2 = 3.36, n_3 = 1.0, D = 1\mu m, d = 0.8\mu m, L = 3\mu m, \lambda = 1.55\mu m$

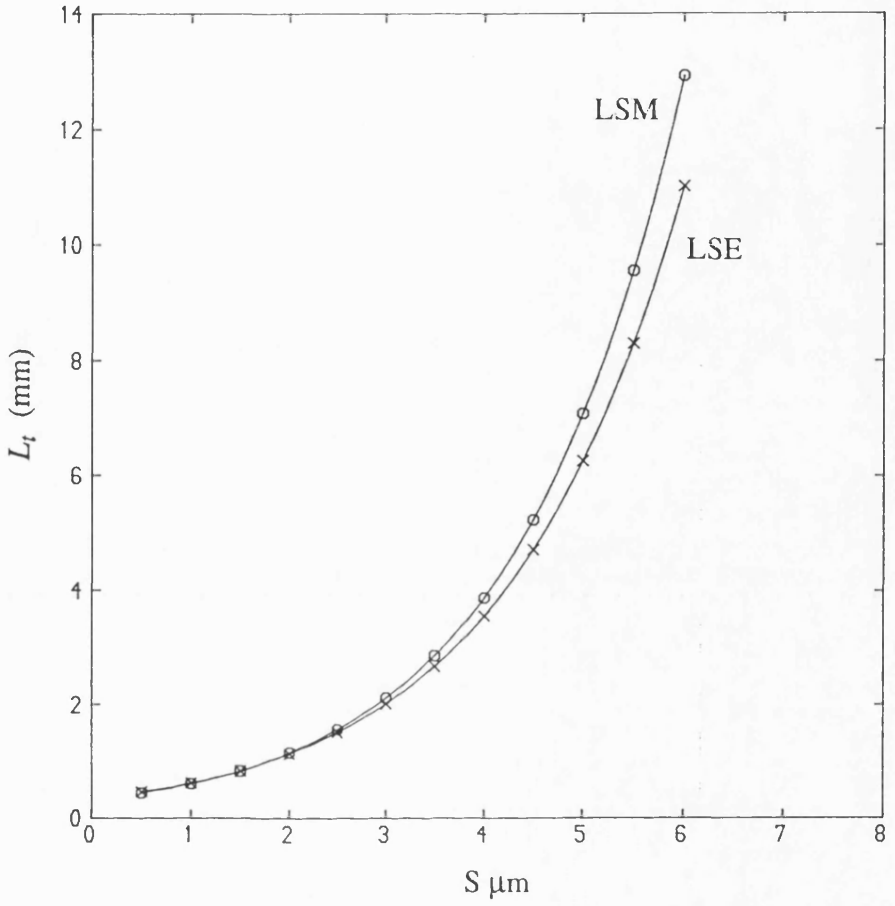

Fig. 5.7 Variation of the transfer length L_t as a function of guides separation S for directional coupler ST4.

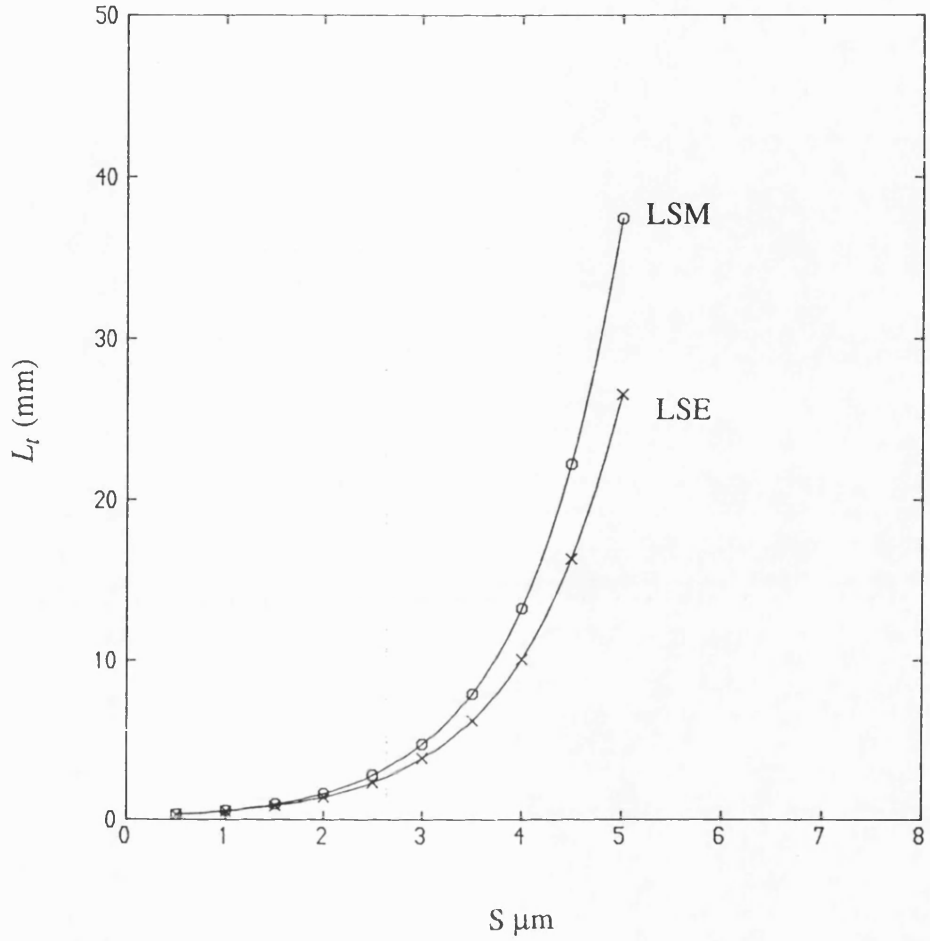

Fig. 5.8 Variation of the transfer length L_t as a function of guides separation S for directional coupler ST5.

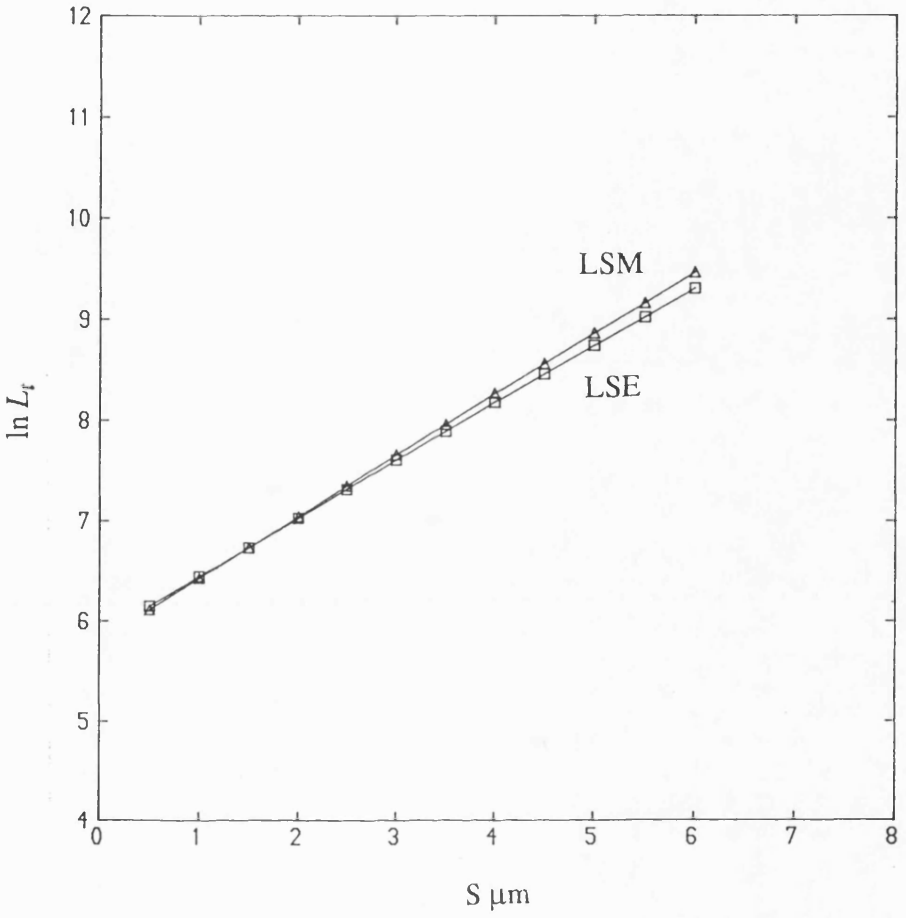

Fig. 5.9 Variation of ln L_t as a function of guides separation S for directional coupler ST4.

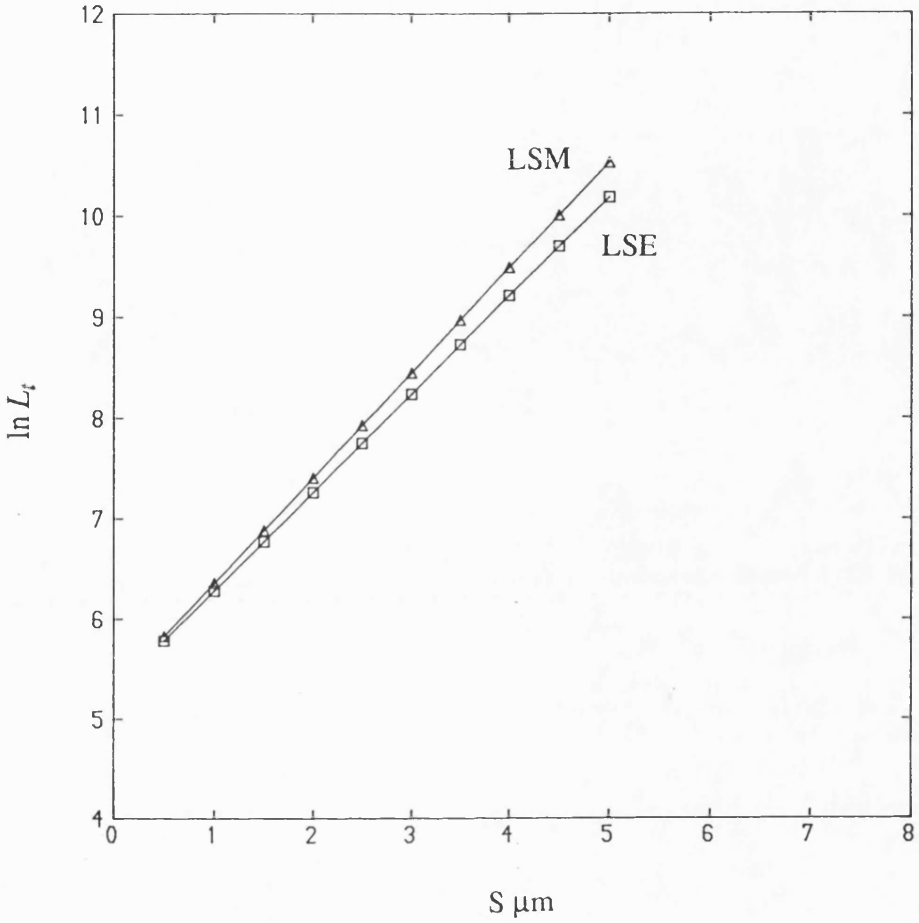

Fig. 5.10 Variation of ln L_t as a function of guides separation S for directional coupler ST5.

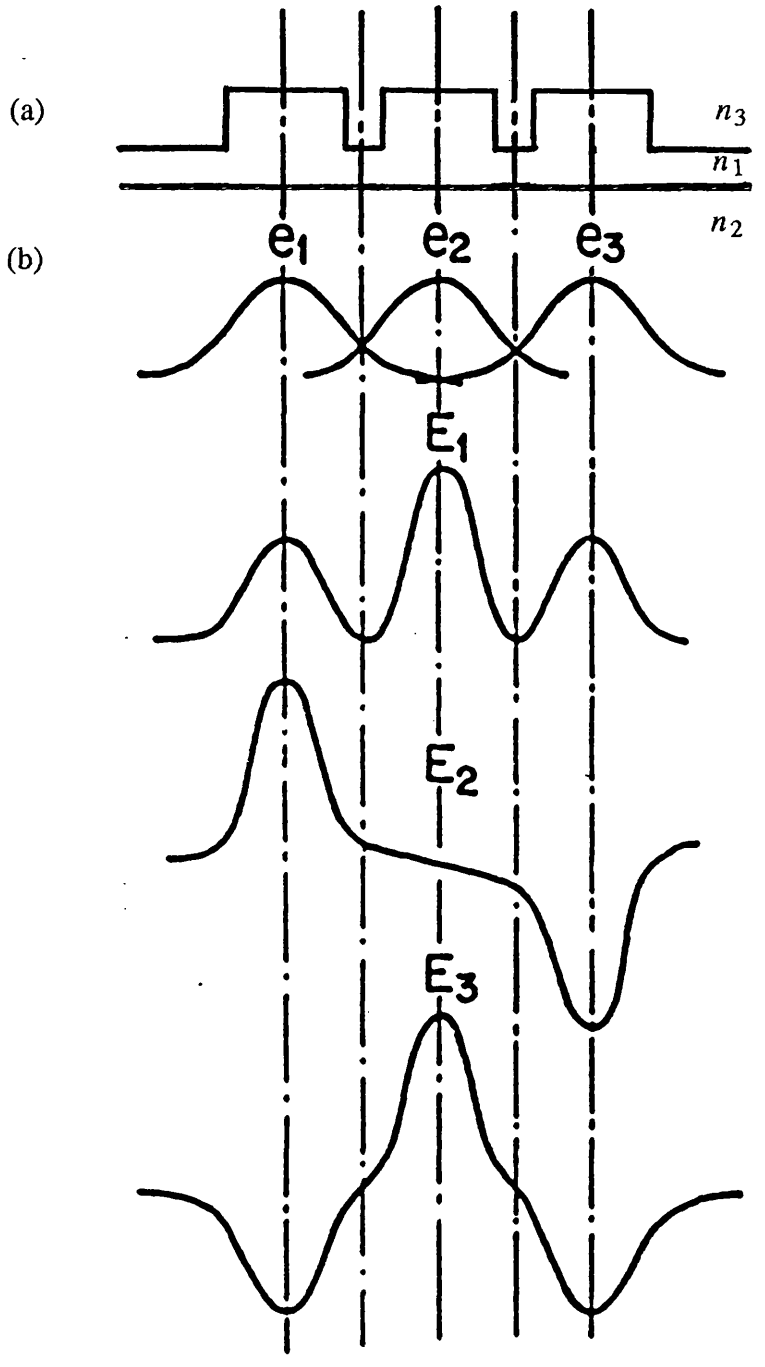

Fig. 5.11 a) Cross sectional geometry of three identical rib waveguide coupler ; b) The transverse field profiles of the overlapping guides modes and the modes of the coupled structure.

moded. Before applying the present method of analysis, it is instructive to consider the modal characteristics of this structure. The transverse field profiles of the overlapping guides modes and the modes of the coupled structure in Fig. 5.11a are shown in Fig. 5.11b . The coupled structure has three modes, two are even with propagation constants β_1 and β_2 and one is odd with propagation constant β_3. In [8], a similar configuration has been analysed using the EDC technique and it has been shown that the propagation constants of the three modes obey the following conditions,

$$\beta_1 > \beta$$

$$\beta_2 < \beta$$

$$\beta_3 \lessgtr \beta \quad ; \textit{depending on the guide parameters}$$

$$(\beta_3 - \beta) \leq (\beta_1 - \beta) \textit{ or } (\beta_2 - \beta) \tag{5.19}$$

where β is the modal propagation constant of a single isolated rib waveguide.

There are two possible ways to excite the structure in Fig. 5.11a . In the first case, the structure is excited symmetrically through the centre guide and this configuration may be used as a power divider. In this case only modes 1 and 2 are excited, such that at $z = 0$ their fields are in phase i.e additive in the centre guide and subtractive in the outside guides. At some distance z down the line, modes 1 and 2 get out of phase, their fields interfere destructively in the centre guide and constructively in the outside guides, accounting for the transfer of power from the centre guide to the outside guides. This occurs at multiples of the coupling length given by [8],

$$L_{ct} = \frac{\pi}{\beta_1 - \beta_2} \tag{5.20}$$

In the second case, the three guide coupler is excited antisymmetrically through either one of the outer guides. Such configuration may be used to transfer power from one of the outer guides to the other outer guide. The feasibility of using such device as an improved sampler has been demonstrated in [9]. At $z = 0$, modes 1 and 2 are excited out of phase so that they are in antiphase in the centre guide and in phase in the outer guides.

Mode 3 is excited so it is in phase with modes 1 and 2 in the input outer guide and antiphase in the other outer guide. In this case, the situation is more complex and beats periodic with distance down the coupler can only be obtained with high power transfer efficiency between guides if the phase velocities of the modes are related to each other in a simple manner. Under the condition of loose coupling most of the power will be transferred from one outer guide to the other at a length given by [8],

$$L_{ot} = \frac{2\pi}{\beta_1 - \beta_2} \tag{5.21}$$

i.e the coupling length is twice that required to symmetrically transfer power from the centre guide to the two outer guides.

Again the key parameter in the analysis of the three guide coupler is the accurate evaluation of β_1, β_2 , and β_3. In this numerical example, three guides of the geometry used in the analysis of the directional couplers i.e ST4 will be analyzed. The resulting equivalent circuit is similar to that of Fig. 5.4c but includes two additional network sections corresponding to the third guide. Solving the equivalent circuit yields all the β's values. Equation (5.19) is used as a reference in the identification of β value for the two even modes and odd mode. The variation of the effective indices of the even modes and odd mode as a function of separation between the guides S are shown in Fig. 5.12. The straight line is the effective index of the single isolated rib waveguide. Using Fig. 5.12 the length required to transfer power from the centre guide to the outer guides L_{ct} can be calculated using (5.20) and that to transfer power from one of the outer guide to the other L_{ot} can be obtained from (5.21). The variation of ln L_{ct} and ln L_{ot} as a function of guides separation S is plotted in Fig. 5.13. In Fig. 5.14 the variation of the transfer length of the three guide coupler and of the directional coupler is shown as a function of guides separation S. Comparing the two curves, it can be seen that for strongly coupled structures the ratio of the two transfer lengths is between 1.45 and 1.5. Only for loosely coupled structures does the ratio become very close to $\sqrt{2}$, i.e the prediction of coupled

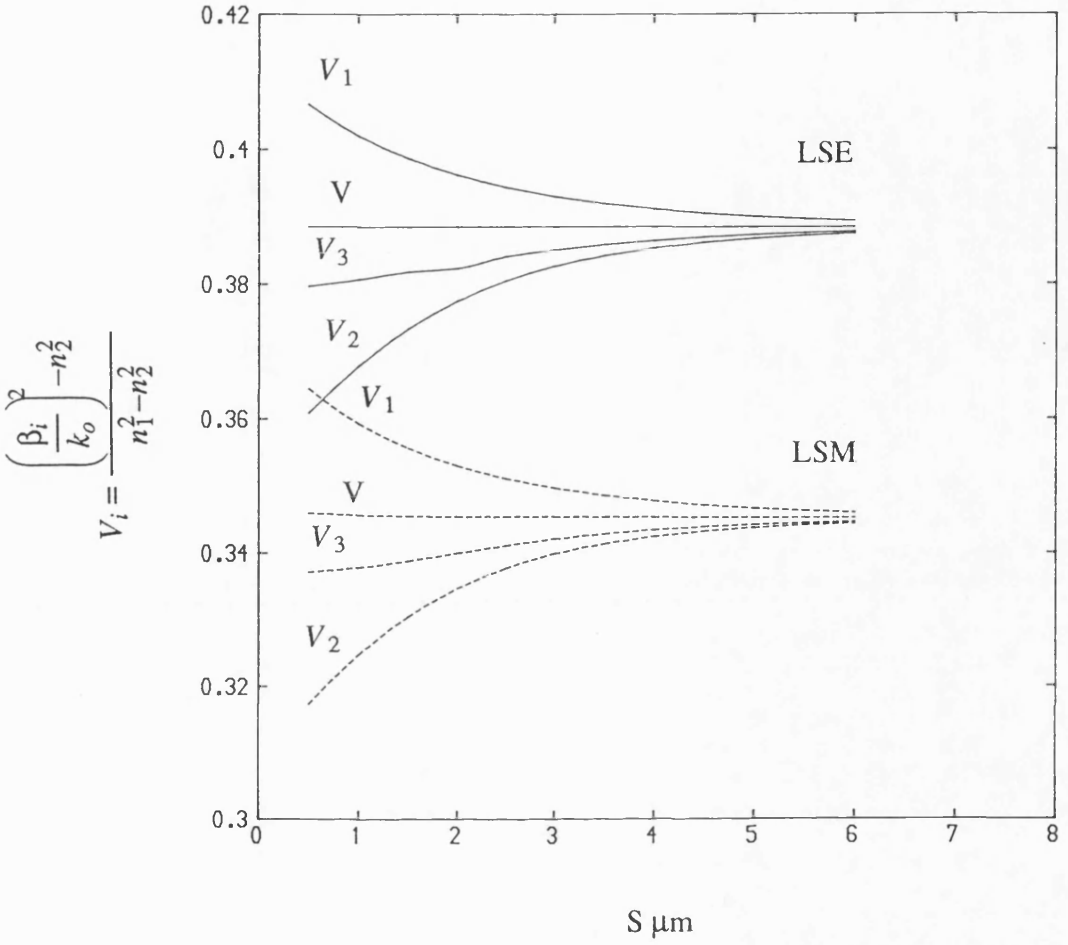

Fig. 5.12 Variation of the normalised modal indices of the even and odd modes as a function of guides separation S for three guide coupler.
V_1 , V_2 - Even modes, V_3 - Odd mode, V - Mode of single guide.

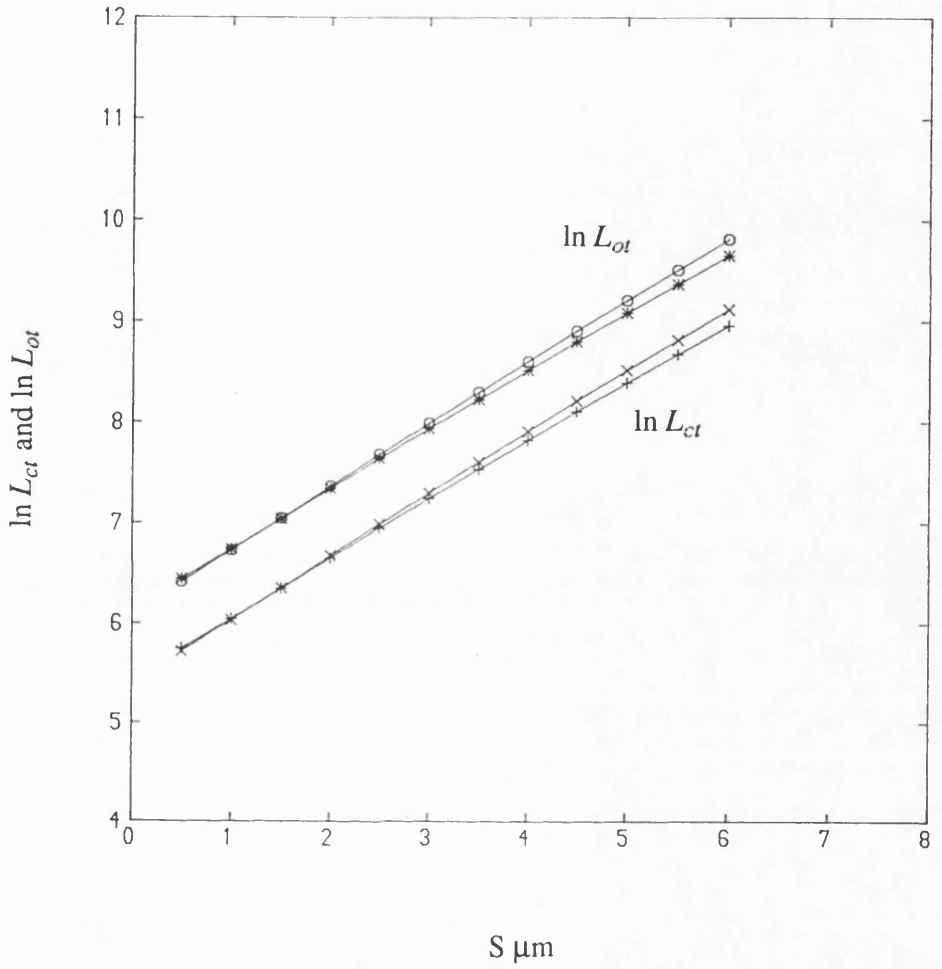

Fig. 5.13 Variation of ln L_{ct} and ln L_{ot} as a function of guides separation S for three guide coupler.

✳ + LSE analysis

○ × LSM analysis

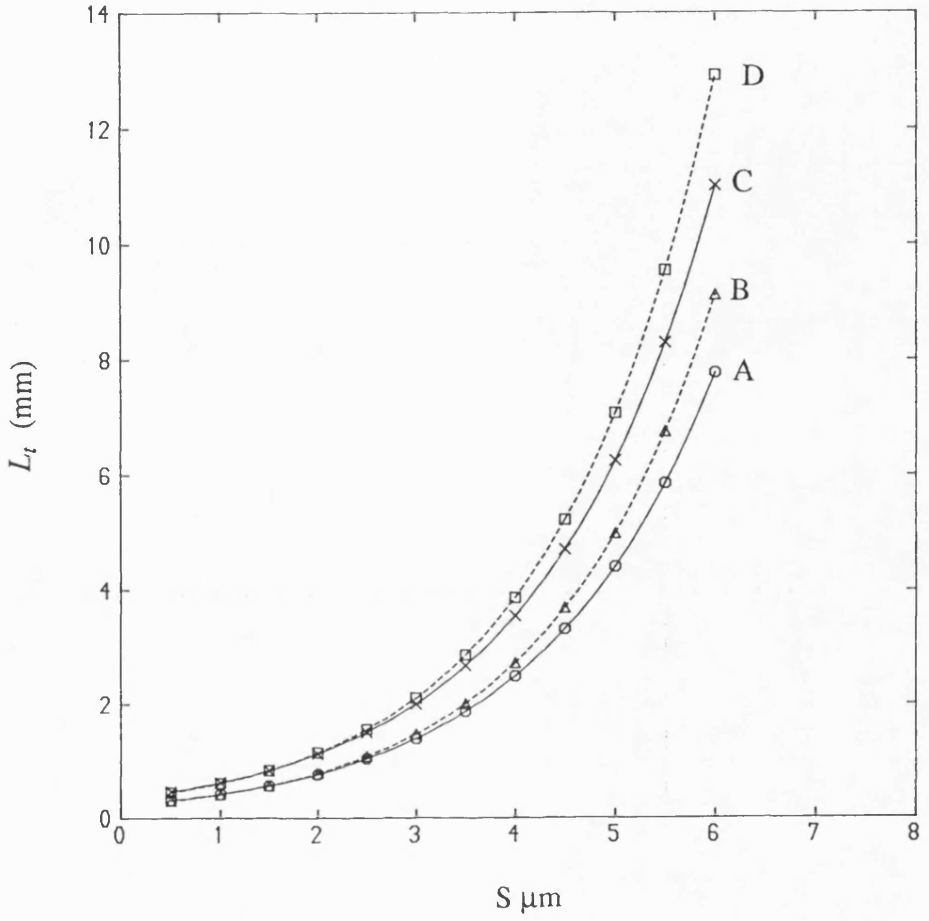

Fig. 5.14 Variation of the transfer length of the three guide coupler L_{ct} (curves A and B) and of the directional coupler L_t (curves C and D) as a function of guides separation S.

——— LSE analysis

— — — — LSM analysis

mode theory. There are two points to be noted from this observation. Firstly, accurate analyses should be employed even for most practical devices. Secondly, one must beware when using data derived from two guide couplers to design devices with three guide couplers. In fact, a simple $\sqrt{2}$ relationship between the transfer lengths predicted by coupled mode theory does not hold for strongly coupled situations.

5.33 STRONGLY COUPLED UNEQUAL GUIDES

The theory developed in section 5.2 applies not only to structures with identical rib waveguides but also to structures with rib guides of different dimensions. As an example, we investigate the propagation constants of nonidentical guides where the geometrical dimensions of guide 1 is fixed and the rib width or rib height of guide 2 varies. The other dimensions of guide 2 are fixed. The optical parameters of the guides are $n_1 = 3.44$, $n_2 = 3.40$, $n_3 = 1.0$, and $\lambda = 1.15\mu m$. Their geometrical dimensions are shown in the figure. The results for the modal indices as a function of the guides separation are shown in Fig. 5.15 and Fig. 5.16. From the figures it can be seen that the fundamental modes of the two rib waveguides are not synchronous where each of the two modes favours one of the two rib waveguides. Thus, each mode is nearly equal to the mode of one or the other rib waveguide taken in isolation. For sufficiently large guides separation the two guides decoupled. These two fundamental modes would have even and odd symmetry if both rib waveguides were identical. From this observation it can be seen that in order to achieve a nonidentical guides coupler the two guides ought to be strongly coupled and in synchronism so that the two modes can be superimposed such that at the input end of the coupler their fields nearly cancel in one guide while they reinforce each other in the opposite guide. At a distance $L_t = \frac{\pi}{\beta_2 - \beta_1}$ the mode fields reinforce each other in the opposite sense, accounting for the transfer of power between the two guides. In order to achieve synchronism of the two guides the rib width or the rib height may be adjusted.

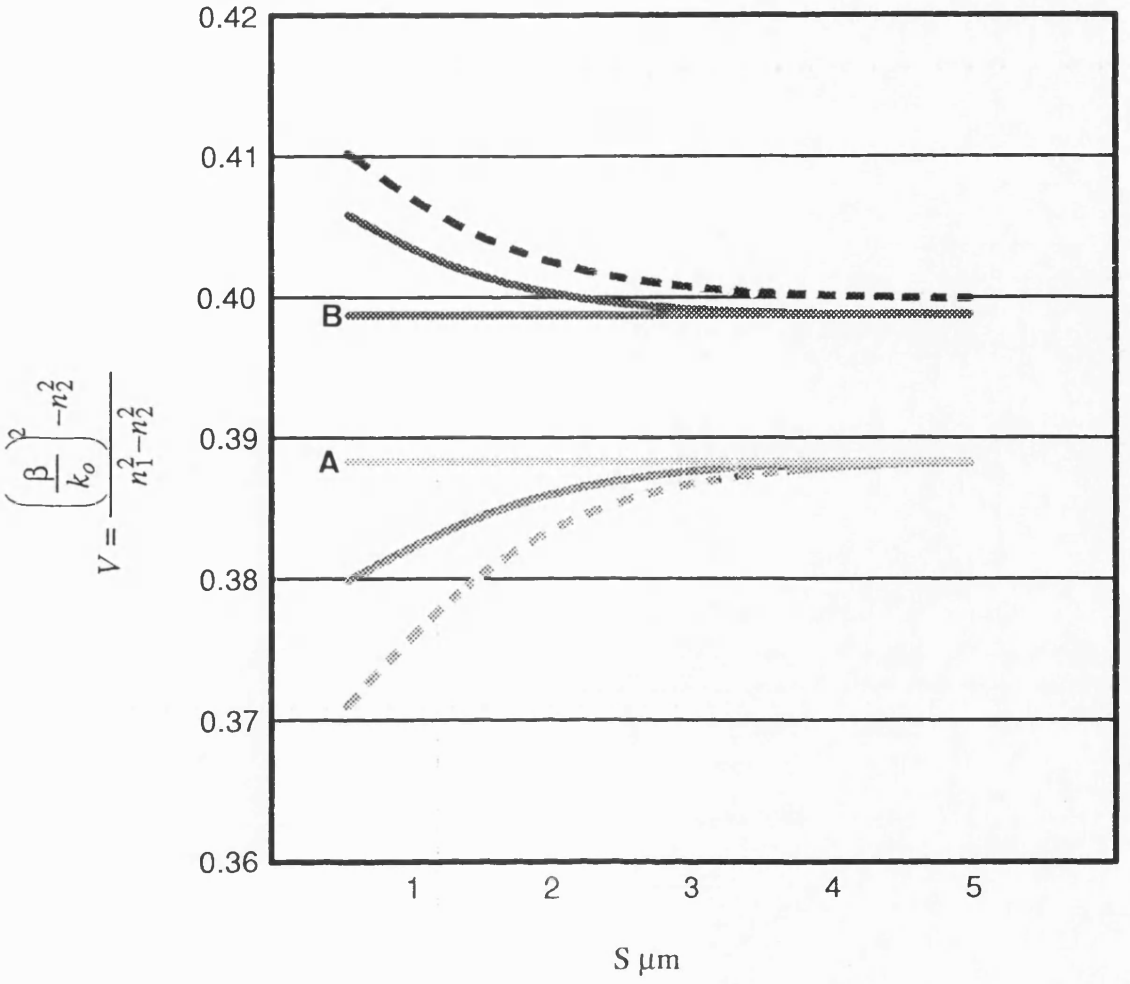

Fig. 5.15 Variation of the normalised modal indices (LSE) of the fundamental modes as a function of guide spacing for closely coupled nonidentical guide. Curve A and B are V's for uncoupled guide of $L = 3.0\mu m$ and $4.0\mu m$ respectively and $D' = 1.0\mu m$,$d = 0.9\mu m$.

——— $L_1 = 3.0\mu m, L_2 = 4.0\mu m, d = 0.9\mu m, D' = 1.0\mu m.$

– – – – $L_1 = 3.0\mu m, L_2 = 4.0\mu m, d = 0.9\mu m, D' = 1.2\mu m.$

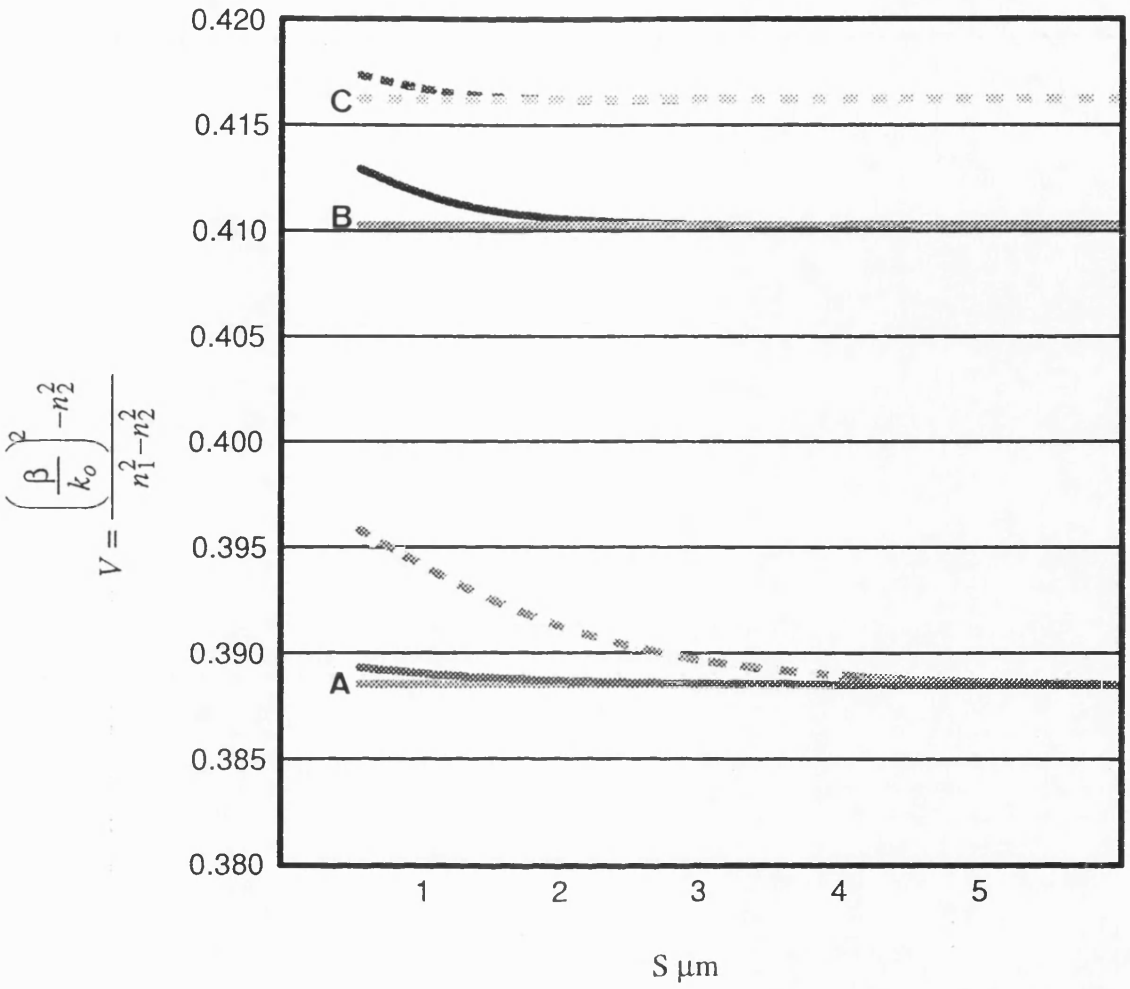

Fig. 5.16 Variation of the normalised modal indices (LSE) of the fundamental modes as a function of guide spacing for closely coupled nonidentical guide. Curve A,B and C are V's for uncoupled guide of $L = 3.0\mu m, 6.0\mu m$ and $8.0\mu m$ respectively and $D' = 1.0\mu m$,$d = 0.9\mu m$.

——— $L_1 = 3.0\mu m, L_2 = 6.0\mu m, d = 0.9\mu m, D' = 1.0\mu m.$

— — — — $L_1 = 3.0\mu m, L_2 = 8.0\mu m, d = 0.9\mu m, D' = 1.0\mu m.$

5.34 WAVEGUIDE ARRAYS

An array of coupled rib waveguides is shown in Fig. 5.17a. This configuration has been used to design coupled laser arrays [10]. The operation of coupled waveguide arrays is more complicated than that of a two or three-guide couplers because of the higher number of modes which can exist in the structures. If the individual guides are single moded, then the number of possible guided modes of coupled arrays is generally equal to the number of guides in the array [7]. The propagation constants of the structure can be obtained by using the theory developed in section 5.2 . In the case of finite arrays, the numerical evaluation of the propagation constant is similar to that of a three guide coupler with little additional computation. The increase in computation time is small since we are dealing only with an additional multiplication of the transfer matrices and there is no need to calculate an additional equivalent circuit parameters.

If the array is large and periodic we may approximate its propagation constant, in a manner similar to the determination of the propagation constant of a cascaded transmission line. To solve a periodic structure let us consider the unit element of the periodic structure and its equivalent circuit shown in Fig. 5.17 . The relationship between voltages and currents at A and A' is given by

$$\begin{bmatrix} V \\ I \end{bmatrix} = T_1 \cdot T_2 \begin{bmatrix} V' \\ I' \end{bmatrix} \tag{5.22}$$

where T is the transfer matrix for each uniform section, already derived in section 5.2 and section 5.31 .

The periodicity condition requires

$$\begin{bmatrix} V' \\ I' \end{bmatrix} = e^{-jk_x l} \begin{bmatrix} V \\ I \end{bmatrix} \tag{5.23}$$

where l is the length of the period and k_x is the propagation constant of the periodic structure. Substituting (5.23) in to (5.22) gives the approximate eigenvalue equation for

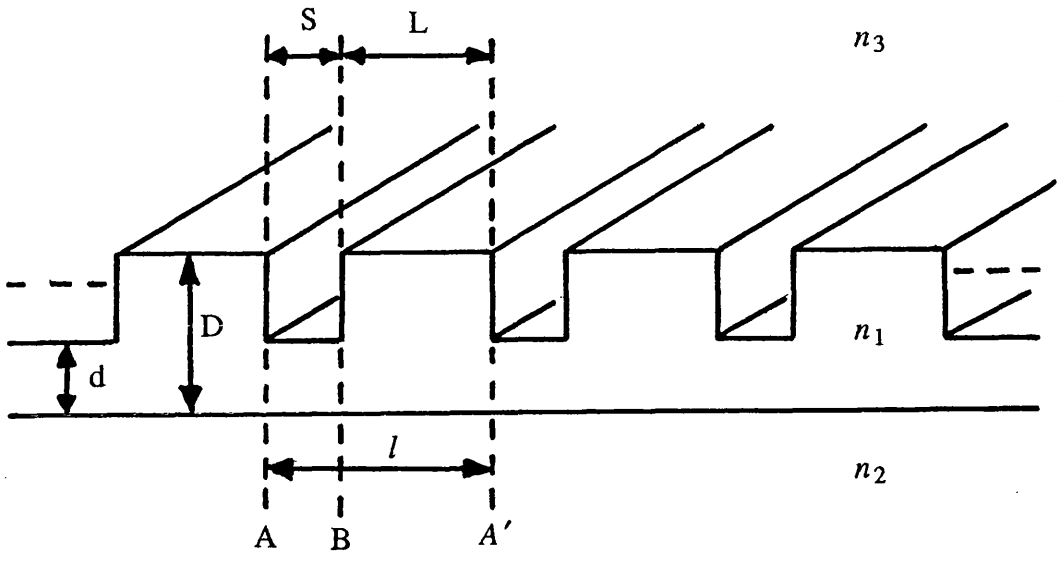

(a)

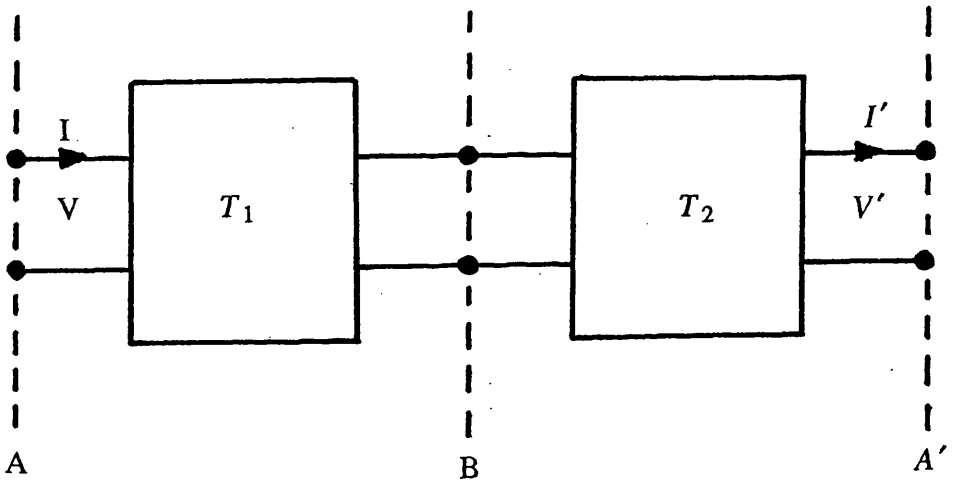

(b)

Fig. 5.17 a) Rib waveguide arrays ; b) Equivalent circuit representation for the unit element of the periodic cascade.

the periodic structure, that is

$$T_1^{-1} \cdot T_2^{-1} \begin{bmatrix} V \\ I \end{bmatrix} = e^{-jk_x l} \begin{bmatrix} V \\ I \end{bmatrix} \tag{5.24}$$

5.4 CONCLUSION

In this chapter, we develop a simple and effective rigorous solution for coupled rib waveguides. The problem is seen as that of cascaded step discontinuities in the transverse direction. The use of a "transition function" at the discontinuous interfaces not only simplifies the calculation, avoiding the use of large matrices but it also yields a simple cascaded two port network representation of the coupled structure.

The accurate determination of the propagation constants of the modes of the coupled structure is very important in determining the coupling between waveguides. The method developed in this work is believed to be accurate and is valid under all circumstances of strong and weak coupling. The accuracy of the method was demonstrated by comparing the results with the results of FDM calculations. Numerical examples were carried out and where comparison is available, it has been found the method yields results that compare very favourably with those produced by FDM. Numerical simulations also show that the results of coupled mode theory agree with our accurate results only for weakly coupled structures. As most practical devices are in fact tightly coupled, a more accurate analysis such as the present method should be employed in their study.

The additional computational effort required to analyse multiple guide couplers including arrays and non identical guides using the present method is only marginally higher than that required for a single guide. This is the important advantage of this method over numerical methods where the computational effort increases as the area of the cross section increases.

REFERENCES

[1] M.R. Knox and P.P. Toulios, " Integrated circuits for the millimetre through optical frequency range ", Proceedings of the symposium on submillimetre waves. Polytechnic, N.Y., 1970, pp 497-516

[2] W.V. Mc Levige, T. Itoh, R. Mittra, " New waveguide structure for millimetre wave and optical integrated circuits ", I.E.E.E. Trans. Microwave Theory Techniques, vol. MTT-23, No. 10, Oct. 1975, pp. 788-794

[3] A. Yariv, " Coupled mode theory for guided wave optics " , I.E.E.E J. Quantum Electron., vol. QE-9, pp 919, 1973

[4] A. Hardy and W. Sreifer, " Coupled mode solutions of multiwaveguide systems ", I.E.E.E J. Quantum Electrons. , vol. QE-22, pp 528-534, April 1986

[5] H.A. Haus, W.P. Huang, S. Kawakami and N.A. Whitaker ", Coupled mode theory of optical waveguides ", J. Lightwave Technology, vol. LT-5, No. 1, Jan 1987, pp 16-23

[6] M.J. Robertson, S. Ritchie and P. Dayan, " Semiconductor waveguides: Analysisof optical propagation in single rib structures and directional couplers ", I.E.E Proceeding, vol. 132, Pt. J, No. 6, Dec. 1985

[7] T. Rozzi, G.H. In't Veld, " Field and network analysis of interacting step discontinuities in planar dielectric waveguide " , I.E.E.E. Trans. Microwave Theory Techniques, vol. MTT-27, No. 4, April 1979 , pp 303-309

[8] J.P. Donnely, N.L. De Meo and G.A. Ferrante, " Three guide couplers in Ga As ", I.E.E.E J. Lightwave Technology, vol. LT-1, No. 2, pp 417-424, June 1983

[9] H.A. Haus and C.G. Fonstad, " Three waveguide couplers for improved sampling and filtering", I.E.E.E J. Quantum Electrons., vol. QE-14, pp 843-847, Nov. 1981

[10] Y. Twu, A. Dienes, S. Wang, and J.R. Whinnery, " High power coupled ridge waveguide semiconductor laser arrays " , Appl. Phys. Lett. 45(7), 1 Oct. 1984, pp. 709-711

CHAPTER 6

THE COMPLETE SPECTRUM OF RIB WAVEGUIDE

6.1 INTRODUCTION

Being an open structure the rib waveguide spectrum comprises discrete modes and a continuum, partly radiative and partly reactive. Excitation of the latter takes place due to discontinuities such as steps, gaps and bends. Therefore, in order to develop an accurate rigorous approach to analyzing practical components in rib waveguide, it is essential to obtain its complete spectrum, inclusive of the continuum. Once the complete spectrum is found, it can be used to formulate the appropriate Green's function of the guide for use in the treatment of discontinuity problems.

The determination of a complete orthonormal mode spectrum of open waveguide is only established for one - dimensional or two - dimensional separable cross sections. An analytical solution for the complete mode spectrum for the two - dimensional, non separable cross section, open waveguide structure especially for rib waveguides, is not readily available. The discrete components, however, can be found by a variety of methods such as those discussed in chapter two. In chapter three and four we have presented an accurate TRD solution of the problem which is sufficient to describe guided field distribution in the rib waveguide. The discrete modes found, can be normalised over the two - dimensional cross section and this problem is the subject of discussion in section 6.2. The continuum, however, is not known and no method seems to exist to extract this part of the spectrum. The non availability of the continuum has hindered the progress in the study of discontinuity problems in rib waveguide. Although the FEM/FDM method may be used to solve this class of problem [1,2], its complexity is well appreciated. Furthermore, the FEM/FDM method cannot be used for determining the far field radiation. Therefore, the motivation of the work presented in this chapter is

to develop a method of solution for the determination of the orthonormalised continuous spectrum specifically for the rib waveguide shown in Fig. 3.1. The approach adopted stems from a generalization of the method of Marcuvitz [3]. The analysis will be developed for the LSE polarization, having $E_y = 0$ and, H_y and E_x as the main field components. The LSM analysis can be obtained by following analogous procedure. Furthermore, globally hybrid radiation field can be represented by a superposition of LSE and LSM radiation modes [4], or derived directly [5].

In order to obtain a complete orthonormalised mode spectrum of the guide, we will consider first the question of the normalisation of the discrete spectrum found in chapter three. This is followed by the formal development of the orthonormalised continuous spectrum, the main objective of this chapter.

6.2 NORMALISATION OF THE DISCRETE MODE SPECTRUM - LSE/LSM

The unnormalised discrete modes were derived in chapter three by means of the Transverse Resonance Diffraction method in the LSE and LSM polarizations. These are reproduced here for the ease of reference.

For LSE polarization, $h_s(x,y) = H_y$ is given by

$$h_s(x,y) = V_s\,\phi_{sh}(y)\,\frac{\cos(q_{sh}(x+a))}{\cos(q_{sh}a)} + \sum_{\mu=e,o}\int_0^{\infty} d\rho\, V_\mu(\rho)\,\phi_{h\mu}(y,\rho)\,\frac{\cosh(\gamma(x+a))}{\cosh(\gamma a)}$$

$$+\int_0^{\nu} d\sigma\, V(\sigma)\,\phi_h(y,\sigma)\,\frac{\cosh(\eta(x+a))}{\cosh(\eta a)} \quad ;x\le 0 \;\; ;-\infty\le y\le\infty$$

$$h_s(x,y) = V'_s\,\psi_{sh}(y)\,e^{-\gamma_{sh}x} + \sum_{\mu=e,o}\int_0^{\infty} d\rho\, V'_\mu(\rho)\,\psi_{h\mu}(y,\rho)\,e^{-\gamma x} +$$

$$+\int_0^{\nu} d\sigma\, V'(\sigma)\,\psi_h(y,\sigma)\,e^{-\eta x} \quad ;x\ge 0 \;\; ;-\infty\le y\le\infty \qquad (6.1)$$

For LSM polarization, $e_s(x,y) = E_y$ is given by

$$e_s(x,y) = I_s\,\phi_{se}(y)\,\frac{\cos(q_{se}(x+a))}{\cos(q_{se}a)} + \sum_{\mu=e,o}\int_0^{\infty} d\rho\, I_\mu(\rho)\,\phi_{e\mu}(y,\rho)\,\frac{\cosh(\gamma(x+a))}{\cosh(\gamma a)}$$

$$+\int_0^{\nu} d\sigma\, I(\sigma)\,\phi_e(y,\sigma)\,\frac{\cosh(\eta(x+a))}{\cosh(\eta a)} \quad ;x\le 0 \;\; ;-\infty\le y\le\infty$$

$$e_s(x,y) = I'_s\,\psi_{se}(y)\,e^{-\gamma'_{se}x} + \sum_{\mu=e,o}\int_0^{\infty} d\rho\, I'_\mu(\rho)\,\psi_{e\mu}(y,\rho)\,e^{-\gamma x} +$$

$$+\int_0^{\nu} d\sigma\, I'(\sigma)\,\psi_e(y,\sigma)\,e^{-\eta x} \quad ;x\ge 0 \;\; ;-\infty\le y\le\infty \qquad (6.2)$$

We want to consider the question of their normalisation such that,

For LSE polarisation,

$$\iint_s h_{s\nu}(x,y)\,h_{s\mu}(x,y)\,dxdy = \delta_{\nu\mu} \qquad (6.3)$$

For LSM polarization

$$\iint_s e_{s\nu}(x,y)\,e_{s\mu}(x,y)\,dxdy = \delta_{\nu\mu} \qquad (6.4)$$

In (6.4) it is noted that the weight factor $\frac{1}{\varepsilon_r(y)}$ is already built in the normalisation of the slab mode spectrum. Generally, the value of the normalisation constant of the discrete mode can be found readily either by direct integration over the cross section or by using their equivalent circuit of Fig. 3.2 and Fig. 3.8 for the LSE and LSM polarizations respectively. We choose to use the latter method as it is more effective and it is also applicable to multiport situation (where the unknown field at the reference plane $x = 0$ is expanded in terms of discrete set of expanding function). In fact, the latter method is similar in principle to the method used in normalising discrete spectrum of a slab waveguide [3], and it has been successfully employed in normalising the discrete spectrum of two dimensional problem of inset dielectric guide [6] and image line [4]. For a bound mode of rib waveguide, the transverse wavenumber $k_{is}^2 = k_{xs}^2 + k_{ys}^2 = k_o^2 - \beta_s^2$ is fixed by the transverse resonance condition. By using the equivalent network of Fig. 3.2 (LSE) and Fig. 3.8 (LSM), we can write almost by

inspection the total transverse impedance Z (LSE) and admittance Y (LSM), as seen at the reference plane at the interface. They have been derived in chapter three and are reproduced here for the ease of reference.

For LSE polarization, the transverse impedance is given by:

$$Z = -j\omega\mu_0 \left[\frac{-q_{sh}\tan(q_{sh}a)}{q_{sh}^2+\beta_s^2} + \frac{\gamma'_{sh} < H(y)\,,\,\psi_{sh}(y) >^2}{(\beta_s^2-\gamma'^2_{sh}) < H(y)\,,\,\phi_{sh}(y) >^2} \right.$$
$$+ \sum_{\mu=e,o} \int_0^{\infty} \frac{d\rho}{k_o^2-\rho^2}\gamma \left[\frac{\tanh(\gamma a) < H(y)\,,\,\phi_{h\mu}(y,\rho) >^2 + < H(y)\,,\,\psi_{h\mu}(y,\rho) >^2}{< H(y)\,,\,\phi_{sh}(y) >^2} \right]$$
$$\left. + \int_0^{\nu} \frac{d\sigma}{\varepsilon_2 k_o^2-\sigma^2}\eta \left[\frac{\tanh(\eta a) < H(y)\,,\,\phi_h(y,\sigma) >^2 + < H(y)\,,\,\psi_h(y,\sigma) >^2}{< H(y)\,,\,\phi_{sh}(y) >^2} \right] \right] \qquad (6.5)$$

For LSM polarization, the transverse admittance is given by:

$$Y = -j\omega\varepsilon_0 \left[\frac{-q_{se}\tan(q_{se}a)}{q_{se}^2+\beta_s^2} + \frac{\gamma'_{se} < E(y)\,,\,\psi_{se}(y) >^2}{(\beta_s^2-\gamma'^2_{se}) < E(y)\,,\,\phi_{se}(y) >^2} \right.$$
$$+ \sum_{\mu=e,o} \int_0^{\infty} \frac{d\rho}{k_o^2-\rho^2}\gamma \left[\frac{\tanh(\gamma a) < E(y)\,,\,\phi_{e\mu}(y,\rho) >^2 + < E(y)\,,\,\psi_{e\mu}(y,\rho) >^2}{< E(y)\,,\,\phi_{se}(y) >^2} \right]$$
$$\left. + \int_0^{\nu} \frac{d\sigma}{\varepsilon_2 k_o^2-\sigma^2}\eta \left[\frac{\tanh(\eta a) < E(y)\,,\,\phi_e(y,\sigma) >^2 + < E(y)\,,\,\psi_e(y,\sigma) >^2}{< E(y)\,,\,\phi_{se}(y) >^2} \right] \right] \qquad (6.6)$$

To normalise the surface modes it is necessary to determine the residue of the transverse Green's function at its singularities. For the LSE polarization, the Green's function may be constructed from two independent solutions of the transverse equivalent network of Fig. 3.2 . This is given by

$$G(r;k_{ts}) = \frac{I^-(r;k_{ts}^2)\,I^+(r;k_{ts}^2)}{j\omega\varepsilon_0 Z(k_{ts}^2)}$$

where Z is the total impedance of the transverse equivalent network. The singularity of $G(r;k_{ts})$ coincides with the resonance of the equivalent network i.e. the vanishing of the total reactance of the transverse equivalent network. Hence, the normalisation constant

N_s is given by,

$$N_s^2 = j\omega\varepsilon_0 \frac{\partial Z}{\partial k_t^2}\,(k_t^2 = k_{ts}^2)$$

$$= \frac{1}{2\,q_{sh}}\left[\, q_{sh}a\, sec^2(q_{sh}a) + \tan(q_{sh}a)\,\right] < H(y)\,,\,\phi_{sh}(y) >^2 + \frac{< H(y)\,,\,\psi_{sh}(y) >^2}{2\,\gamma'_{sh}}$$

$$+ \sum_{\mu=e,o} \int_0^\infty d\rho\, \frac{1}{2\gamma}\Big[\, (\gamma a\, sech^2(\gamma a) + \tanh(\gamma a)) < H(y)\,,\,\phi_{h\mu}(y,\rho) >^2$$

$$+ < H(y)\,,\,\psi_{h\mu}(y,\rho) >^2 \,\Big]$$

$$+ \int_0^\nu d\sigma\, \frac{1}{2\eta}\Big[\, (\eta a\, sech^2(\eta a) + \tanh(\eta a)) < H(y)\,,\,\phi_h(y,\sigma) >^2 \qquad (6.7)$$

$$+ < H(y)\,,\,\psi_h(y,\sigma) >^2 \,\Big]$$

By similar argument, we have for the LSM modes

$$N_s^2 = j\omega\mu_0 \frac{\partial Y}{\partial k_t^2}\,(k_t^2 = k_{ts}^2)$$

$$= \frac{1}{2\,q_{se}}\left[\, q_{se}a\, sec^2(q_{se}a) + \tan(q_{se}a)\,\right] < E(y)\,,\,\phi_{se}(y) >^2 + \frac{< E(y)\,,\,\psi_{se}(y) >^2}{2\,\gamma'_{se}}$$

$$+ \sum_{\mu=e,o} \int_0^\infty d\rho\, \frac{1}{2\gamma}\Big[\, (\gamma a\, sech^2(\gamma a) + \tanh(\gamma a)) < E(y)\,,\,\phi_{e\mu}(y,\rho) >^2$$

$$+ < E(y)\,,\,\psi_{e\mu}(y,\rho) >^2 \,\Big]$$

$$+ \int_0^\nu d\sigma\, \frac{1}{2\,\eta}\left[\, (\eta a\, sech^2(\eta a) + \tanh(\eta a)) < E(y)\,,\,\phi_e(y,\sigma) >^2 \qquad (6.8)\right.$$

$$+ < E(y)\,,\,\psi_e(y,\sigma) >^2 \,\Big]$$

It is straight forward to check by direct integration over the cross section that the expressions in equation (6.7) and (6.8) equals

$$N_s^2 = \int_{-\infty}^{\infty} dy \int_{-a}^{\infty} dx\, \psi_s^2(x,y)$$

where,

$\psi_s(x,y) = h_s(x,y)$; for *LSE polarization*

$= e_s(x,y)$; for *LSM polarization*

and $h_s(x,y)$ and $e_s(x,y)$ are given by (6.1) and (6.2) respectively.

6.3 DETERMINATION OF THE ORTHONORMALISED CONTINUOUS SPECTRUM OF THE RIB WAVEGUIDE

The determination of the continuum of an open waveguide with a non separable cross section does not seem so far, to have drawn the attention of the researchers. The only work on this subject reported in the literature are those for the inset guide [6] and image line [4]. The approach considers an expansion of the field in the air region above the dielectric - air interface in terms of partial plane waves without enforcing satisfaction of boundary and edge conditions on each individual component of the continuum. The problem with this approach is that the solution is often slow to converge. In order to improve the technique, a procedure which takes in to account the simultaneous excitation of the whole "wave packet" satisfying boundary and edge conditions is required. This is the approach adopted in this work and the analysis is developed to derive the continuum for pure LSE polarisation. This involves constructing the transverse Green's function from an outward and inward travelling wave at the reference plane at the interface $x = 0$. Transverse resonance condition is imposed and the branch cut singularity, where the impedance does not vanish gives rise to the continuum. It is worth remarking here that, this approach is in fact, the generalization of the Marcuvitz method [3] to the two - dimensional non separable problem. The basic concepts and notations used in the discussion in chapter two are, therefore, needed in the following development.

6.31 COMPLETENESS OF THE SPECTRUM

The completeness of the LSE spectrum of the rib waveguide may be stated as,

$$\sum_{\nu=1}^{N} h_{s\nu}(x,y)\, h_{s\nu}(x',y') + \int_0^{\infty} dk_t \sum_{\nu} h_{\nu}(x,y;k_t)\, h_{\nu}(x',y';k_t) = \delta(r-r') \tag{6.10}$$

The summation is over the finite number of discrete bound modes where energy is guided indefinitely along a waveguide. The integral is over the continuum and the orthonormalization is such that

$$\iint_s h_{s\mu}(x,y)\, h_{s\nu}(x,y)\, dx\, dy = \delta_{\mu\nu} \tag{6.11a}$$

$$\iint_s h_{\mu}(x,y;k_t)\, h_{\nu}(x,y;k_t')\, dx\, dy = \delta_{\mu\nu} \cdot \delta(k_t - k_t') \tag{6.11b}$$

where

$$\iint_s h_{\mu}(x,y;k_t)\, h_{\nu}(x,y;k_t)\, dx\, dy = 0$$

Here, we emphasize that orthogonality holds when $\mu = \nu$ provide that values of k_t and k_t' differ. In other words, a continuous mode is orthogonal to it self for different values of k_t.

The discrete set bound mode propagation constants means that the fields of the waveguide in the resonance state are given by the finite sum over all bound modes. In contrast, each radiation and evanescent continuous mode can take any of the continuum of propagation constant values, and thus an integration over all values of k_t is necessary. However, like bound modes, the continuous modes requires summation over the subscript ν to account for the different transverse distributions corresponding to the same value of k_t. Hence, in (6.10) a component of the continuum is labelled by means of two indices, one discrete ν, the other continuous.

The representation in equation (6.10) is analogous to the completeness equation (2.31) for the slab waveguide we met in chapter two, and consequently, it is also identical to

the contour integral of the Green's function of the transverse wave equation

$$\nabla_t^2 h_v + (\varepsilon_r k_o^2 - \beta^2)\, h_v = 0 \tag{6.12}$$

integrated over a path C in the complex k_t^2 - plane to include all singularities. The singularities are constituted by the set of discrete poles corresponding to the discrete spectrum and branch cut corresponding to the continuum, namely

$$-\frac{1}{j2\pi}\oint_c g(r,r';k_t^2)\, dk_t^2 = \delta(r-r') \tag{6.13}$$

In (6.12), h_v is the magnetic field transverse to x namely h_{vy}. For each value of k_t^2, the Green's function in (6.13) is constructed from two independent wave solutions with boundary condition appropriate for H_y for propagation in x direction namely, a standing wave solution I^- satisfying boundary condition for $x < 0$ and travelling wave solution I^+ satisfying boundary condition for $x > 0$, given by

$$\begin{aligned} I^+(x,y;k_t^2) = {} & \phi_{sh}(y)\, \tilde{H}_{vs}^- \frac{\cos(k_{x1}(x+a))}{\cos(k_{x1}a)} \\ & + \sum_{\mu=e,o} \int_0^\infty d\rho\, \tilde{H}_{v\mu}^-(\rho;k_t)\, \phi_{h\mu}(y,\rho) \frac{\cos(k_{x1}(\rho)(x+a))}{\cos(k_{x1}(\rho)a)} \\ & + \int_0^v d\sigma\, \tilde{H}_v^-(\sigma;k_t)\, \phi_h(y,\sigma) \frac{\cos(k_{x1}(\sigma)(x+a))}{\cos(k_{x1}(\sigma)a)} \end{aligned} \tag{6.14a}$$

$$\begin{aligned} I^-(x,y;k_t^2) = {} & \psi_{sh}(y)\, \tilde{H}_{vs}^+ e^{-jk_{x2}x} + \sum_{\mu=e,o} \int_0^\infty d\rho\, \tilde{H}_{v\mu}^+(\rho;k_t)\, \psi_{h\mu}(y,\rho)\, e^{-jk_{x2}(\rho)x} \\ & + \int_0^v d\sigma\, \tilde{H}_v^+(\sigma;k_t)\, \psi_h(y,\sigma)\, e^{-jk_{x2}(\sigma)x} \end{aligned} \tag{6.14b}$$

At the interface plane $x = 0$, we have

$$I^-(0,y;k_t^2) = I^+(0,y;k_t^2) = H_v(y;k_t) \tag{6.15}$$

where $H_v(y;k_t)$ is an interface field function normalised to unity over the interface domain satisfying edge and boundary conditions.

We have then the Green's function,

$$g(x,y,x',y';k_t^2) = \sum_{\nu} \frac{I^-(x,y;k_t^2)\, I^+(x,y;k_t^2)}{-j\omega\varepsilon_0\, Z_\nu(k_t^2)} \tag{6.16}$$

where $Z_\nu(k_t^2)$ is the total transverse impedance of the ν - th solution for a given value of k_t^2.

It is noted that the occurrence of a pole of g in the complex k_t^2 - plane corresponding to the existence of discrete modes coincides with the vanishing of the total transverse impedance Z_ν. The non vanishing of Z_ν corresponding to branch line singularity give rise to the continuum part of the spectrum. To recover (6.10) from (6.16) , it is required to isolate the residues of the poles and modify the integration path so as to go around the branch line in the positive k_t^2 axis, by which process using (6.10), (6.13) and (6.16) , we recover the required completeness relationship given by

$$\sum_{\nu=1}^{N} \frac{I_\nu^-(x,y;k_{ts}^2)\, I_\nu^+(x,y;k_{ts}^2)}{-j\omega\varepsilon_0 \left.\dfrac{\partial Z_\nu}{\partial k_{ts}^2}\right|_{k_{ts}^2}} + \frac{2}{\pi}\int_0^\infty dk_t\, k_t\, \mathrm{Im} \sum_{\nu} \frac{I_\nu^-(x,y;k_t^2)\, I_\nu^+(x,y;k_t^2)}{-j\omega\varepsilon_0\, Z_\nu(k_t^2)}$$

$$= \sum_{\nu=1} h_{s\nu}(x,y)\, h_{s\nu}(x',y') + \int_0^\infty dk_t \sum_{\nu} h_\nu(x,y;k_t)\, h_\nu(x',y';k_t) \tag{6.17}$$

The contribution of the discrete modes which is characterized by the finite summation have been treated in chapter three by means of TRD approach and their normalisation over the guide cross section was discussed in section 6.2. The integral characterized the contribution of the continuous part of the spectrum and the method of determining them is the subject of the following discussion. In fact, from the above discussion one notices that the Marcuvitz formalism is not needed in the direct approach that follows.

6.32 CONSTRUCTION OF EIGENVALUE EQUATION AND MODE SPECTRUM

To generalise the concept of transverse resonance used in the discrete case to this problem, we need to formulate the eigenvalue equation at the interface plane $x = 0$. In (6.15), $H_\nu(y,k_t)$ is a real interface field eigenfunction of the complex impedance

operator $\tilde{Z}(k_t)$ evaluated at $x = 0$. There, the impedance operator $\tilde{Z}(k_t)$ may be written as

$$\tilde{Z}(0,y,x'=0,y';k_t) = \tilde{Z}^{-}(k_t) + \tilde{Z}^{+}(k_t) \tag{6.18}$$

where $\tilde{Z}^{-}(k_t)$ and $\tilde{Z}^{+}(k_t)$ are the complex impedance operator which link the transverse to x electric and magnetic field to the left and right of the interface plane respectively. In order to establish the expression of these operators and hence the eigenvalue equation of the problem, we express the transverse to x field at each side of the interface plane separately as given by,

For $x < 0$,

$$\begin{aligned} H_{vy}(x,y;k_t) = {} & \tilde{H}^{-}_{vs}\,\phi_{sh}(y)\,\frac{\cos(k_{x1}(x+a))}{\cos(k_{x1}a)} \\ & + \sum_{\mu=e,o}\int_0^{\infty} d\rho\,\tilde{H}^{-}_{v\mu}(\rho;k_t)\,\phi_{h\mu}(y,\rho)\,\frac{\cos(k_{x1}(\rho)(x+a))}{\cos(k_{x1}(\rho)a)} \\ & + \int_0^{v} d\sigma\,\tilde{H}^{-}_{v}(\sigma;k_t)\,\phi_{h}(y,\sigma)\,\frac{\cos(k_{x1}(\sigma)(x+a))}{\cos(k_{x1}(\sigma)a)} \end{aligned} \tag{6.19a}$$

$$\begin{aligned} E_{vz}(x,y;k_t) = j\omega\mu_0 \Bigg[& \frac{k_{x1}}{k_{x1}^2+\beta^2}\,\tilde{H}^{-}_{vs}\,\phi_{sh}(y)\,\frac{\sin(k_{x1}(x+a))}{\cos(k_{x1}a)} \\ & + \sum_{\mu=e,o}\int_0^{\infty} \frac{d\rho}{k_o^2-\rho^2}\,\tilde{H}^{-}_{v\mu}\,\phi_{h\mu}(y,\rho)\,k_{x1}(\rho)\,\frac{\sin(k_{x1}(\rho)(x+a))}{\cos(k_{x1}(\rho)a)} \\ & + \int_0^{v} \frac{d\sigma}{\varepsilon_2 k_o^2-\sigma^2}\,\tilde{H}^{-}_{v}\phi_{h}(y,\sigma)\,k_{x1}(\sigma)\,\frac{\sin(k_{x1}(\sigma)(x+a))}{\cos(k_{x1}(\sigma)a)} \Bigg] \end{aligned} \tag{6.19b}$$

and for $x > 0$,

$$\begin{aligned} H_{vy}(x,y;k_t) = {} & \tilde{H}^{+}_{vs}\,\psi_{sh}(y)\,e^{-jk_{x2}x} + \sum_{\mu=e,o}\int_0^{\infty} d\rho\,\tilde{H}^{+}_{v\mu}(\rho;k_t)\,\psi_{h\mu}(y,\rho)\,e^{-jk_{x2}(\rho)x} \\ & + \int_0^{v} d\sigma\,\tilde{H}^{+}_{v}(\sigma;k_t)\,\psi_{h}(y,\sigma)\,e^{-jk_{x2}(\sigma)x} \end{aligned} \tag{6.20a}$$

$$E_{vz}(x,y;k_t) = \omega\mu_0 \left[\frac{k_{x2}}{k_{x2}^2 + \beta^2} \tilde{H}_{vs}^{+} \psi_{sh}(y)\, e^{-jk_{x2}x} \right.$$

$$+ \sum_{\mu=e,o} \int_0^{\infty} \frac{d\rho}{k_o^2 - \rho^2} \tilde{H}_{v\mu}^{+} \psi_{h\mu}(y,\rho)\, k_{x2}(\rho)\, e^{-jk_{x2}(\rho)x} +$$

$$\left. + \int_0^{v} \frac{d\sigma}{\varepsilon_2 k_o^2 - \sigma^2} \tilde{H}_{v}^{+} \psi_{h}(y,\sigma)\, k_{x2}(\sigma)\, e^{-jk_{x2}(\sigma)x} \right] \qquad (6.20b)$$

By applying the continuity of the transverse field at the interface plane, we have

$$H_{vy}(0,y;k_t) = H_v(y;k_t)$$

$$= \tilde{H}_{vs}^{+} \psi_{sh}(y) + \sum_{\mu=e,o} \int_0^{\infty} d\rho\, \tilde{H}_{v\mu}^{+}(\rho;k_t)\, \psi_{h\mu}(y,\rho)$$

$$+ \int_0^{v} d\sigma\, \tilde{H}_{v}^{+}(\sigma;k_t)\, \psi_{h}(y,\sigma)$$

$$= \tilde{H}_{vs}^{-} \phi_{sh}(y) + \sum_{\mu=e,o} \int_0^{\infty} d\rho\, \tilde{H}_{v\mu}^{-}(\rho;k_t)\, \phi_{h\mu}(y,\rho)$$

$$+ \int_0^{v} d\sigma\, \tilde{H}_{v}^{-}(\sigma;k_t)\, \phi_{h}(y,\sigma) \qquad (6.21)$$

and from the orthogonality of the slab mode function we recover,

$$\tilde{H}_{vs}^{+} = \int_{-\infty}^{\infty} \psi_{sh}(y)\, H_v(y;k_t)\, dy \qquad (6.22a)$$

$$\tilde{H}_{v\mu}^{+}(\rho;k_t) = \int_{-\infty}^{\infty} \psi_{h\mu}(y,\rho)\, H_v(y;k_t)\, dy \qquad (6.22b)$$

$$\tilde{H}_{v}^{+}(\sigma;k_t) = \int_{-\infty}^{\infty} \psi_{h}(y,\sigma)\, H_v(y;k_t)\, dy \qquad (6.22c)$$

$$\tilde{H}_{vs}^{-} = \int_{-\infty}^{\infty} \phi_{sh}(y)\, H_v(y;k_t)\, dy \qquad (6.22d)$$

$$\tilde{H}_{v\mu}^{-}(\rho;k_t) = \int_{-\infty}^{\infty} \phi_{h\mu}(y,\rho)\, H_v(y;k_t)\, dy \qquad (6.22e)$$

$$\tilde{H}_{v}^{-}(\sigma;k_t) = \int_{-\infty}^{\infty} \phi_{h}(y,\sigma)\, H_v(y;k_t)\, dy \qquad (6.22f)$$

Substituting (6.22a to 6.22c) in to (6.20b) and (6.22d to 6.22f) in to (6.19b) and rearranging gives the integral operator $\tilde{Z}^{+}(k_t)$ and $\tilde{Z}^{-}(k_t)$ on the R.H.S. and L.H.S. of the discontinuous interface plane respectively which may be written as,

$$E_{vz}^{x<0}(0,y;k_t) = \int_{-\infty}^{\infty} Z^{-} H_v(y';k_t)\, dy' = \tilde{Z}^{-} \cdot H_v(y;k_t) \tag{6.23a}$$

$$E_{vz}^{x>0}(0,y;k_t) = \int_{-\infty}^{\infty} Z^{+} H_v(y';k_t)\, dy' = \tilde{Z}^{+} \cdot H_v(y;k_t) \tag{6.23b}$$

where the kernels of the above complex impedance operators are given by

$$\begin{aligned} Z^{-}(x,y,x',y';k_t) = j\omega\mu_0 \Bigg[& \frac{k_{x1}}{k_{x1}^2 + \beta^2} \tan(k_{x1}a)\, \phi_{sh}(y)\, \phi_{sh}(y') \\ & + \sum_{\mu=e,o} \int_0^{\infty} \frac{d\rho}{k_o^2 - \rho^2} k_{x1}(\rho) \tan(k_{x1}(\rho)a)\, \phi_{h\mu}(y,\rho)\, \phi_{h\mu}(y',\rho) \\ & + \int_0^{\nu} \frac{d\sigma}{\varepsilon_2 k_o^2 - \sigma^2} k_{x1}(\sigma) \tan(k_{x1}(\sigma)a)\, \phi_h(y,\sigma)\, \phi_h(y',\sigma) \Bigg] \end{aligned} \tag{6.24a}$$

$$\begin{aligned} Z^{+}(x,y,x',y';k_t) = \omega\mu_0 \Bigg[& \frac{k_{x2}}{k_{x2}^2 + \beta^2} \psi_{sh}(y)\, \psi_{sh}(y') \\ & + \sum_{\mu=e,o} \int_0^{\infty} \frac{d\rho}{k_o^2 - \rho^2} k_{x2}(\rho)\, \psi_{h\mu}(y,\rho)\, \psi_{h\mu}(y',\rho) \\ & + \int_0^{\nu} \frac{d\sigma}{\varepsilon_2 k_o^2 - \sigma^2} k_{x2}(\sigma)\, \psi_h(y,\sigma)\, \psi_h(y',\sigma) \Bigg] \end{aligned} \tag{6.24b}$$

The wavenumbers appearing in equation (6.19 to 6.24) are defined as,

$$k_{x1}^2 = \varepsilon_{eh1} k_o^2 - \beta^2 = (\varepsilon_{eh1} - 1)k_o^2 + k_t^2$$

$$k_{x1}^2(\rho) = k_t^2 - \rho^2$$

$$i.e. \quad k_{x1}(\rho) = \sqrt{k_t^2 - \rho^2} \quad ; k_t \geq \rho$$

$$= -j\sqrt{\rho^2 - k_t^2} = -j\gamma \quad ; k_t \leq \rho$$

$$k_{x1}^2(\sigma) = (\varepsilon_2 - 1)k_o^2 + k_t^2 - \sigma^2$$

$$k_{x2}^2 = (\varepsilon_{eh2} - 1)k_o^2 + k_t^2$$

$$k_{x2}(\rho) = \sqrt{k_t^2 - \rho^2} \qquad ; k_t \geq \rho$$

$$= -j\gamma \qquad ; k_t \leq \rho$$

$$k_{x2}^2(\sigma) = (\varepsilon_2 - 1)k_o^2 + k_t^2 - \sigma^2$$

ε_{eh1} and ε_{eh2} is the the effective dielectric constant of the slab to the left and to the right of the interface plane respectively.

Imposing the continuity of E_{vz} defined in equation (6.23) at the discontinuous interface $x = 0$, is equivalent to requiring $H_v(y;k_t)$ to be a real eigenfunction of the complex operator $\tilde{Z}(k_t)$. This constraint can be satisfied if we make $H_v(y;k_t)$ to be a common eigenfunction to the real and imaginary part of the complex operator $\tilde{Z}(k_t)$, which exists as the eigen solution of the eigenvalue problem given by

$$\text{Im}\,\tilde{Z}(k_t)\, H_v(y;k_t) = \tan(\alpha_v(k_t))\, \text{Re}\,\tilde{Z}(k_t)\, H_v(y;k_t) \tag{6.25}$$

From (6.18) and (6.24) we have,

$$\text{Re}\,\tilde{Z}(k_t) = \omega\mu_0 \left[\frac{k_{x2}}{k_{x2}^2 + \beta^2} \psi_{sh}(y)\, \psi_{sh}(y') \right.$$

$$+ \sum_{\mu=e,o} \int_0^{k_t} \frac{d\rho}{k_o^2 - \rho^2} k_{x2}(\rho)\, \psi_{h\mu}(y,\rho)\, \psi_{h\mu}(y',\rho)$$

$$\left. + \int_0^{v} \frac{d\sigma}{\varepsilon_2 k_o^2 - \sigma^2} k_{x2}(\sigma)\, \psi_h(y,\sigma)\, \psi_h(y',\sigma) \right] \tag{6.26}$$

$$\text{Im}\,\tilde{Z}(k_t) = \omega\mu_0 \left[\frac{k_{x1}}{k_{x1}^2 + \beta^2} \tan(k_{x1}a)\, \phi_{sh}(y)\, \phi_{sh}(y') \right.$$

$$+ \sum_{\mu=e,o} \int_0^{\infty} \frac{d\rho}{k_o^2 - \rho^2} k_{x1}(\rho) \tan(k_{x1}(\rho)a)\, \phi_{h\mu}(y,\rho)\, \phi_{h\mu}(y',\rho)$$

$$\left. - \sum_{\mu=e,o} \int_{k_t}^{\infty} \frac{d\rho}{k_o^2 - \rho^2} \gamma\, \psi_{h\mu}(y,\rho)\, \psi_{h\mu}(y',\rho) \right.$$

$$+\int_0^{\nu}\frac{d\sigma}{\varepsilon_2 k_o^2-\sigma^2}\,k_{x1}(\sigma)\tan(k_{x1}(\sigma)a)\,\phi_h(y,\sigma)\,\phi_h(y',\sigma)\Bigg] \tag{6.27}$$

and

$$\tilde{Z}(k_t)=\mathrm{Re}\,\tilde{Z}(k_t)+j\,\mathrm{Im}\,\tilde{Z}(k_t) \tag{6.28}$$

Hence, using (6.28) we may write (6.25) as,

$$\begin{aligned}\tilde{Z}\cdot H_\nu(y;k_t)&=(1+j\tan(\alpha_\nu(k_t)))\,\mathrm{Re}\,\tilde{Z}(k_t)\,H_\nu(y;k_t)\\&=Z_\nu\,\mathrm{Re}\,\tilde{Z}(k_t)\,H_\nu(y;k_t)\end{aligned} \tag{6.29}$$

and

$$Z_\nu=1+j\tan(\alpha_\nu(k_t)) \tag{6.30}$$

By using equation (6.14), (6.17) and (6.30) one recover the normalized continuous modes as

$$\begin{aligned}h_\nu(x,y;k_t)=\sqrt{\frac{2}{\pi}k_t}\cos(\alpha_\nu(k_t))\Bigg[&\tilde{H}^-_{\nu s}\,\phi_{sh}(y)\,\frac{\cos(k_{x1}(x+a))}{\cos(k_{x1}a)}\\&+\sum_{\mu=e,o}\int_0^{\infty}d\rho\,\tilde{H}^-_{\nu\mu}(\rho;k_t)\,\phi_{h\mu}(y,\rho)\,\frac{\cos(k_{x1}(\rho)(x+a))}{\cos(k_{x1}(\rho)a)}\\&+\int_0^{\nu}d\sigma\,\tilde{H}^-_{\nu}(\sigma;k_t)\,\phi_h(y,\sigma)\,\frac{\cos(k_{x1}(\sigma)(x+a))}{\cos(k_{x1}a)}\Bigg]\qquad;x\le 0\\=\sqrt{\frac{2}{\pi}k_t}\Bigg[&\tilde{H}^+_{\nu s}\,\psi_{sh}(y)\cos(k_{x2}x+\alpha_\nu)\\&+\sum_{\mu=e,o}\int_0^{k_t}d\rho\tilde{H}^+_{\nu\mu}(\rho;k_t)\,\psi_{h\mu}(y,\rho)\cos(k_{x2}(\rho)x+\alpha_\nu)\\&+\cos(\alpha_\nu)\sum_{\mu=e,o}\int_{k_t}^{\infty}d\rho\,\tilde{H}^+_{\nu\mu}(\rho;k_t)\,\psi_{h\mu}(y,\rho)\,e^{-\gamma x}\end{aligned}$$

$$+\int_0^{\nu} d\sigma\, \tilde{H}_{\nu}^{+}(\sigma;k_t)\, \psi_h(y,\sigma) \cos(k_{x2}(\sigma)x + \alpha_{\nu}) \Bigg] \quad ; x \geq 0 \tag{6.31}$$

The orthonormality condition of $h_{\nu}(x,y;k_t)$ and $h_{\mu}(x,y;k_t')$ is checked out explicitly in appendix at the end of the chapter.

6.33 SOLUTION OF THE EIGENVALUE EQUATION

The application of the continuous spectrum developed in the previous section depends on efficiently solving the eigenvalue equation (6.25) for each value of k_t ($0 \leq k_t < \infty$). The eigenvalue equation can be solved by a variety of ways, the one proposed to be used here being the Ritz - Galerkin variational approach. This requires an orthonormal basis function which incorporates all the boundary and edge conditions at the interface to expand the interface field $H_{\nu}(y;k_t)$. In order to use the method of solution we need to construct the variational expression for the eigenvalue $\tan(\alpha_{\nu})$. Multiplying (6.25) by $H_{\nu}(y;k_t)$ and integrating with respect to y from $-\infty$ to ∞ we obtain the variational expression for $\tan(\alpha_{\nu})$ given by

$$\tan(\alpha_{\nu}) \int_{-\infty}^{\infty} dy \int_{-\infty}^{\infty} dy'\, H_{\nu}(y;k_t)\, H_{\nu}(y';k_t)\, \mathrm{Re}\, Z(y,y';k_t)$$

$$= \int_{-\infty}^{\infty} dy \int_{-\infty}^{\infty} dy'\, H_{\nu}(y;k_t)\, H_{\nu}(y';k_t)\, \mathrm{Im}\, Z(y,y';k_t) \tag{6.32}$$

where,

$$\mathrm{Re}\, Z(y,y';k_t) = \frac{k_{x2}}{k_{x2}^2 + \beta^2}\, \psi_{sh}(y)\, \psi_{sh}(y')$$

$$+ \sum_{\mu=e,o} \int_0^{k_t} \frac{d\rho}{k_o^2 - \rho^2}\, k_{x2}(\rho)\, \psi_{h\mu}(y,\rho)\, \psi_{h\mu}(y',\rho)$$

$$+ \int_0^{\nu} \frac{d\sigma}{\varepsilon_2 k_o^2 - \sigma^2}\, k_{x2}(\sigma)\, \psi_h(y,\sigma)\, \psi_h(y',\sigma) \tag{6.33}$$

$$\text{Im}\, Z(y,y';k_t) = \frac{k_{x1}}{k_{x1}^2+\beta^2}\tan(k_{x1}a)\,\phi_{sh}(y)\,\phi_{sh}(y')$$

$$+\sum_{\mu=e,o}\int_0^{\infty}\frac{d\rho}{k_o^2-\rho^2}\,k_{x1}(\rho)\tan(k_{x1}(\rho)a)\,\phi_{h\mu}(y,\rho)\,\phi_{h\mu}(y',\rho)$$

$$+\int_0^{\nu}\frac{d\sigma}{\varepsilon_2 k_o^2-\sigma^2}\,k_{x1}(\sigma)\tan(k_{x1}(\sigma)a)\,\phi_h(y,\sigma)\,\phi_h(y',\sigma)$$

$$-\sum_{\mu=e,o}\int_{k_t}^{\infty}\frac{d\rho}{k_o^2-\rho^2}\,\gamma\,\psi_{h\mu}(y,\rho)\,\psi_{h\mu}(y',\rho) \qquad (6.34)$$

The interface field $H_\nu(y;k_t)$ is expanded by means of orthogonal complete basis $f_n(y)$ satisfying boundary and edge conditions such that

$$H_\nu(y;k_t) = \sum_n X_{\nu n}\, f_n(y) \qquad (6.35)$$

Substituting (6.35) in (6.32), $\text{Re}\,\tilde{Z}$ and $\text{Im}\,\tilde{Z}$ becomes a square matrix and equation (6.32) becomes a matrix eigenvalue equation given by

$$\tan(\alpha_\nu)\,\underline{X}_\mu^T\,\text{Re}\,\underline{\underline{Z}}\,\underline{X}_\nu = \underline{X}_\mu^T\,\text{Im}\,\underline{\underline{Z}}\,\underline{X}_\nu \qquad (6.36)$$

with,

$$\underline{\underline{Z}}_{pq}^R = \text{Re}\,\underline{\underline{Z}}_{pq} = \frac{Q_p\,Q_q\,k_{x2}}{k_{x2}^2+\beta^2} + \sum_{\mu=e,o}\int_0^{k_t}\frac{d\rho}{k_o^2-\rho^2}\,k_{x2}(\rho)\,Q_{p\mu}(\rho)\,Q_{q\mu}(\rho)$$

$$+\int_0^{\nu}\frac{d\sigma}{\varepsilon_2 k_o^2-\sigma^2}\,k_{x2}(\sigma)\,Q_p(\sigma)\,Q_q(\sigma) \qquad (6.37a)$$

$$\underline{\underline{Z}}_{pq}^I = \text{Im}\,\underline{\underline{Z}}_{pq} = \frac{k_{x1}}{k_{x1}^2+\beta^2}\tan(k_{x1}a)\,P_p\,P_q$$

$$+\sum_{\mu=e,o}\int_0^{\infty}\frac{d\rho}{k_o^2-\rho^2}\,k_{x1}(\rho)\tan(k_{x1}(\rho)a)\,P_{p\mu}\,P_{q\mu}$$

$$+\int_0^{\nu}\frac{d\sigma}{\varepsilon_2 k_o^2-\sigma^2}\,k_{x1}(\sigma)\tan(k_{x1}(\sigma)a)\,P_p(\sigma)\,P_q(\sigma)$$

$$-\sum_{\mu=e,o}\int_{k_t}^{\infty}\frac{d\rho}{k_o^2-\rho^2}\,\gamma\,Q_{p\mu}\,Q_{q\mu} \qquad (6.37b)$$

Hence, we have a matrix eigenvalue equation for α_ν and X_ν, given by

$$\tan(\alpha_\nu)\underline{\underline{Z}}^R \cdot \underline{X}_\nu = \underline{\underline{Z}}^I \cdot \underline{X}_\nu \tag{6.38}$$

In (6.38), X_ν's are orthogonal w.r.t. $\underline{\underline{Z}}^R$ [7], and hence

$$\underline{X}_\mu^T \cdot \underline{\underline{Z}}^R \cdot \underline{X}_\nu = \delta_{\mu\nu} \tag{6.39}$$

Solving (6.38) gives the eigenvectors X_ν's and the continuous modes of the guide $h_\nu(x,y;k_t)$ can then be obtained from $H_\nu(y;k_t)$ through (6.22).

It is noted that the practical choice of basis function $f_n(y)$ in (6.35) is very limited. However, the polynomials $F_n(y)$ constructed from the "transition function" developed in chapter 3 provide an appropriate basis to expand the interface field.

FIRST ORDER VARIATIONAL SOLUTION

In order to overcome the computation complexity and to improve the effeciency of solving the eigenvalue problem, we investigate the application of a single "transition function" as a trial field to expand the interface field $H(y;k_t)$. Clearly, this is an approximation but it has been proved to be a successful and accurate one for the discrete modes. Approximating $H(y;k_t)$ by a "transition function" gives,

$$H(y;k_t) \approx \overline{U}_{sh}(y) \tag{6.40}$$

From (6.32) we have

$$\tan(\alpha(k_t)) = \frac{\int_{-\infty}^{\infty}\int_{-\infty}^{\infty} dy\, dy'\, H(y;k_t)\, H(y';k_t)\, \mathrm{Im}\, Z(y,y';k_t)}{\int_{-\infty}^{\infty}\int_{-\infty}^{\infty} dy\, dy'\, H(y;k_t)\, H(y';k_t)\, \mathrm{Re}\, Z(y,y';k_t)} \tag{6.41}$$

Substituting (6.40) in to (6.41) we obtain

$$\tan(\alpha(k_t)) = \Bigg[\frac{k_{x1}}{k_{x1}^2+\beta^2} P^2 \tan(k_{x1}a) + \sum_{\mu=e,o} \int_0^{\infty} \frac{d\rho}{k_o^2-\rho^2} P_\mu^2(\rho)\, k_{x1}(\rho) \tan(k_{x1}(\rho)a)$$

$$+ \int_0^{\nu} \frac{d\sigma}{\varepsilon_2 k_o^2-\sigma^2} P^2(\sigma)\, k_{x1}(\sigma) \tan(k_{x1}(\sigma)a)$$

$$- \sum_{\mu=e,o} \int_{k_t}^{\infty} \frac{d\rho}{k_o^2-\rho^2} \gamma Q_\mu^2(\rho) \Bigg] \times$$

$$\Bigg[\frac{k_{x2}}{k_{x2}^2+\beta^2} Q^2 + \sum_{\mu=e,o} \int_0^{k_t} \frac{d\rho}{k_o^2-\rho^2} k_{x2}(\rho)\, Q_\mu^2(\rho) \qquad (6.42)$$

$$+ \int_0^{\nu} \frac{d\sigma}{\varepsilon_2 k_o^2-\sigma^2} k_{x2}(\sigma)\, Q^2(\sigma) \Bigg]^{-\frac{1}{2}}$$

where we have defined,

$$P = < \overline{U}_{sh}(y) , \phi_h(y) >$$

$$P_\mu(\rho) = < \overline{U}_{sh}(y) , \phi_{h\mu}(y,\rho) >$$

$$P(\sigma) = < \overline{U}_{sh}(y) , \phi_h(y,\sigma) >$$

$$Q = < \overline{U}_{sh}(y) , \psi_h(y) >$$

$$Q_\mu(\rho) = < \overline{U}_{sh}(y) , \psi_h(y,\rho) >$$

$$Q(\sigma) = < \overline{U}_{sh}(y) , \psi_h(y,\sigma) >$$

Using (6.42), $\alpha(k_t)$ can be evaluated for each value of k_t and, hence, the continuous mode in (6.31) is completely defined.

If the small - step approximation is made, i.e $\phi_{sh} \approx \psi_{sh} \approx \overline{U}_{sh}(y)$, then, by orthogonality, the contributions of air and substrate modes vanish and equation (6.42) becomes

$$\tan(\alpha(k_t)) = \frac{k_{x1}\, \varepsilon_{eh2}}{k_{x2}\, \varepsilon_{eh1}} \tan(k_{x1}a) \qquad (6.43)$$

Furthermore, for a small step $\varepsilon_{eh1} \approx \varepsilon_{eh2}$, then equation (6.43) can be written as,

$$\tan(\alpha(k_t)) \approx \frac{k_{x1}}{k_{x2}} \tan(k_{x1} a) \qquad (6.44)$$

In order to examine the validity of this approximation we compute α values for rib waveguide whose parameters are $n_1 = 3.44$, $n_2 = 3.40$, $n_3 = 1$, $\lambda = 1.15\mu m$, $D = 1\mu m$, $W = 3\mu m$ and $d = 0.6\mu m$, $0.9\mu m$. Outer slab thickness $d = 0.6\mu$m and 0.9μm represents the situation for a guide with outer slab near cutoff and beyond cutoff respectively. The results for α vs k_t predicted from equations (6.42) and (6.43) are plotted in Fig. 6.1 and Fig. 6.2 for $d = 0.9\mu m$ and $0.6\mu m$ respectively. Results for α vs k_t predicted from equation (6.43) are shown by the dashed line. From the figures it is observed that the difference between the two curves is very small even for large steps as long as the outer slab supporting surface modes. The remarkable accuracy of (6.43) in approximating α values when the step is not small can be justified by the following arguments. Firstly, when ϕ_{sh} and ψ_{sh} differ from each other and from $\overline{U}_{sh}$, the ratio of Q to P is still fairly close to unity. Secondly, it was observed in chapter three that the contributions of air and substrate modes of thicker slab as well as the outer slab (when the outer slab suppport surface wave) is small and can be neglected. Hence, equation (6.42) reduces approximately to equation (6.43). This approximation will prove extremely useful in obtaining practical results. However, for cases where the outer slab is below cutoff, the approximation (6.43) does not hold and equation (6.42) must be used in obtaining α values for the spectral components.

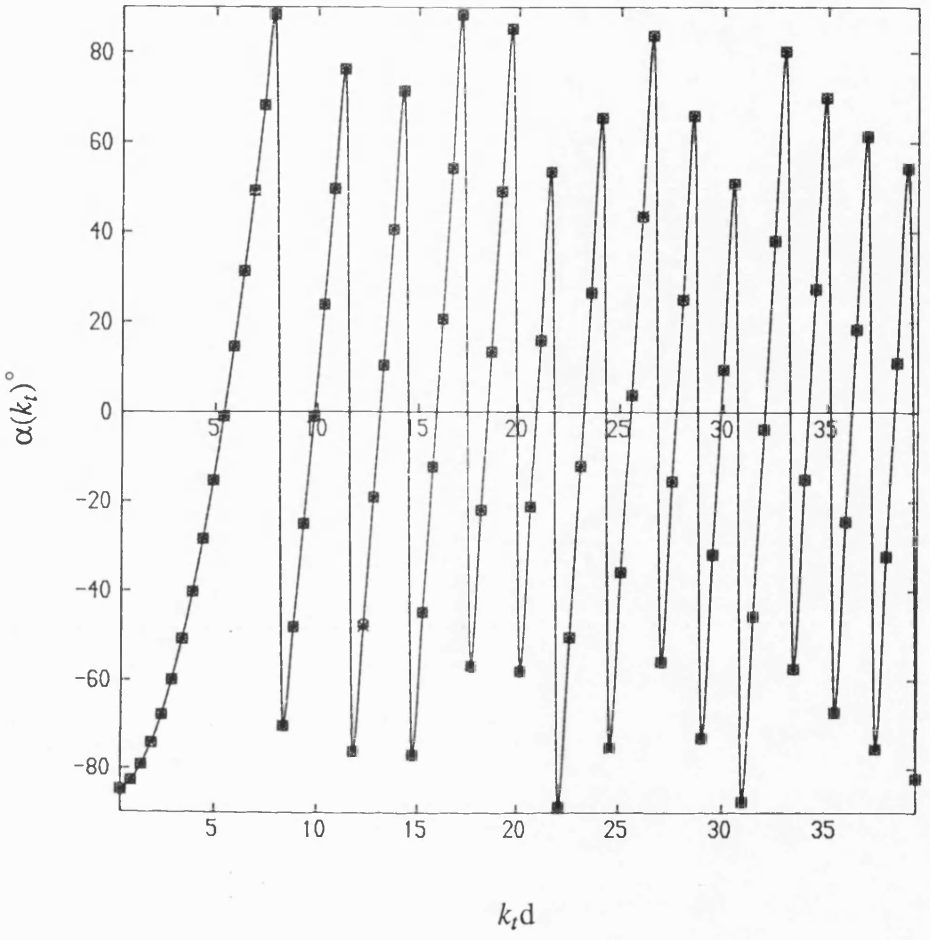

Fig. 6.1 Plot of α as a function of k_t for $d = 0.9\mu$m and $D = 1.0\mu$m.

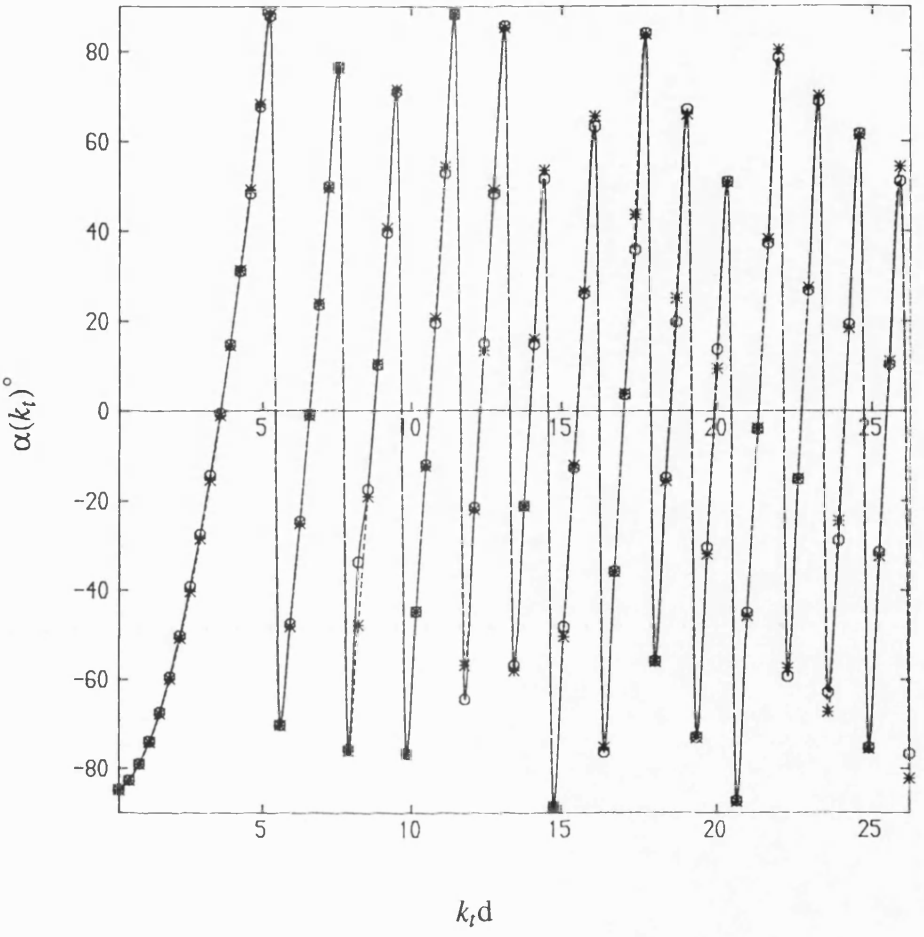

Fig. 6.2 Plot of α as a function of k_t for $d = 0.6\mu$m and $D = 1.0\mu$m.

REFERENCES

[1] B.M.A. Rahman and J.B. Davies, " Analysis of optical waveguides and some discontinuity problems ", I.E.E. Proc., vol. 135, Pt. J, No. 5, Oct. 1988, pp. 339-342.

[2] A. Yi-Yan, P. Correc and H. Carru, " Narrow band rib waveguide grating resonator filters ", I.E.E. Proc., vol. 137, Pt. J, No. 2, April 1990, pp. 132-138.

[3] N. Marcuvitz, L. Felsen, " Radiation and scattering of waves ", Englewood Cliffs, N.J., Prentice Hall, 1973, ch. 3, pp 278-282

[4] T. Rozzi, J.S. Kot, " The Complete Spectrum of Image Line ", I.E.E.E Trans. on Microwave Theory and Techniques, vol. MTT-37, No. 5, May 1989, pp 868-874

[5] T. Rozzi, P. Sewell, " The continuous spectrum of open waveguides of non separable cross section ", To be submitted for publication.

[6] T. Rozzi, L. Ma, " Mode completeness, normalization and Green's function of the inset dielectric guide ", I.E.E.E Trans. Microwave Theory and Techniques , vol. MTT-36, pp 542-551, March 1988

[7] R. Collin, " Field Theory of Guided Waves ", New York: McGraw-Hill, 1964 , pp. 570

APPENDIX

We want to verify that the condition

$$\iint dx\, dy\, h_{\nu}(x,y;k_t)\, h_{\mu}(x,y;k_t') = \delta(k_t - k_t') \tag{A-1}$$

is satisfied by direct integration. Define $I^{x<0}$ the integral over the thicker slab region. This is given by

$$I^{x<0} = \sqrt{k_t k_t'} \int_{-\infty}^{\infty} dy \int_{-a}^{0} dx \sum_n \tilde{H}^{-}_{\nu n}(k_y)\, \tilde{H}^{-\prime}_{\mu n}(k_y') \cos(\alpha_\nu) \cos(\alpha_\mu')\, \phi_{hn}(y)\, \phi_{hn}(y')$$

$$\frac{2}{\pi} \frac{\cos(k_{x1n}(x+a))}{\cos(k_{x1n}a)} \frac{\cos(k_{x1n}'(x+a))}{\cos(k_{x1n}'a)}$$

For compactness and clarity we have written the discrete sum and integrals for $x \le 0$ in (6.31) together where n stands for a component, discrete or continuous, of the spectrum and the summation for a discrete sum or integrals over ρ and σ ; and ϕ_{hn} denotes the slab mode distribution.

The wavenumbers are given by

$$k_{x1n}^2 = \varepsilon_r k_o^2 - \beta^2 - k_{yn}^2 = (\varepsilon_r - 1)k_o^2 + k_t^2 - k_{yn}^2$$

$$k_{x1n}^2 = k_t^2 - k_{yn}^2 \quad (\textit{in air})$$

The quantity k_{yn} denotes either the y - directed wavenumber of the slab surface wave k_{ys} or the continuous wavenumber ρ and σ in air and substrate respectively.

Upon integration w.r.t. y from $-\infty$ to ∞, by orthogonality of the ϕ_{hn}, we have

$$I^{x<0} = \sqrt{k_t k_t'} \int_{-a}^{0} dx \sum_n \tilde{H}^{-}_{\nu n}(k_y)\, \tilde{H}^{-\prime}_{\mu n}(k_y') \cos(\alpha_\nu) \cos(\alpha_\mu') \frac{2}{\pi} \frac{\cos(k_{x1n}(x+a))}{\cos(k_{x1n}a)} \frac{\cos(k_{x1n}'(x+a))}{\cos(k_{x1n}'a)}$$

$$= \sqrt{k_t k_t'}\, \frac{2}{\pi} \frac{\cos(\alpha_\nu)\cos(\alpha_\mu')}{k_t^2 - k_t'^2} \sum_n \tilde{H}^{-}_{\nu n}(k_y)\, \tilde{H}^{-\prime}_{\mu n}(k_y') \times$$

$$\left[k_{x1n} \tan(k_{x1n}a) - k_{x1n}' \tan(k_{x1n}'a) \right] \tag{A-2}$$

Define $I^{x>0}$ the integral over the thinner slab region. This is given by

$$I^{x>0} = \int_{-\infty}^{\infty} dy \int_{0}^{\infty} dx\, h_{\nu}(x,y;k_t)\, h_{\mu}(x,y;k_t')$$

Integration over y and by orthogonality of ψ_{hn} gives

$$I^{x>0} = \sqrt{k_t k_t'} \int_{0}^{\infty} dx \left[\tilde{H}_{\nu s}^{+}(k_y)\, \tilde{H}_{\mu s}^{+\prime}(k_y')\, \frac{2}{\pi} \cos(k_{x2}x + \alpha_{\nu}) \cos(k_{x2}'x + \alpha_{\mu}') \right.$$

$$+ \int_{0}^{k_t'} d\rho\, \tilde{H}_{\nu}^{+}(\rho;k_t)\, \tilde{H}_{\mu}^{+\prime}(\rho;k_t')\, \frac{2}{\pi} \cos(k_{x2}(\rho)x + \alpha_{\nu}) \cos(k_{x2}'(\rho)x + \alpha_{\mu}')$$

$$+ \int_{k_t'}^{k_t} d\rho\, \tilde{H}_{\nu}^{+}(\rho;k_t)\, \tilde{H}_{\mu}^{+\prime}(\rho;k_t')\, \frac{2}{\pi} \cos(k_{x2}(\rho)x + \alpha_{\nu})\, e^{-\gamma x} \cos(\alpha_{\mu}')$$

$$+ \int_{k_t}^{\infty} d\rho\, \tilde{H}_{\nu}^{+}(\rho;k_t)\, \tilde{H}_{\mu}^{+\prime}(\rho;k_t')\, \frac{2}{\pi}\, e^{-(\gamma+\gamma')x} \cos(\alpha_{\nu}) \cos(\alpha_{\mu}')$$

$$\left. + \int_{0}^{\nu} d\sigma\, \tilde{H}_{\nu}^{+}(\sigma;k_t)\, \tilde{H}_{\mu}^{+\prime}(\sigma;k_t')\, \frac{2}{\pi} \cos(k_{x2}(\sigma)x + \alpha_{\nu}) \cos(k_{x2}'(\sigma)x + \alpha_{\mu}') \right]$$

$$= \sqrt{k_t k_t'} \left[\tilde{H}_{\nu s}^{+}(k_y)\, \tilde{H}_{\mu s}^{+\prime}(k_y') \left[\delta(k_{x2} - k_{x2}') \right.\right.$$

$$\left. - \frac{2}{\pi} \frac{\cos(\alpha_{\nu}) \cos(\alpha_{\mu}')}{k_{x2}^2 - k_{x2}'^2} \left(k_{x2} \tan(\alpha_{\nu}) - k_{x2} \tan(\alpha_{\mu}')\right) \right]$$

$$+ \int_{0}^{k_t'} d\rho\, \tilde{H}_{\nu}^{+}(\rho;k_t)\, \tilde{H}_{\mu}^{+\prime}(\rho;k_t') \left[\delta(k_{x2}(\rho) - k_{x2}'(\rho)) \right.$$

$$\left. \left. - \frac{2}{\pi} \frac{\cos(\alpha_{\nu}) \cos(\alpha_{\mu}')}{k_{x2}^2(\rho) - k_{x2}'^2(\rho)} \left(k_{x2}(\rho) \tan(\alpha_{\nu}) - k_{x2}'(\rho) \tan(\alpha_{\mu}')\right) \right] \right.$$

$$+ \int_{k_t'}^{k_t} d\rho\, \tilde{H}_{\nu}^{+}(\rho;k_t)\, \tilde{H}_{\mu}^{+\prime}(\rho;k_t')\, \frac{2}{\pi} \frac{\cos(\alpha_{\nu}) \cos(\alpha_{\mu}')}{k_{x2}^2(\rho) - k_{x2}'^2(\rho)} \left[\gamma - k_{x2}(\rho) \tan(\alpha_{\nu}) \right]$$

$$+\int_{k_t}^{\infty} d\rho\, \tilde{H}_{\nu}^{+}(\rho;k_t)\, \tilde{H}_{\mu}^{+\prime}(\rho;k_t')\, \frac{2}{\pi}\, \frac{\cos(\alpha_\nu)\cos(\alpha_\mu')}{k_{x2}^2(\rho)-k_{x2}'^2(\rho)} \Big[\gamma-\gamma\Big]$$

$$+\int_{0}^{\nu} d\sigma\, \tilde{H}_{\nu}^{+}(\sigma;k_t)\, \tilde{H}_{\mu}^{+\prime}(\sigma;k_t') \Big[\, \delta(k_{x2}(\sigma)-k_{x2}'(\sigma))$$

$$-\frac{2}{\pi}\, \frac{\cos(\alpha_\nu)\cos(\alpha_\mu')}{k_{x2}^2(\sigma)-k_{x2}'^2(\sigma)}\, (k_{x2}(\sigma)\tan(\alpha_\nu)-k_{x2}'(\sigma)\tan(\alpha_\mu'))\Big] \qquad \text{(A-3)}$$

$$I^{x<0}+I^{x>0}=\sqrt{k_t k_t'}\Big[\, \tilde{H}_{\nu s}^{+}(k_y)\, \tilde{H}_{\mu s}^{+\prime}(k_y')\, \delta(k_{x2}-k_{x2}')$$

$$+\int_{0}^{k_t} d\rho\, \tilde{H}_{\nu}^{+}(\rho;k_t)\, \tilde{H}_{\mu}^{+}(\rho;k_t')\, \delta(k_{x2}(\rho)-k_{x2}'(\rho))$$

$$+\int_{0}^{\nu} d\sigma\, \tilde{H}_{\nu}(\sigma;k_t)\, \tilde{H}_{\mu}^{+\prime}(\sigma;k_t')\, \delta(k_{x2}(\sigma)-k_{x2}'(\sigma))\Big]$$

$$+\sqrt{k_t k_t'}\, \frac{2}{\pi}\, \frac{\cos(\alpha_\nu)\cos(\alpha_\mu')}{k_t^2-k_t'^2}\Big[\, \tilde{H}_{\nu s}^{+}(k_y)\, \tilde{H}_{\mu s}^{+\prime}(k_y')\, k_{x2}\tan(\alpha_\mu')$$

$$+\int_{0}^{k_t'} d\rho\, \tilde{H}_{\nu}^{+}(\rho;k_t)\, \tilde{H}_{\mu}^{+\prime}(\rho;k_t')\, k_{x2}(\rho)\tan(\alpha_\mu')+\int_{k_t'}^{\infty} d\rho\, \tilde{H}_{\nu}^{+}(\rho;k_t)\, \tilde{H}_{\mu}^{+\prime}(\rho;k_t')\, \gamma$$

$$+\int_{0}^{\nu} d\sigma\, \tilde{H}_{\nu}^{+}(\sigma;k_t)\, \tilde{H}_{\mu}^{+\prime}(\sigma;k_t')\, k_{x2}(\sigma)\tan(\alpha_\mu')$$

$$-\Big[\, \tilde{H}_{\nu s}^{+}(k_y)\, \tilde{H}_{\mu s}^{+\prime}(k_y')\, k_{x2}\tan(\alpha_\nu)+\int_{0}^{k_t} d\rho\, \tilde{H}_{\nu}^{+}(\rho;k_t)\, \tilde{H}_{\mu}^{+\prime}(\rho;k_t')\, k_{x2}(\rho)\tan(\alpha_\nu)$$

$$+\int_{k_t}^{\infty} d\rho\, \tilde{H}_{\nu}^{+}(\rho;k_t)\, \tilde{H}_{\mu}^{+\prime}(\rho;k_t')\, \gamma+\int_{0}^{\nu} d\sigma\, \tilde{H}_{\nu}^{+}(\sigma;k_t)\, \tilde{H}_{\mu}^{+\prime}(\sigma;k_t')\, k_{x2}(\sigma)\tan(\alpha_\nu)\Big]$$

$$+\sum_{n} \tilde{H}_{\nu n}^{-}(k_y)\, \tilde{H}_{\mu n}^{-\prime}(k_y')\Big[\, k_{x1n}\tan(k_{x1n}a)-k_{x1n}'\tan(k_{x1n}'a)\Big]\Big]$$

In order to obtain the required proof, (A-2) and (A-3), apart from the delta , must balance out. This gives,

$$\tilde{H}^{+}_{\nu s}(k_y)\,\tilde{H}^{+\prime}_{\mu s}(k'_y)\,k'_{x2}\,\tan(\alpha'_\mu)+\int_0^{k'_t} d\rho\,\tilde{H}^{+}_{\nu}(\rho;k_t)\,\tilde{H}^{+\prime}_{\mu}(\rho;k'_t)\,k'_{x2}(\rho)\tan(\alpha'_\mu)$$

$$+\int_{k'_t}^{\infty} d\rho\,\tilde{H}^{+}_{\nu}(\rho;k_t)\,\tilde{H}^{+\prime}_{\mu}(\rho;k'_t)\,\gamma'+\int_0^{\nu} d\sigma\,\tilde{H}^{+}_{\nu}(\sigma;k_t)\,\tilde{H}^{+\prime}_{\mu}(\sigma;k'_t)\,k'_{x2}(\sigma)\tan(\alpha'_\mu)$$

$$=\sum_n \tilde{H}^{-}_{\nu n}(k_y)\,\tilde{H}^{-\prime}_{\mu n}(k'_y)\,k'_{x1n}\tan(k'_{x1n}a)$$

and

$$\tilde{H}^{+}_{\nu s}(k_y)\,\tilde{H}^{+\prime}_{\mu s}(k'_y)\,k_{x2}\tan(\alpha_\nu)+\int_0^{k_t} d\rho\,\tilde{H}^{+}_{\nu}(\rho;k_t)\,\tilde{H}^{+\prime}_{\mu}(\rho;k'_t)\,k_{x2}(\rho)\tan(\alpha_\nu)$$

$$+\int_{k_t}^{\infty} d\rho\,\tilde{H}^{+}_{\nu}(\rho;k_t)\,\tilde{H}^{+\prime}_{\mu}(\rho;k'_t)\,\gamma+\int_0^{\nu} d\sigma\,\tilde{H}^{+}_{\nu}(\sigma;k_t)\,\tilde{H}^{+\prime}_{\mu}(\sigma;k'_t)\,k_{x2}(\sigma)\tan(\alpha_\nu)$$

$$=\sum_n \tilde{H}^{-}_{\nu n}(k_y)\,\tilde{H}^{-\prime}_{\mu n}(k'_y)\,k_{x1n}\tan(k_{x1n}a)$$

Rearranging we have,

$$\tan(\alpha_\nu)\left[\tilde{H}^{+}_{\nu s}(k_y)\,\tilde{H}^{+\prime}_{\mu s}(k'_y)\,k_{x2}+\int_0^{k_t} d\rho\,\tilde{H}^{+}_{\nu}(\rho;k_t)\,\tilde{H}^{+\prime}_{\mu}(\rho;k'_t)\,k_{x2}(\rho)\right.$$

$$\left.+\int_0^{\nu} d\sigma\,\tilde{H}^{+}_{\nu}(\sigma;k_t)\,\tilde{H}^{+\prime}_{\mu}(\sigma;k'_t)\,k_{x2}(\sigma)\tan(\alpha_\nu)\right]$$

$$=\sum_n \tilde{H}^{-}_{\nu n}(k_y)\,\tilde{H}^{-\prime}_{\mu n}(k'_y)\,k_{x1n}\tan(k_{x1n}a)-\int_{k_t}^{\infty} d\rho\,\tilde{H}^{+}_{\nu}(\rho;k_t)\,\tilde{H}^{+\prime}_{\mu}(\rho;k'_t)\,\gamma \qquad \text{(A-4)}$$

Discretizing (A-4) with $H_\nu(k_y)=\sum_m A_{m\nu}\,f_m(k_y)$, we obtain

$$\tan(\alpha_\nu)\,\underline{A}^{T}_{\mu}\cdot\underline{\underline{Z}}^{R}\cdot\underline{A}_\nu=\underline{A}^{T}_{\mu}\cdot\underline{\underline{Z}}^{I}\cdot\underline{A}_\nu$$

where

$$\underline{\underline{Z}}^{R}=Q_p\,Q_q\,k_{x2}+\int_0^{k_t} d\rho\,Q_p(\rho)\,Q_q(\rho)\,k_{x2}(\rho)+\int_0^{\nu} d\sigma\,Q_p(\sigma)\,Q_q(\sigma)\,k_{x2}(\sigma)$$

$$\underline{\underline{Z}}^I = \sum_n P_{pn}\, Q_{qn}\, k_{x1n} \tan(k_{x1n} a) - \int_{k_t}^{\infty} d\rho\, Q_p(\rho)\, Q_q(\rho)\, \gamma$$

From [7], A_ν's are orthogonal w. r. t. $\underline{\underline{Z}}^R$. Hence

$$\underline{A}_\mu^T \cdot \underline{\underline{Z}}^R \cdot \underline{A}_\nu = \delta_{\mu\nu}$$

Let now consider the first term of (A-3). This yields

$$\sqrt{k_t k_t'} \left[\tilde{H}_{\nu s}^+(k_y)\, \tilde{H}_{\mu s}^{+\prime}(k_y')\, \delta(k_{x2} - k_{x2}') + \int_0^{k_t} d\rho\, \tilde{H}_\nu^+(\rho;k_t)\, \tilde{H}_\mu^{+\prime}(\rho;k_t')\, \delta(k_{x2}(\rho) - k_{x2}'(\rho)) \right.$$

$$\left. + \int_0^{\nu} d\sigma\, \tilde{H}_\nu^+(\sigma;k_t)\, \tilde{H}_\mu^{+\prime}(\sigma;k_t)\, \delta(k_{x2}(\sigma) - k_{x2}'(\sigma)) \right]$$

$$= \sqrt{k_t k_t'} \left[\tilde{H}_{\nu s}^+(k_y)\, \tilde{H}_{\mu s}^{+\prime}(k_y')\, \delta(k_t - k_t')\, \frac{k_{x2}}{k_t} + \int_0^{k_t} d\rho\, \tilde{H}_\nu^+(\rho;k_t)\, \tilde{H}_\mu^{+\prime}(\rho;k_t')\, \delta(k_t - k_t')\, \frac{k_{x2}(\rho)}{k_t} \right.$$

$$\left. + \int_0^{\nu} d\sigma\, \tilde{H}_\nu^+(\sigma;k_t)\, \tilde{H}_\mu^{+\prime}(\sigma;k_t)\, \delta(k_t - k_t')\, \frac{k_{x2}(\sigma)}{k_t} \right]$$

$$= \delta(k_t - k_t') \left[\tilde{H}_{\nu s}^+(k_y)\, \tilde{H}_{\mu s}^{+\prime}\, k_{x2} + \int_0^{k_t} d\rho\, \tilde{H}_\nu^+(\rho;k_t)\, \tilde{H}_\mu^{+\prime}(\rho;k_t')\, k_{x2}(\rho) \right.$$

$$\left. + \int_0^{\nu} d\sigma\, \tilde{H}_\nu^+(\sigma;k_t)\, \tilde{H}_\mu^{+\prime}(\sigma;k_t)\, k_{x2}(\sigma) \right]$$

$$= \delta(k_t - k_t')\, \underline{A}_\mu^T \cdot \underline{\underline{Z}}^R \cdot \underline{A}_\nu$$

$$= \delta(k_t - k_t')\, \delta_{\mu\nu}$$

Hence,

$$< h_\nu(x,y;k_t)\, ,\, h_\mu(x,y;k_t') > = I^{x<0} + I^{x>0}$$

$$= \delta_{\mu\nu}\, \delta(k_t - k_t') \qquad \text{Q.E.D.}$$

CHAPTER 7

ANALYSIS OF DISCONTINUITY PROBLEMS IN RIB WAVEGUIDES

7.1 INTRODUCTION

In order to demonstrate the validity of the modal spectrum of a rib waveguide developed in chapter six, in this chapter we formulate rigorously the discontinuity problems involving rib waveguides. The problems we addressed in this chapter are the analysis of scattering of bound modes in an abruptly terminated rib waveguide and the analyses of different types of discontinuities between two rib waveguides. The problem of abruptly terminated rib waveguide is of great importance in resonator design and in other areas of activity such as in solid state laser devices and in millimeter wave antenna application. In particular, for a laser cavity, the reflection and the diffraction of bound modes at end facet are crucial parameters for determining both its oscillation condition and its radiation output in free space. On the other hand, for millimeter wave antennas, the usual parameters required are the terminal impedance and the near as well as the far fields. The discontinuity problem between two rib waveguides, such as a change in rib width and in rib height is also of great importance in device design. An extension of the analysis used for that problem could also cover the problem of the tapered waveguide, the bend section, as well as waveguide grating and filters.

In as much as the complete normalized mode spectrum of the rib waveguide is now known, the approach to be adopted in order to treat the above mentioned problems, is in essence, similar to those used on abrupt junctions in dielectric slab waveguides [1,2], i.e the modal approach. In the development of the modal analysis throughout the present work the rib waveguide is assumed monomodal.

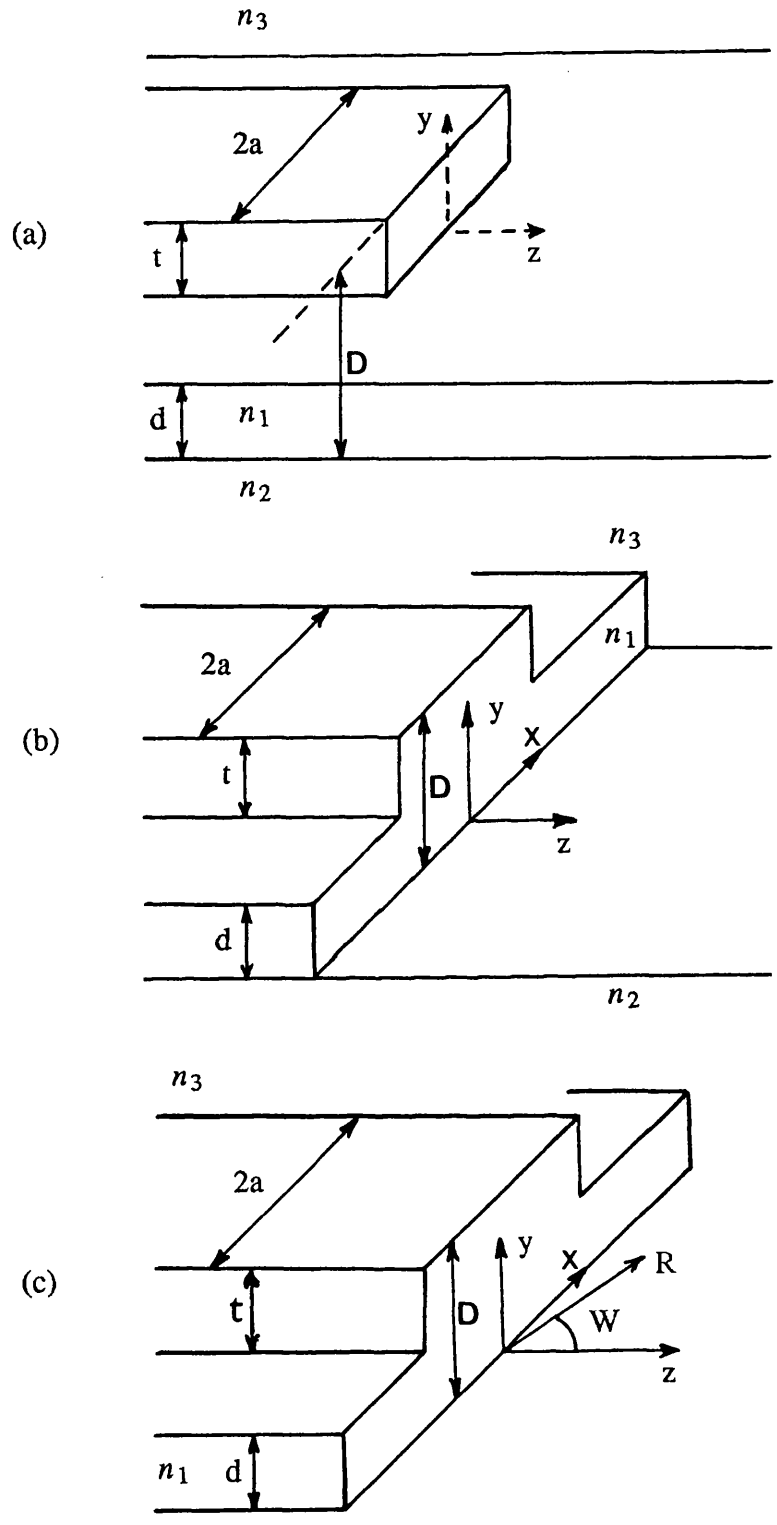

Fig. 7.1 Abruptly terminated rib waveguide a) Only the rib is terminated
b) The guide and surrounding slab is terminated
c) The whole guide is terminated

7.2 ABRUPTLY TERMINATED RIB WAVEGUIDE

7.21 FORMULATION OF THE PROBLEM

The basic configuration of an abruptly terminated rib waveguide under consideration is shown in Fig. 7.1 . The structure is terminated abruptly at $z = 0$. Three cases of terminating the guide being examined are;

a) The rib is terminated abruptly at $z = 0$ as shown in Fig. 7.1a . Region $z \geq 0$ is represented by an asymmetrical slab waveguide of thickness 'd'.

b) The guide slab and the surrounding slab is terminated abruptly at $z = 0$ as shown in Fig. 7.1b . In this case region $z \geq 0$ is represented by an air- substrate half space.

c) The whole guide is terminated at $z = 0$ as shown in Fig. 7.1c . In this case region $z \geq 0$ is represented by air half space or facet with mirror.

We assume that the rib waveguide is excited by the dominant mode and the field is pure LSE. The main transverse field components are E_x and H_y. We consider the case where an electric wall is placed at $x = 0$ and the field is even to x. The various mode functions $\psi_s(x,y)$ and $\psi_c(x,y;k_t)$ with their proper normalizations can be found in chapter six. For all cases considered, the spectral distribution for region $z \geq 0$ is described by means of a superposition of spectral components of the type

$$\psi_a(x,y;k_t) = \sqrt{\frac{2}{\pi}}\, cos(k_x x)\, \chi_h(y,k_y)$$

where $\chi_h(y,k_y)$ is defined below.

For case (a), $\chi_h(y,k_y)$ is constituted by the complete spectrum of an asymmetrical slab guide of thickness 'd' given by

$$\chi_h(y,k_y = \rho) = \psi_{sh}(y) + \sum_{\mu=e,o} \int_0^\infty d\rho \psi_{h\mu}(y,\rho) + \int_0^\nu d\sigma \psi_h(y,\sigma)$$

For case (b), $\chi_h(y,k_y)$ is constituted by the limiting case of the spectrum of air modes of an asymmetrical slab guide obtained by letting the film thickness go to zero and the wavenumber in the film h go over to its free-space counterpart, ρ. Thus $\chi_h(y,k_y)$ is given by

$$\chi_h(y,k_y=\rho)=\sqrt{\frac{2}{\pi}}\left[A^e cos(\rho y)+A^o sin(\rho y)\right] \qquad ;y\geq 0$$

$$=\sqrt{\frac{2}{\pi}}\left[A^e cos(\sigma y)+A^o sin(\sigma y)\right] \qquad ;y\leq 0$$

where

$$A^e=\sqrt{\frac{\rho}{\rho+\sigma}} \quad \text{and} \quad A^o=\sqrt{\frac{\sigma}{\rho+\sigma}}$$

For case (c), $\chi_h(y,k_y)$ is represented by the plane wave in air given by

$$\chi_h(y,k_y)=\sqrt{\frac{2}{\pi}}\left[A^e\, cos(\rho y)+A^o\, sin(\rho y)\right]$$

where $A^e=A^o=\sqrt{\frac{1}{2}}$

Orthonormalisation is of the type

$$\int_{-\infty}^{\infty} dy \int_{0}^{\infty} dx\ \psi_a(x,y;k_t)\psi_a(x,y;k_t')=\delta(k_t-k_t') \qquad ;k_t^2=k_o-\beta^2$$

$$0\leq k_t,k_t'<\infty$$

Let us consider a surface wave propagating in the rib guide along z. At $z=0$, the incoming surface wave couples to the continuous spectrum of the rib waveguide and the spectrum of region $z\geq 0$. Let the electric field amplitude of the incoming and reflected waves at $z=0$ be expressed by a_o and b_o respectively. Let $b_c(k_t)$ and $b_a(k_t)$ denote the amplitude of the scattered modes of the continuous spectrum in region $z\leq 0$ and in region $z\geq 0$ respectively. To derive the variational expression for the reflection coefficient at the discontinuous step at $z=0$ let consider case (a) shown in Fig. 7.1a .

For $z \leq 0$, the transverse fields in the region may be expressed in the form

$$E_x(x,y) = (a_o + b_o)Z_o\psi_s(x,y) + \int_0^{\infty} dk_x \left[b_{cs}(k_x)Z_{cs}(k_x)\psi_{cs}(x,y;k_x) \right.$$

$$\left. + \int_0^{\nu} d\sigma b_{c\sigma}Z_{c\sigma}(k_t)\psi_{c\sigma}(x,y;k_t) + \int_0^{\infty} d\rho b_{c\rho}Z_{c\rho}(k_t)\psi_{c\rho}(x,y;k_t) \right] \tag{7.1a}$$

$$H_y(x,y) = (a_o - b_o)\psi_s(x,y) - \int_0^{\infty} dk_x \left[b_{cs}(k_x)\psi_{cs}(x,y;k_x) \right.$$

$$\left. + \int_0^{\nu} d\sigma b_{c\sigma}\psi_{c\sigma}(x,y;k_t) + \int_0^{\infty} d\rho b_{c\rho}\psi_{c\rho}(x,y;k_t) \right] \tag{7.1b}$$

where,

$$Z_o = \frac{\omega\mu_0\beta_s}{q_h^2 + \beta_s^2} \tag{7.2a}$$

$$Z_{cs}(k_x) = \frac{\omega\mu_0\beta}{k_{xs}^2 + \beta^2} \tag{7.2b}$$

$$Z_{c\sigma}(k_t) = \frac{\omega\mu_0\beta}{k_x^2(\sigma) + \beta^2} \tag{7.2c}$$

$$Z_{c\rho}(k_t) = \frac{\omega\mu_0\beta}{k_x^2(\rho) + \beta^2} \tag{7.2d}$$

Z_o is the characteristic impedance of the bound mode. $Z_{cs}(k_x)$, $Z_{c\sigma}(k_t)$ and $Z_{c\rho}(k_t)$ is the characteristic impedance of the continuum in the film, substrate and air respectively. The various variable appearing in (7.2a-7.2d) have been defined previously in chapters three and six.

For $z \geq 0$, the transverse fields in the region take the form

$$E_x(x,y) = \int_0^{\infty} dk_x \left[b_{as}(k_x) Z_{as}(k_x) \psi_{as}(x,y;k_x) + \int_0^{\nu} b_{a\sigma}(k_t) Z_{a\sigma}(k_t) \psi_{a\sigma}(x,y;k_t) \right.$$

$$\left. + \int_0^{\infty} d\rho b_{a\rho}(k_t) Z_{a\rho}(k_t) \psi_{a\rho}(x,y;k_t) \right] \tag{7.3a}$$

$$H_y(x,y) = \int_0^{\infty} dk_x \left[b_{as}(k_x) \psi_{as}(x,y;k_x) + \int_0^{\nu} b_{a\sigma}(k_t) \psi_{a\sigma}(x,y;k_t) \right.$$

$$\left. + \int_0^{\infty} d\rho b_{a\rho}(k_t) \psi_{a\rho}(x,y;k_t) \right] \tag{7.3b}$$

where,

$$Z_{as}(k_x) = \frac{\omega\mu_0\beta}{k_{xs}^2 + \beta^2} \tag{7.4a}$$

$$Z_{a\sigma}(k_t) = \frac{\omega\mu_0\beta}{\varepsilon_2 k_o^2 - \sigma^2} \tag{7.4b}$$

$$Z_{a\rho}(k_t) = \frac{\omega\mu_0\beta}{k_o^2 - \rho^2} \tag{7.4c}$$

Equations (7.4a-7.4c) define the characteristic impedance of the spectral distribution component for region $z \geq 0$ in film, substrate and air respectively. The continuity of the transverse fields at $z = 0$, gives

$$E_x(x,y) = (a_o + b_o) Z_o \psi_s(x,y) + \int_0^{\infty} dk_x \left[b_{cs}(k_x) Z_{cs}(k_x) \psi_{cs}(x,y;k_x) \right.$$

$$\left. + \int_0^{\nu} d\sigma b_{c\sigma} Z_{c\sigma}(k_t) \psi_{c\sigma}(x,y;k_t) + \int_0^{\infty} d\rho b_{c\rho} Z_{c\rho}(k_t) \psi_{c\rho}(x,y;k_t) \right]$$

$$= \int_0^{\infty} dk_x \left[b_{as}(k_x) Z_{as}(k_x) \psi_{as}(x,y;k_x) + \int_0^{\nu} b_{a\sigma}(k_t) Z_{a\sigma}(k_t) \psi_{a\sigma}(x,y;k_t) \right.$$

$$\left. + \int_0^{\infty} d\rho b_{a\rho}(k_t) Z_{a\rho}(k_t) \psi_{a\rho}(x,y;k_t) \right] \tag{7.5a}$$

and

$$H_y(x,y) = (a_o - b_o) - \int_0^{\infty} dk_x \left[b_{cs}(k_x)\psi_{cs}(x,y;k_x) + \int_0^{\nu} d\sigma b_{c\sigma}\psi_{c\sigma}(x,y;k_t) + \int_0^{\infty} d\rho b_{c\rho}\psi_{c\rho}(x,y;k_t) \right]$$

$$= \int_0^{\infty} dk_x \left[b_{as}(k_x)\psi_{as}(x,y;k_x) + \int_0^{\nu} b_{a\sigma}(k_t)\psi_{a\sigma}(x,y;k_t) + \int_0^{\infty} d\rho b_{a\rho}(k_t)\psi_{a\rho}(x,y;k_t) \right] \tag{7.5b}$$

From the orthogonality conditions, the wave amplitudes in (7.5a) can be determined from (7.5b), namely, denoting by the symbol <<...>> integration over the guide cross-section, we have:

$$(a_o - b_o) = \int_{-\infty}^{\infty} dy \int_0^{\infty} dx \psi_s(x,y) H_y(x,y) = \ll \psi_s(x,y), H_y(x,y) \gg \tag{7.6}$$

$$b_{cs}(k_x) = - \ll \psi_{cs}(x,y;k_x), H_y(x,y) \gg \tag{7.7}$$

$$b_{c\sigma}(k_t) = - \ll \psi_{c\sigma}(x,y;k_t), H_y(x,y) \gg \tag{7.8}$$

$$b_{c\rho}(k_t) = - \ll \psi_{c\rho}(x,y;k_t), H_y(x,y) \gg \tag{7.9}$$

$$b_{as}(k_x) = \ll \psi_{as}(x,y;k_x), H_y(x,y) \gg \tag{7.10}$$

$$b_{a\sigma}(k_t) = \ll \psi_{a\sigma}(x,y;k_t), H_y(x,y) \gg \tag{7.11}$$

$$b_{a\rho}(k_t) = \ll \psi_{a\rho}(x,y;k_t), H_y(x,y) \gg \tag{7.12}$$

From (7.6) the reflected wave amplitude is given by

$$b_o = a_o - \ll \psi_s(x,y), H_y(x,y) \gg = \Gamma a_o$$

If the incident amplitude is taken as unity, then the reflected wave amplitude may be expressed as

$$b_o = \Gamma = 1 - \ll \psi_s(x,y), H_y(x,y) \gg = 1 - \delta \tag{7.13}$$

where Γ defines the reflection coefficient at the discontinuity $z = 0$.

Substituting (7.6) to (7.12) in to (7.5a) we obtain,

$$
\begin{aligned}
Z_o\psi_s(x,y) = \frac{1}{2}\Big[& \ll \psi_s(x,y), H_y(x,y) \gg Z_o\psi_s(x,y) \\
& + \int_0^{\infty} dk_x \Big[\ll \psi_{cs}(x,y;k_x), H_y(x,y) \gg Z_{cs}(k_x)\psi_{cs}(x,y;k_x) \\
& + \ll \psi_{as}(x,y;k_x), H_y(x,y) \gg Z_{as}(k_x)\psi_{as}(x,y;k_x) \Big] \\
& + \int_0^{\infty} dk_x \int_0^{\nu} d\sigma \Big[\ll \psi_{c\sigma}(x,y;k_t), H_y(x,y) \gg Z_{c\sigma}(k_t)\psi_{c\sigma}(x,y;k_t) \\
& + \ll \psi_{a\sigma}(x,y;k_t), H_y(x,y) \gg Z_{a\sigma}(k_t)\psi_{a\sigma}(x,y;k_t) \Big] \\
& + \int_0^{\infty} dk_x \int_0^{\infty} d\rho \Big[\ll \psi_{c\rho}(x,y;k_t), H_y(x,y) \gg Z_{c\rho}(k_t)\psi_{c\rho}(x,y;k_t) \\
& + \ll \psi_{a\rho}(x,y;k_t), H_y(x,y) \gg Z_{a\rho}(k_t)\psi_{a\rho}(x,y;k_t) \Big] \Big]
\end{aligned}
\tag{7.14}
$$

By multiplying (7.14) by $H_y(x,y)$ and integrating with respect to x and y and dividing through by $\ll \psi_s(x,y), H_y(x,y) \gg . \ll Z_o\psi_s(x,y), H_y(x,y) \gg$ we obtain the variational expression for $\frac{1}{\delta}$ given by,

$$
\begin{aligned}
\frac{1}{\delta} &= \frac{\ll Z_o\psi_s(x,y), H_y(x,y) \gg}{\ll \psi_s(x,y), H_y(x,y) \gg . \ll Z_o\psi_s(x,y), H_y(x,y) \gg} \\
&= \frac{\ll H_y(x,y)\,,\, Z(x,y;x',y')\,,\, H_y(x',y') \gg}{\ll \psi_s(x,y), H_y(x,y) \gg . \ll Z_o\psi_s(x,y), H_y(x,y) \gg}
\end{aligned}
\tag{7.15}
$$

where,

$$Z(x,y;x',y') = \frac{1}{2}\Big[Z_o\psi_s(x,y)\psi_s(x',y') +$$

$$\int_0^\infty dk_x \Big[\psi_{cs}(x,y;k_x)Z_{cs}(k_x)\psi_{cs}(x',y';k_x) + Z_{as}(k_x)\psi_{as}(x,y;k_x)\psi_{as}(x',y';k_x) \Big]$$

$$+ \int_0^\infty dk_x \int_0^\nu d\sigma \Big[\psi_{c\sigma}(x,y;k_t)Z_{c\sigma}(k_t)\psi_{c\sigma}(x',y';k_t)$$

$$+ Z_{a\sigma}(k_t)\psi_{a\sigma}(x,y;k_t)\psi_{a\sigma}(x',y';k_t) \Big]$$

$$+ \int_0^\infty dk_x \int_0^\infty d\rho \Big[\psi_{c\rho}(x,y;k_t)Z_{c\rho}(k_t)\psi_{c\rho}(x',y';k_t)$$

$$+ \psi_{a\rho}(x,y;k_t)Z_{a\rho}(k_t)\psi_{a\rho}(x',y';k_t) \Big]\Big] \qquad (7.16)$$

Equations (7.13) and (7.15), express the sought variational expression for the reflection coefficient at the discontinuity $z = 0$.

For case (b), the appropriate variational expression for the reflection coefficient can be deduced from equations (7.13) and (7.15) where now $Z(x,y;x',y')$ is defined by

$$Z(x,y;x',y') = \frac{1}{2}\Big[Z_o\psi_s(x,y)\psi_s(x',y')$$

$$+ \int_0^\infty dk_x\, \psi_{cs}(x,y;k_x)Z_{cs}(k_x)\psi_{cs}(x',y';k_x)$$

$$+ \int_0^\infty dk_x \int_0^\nu d\sigma\, \psi_{c\sigma}(x,y;k_t)Z_{c\sigma}(k_t)\psi_{c\sigma}(x',y';k_t)$$

$$+ \int_0^\infty dk_x \int_0^\infty d\rho \Big[\psi_{c\rho}(x,y;k_t)Z_{c\rho}(k_t)\psi_{c\rho}(x',y';k_t)$$

$$+ Z_{a\rho}\psi_a(x,y;k_t)\psi_a(x',y';k_t) \Big]\Big] \qquad (7.17)$$

Similar expression as (7.17) holds for case (c). $\psi_a(x,y;k_t)$ for the two cases considered is defined at the beginning of the section.

7.22 VARIATIONAL SOLUTION

The variational expression for δ in equation (7.15) contains the unknown interface field $H_y(x,y)$. The two dimensional nature of $H_y(x,y)$ means that we require a two dimensional trial field function to represent the field unknown. The choice of a suitable trial function which satisfies the appropriate boundary conditions is not readily available. The obvious choice is to use the bound mode function of the rib waveguide. However, if the bound mode function is used as a trial field, then the contribution of the continuum cancels because of its orthogonality to the bound mode there by neglecting backward radiation. In order to overcome this problem we choose to use the bound mode of an intermediate rib waveguide , $\psi_I(x,y)$, whose height d_I is intermediate between those of the guide 'D' and the slab 'd' to the left and to the right of the step respectively. The outer slab dimension of both guides is kept the same. As the surface waves carry most of the power the criterion used in choosing the height d_I is to maximize the ratio of $\dfrac{\ll H_y(x,y),\psi_{sh}(y) \gg}{\ll H_y(x,y),\psi_s(x,y) \gg}$ where $\ll H_y(x,y),\psi_{sh}(y) \gg$ and $\ll H_y(x,y),\psi_s(x,y) \gg$ is the overlapping integral between the trial function and the bound mode of the asymmetrical slab and the rib waveguide respectively. In the case where no guidance is present in region $z \geq 0$ i.e. for cases (b) and (c) in section 7.21, the above criterion breaks down. For these cases, we choose d_I equals to $\bar{d}$ defined in chapter 3. This is a reasonable approximation since $\bar{d}$ provides a good transition between the inner and the outer regions of the guide. Furthermore, in order to avoid the computational complexity in the evaluation of the various inner products involving integrals over the continuum we suppressed the continuum in the expression of $\psi_I(x,y)$. This approximation can be justified by the following arguments. As discussed in chapter three in the context of solving the dispersion equation, the contribution of the continuum was found to be small even for rib waveguide with surrounding slab near cutoff. Hence, suppressing the continuum terms will not seriously distort the form of the field. Moreover , since we are dealing with a variational solution, the exact form of the trial

field function is not critical and any reasonable form of the trial function may gives reasonably accurate results. Hence, $\psi_I(x,y)$ is defined as

$$\psi_I(x,y) = \frac{1}{N_I} P_I \phi_I(y) \frac{\cos(q_{sI}x)}{\cos(q_{sI}a)} \qquad ;x \le a$$

$$= \frac{1}{N_I} P'_I \psi_I(y) e^{-\gamma_{sI}(x-a)} \qquad ;x \ge a \tag{7.18}$$

and

$$N_I^2 = \frac{P_I^2}{2q_{sI}} \left[q_{sI}a \sec^2(q_{sI}a) + \tan(q_{sI}a) \right] + \frac{P_I'^2}{2\gamma_{sI}}$$

The subscript I denotes the intermediate function and the various quantities appearing in (7.18) are defined similar to those found in chapter three.

Substituting (7.18) in to equation (7.15) we obtain

$$\frac{1}{\delta} = \left[P_{rib}P'_{rib} + \omega\mu_0 \int_0^\infty dk_x \frac{\beta}{k_{xs}^2 + \beta^2} \left[Q_{cs}^2(k_x) + Q_{as}^2(k_x) \right] \right.$$

$$+ \omega\mu_0 \int_0^\infty dk_x \int_0^\nu d\sigma \frac{\beta}{\varepsilon_2 k_o^2 - \sigma^2} \left[Q_{c\sigma}(k_t) + Q_{a\sigma}(k_t) \right]$$

$$\left. + \omega\mu_0 \int_0^\infty dk_x \int_0^\infty d\rho \frac{\beta}{k_o^2 - \rho^2} \left[Q_{c\rho}(k_t) + Q_{a\rho}(k_t) \right] \right] / 2P_{rib}P'_{rib} \tag{7.19}$$

where the various coefficients are defined by

$$P_{rib} = \ll \psi_I(x,y), \psi_s(x,y) \gg$$

$$P'_{rib} = \ll \psi_I(x,y), Z_o\psi_s(x,y) \gg$$

$$Q_{cs}(k_x) = \ll \psi_I(x,y), \psi_{cs}(x,y;k_x) \gg$$

$$Q_{as}(k_x) = \ll \psi_I(x,y), \psi_{as}(x,y;k_x) \gg$$

$$Q_{c\sigma}(k_t) = \ll \psi_I(x,y), \psi_{c\sigma}(x,y;k_t) \gg$$

$$Q_{a\sigma}(k_t) = \ll \psi_I(x,y), \psi_{a\sigma}(x,y;k_t) \gg$$

$$Q_{c\rho}(k_t) = \ll \psi_I(x,y), \psi_{c\rho}(x,y;k_t) \gg$$

$$Q_{a\rho}(k_t) = \ll \psi_{(x,y)}, \psi_{a\rho}(x,y;k_t) \gg$$

The integrals in (7.19) are more effectively performed in the complex θ plane. The transformations of variables are defined below;

For the integral over the semi infinite k_x - interval the transformation is given by

$$k_x = \sqrt{\varepsilon_e}\, k_o \sin\theta \qquad ; 0 \le k_x \le \sqrt{\varepsilon_e}\, k_o$$

$$k_x = \sqrt{\varepsilon_e}\, k_o \cosh\theta \qquad ; \sqrt{\varepsilon_e}\, k_o \le k_x \le \infty$$

Upon using the above tranformation of variables the integral becomes

$$\int_0^\infty dk_x \frac{\beta}{k_{xs}^2 + \beta^2} \left[Q_{cs}^2(k_x) + Q_{as}^2(k_x) \right]$$

$$= \int_0^{\frac{\pi}{2}} d\theta \cos^2\theta \left[Q_{cs}^2(\sqrt{\varepsilon_e}\, k_o \sin\theta) + Q_{as}^2(\sqrt{\varepsilon_e}\, k_o \sin\theta) \right]$$

$$+ j \int_0^\infty d\theta \sinh^2\theta \left[Q_{cs}^2(\sqrt{\varepsilon_e}\, k_o \cosh\theta) + Q_{as}^2(\sqrt{\varepsilon_e}\, k_o \cosh\theta) \right]$$

For the integral over the semi infinite k_x and finite σ intervals , we set

$$k_x = \sqrt{\varepsilon_2 k_o - \sigma^2}\, \sin\theta \qquad ; 0 \le k_x \le \sqrt{\varepsilon_2 k_o - \sigma^2}$$

$$k_x = \sqrt{\varepsilon_2 k_o - \sigma^2}\, \cosh\theta \qquad ; \sqrt{\varepsilon_e k_o - \sigma^2} \le k_x \le \infty$$

Upon using the above tranformation the integral becomes

$$\int_0^{\infty} dk_x \int_0^{\nu} d\sigma \frac{\beta}{\varepsilon_2 k_o^2 - \sigma^2} \left[Q_{c\sigma}^2(k_t) + Q_{a\sigma}^2(k_t) \right]$$

$$= \int_0^{\nu} d\sigma \left[\int_0^{\frac{\pi}{2}} d\theta \cos^2\theta \left[Q_{c\sigma}^2(\sqrt{\varepsilon_2 k_o - \sigma^2}\sin\theta) + Q_{a\sigma}^2(\sqrt{\varepsilon_2 k_o - \sigma^2}\sin\theta) \right] \right.$$

$$\left. + j \int_0^{\infty} d\theta \sinh^2\theta \left[Q_{c\sigma}^2(\sqrt{\varepsilon_2 k_o - \sigma^2}\cosh\theta) + Q_{a\sigma}^2(\sqrt{\varepsilon_2 k_o - \sigma^2}\cosh\theta) \right] \right]$$

For the integral over the semi infinite k_x and ρ intervals we define

$$\beta = k_o \cos\eta \quad ; k_t = k_o \sin\eta \quad ; k_x = k_t \cos\theta \quad ; \rho = k_t \sin\theta$$

$$d\rho dk_x = k_t dk_t d\theta$$

Upon using the above tranformation of variables the integral becomes

$$\int_0^{\infty} dk_x \int_0^{\infty} d\rho \frac{\beta}{k_o^2 - \rho^2} \left[Q_{c\rho}^2(k_t) + Q_{a\rho}^2(k_t) \right]$$

$$= \int_0^{\frac{\pi}{2}} d\theta \int_0^{\frac{\pi}{2}} d\eta \left[k_o \cos^2\eta \sin\eta \left[Q_{c\rho}^2(k_o \sin\eta\cos\theta, k_o \sin\eta\sin\theta) \right. \right.$$

$$\left. \left. + Q_{a\rho}^2(k_o \sin\eta\cos\theta, k_o \sin\eta\sin\theta) \right] \right] / \left[1 - \sin^2\eta\sin^2\theta \right]$$

$$- j \int_0^{\frac{\pi}{2}} d\theta \int_0^{\infty} d\eta \left[k_o \sinh^2\eta\cosh\eta \left[Q_{c\rho}^2(k_o \cosh\eta\cos\theta, k_o \cosh\eta\sin\theta) \right. \right.$$

$$\left. \left. + Q_{a\rho}^2(k_o \cosh\eta\cos\theta, k_o \cosh\eta\sin\theta) \right] \right] / \left[1 - \cosh^2\eta\sin^2\theta \right]$$

Similar transformations are used for solving the variational expression for case (b) and (c).

7.23 FAR FIELD OF ABRUPTLY TERMINATED RIB WAVEGUIDE

We consider the rib waveguide shown in Fig. 7.1c . The computation of the far field is based on the saddle point method. The electric field of the continuous spectrum can be written as,

$$E_x(x,y,z) = \int_0^\infty dk_x \int_0^\infty d\rho\, b_a(k_t) Z_a(k_t) \psi_a(x,y;k_t) e^{-j\beta z} \tag{7.20a}$$

for $z > 0$ and

$$E_x(x,y,z) = \int_0^\infty dk_x \int_0^\infty d\rho\, b_c(k_t) Z_c(k_t) \psi_c(x,y;k_t) e^{-j\beta z} \tag{7.20b}$$

for $z < 0$.

The double integral in the wavenumber space is conveniently carried out by trigonometric transformations given by,

$$\beta = k_o \cos\eta \quad ; k_x = k_t \cos\theta \quad ; \rho = k_t \sin\theta \quad ; k_t = k_o \sin\eta$$

Since we have chosen k_x and ρ real and such that $0 \le k_x, \rho < \infty$, then the path of the integration in the θ- plane runs over real interval

$$0 \le \theta \le \frac{\pi}{2}$$

The integration in the complex η- plane, however, runs over

$$0 \le \mathrm{Re}\,\eta \le \frac{\pi}{2} \qquad ; \text{corresponding to } k_t \le k_o$$

and

$$\mathrm{Re}\,\eta = \frac{\pi}{2},\ 0 \le \mathrm{Im}\,\eta < \infty \qquad ; \text{corresponding to } k_t > k_o$$

In the evaluation of the far field the non radiative continuum corresponding to $k_t > k_o$ is neglected and η is a real angle in the interval

$$0 \le \eta \le \frac{\pi}{2}$$

Considering the y-z plane and taking even parity with respect to ρ, the radiation field for $z > 0$ may be expressed as

$$E_x = \frac{\omega\mu_0}{2}\sqrt{\frac{1}{\pi}}\int_0^{\infty} dk_x \int_{-\infty}^{\infty} d\rho b_a(k_t)\frac{\beta}{k_x^2+\beta^2}e^{-j\rho y}e^{-j\beta z} \tag{7.21}$$

The evaluation of the far field is effected by going over to cylindrical coordinates as shown in Fig. 7.1c .

$$z = R\cos W \qquad ; \; y = R\sin W$$

The radiation integral (7.21) may be written as

$$E_x = \frac{\omega\mu_0}{2}\sqrt{\frac{1}{\pi}}\int_0^{\frac{\pi}{2}} d\eta \int_0^{\frac{\pi}{2}} d\theta f(\theta,\eta)e^{-jk_oR\cos\eta\cos W}e^{-jk_oR\sin\eta\sin\theta\sin W}$$

where

$$f(\theta,\eta) = b_a(k_o\sin\eta)\frac{k_o\sin\eta\cos^2\eta}{\sin^2\eta\cos^2\theta+\cos^2\eta}$$

There is no pole in (7.21) and upon using the saddle point method we obtain

$$E_x(R,W) = \frac{\omega\mu_0\sqrt{\pi}}{k_oR\sin W}f(\frac{\pi}{2},W)e^{-j(k_oR-\frac{\pi}{2})} \tag{7.22}$$

Hence, the radiation pattern is proportional to the spectral power density of the radiation modes $\left|b_a(k_t)\right|$.

By similar procedure the radiation field for $z < 0$ may be derived as

$$E_x(R,W) = \frac{\sqrt{2\pi}\,\omega\mu_0}{k_oR\sin W}g(\frac{\pi}{2},W)e^{-j(k_oR-\frac{\pi}{2})} \tag{7.23}$$

where

$$g\left(\frac{\pi}{2},W\right)=\sqrt{k_o\sin\eta}\cos\alpha(k_o\sin\eta)A(\theta,\eta)\tilde{H}(\theta,\eta)b_c(k_o\sin\eta)e^{-j[\alpha_D(\theta)-k_o\sin\eta\sin\theta D]}$$

$$\frac{k_o\sin\eta\cos^2\eta}{\sin^2\eta\cos^2\theta+\cos^2\eta}$$

and $A(\theta,\eta)$ is the modal amplitude of $\psi_h(y,\rho)$

7.24 NUMERICAL RESULTS

The parameters of the rib waveguide considered are $n_1=3.40$, $n_2=3.40$, $n_3=1.0$, $D=1.0\mu m$, $2a=3.0\mu m$, $d=0.1$–$0.9\mu m$ and $\lambda=1.15\mu m$. The variation of the reflection coefficient plotted against the outer slab thickness 'd' for the configuration in Fig. 7.1a to 7.1c is shown in Fig. 7.2, Fig. 7.3 and Fig. 7.4 respectively. In the case of configuration Fig. 7.1a where only the rib is terminated at $z=0$ the reflection coefficient decreases as d increases. This is to be expected as d increases the rib waveguide approaches the asymmetrical slab guide at $z\geq 0$ and most of the incident wave from the rib waveguide will pass through in to the asymmetrical slab guide for $z\geq 0$. As the confinement increases i.e d decreases the reflection coefficient of configuration Fig.7.1a approaches the reflection coefficient of configuration Fig. 7.1b. This is true because as d decreases the slab at $z\geq 0$ will not support surface waves and there is no guiding. The reflection coefficient of the configuration of Fig. 7.1c where the guide is terminated by the air half space is slightly higher than those of Fig.7.1b or Fig. 7.1a with a slab below cutoff. This suggests that some of incident wave leaks through the substrate. However, the difference in the reflection coefficients of the two different terminations is not large.

The radiation pattern of the far field for configuration Fig. 7.1c is shown in Fig. 7.5 .

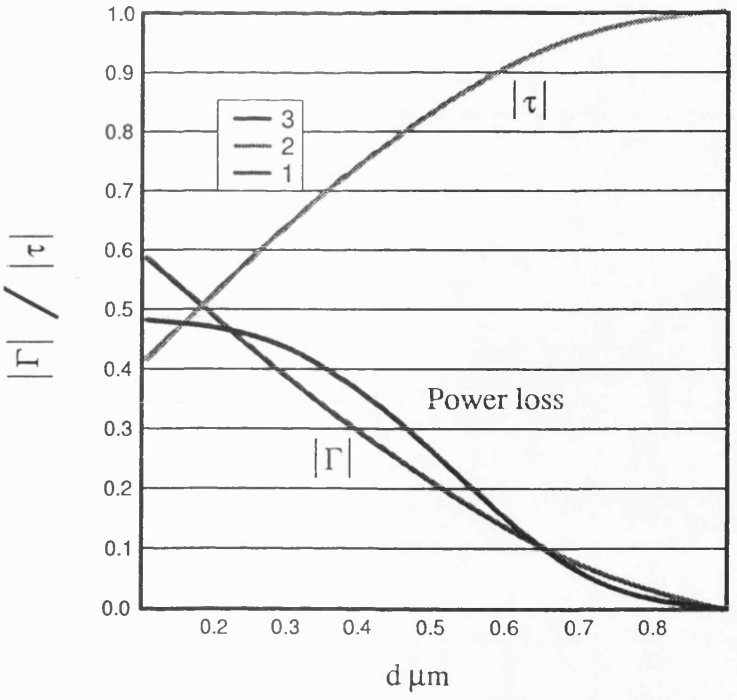

(a)

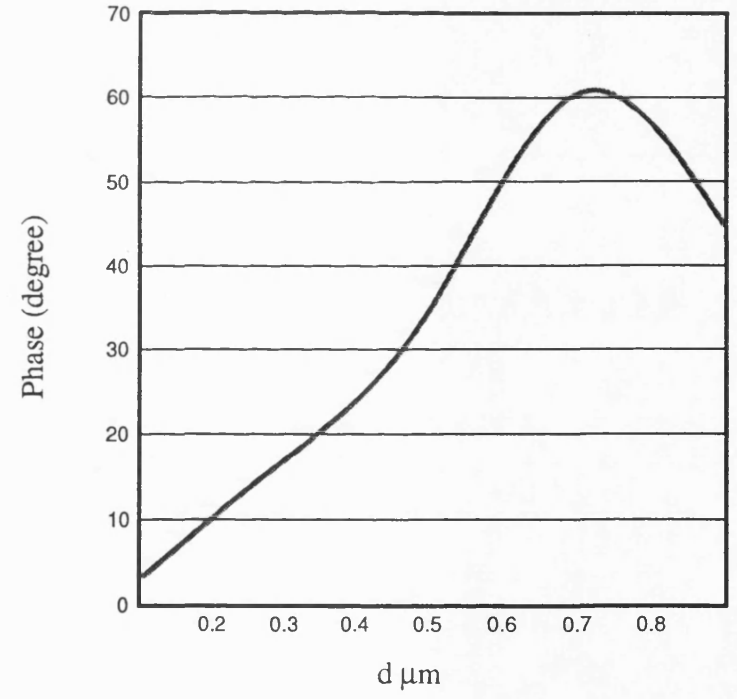

(b)

Fig. 7.2 Variation of the reflection coefficient against the outer slab thickness d for configuration of Fig. 7.1a ;
a) Modulas of the reflection coefficient b) Phase of the reflection coefficient.

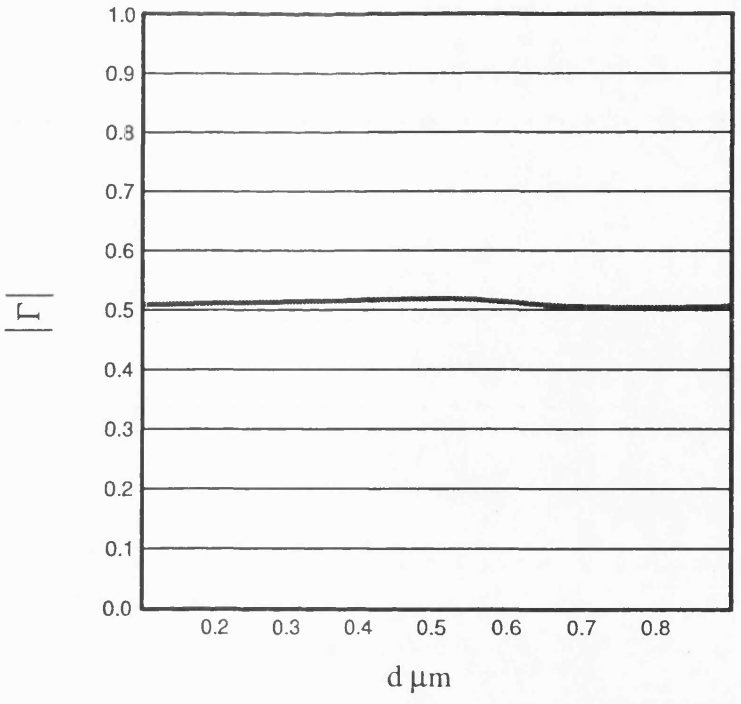

(a)

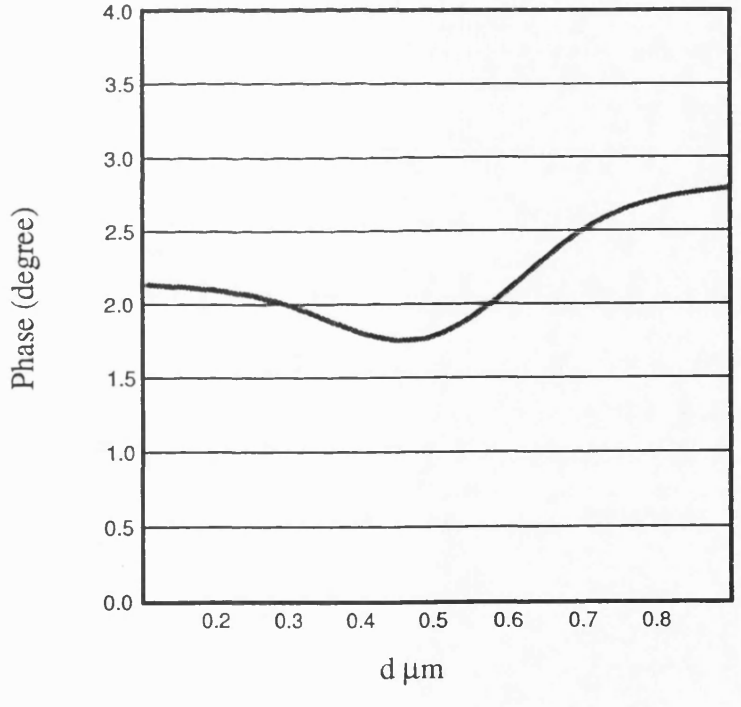

(b)

Fig. 7.3 Variation of the reflection coefficient against the outer slab thickness d for configuration of Fig. 7.1b ;
a) Modulas of the reflection coefficient b) Phase of the reflection coefficient.

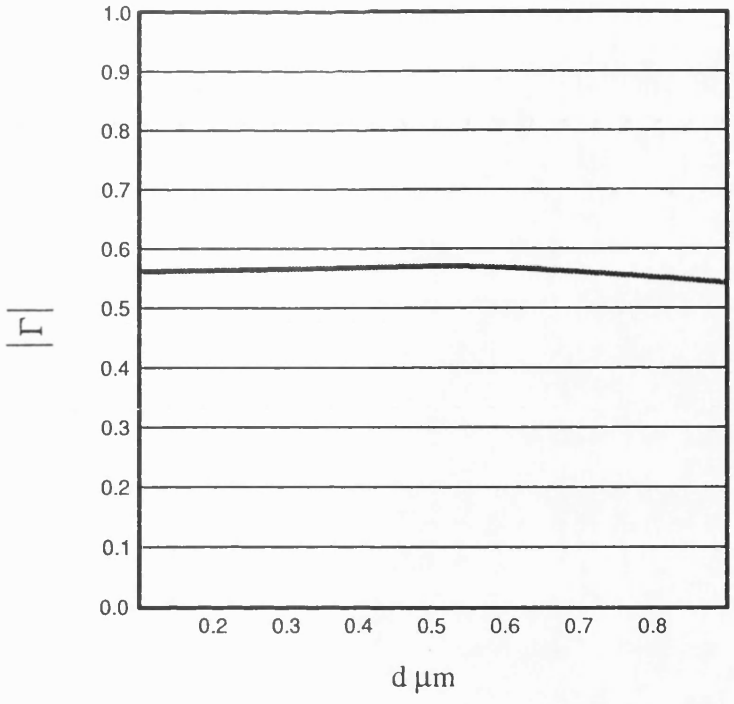

(a)

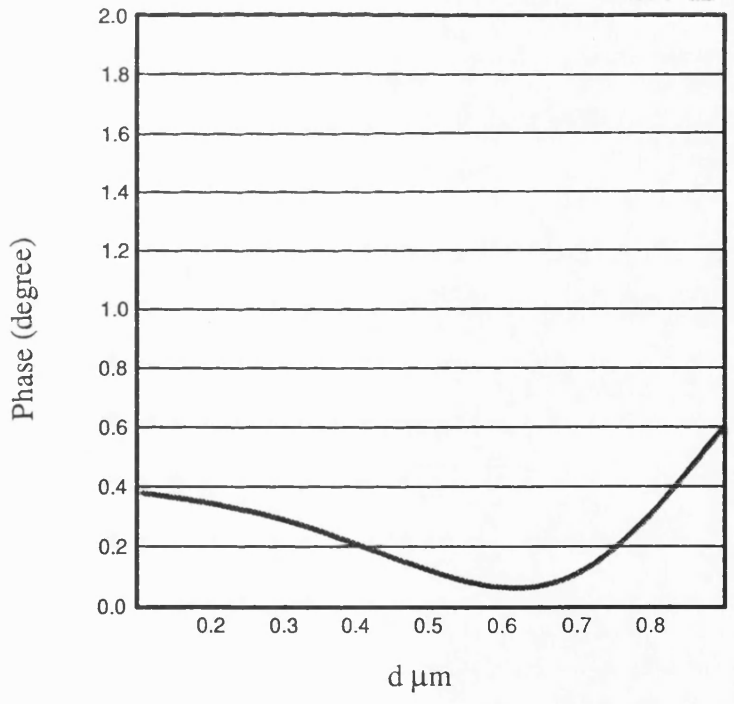

(b)

Fig. 7.4 Variation of the reflection coefficient against the outer slab thickness d for configuration of Fig. 7.1c ;
a) Modulas of the reflection coefficient b) Phase of the reflection coefficient.

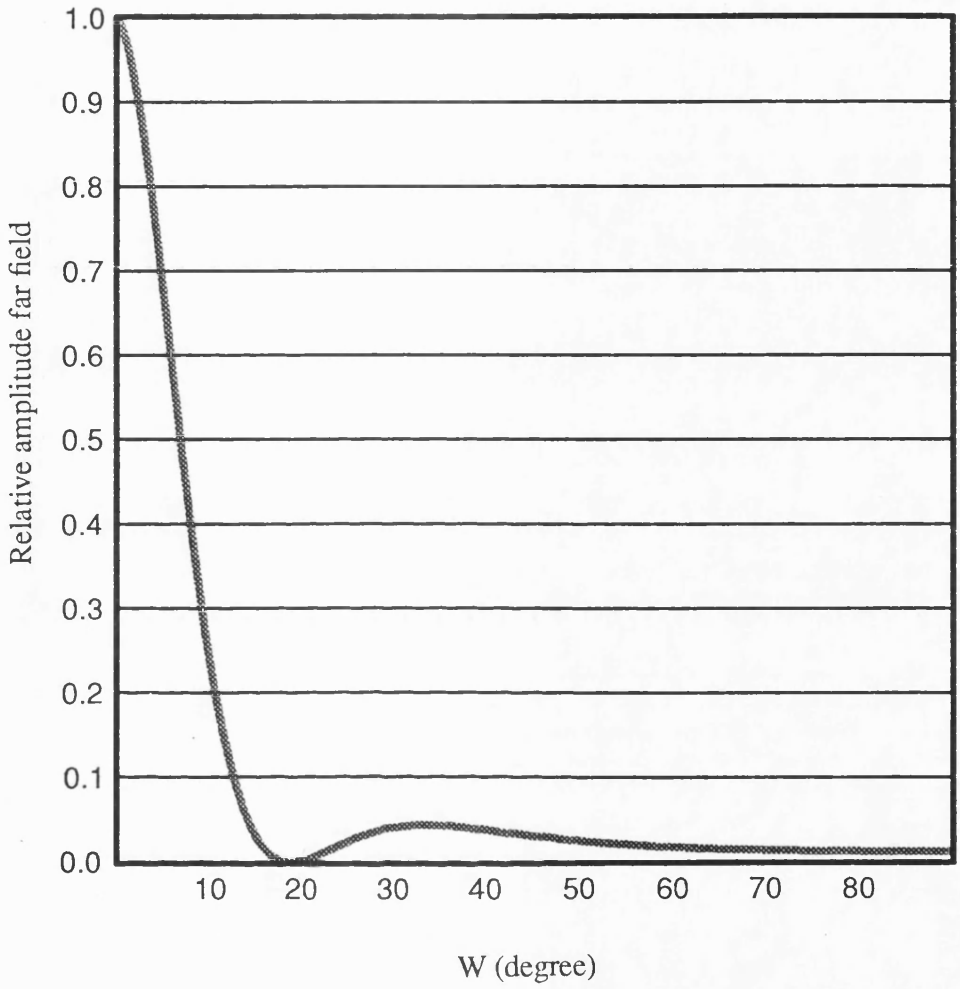

Fig. 7.5 The far field for configuration of Fig. 7.1c

7.3 DISCONTINUITY BETWEEN TWO RIB WAVEGUIDES

7.31 CHANGE IN RIB WIDTH

To investigate the effect of change in rib width between two rib waveguides we consider the configuration shown in Fig. 7.6 . The method of analysis of this structure is similar to those adopted in section 7.2 . Therefore, we will quote only the important expressions without repeating the whole analysis.

For $z \leq 0$, the transverse fields in the region may be expressed in the form

$$E_x(x,y) = (a_{o1} + b_{o1})Z_{o1}\psi_{s1}(x,y) + \int_0^\infty dk_x \Big[b_{cs1}(k_x)Z_{cs1}(k_x)\psi_{cs1}(x,y;k_x) + \int_0^\nu d\sigma b_{c\sigma1}Z_{c\sigma1}(k_t)\psi_{c\sigma1}(x,y;k_t) + \int_0^\infty d\rho b_{c\rho1}Z_{c\rho1}(k_t)\psi_{c\rho1}(x,y;k_t) \Big] \tag{7.24a}$$

$$H_y(x,y) = (a_{o1} - b_{o1})\psi_{s1}(x,y) - \int_0^\infty dk_x \Big[b_{cs1}(k_x)\psi_{cs1}(x,y;k_x) + \int_0^\nu d\sigma b_{c\sigma1}\psi_{c\sigma1}(x,y;k_t) + \int_0^\infty d\rho b_{c\rho1}\psi_{c\rho1}(x,y;k_t) \Big] \tag{7.24b}$$

For $z \geq 0$, the transverse fields in the region take the form

$$E_x(x,y) = (-a_{o2} + b_{o2})Z_{o2}\psi_{s2}(x,y) + \int_0^\infty dk_x \Big[b_{cs2}(k_x)Z_{cs2}(k_x)\psi_{cs2}(x,y;k_x) + \int_0^\nu d\sigma b_{c\sigma2}Z_{c\sigma2}(k_t)\psi_{c\sigma2}(x,y;k_t) + \int_0^\infty d\rho b_{c\rho2}Z_{c\rho2}(k_t)\psi_{c\rho2}(x,y;k_t) \Big] \tag{7.25a}$$

$$H_y(x,y) = (a_{o2} - b_{o2})\psi_{s2}(x,y) - \int_0^\infty dk_x \Big[b_{cs2}(k_x)\psi_{cs2}(x,y;k_x) + \int_0^\nu d\sigma b_{c\sigma2}\psi_{c\sigma2}(x,y;k_t) + \int_0^\infty d\rho b_{c\rho2}\psi_{c\rho2}(x,y;k_t) \Big] \tag{7.25b}$$

Subscripts 1 and 2 appearing in (7.24-7.25) refer to guide 1 and 2 respectively. Z_o,

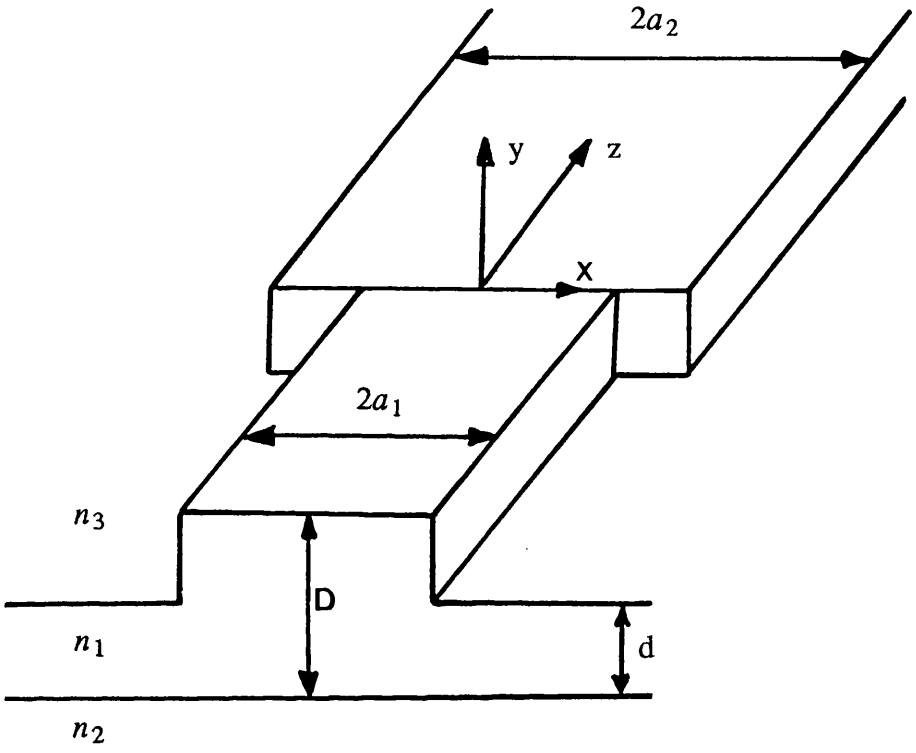

Fig. 7.6 Change in rib width between two rib waveguides.

$Z_{cs}(k_t)$, $Z_{c\sigma}(k_t)$, $Z_{c\rho}(k_t)$ were already defined in equation (7.2). Following similar development adopted in section 7.2 we obtain variational expression for δ given by,

$$\frac{1}{\delta} = \frac{\ll Z_{o1}\psi_{s1}(x,y), H_y(x,y) \gg}{\ll \psi_{s1}(x,y), H_y(x,y) \gg . \ll Z_{o1}\psi_{s1}(x,y), H_y(x,y) \gg}$$

$$= \frac{\ll H_y(x,y)\,,\, Z(x,y;x',y')\,,\, H_y(x',y') \gg}{\ll \psi_{s1}(x,y), H_y(x,y) \gg . \ll Z_{o1}\psi_{s1}(x,y), H_y(x,y) \gg} \qquad (7.26)$$

where,

$$Z(x,y;x',y') = \frac{1}{2}\Big[\Big[Z_{o1}\psi_{s1}(x,y)\psi_{s1}(x',y') + Z_{o2}\psi_{s2}(x,y)\psi_{s2}(x',y') \Big] +$$

$$\int_0^\infty dk_x \Big[\psi_{cs1}(x,y;k_x) Z_{cs1}(k_x) \psi_{cs1}(x',y';k_x)$$

$$+ Z_{cs2}(k_x)\psi_{cs2}(x,y;k_x)\psi_{cs2}(x',y';k_x) \Big]$$

$$+ \int_0^\infty dk_x \int_0^\nu d\sigma \Big[\psi_{c\sigma 1}(x,y;k_t) Z_{c\sigma 1}(k_t) \psi_{c\sigma 1}(x',y';k_t)$$

$$+ Z_{c\sigma 2}(k_t)\psi_{c\sigma 2}(x,y;k_t)\psi_{c\sigma 2}(x',y';k_t) \Big]$$

$$+ \int_0^\infty dk_x \int_0^\infty d\rho \Big[\psi_{c\rho 1}(x,y;k_t) Z_{c\rho 1}(k_t) \psi_{c\rho 1}(x',y';k_t)$$

$$+ \psi_{c\rho 2}(x,y;k_t) Z_{a\rho 2}(k_t) \psi_{a\rho 2}(x',y';k_t) \Big]\Big] \qquad (7.27)$$

Equations (7.26) and (7.15), express the sought variational expression for the reflection coefficient at the discontinuity $z = 0$.

7.311 CHOICE OF TRIAL FIELD

In order to solve the variational expression (7.26) we require a two dimensional trial field function to represent the field unknown. As in section 7.2 we use the bound mode of an intermediate rib waveguide , $\psi_I(x,y)$, whose height d_I is intermediate between those of the thicker slab 'D' and the surrounding slab 'd', and rib width a_I intermediate

between those of guide 1 and guide 2 respectively. The outer slab dimension of both guides is kept the same. The criterion used in choosing the height d_I and the rib width a_I is to maximize the ratio of $\frac{\ll H_y(x,y),\psi_{s2}(x,y)\gg}{\ll H_y(x,y),\psi_{s1}(x,y)\gg}$ where $\ll H_y(x,y),\psi_{s1}(x,y)\gg$ and $\ll H_y(x,y),\psi_{s2}(x,y)\gg$ is the overlapping integral between the trial function and the bound mode of guides 1 and 2 respectively. The trial function is a function of two variables and with a view to minimising the computational complexity, we fixed one of the variables. As the height 'D' and 'd' of the two guides are the same, we choose to set $d_I = \bar{d}$ (where $\bar{d}$ defined as in chapter three). Justification for this choice was explained in section 7.2 . Furthermore, in the maximisation process we consider only the first term of $\psi_{s1}(x,y)$ and $\psi_{s2}(x,y)$ as these terms carry most of the power. As it turns out, a_I resulting from the above process is very close to the rib width of guide 1 and hence we use a_1. Therefore, $\psi_I(x,y)$ is chosen as,

$$\psi_I(x,y) = \frac{1}{N_I} P_I \phi_I(y) \frac{\cos(q_{sI}x)}{\cos(q_{sI}a_{1)}} \qquad ;x \le a_1$$

$$= \frac{1}{N_I} P'_I \psi_I(y) e^{-\gamma_{sI}(x-a_1)} \qquad ;x \ge a_1 \tag{7.28}$$

and

$$N_I^2 = \frac{P_I^2}{2q_{sI}} \left[q_{sI}a_1 \, sec^2(q_{sI}a_1) + tan(q_{sI}a_1) \right] + \frac{P_I'^2}{2\gamma_{sI}}$$

Substituting (7.28) in to equation (7.26), we obtain

$$\frac{1}{\delta} = \Bigg[\left[P_{rib1}P'_{rib1} + P_{rib2}P'_{rib2} \right] + \omega\mu_0 \int_0^\infty dk_x \frac{\beta}{k_{xs}^2 + \beta^2} \left[Q_{cs1}^2(k_x) + Q_{cs2}^2(k_x) \right]$$

$$+ \omega\mu_0 \int_0^\infty dk_x \int_0^\nu d\sigma \frac{\beta}{\varepsilon_2 k_o^2 - \sigma^2} \left[Q_{c\sigma 1}(k_t) + Q_{c\sigma 2}(k_t) \right]$$

$$+ \omega\mu_0 \int_0^\infty dk_x \int_0^\infty d\rho \frac{\beta}{k_o^2 - \rho^2} \left[Q_{c\rho 1}(k_t) + Q_{c\rho 2}(k_t) \right] \Bigg] / 2P_{rib1}P'_{rib1} \tag{7.29}$$

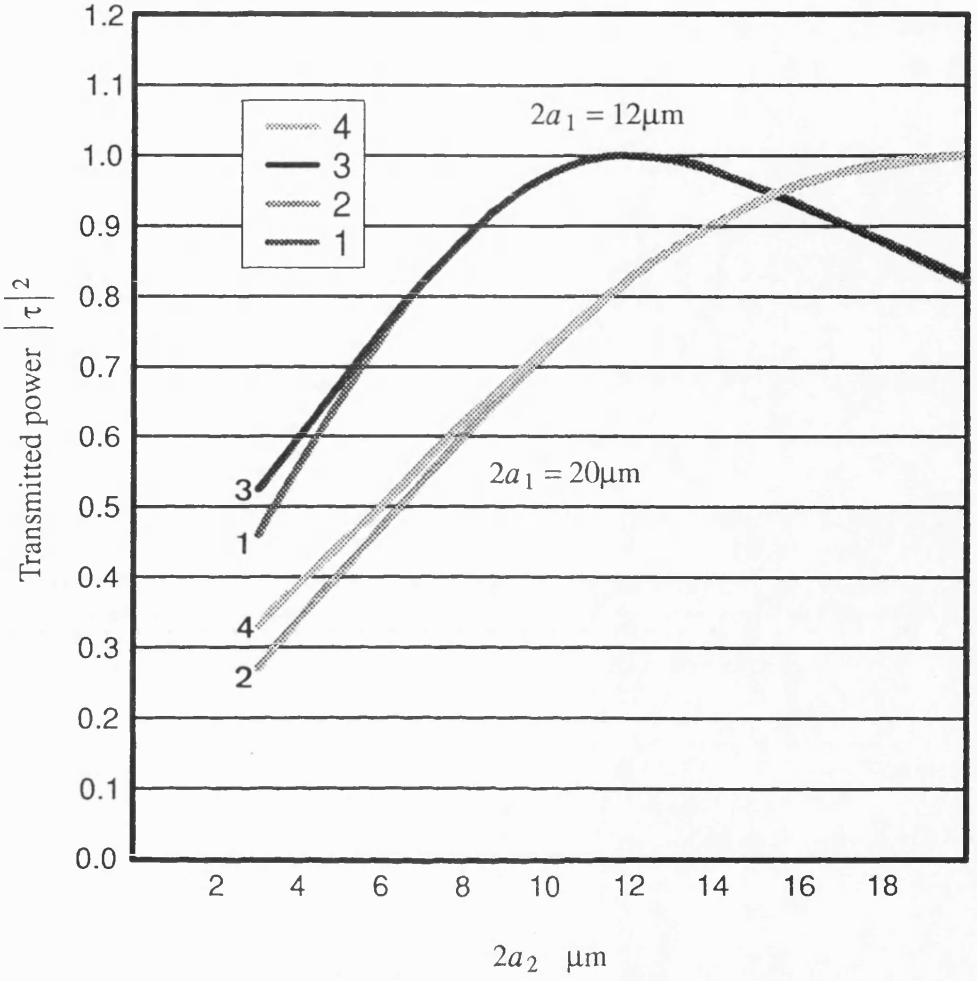

Fig. 7.7 Variation of the transmitted power in guide two as a function of the rib width of guide two.

1&2 – Present analysis

3&4 – Reference [3]

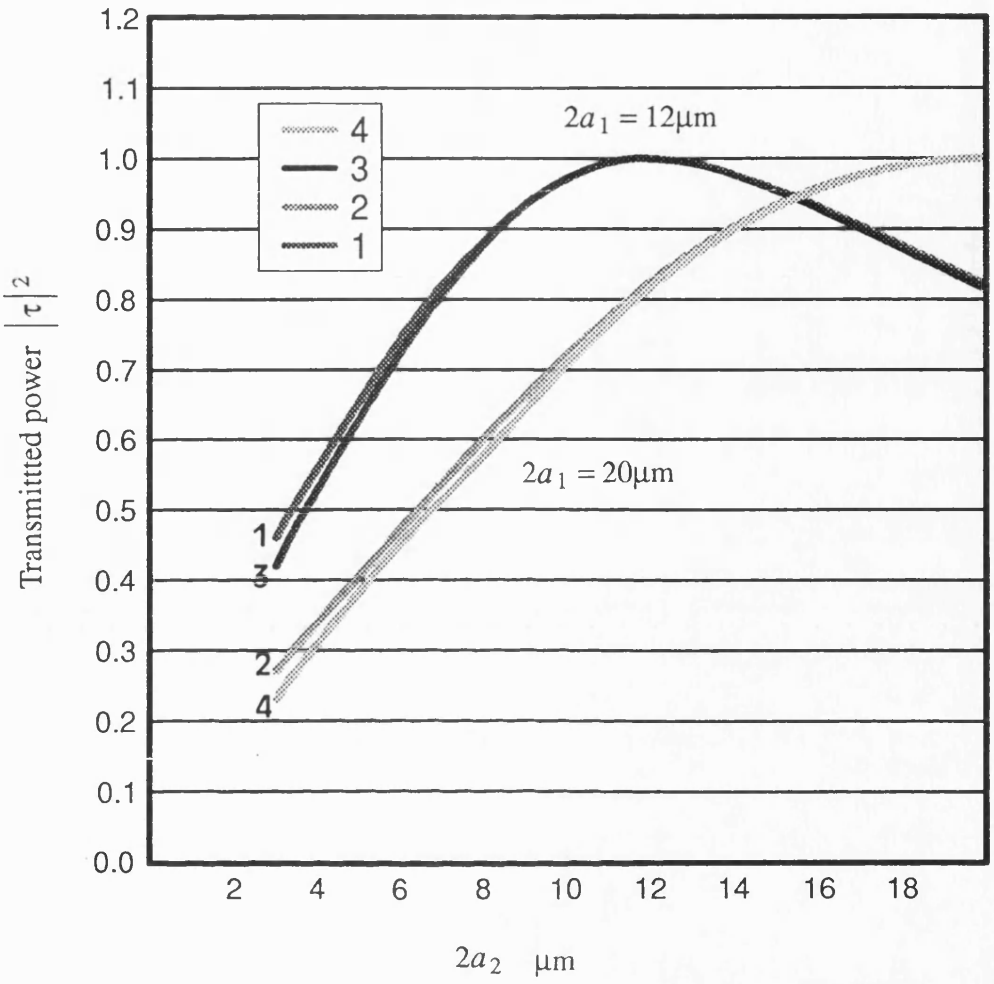

Fig. 7.8 Variation of the transmitted power in guide two as a function of the rib width of guide two at $\lambda = 1.15\mu m$ and $\lambda = 1.55\mu m$

3 & 4 $-\lambda = 1.15\mu m$

1 & 2 $-\lambda = 1.55\mu m$

where the various coefficients are defined by

$$P_{rib\,1,2} = \ll \psi_I(x,y), \psi_{s\,1,2}(x,y) \gg$$

$$P'_{rib\,1,2} = \ll \psi_I(x,y), Z_{o\,1,2}\psi_{s\,1,2}(x,y) \gg$$

$$Q_{cs\,1,2}(k_x) = \ll \psi_I(x,y), \psi_{cs\,1,2}(x,y;k_x) \gg$$

$$Q_{c\sigma 1,2}(k_t) = \ll \psi_I(x,y), \psi_{c\sigma 1,2}(x,y;k_t) \gg$$

$$Q_{c\rho 1,2}(k_t) = \ll \psi_I(x,y), \psi_{c\rho 1,2}(x,y;k_t) \gg$$

7.312 NUMERICAL RESULTS

In order to assess the accuracy of the method, we apply the above analysis to a guide whose parameters are given by $n_1 = 3.4406$, $n_2 = 3.4145$, $n_3 = 1.0$, $D = 1.5\mu m$, $d = 0.5\mu m$ with $\lambda = 1.55\mu$ m. This particular structure has been analyzed by [3] using finite element method and field matching. The results of the present analysis, shown by solid lines, together with the results of [3], shown by dotted lines, are plotted in Fig. 7.7 . The agreement between the two sets of results is good and this validates the accuracy of our approach. A similar structure is also analyzed at $\lambda = 1.15\mu m$ and the results are shown in Fig. 7.8 . It is seen that the transmitted power at $\lambda = 1.15\mu m$ decreases slightly as the mismatch between the two guides (i.e. $a_1 > a_2$ or $a_1 < a_2$) increases, particularly when $a_2 < a_1$.

7.32 HORIZONTAL MISALINGMENT

The configuration under study is shown in Fig. 7.9 where the second guide is shifted horizontally by Δx at $z = 0$. The geometrical and electrical parameters of the two guides are kept the same. The method of analysis of this structure is similar to that adopted in previous sections and hence the development of the required variational expression for the reflection coefficient at $z = 0$ will not be repeated. The transverse fields in the first guide take the form similar to that given in equation (7.24) and the transverse fields in the second guide $z \geq 0$ may be expressed as,

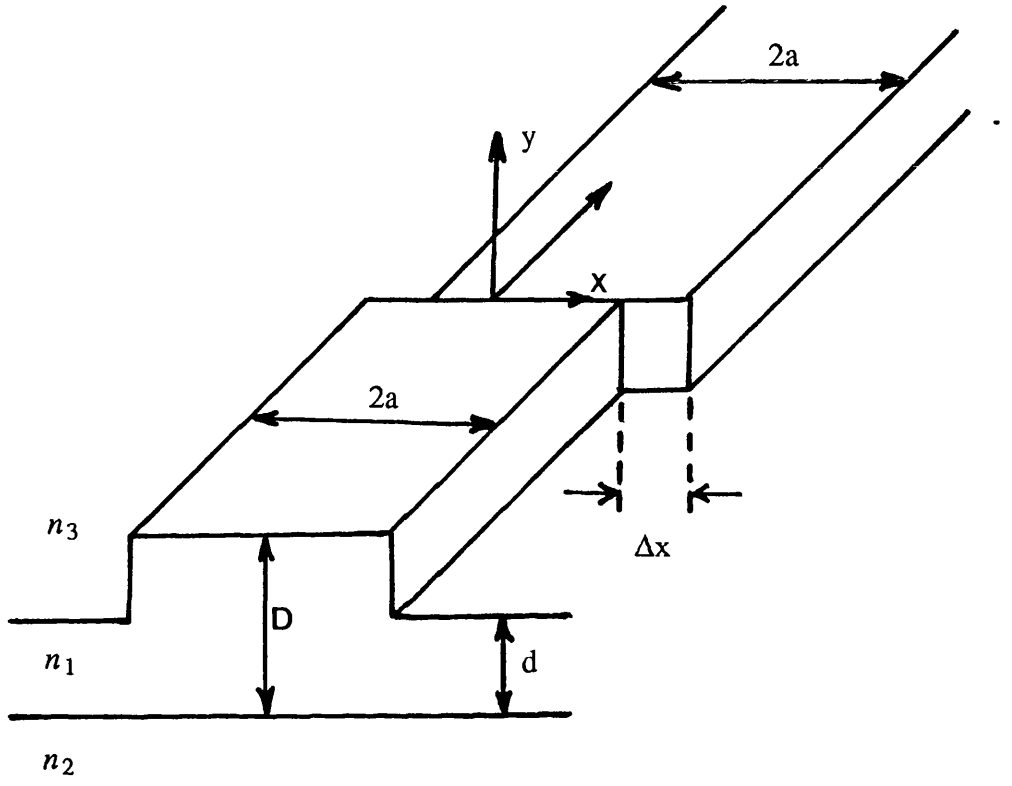

Fig. 7.9 Horizontal misalingment between two identical rib waveguides.

$$E_x(x,y) = (-a_{o2} + b_{o2})Z_{o2}\psi_{s2}(x+\Delta x,y) + \int_0^{\infty} dk_x \Big[b_{cs2}(k_x)Z_{cs2}(k_x)\psi_{cs2}(x+\Delta x,y;k_x)$$

$$+ \int_0^{\nu} d\sigma b_{c\sigma 2}Z_{c\sigma 2}(k_t)\psi_{c\sigma 2}(x+\Delta x,y;k_t)$$

$$+ \int_0^{\infty} d\rho b_{c\rho 2}Z_{c\rho 2}(k_t)\psi_{c\rho 2}(x+\Delta x,y;k_t) \Big] \qquad (7.30a)$$

$$H_y(x,y) = (a_{o2} - b_{o2})\psi_{s2}(x+\Delta x,y) - \int_0^{\infty} dk_x \Big[b_{cs2}(k_x)\psi_{cs2}(x+\Delta x,y;k_x)$$

$$+ \int_0^{\nu} d\sigma b_{c\sigma 2}\psi_{c\sigma 2}(x+\Delta x,y;k_t) + \int_0^{\infty} d\rho b_{c\rho 2}\psi_{c\rho 2}(x+\Delta x,y;k_t) \Big] \qquad (7.30b)$$

The appropriate variational expression for $\frac{1}{\delta}$ is essentially the same as in equation (7.26) where now the kernel of the integral operator is given by,

$$Z(x,y;x',y') = \frac{1}{2}\Big[\Big[Z_{o1}\psi_{s1}(x+\Delta x,y)\psi_{s1}(x'+\Delta x',y')$$

$$+ Z_{o2}\psi_{s2}(x+\Delta x)\psi_{s2}(x'+\Delta x',y') \Big]$$

$$+ \int_0^{\infty} dk_x \Big[\psi_{cs1}(x+\Delta x,y;k_x)Z_{cs1}(k_x)\psi_{cs1}(x'+\Delta x',y';k_x)$$

$$+ Z_{cs2}(k_x)\psi_{cs2}(x+\Delta x,y;k_t)\psi_{cs2}(x'+\Delta x',y';k_x) \Big]$$

$$+ \int_0^{\infty} dk_x \int_0^{\nu} d\sigma \Big[\psi_{c\sigma 1}(x+\Delta x,y;k_t)Z_{c\sigma 1}(k_t)\psi_{c\sigma 1}(x'+\Delta x',y';k_t)$$

$$+ Z_{c\sigma 2}(k_t)\psi_{c\sigma 2}(x+\Delta x,y;k_t)\psi_{c\sigma 2}(x'+\Delta x',y';k_t) \Big]$$

$$+ \int_0^{\infty} dk_x \int_0^{\infty} d\rho \Big[\psi_{c\rho 1}(x+\Delta x,y;k_t)Z_{c\rho 1}(k_t)\psi_{c\rho 1}(x'+\Delta x',y';k_t)$$

$$+ \psi_{c\rho 2}(x+\Delta x,y;k_t)Z_{a\rho 2}(k_t)\psi_{a\rho 2}(x'+\Delta x',y';k_t) \Big] \Big] \qquad (7.31)$$

As an example of the numerical simulation we consider guide with $n_1 = 3.44$, $n_2 = 3.40$,

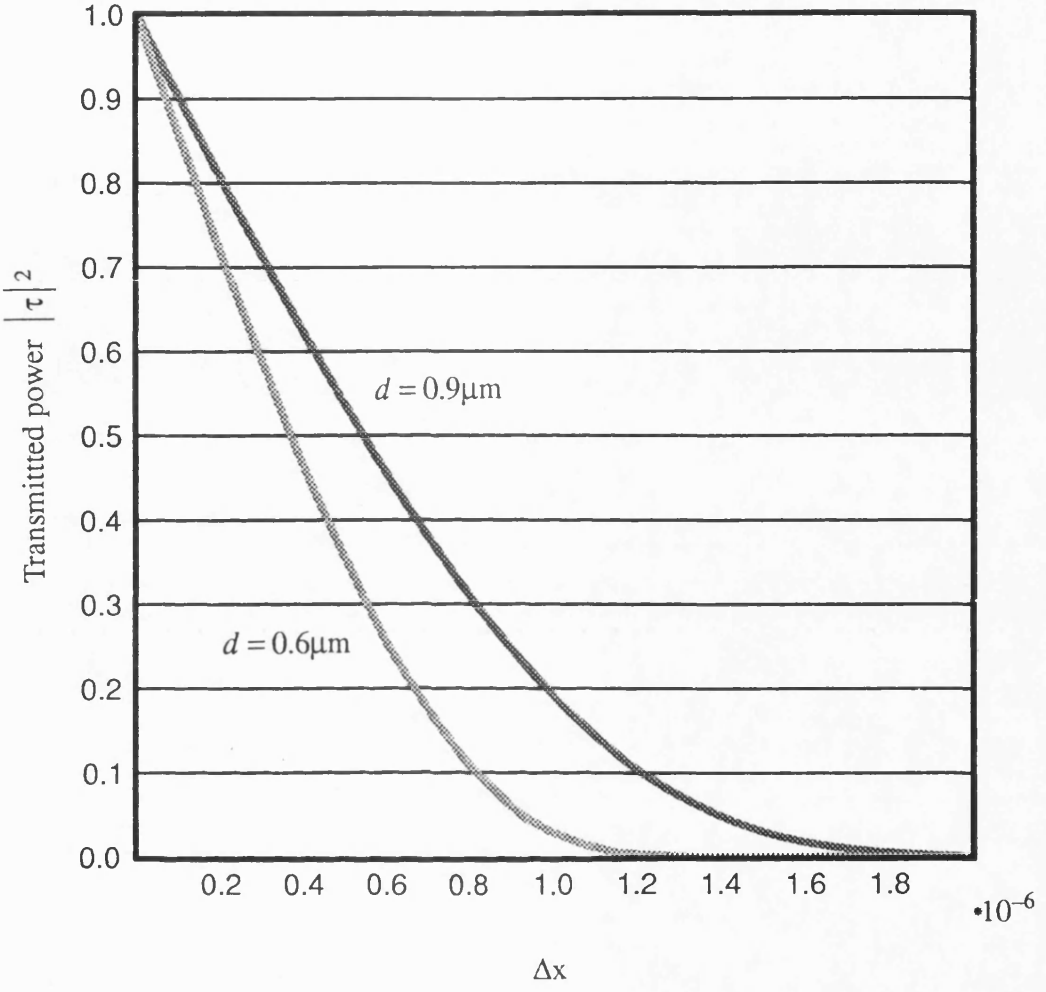

Fig. 7.10 Variation of the transmitted power in guide two as a function of the horizontal displacement Δx

$n_3 = 1.0$, $D = 1.0\mu m$, $d = 0.6\mu m$ and $d = 0.9\mu m$, $2a = 4.0\mu m$ and $\lambda = 1.15\mu m$. The variation of the transmitted power in guide two as a function of horizontal misalingment is shown in Fig. 7.10.

7.33 CHANGE IN RIB HEIGHT

The arrangement under consideration is shown in Fig. 7.11 . The rib height of guide 1 is fixed and that of guide guide 2 is varied. The electrical parameters and other geometrical parameters for both guide are the same. The method of analysis and the solution of the resulting variational expression is similar to those adopted in the previous section. However, in this case the LSM mode is considered to be incident from guide 1 to guide 2. The appropriate variational expression for $\frac{1}{\delta}$ and the kernel of the associated integral operator is given by (7.26) and (7.27) respectively, where now the quantities appropriate for the LSM mode must be used. In the numerical simulation, we consider a guide whose parameters are $n_1 = 3.44$, $n_2 = 3.434$, $n_3 = 1.0$, $2a = 5.0\mu m$, $d = 2.0\mu m$, $D_1 = 3.0\mu m$ and $\lambda = 1.15\mu m$. The variation of the tramsmitted power in guide 2 as a function of the rib height is shown in Fig. 7.12 by solid lines. The dotted line are the results of [3]. From the figure, the close agreement of the two sets of results is clearly visible.

7.4 GENERAL CONCLUSION

In this chapter we have illustrated the analysis of the discontinuity problems in rib waveguide by means of a rigorous variational solution. In the analysis the mode spectrum developed in chapter six was used to expand the fields at the discontinuity. Results are presented on the scattering of bound mode at the abrupt discontinuity at the end of the rib waveguide and the discontinuity between two waveguides. Simulations show that the results of our analysis agrees quite well with the results of [3] and this confirms the accuracy of the mode spectrum. The present analysis could be extended to

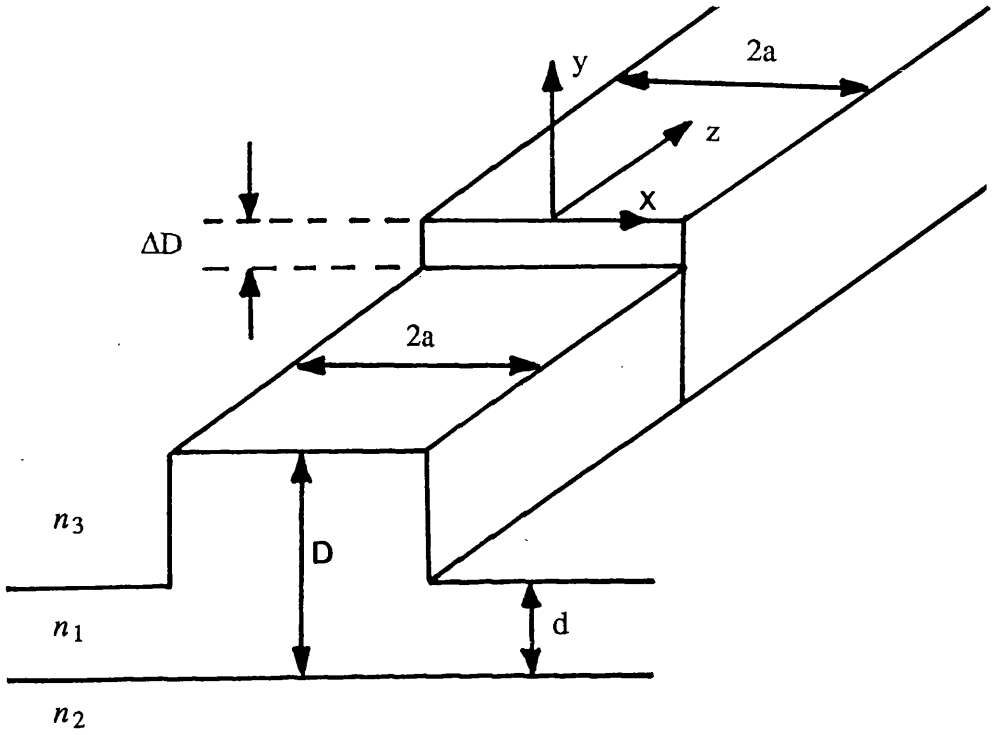

Fig. 7.11 Change in rib height between two rib waveguides.

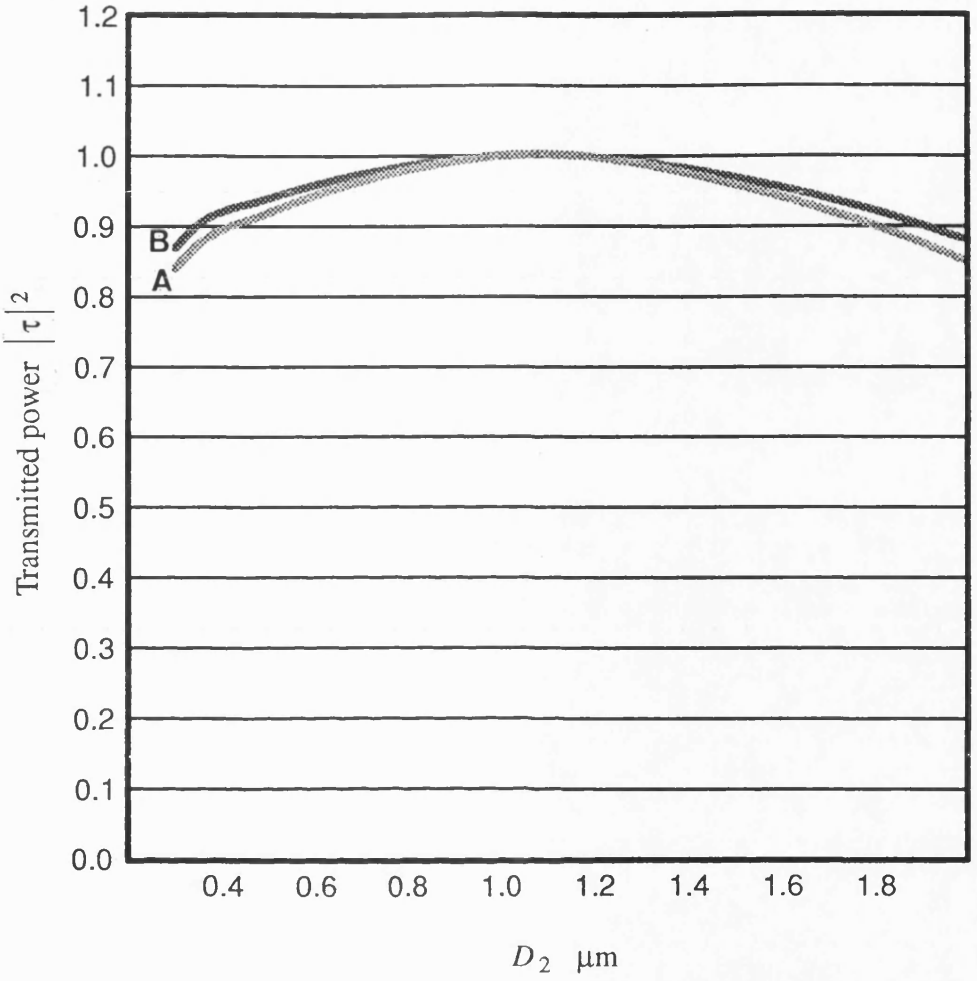

Fig. 7.12 Variation of the transmitted power as a function of rib height of guide two.

A — Present analysis

B — Reference [3]

cover the analysis of other discontinuity problems involving rib waveguides such gratings or filters.

REFERENCES

[1] T.E Rozzi, "Rigorous analysis of the step discontinuity in a planar dielectric waveguide", I.E.E.E. Trans. on Microwave Theory and Techniques, vol. MTT-26, No. 10, Oct. 1978, pp. 738-746.

[2] T.E. Rozzi and G.H. Int't Veld, "Variational Treatment of the diffraction at the facet of d.h. lasers and of dielectric millimeter wave antennas", I.E.E.E Trans. Microwave Theory and Techniques", vol. MTT-28, No. 2, Feb. 1980, pp. 61-73.

[3] B.M.A. Rahman and J.B. Davies, "Analysis of optical waveguides and some discontinuity problems", I.E.E Proc., vol. 135, Pt. J, No. 5, Oct. 1988, pp. 339-342.

CHAPTER 8

CONCLUSIONS AND SUGGESTIONS FOR FURTHER WORK

A theoretical model of the open rib waveguide structure including its complete electromagnetic spectrum has been developed. The theoretical investigation of rib waveguide is complicated by two factors, the non separable waveguide cross section and the open nature of the guide where the electromagnetic field components contain an integral over a continuously varying transverse wave number. The solution adopted in the present work is to view the structure in terms of two basic building components. These are the uniform regions, made up of multilayer slab waveguides, and the step discontinuities where the two regions meet. Each uniform region, then, is described as an infinite region in which the electromagnetic field equations may be solved in a separable form. The unknown electromagnetic field in the waveguide is expressed separately in each region in terms of y-directed Hertzian potentials. The boundary conditions at the interface where the two uniform regions meet is then applied to find the unknown field amplitudes. The problem is formulated as an integral equation in the unknown transverse field component at the interface between regions. The equation is solved using a variational method of Rayleigh - Ritz type, i.e. one where we adopt a single function trial field at the transverse step discontinuity, including all a priori known physical features of the discontinuity. The trial function is represented by the modal distribution of an asymmetrical slab of height intermediate between those of the rib and of the surrounding slab, which we define 'transition function'. The formulation leads to a simple model for the guide dispersion yielding results for the propagation constants which are of comparable accuracy with other numerical techniques and significantly better than the EDC method. The success of a single 'transition function' in representing the field unknown is a considerable advantage as it totally avoids the use of matrices and is consequently more efficient than the direct mode matching technique. In the analysis,

the pure LSE/LSM polarizations and as well as the full hybrid case are considered.

In the calculation of the propagation constant, it is shown that when there are well guided modes in the slab under the rib and the surrounding slab, the effect of the continuous spectra is negligible. When the surrounding slab is cutoff, the continuous spectra has to be included, and the simulation shows that only the substrate modes contribute significantly to the accuracy of the results. This observation makes it possible to simplify the formulation and yet get accurate results with minimum computational effort as we need to consider only the regular integral with finite interval. Accuracy is checked by comparing the results of the present analysis with the results of other numerical techniques that exist in the literature, in particular the vector finite element method [1]. These comparisons demonstrate that the present method of analysis yields accurate results with minimum computational effort. Furthermore, simulations also show that the results of the LSE/LSM polarizations are almost identical to those of the hybrid mode analysis. This observation seem to suggest that LSE/LSM provides a good approximation even though the field is recognized to be hybrid.

Once the propagation constants have been obtained the other field components may be derived from the potential.

The analysis of a single guide is extended to cover coupled rib waveguides. The coupled structure is viewed as a cascade of step discontinuities in the transverse direction. The formulation takes into account not only the bound modes but also the continua between two successive steps. For the purpose of establishing the relationship between E and H fields, the structure is divided in to three basic building blocks where each constituent is represented by uniform slab with step discontinuities at each end. Integral operators are found relating the total E and H fields at various ports and then these are used to relate the total fields at each port to one another. A simple two port model for each constituent block is obtained using variational methods similar to those used for single guides. This way, the analysis of coupled waveguide reduces to that of a cascade of two-port

networks. Network analysis is then used to determine the propagation constants of the coupled structure. Thanks to this formulation the same approach can be used to analyse symmetrical as well as asymmetrical multiple coupled structures. This is a considerable advantage as compared with the numerical techniques where the computational effort increases with the area in which the solution is sought. Numerical examples were worked out for symmetrical coupled waveguides and results are shown to be in agreement with those of the finite difference method. The numerical simulation on three guide couplers indicates that, for closely coupled structures, an accurate technique such as the present approach must be used rather than coupled mode theory which is only valid for loosely coupled systems. Numerical calculations on asymmetrical coupled waveguides are also demonstrated.

In order to complete the characterization of the electromagnetic spectrum, we address the question of determining the continuum. The method adopted in this work uses an eigenfunction approach which describes the continuous modes in a manner analogous to the bound mode description of the guided fields. It starts by defining the completeness relationship of the mode spectrum. From the statement of completeness, we derive the field components of the continuum in terms of H_y. By imposing the continuity of the transverse fields at a chosen interface, we establish an eigenvalue equation for the transverse impedance. The solution of this equation determines the electromagnetic fields of the continuum. Once the complete spectrum is known the longitudinal Green's function of the guide can be derived and used in treating the discontinuity problems in rib waveguides.

With a view to demonstrating validity, an application is given to a few types of basic discontinuities in rib waveguide, such as the abrupt termination of the rib waveguide and the change in rib width and rib height between two rib waveguides. This problem is solved by means of a rigorous variational approach and the results show good agreement with those of the FEM [2].

The method of analysis may be used for a wide variety of practical structures. The discontinuity may be constituted by a single step but also by multiple steps, periodic or aperiodic. Two structures are directly obtainable. The first is the extension of the analysis for the change in rib width to the case of tapered rib waveguides. This involves solving the problems by considering successive changes in rib width. The second is the extension of the analysis of the change in rib height to the analysis of corrugated rib waveguides such as gratings or resonator filters as shown in Fig. 8.1 . The obvious approach to this problem is to proceed along the lines of chapter five. In this approach, the structure is viewed as a cascade of a double step discontinuity in rib waveguide as shown in Fig. 8.2 . By using the method detailed in chapter five, a two-port impedance operator for the section of the rib waveguide $0 \le z \le L$ may be established by the relationship:

$$\begin{bmatrix} E_x(x,y,0) \\ E_x(x,y,L) \end{bmatrix} = \begin{bmatrix} -\hat{Z}_{11} & \hat{Z}_{12} \\ -\hat{Z}_{12} & \hat{Z}_{11} \end{bmatrix} \begin{bmatrix} -H_y(x,y,0) \\ -H_y(x,y,L) \end{bmatrix}$$

where the kernel of the impedance operators is given by

$$Z_{11}(x,y;x',y') = Z_{os2}\coth(\beta_{s2}L)\psi_{s2}(x,y)\psi_{s2}(x',y') + \int_0^\infty\int_0^\infty dk_t Z_{c2}(k_t)\coth(\beta(k_t)L)\psi_{c2}(x,y;k_t)\psi_{c2}(x',y';k_t)$$

$$Z_{12}(x,y;x',y') = Z_{os2}\,\mathrm{cosech}(\beta_{s2}L)\psi_{s2}(x,y)\psi_{s2}(x',y') + \int_0^\infty\int_0^\infty dk_t Z_{c2}(k_t)\,\mathrm{cosech}(\beta(k_t)L)\psi_{c2}(x,y;k_t)\psi_{c2}(x',y';k_t)$$

The impedance operators at $z = 0$ and $z = L$ are given by,

At $z = 0$ we have

$$E_x(x,y,0) = \hat{Z}_1 \left[-H_y(x,y,0) \right]$$

where the kernel of the operator is given by

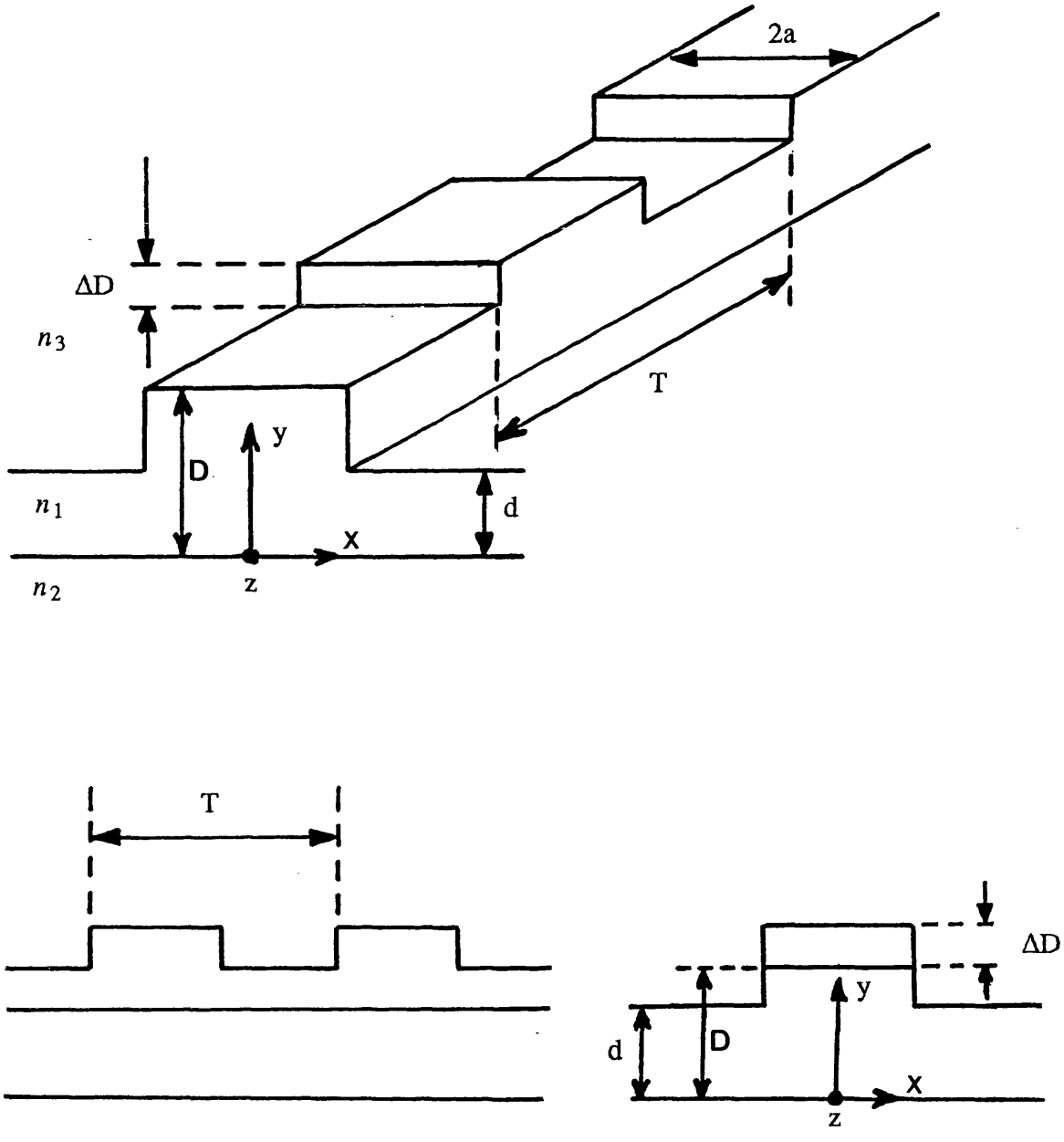

Fig. 8.1 Rib waveguide grating

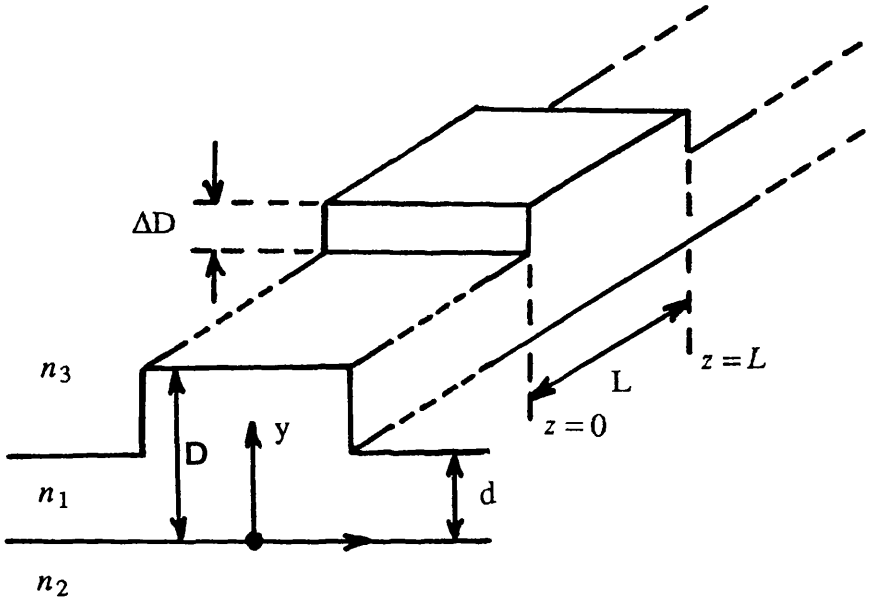

Fig. 8.2 Longitudinal double step discontinuity in rib waveguide.

$$Z_1(x,y;x',y') = Z_{os1}\psi_{s1}(x,y)\psi_{s1}(x',y') + \int_0^\infty\int_0^\infty dk_t Z_{c1}(k_t)\psi_{c1}(x,y;k_t)\psi_{c1}(x',y';k_t)$$

Similarly at $Z = L$ we have

$$E_x(x,y,0) = -\hat{Z}_3\left[-H_y(x,y,L)\right]$$

where the kernel of the operator is given by

$$Z_3(x,y;x',y') = Z_{os3}\psi_{s3}(x,y)\psi_{s3}(x',y') + \int_0^\infty\int_0^\infty dk_t Z_{c3}(k_t)\psi_{c3}(x,y;k_t)\psi_{c3}(x',y';k_t)$$

Where Z_{os} and Z_c are the characteristic impedances of the discrete bound mode and of the continuum respectively.

Once the two-port parameters have been obtained the analysis of the corrugated structure reduces to that of solving the two port in cascade using network methods. By this approach, we can analyse not only structures with periodic gratings but also aperiodic gratings.

REFERENCES

[1] B.M.A. Rahman, J.B. Davies, " Vector H finite element solution of Ga As/Ga Al As rib waveguides ", I.E.E Proc., vol. 132, Pt. J, Dec. 1985, pp 349-353.

[2] B.M.A. Rahman and J.B. Davies, "Analysis of optical waveguides and some discontinuity problems", I.E.E Proc., vol. 135, Pt. J, No. 5, Oct. 1988, pp. 339-342.

APPENDIX 1

TM mode spectrum of an asymmetric three layer slab waveguide

The three layer geometry is the same as under the rib of Fig. 2.1. The modes normalized to unity over the whole interval $-\infty \le y \le \infty$ are given by:

a) Surface modes

$$\phi_{se}(y) = A\, e^{-q(y-D)} \qquad : y \ge D$$

$$= A\, \frac{\cos(hy - \bar{\phi})}{\cos(hD - \bar{\phi})} \qquad : 0 \le y \le D$$

$$= A\, \frac{\cos(\bar{\phi})}{\cos(hD - \bar{\phi})}\, e^{py} \qquad : y \le 0$$

where

$$A = \left\{ \frac{2}{\dfrac{q}{h^2} + \dfrac{1}{q} + \left(\dfrac{D}{\varepsilon_1} + \dfrac{\varepsilon_2 (h^2+p^2)}{p\,(\varepsilon_2^2 h^2 + p^2 \varepsilon_1^2)} \right) \dfrac{1}{\cos^2(hD - \bar{\phi})}} \right\}^{\frac{1}{2}}$$

$$\bar{\phi} = \tan^{-1} \left(\frac{p\, \varepsilon_1}{h\, \varepsilon_2} \right)$$

and the wavenumber are related by the usual quadratic law, namely

$$\varepsilon_1 k_o^2 = h^2 + \beta^2$$

$$\varepsilon_2 k_o^2 = -p^2 + \beta^2$$

$$\varepsilon_3 k_o^2 = -q^2 + \beta^2$$

and the surface modes are normalised as

$$< \phi_{se}(y) , \phi_{se}(y) > = \delta(y)$$

b) Substrate modes

$$\phi_e(y,\sigma) = \sqrt{\frac{2}{\pi}\,\varepsilon_2}\; A_{sb}\cos(hD - \bar{\phi}_{sb})\, e^{-q(y-D)} \qquad : y \geq D$$

$$= \sqrt{\frac{2}{\pi}\,\varepsilon_2}\; A_{sb}\cos(hy - \bar{\phi}_{sb}) \qquad : 0 \leq y \leq D$$

$$= \sqrt{\frac{2}{\pi}\,\varepsilon_2}\;\cos(\sigma y - \alpha_{sb}) \qquad : y \leq 0$$

where

$$\alpha_{sb} = \tan^{-1}\left(\frac{h\,\varepsilon_2}{\sigma\,\varepsilon_1}\tan(\bar{\phi}_{sb})\right)$$

$$\bar{\phi}_{sb} = \tan^{-1}\left(\frac{\frac{h}{\varepsilon_1}\tan(hD) - q}{\frac{h}{\varepsilon_1} + q\,\tan(hD)}\right)$$

$$A_{sb} = \frac{\cos(\alpha_{sb})}{\cos(\bar{\phi}_{sb})}$$

with the above choice of constants, the substrate modes are normalised as

$$< \phi_e(y,\sigma)\,,\, \phi_e(y,\sigma') > = \delta(\sigma - \sigma')$$

and the wavenumber are related by

$$\varepsilon_1\, k_o^2 = h^2 + \beta^2$$

$$\varepsilon_2\, k_o^2 = \sigma^2 + \beta^2$$

$$\varepsilon_3\, k_o^2 = -q^2 + \beta^2$$

c) Even air modes

$$\phi_e(y,\rho) = \sqrt{\frac{2}{\pi}}\; A_e\,\frac{\cos(hD - \bar{\phi}_e)}{\cos(\alpha_{De})}\cos(\rho(y-D) + \alpha_{De}) \qquad : y \geq D$$

$$= \sqrt{\frac{2}{\pi}}\; A_e\cos(hy - \bar{\phi}_e) \qquad : 0 \leq y \leq D$$

$$= \sqrt{\frac{2}{\pi}}\; A_e\,\frac{\cos(\bar{\phi}_e)}{\cos(\alpha_{0e})}\cos(\sigma y - \alpha_{0e}) \qquad : y \leq 0$$

where

$$\alpha_{0e} = \tan^{-1}\left(\frac{h\,\varepsilon_2}{\sigma\,\varepsilon_1}\tan(\bar{\phi}_e)\right)$$

$$\alpha_{De} = \tan^{-1}\left(\frac{h}{\rho\,\varepsilon_1}\tan(hD-\bar{\phi}_e)\right)$$

The angle $\bar{\phi}_e$ is given by the solution of the equation

$$\frac{\sin(2\bar{\phi}_e)}{\sin(2(hD-\bar{\phi}_e))} = \frac{\sigma}{\rho\varepsilon_2}\left[\frac{\rho^2-\frac{h^2}{\varepsilon_1^2}}{\frac{\sigma^2}{\varepsilon_2^2}-\frac{h^2}{\varepsilon_1^2}}\right]$$

$$A_e = \left\{\frac{\sigma}{\rho\,\varepsilon_2}\left(\cos^2(\bar{\phi}_e)+\frac{h^2\,\varepsilon_2^2}{\sigma^2\,\varepsilon_1^2}\sin^2(\bar{\phi}_e)\right)+\frac{h^2}{\varepsilon_1^2\,\rho^2}\sin^2(hD-\bar{\phi}_e)+\cos^2(hD-\bar{\phi}_e)\right\}^{-\frac{1}{2}}$$

with the above choice of constants, the even air modes are normalised as

$$<\phi_e(y,\rho)\,,\,\phi_e(y,\rho')> = \delta(\rho-\rho')$$

and the wavenumber are related by

$$\varepsilon_1\,k_o^2 = h^2+\beta^2$$

$$\varepsilon_2\,k_o^2 = \sigma^2+\beta^2$$

$$\varepsilon_3\,k_o^2 = \rho^2+\beta^2$$

The odd air modes $\phi_o(y,\rho)$ are obtained from the foregoing formulae by replacing all cosine functions by sine and tangent by cotangent.

APPENDIX 2

Let u(y) and $\phi(y)$ be bounded solutions of the following one - dimensional TE - wave equations:

$$\phi'' + (\varepsilon_r k_o^2 - \beta^2) \phi = 0 \qquad \text{(A2.1a)}$$

$$u'' + (\bar{\varepsilon}_r k_o^2 - \bar{\beta}^2) u = 0 \qquad \text{(A2.1b)}$$

Multiplying (A2.1a) by u, and (A2.1b) by ϕ, subtracting one equation from the other and integrating we obtain

$$< \phi'' , u > - < u'' , \phi > + k_o^2 < u , (\varepsilon_r - \bar{\varepsilon}_r) \phi > = (\beta^2 - \bar{\beta}^2) < \phi , u > \qquad \text{(A2.2)}$$

After integration by parts, the first two terms on the LHS reduce to the integrated term:

$$\left[\phi' u - \phi u' \right]_{-\infty}^{\infty}$$

If either u or ϕ vanishes at infinity with its first derivative, (e.g. a surface wave), the integrated term vanishes. If both are only bounded, i.e. being components of the continuum, then this term is proportional to a delta function of the wavenumber k_y. Turning now to the remaining term on the LHS, this integral vanishes wherever $\varepsilon_r = \bar{\varepsilon}_r$. In the specific case of an "intermediate " waveguide, ϕ being ϕ_s of the thicker slab shown in Fig. 3.1, it reduces to

$$k_o^2 (\varepsilon_r - 1) \int_{\bar{d}}^{D} \phi_s \, u \, dy$$

On the RHS, we have for a one - dimensional waveguide:

$$\beta^2 = \varepsilon_r k_o^2 - k_y^2 = \varepsilon_e k_o^2$$

Hence, from (A2.2), we obtain

$$P_s = < \phi , u > = \frac{\varepsilon_r - 1}{\varepsilon_e - \bar{\varepsilon}_e} \int_{\bar{d}}^{D} \phi_s \, u \, dy \qquad \text{(A2.3)}$$

APPENDIX 3

THE COEFFICIENTS $P_{sh}, P_{h\mu}(\rho), P_h(\sigma), P'_{sh}, P'_{h\mu}(\rho)$, AND $P'_h(\sigma)$ OF SECTION 3.231 (LSE)

Using the trial field of the TE "transition function"

$$\bar{U}_{sh} = \bar{A}\, e^{-\bar{q}(y-\bar{d})} \quad ; y \geq \bar{d}$$

$$= \bar{A}\, \frac{\cos(\bar{h}y - \bar{\Phi}_b)}{\cos(\bar{h}\bar{d} - \bar{\Phi}_b)} \quad ; 0 \leq y \leq \bar{d}$$

$$= \bar{A}\, \frac{\cos(\bar{\Phi}_b)}{\cos(\bar{h}\bar{d} - \bar{\Phi}_b)}\, e^{\bar{p}y} \quad ; y \leq 0$$

where

$$\bar{A} = \left(\frac{2}{\frac{1}{\bar{q}} + \bar{d} + \frac{1}{\bar{p}}} \right)^{\frac{1}{2}} \cos(\bar{h}\bar{d} - \bar{\Phi}_b)$$

$$\bar{\Phi}_b = \tan^{-1}\left(\frac{\bar{p}}{\bar{h}} \right)$$

we obtain

$$P_{sh} = \frac{\varepsilon_1 - \varepsilon_3}{\varepsilon_{eh1} - \bar{\varepsilon}_{eh}} \frac{A_1 \bar{A}}{\cos(h_1 D - \bar{\Phi}_1)\,(\bar{q}^2 + h_1^2)} \times$$

$$\left[\bar{q} \cos(h_1 \bar{d} - \bar{\Phi}_1) - h_1 \sin(h_1 \bar{d} - \bar{\Phi}_1) \right.$$

$$\left. - e^{-\bar{q}(D-\bar{d})} \left[\bar{q} \cos(h_1 D - \bar{\Phi}_1) - h_1 \sin(h_1 D - \bar{\Phi}_1) \right] \right.$$

$$P'_{sh} = \frac{\varepsilon_3 - \varepsilon_1}{\varepsilon_{eh2} - \bar{\varepsilon}_{eh}} \frac{A_2 \bar{A}}{\cos(\bar{h}\bar{d} - \bar{\Phi}_b)(q_2^2 + \bar{h}^2)} \times$$

$$\left[e^{-q_2(\bar{d}-d)} \left[\bar{h} \sin(\bar{h}\bar{d} - \bar{\Phi}_b) - q_2 \cos(\bar{h}\bar{d} - \bar{\Phi}_b) \right] \right.$$

$$\left. + q_2 \cos(\bar{h}d - \bar{\Phi}_b) - \bar{h} \sin(\bar{h}d - \bar{\Phi}_b) \right]$$

$$P_h(\sigma) = \sqrt{\frac{2}{\pi}} \frac{\varepsilon_1 - \varepsilon_3}{\varepsilon_{eh1} - \bar{\varepsilon}_{eh}} \frac{A_{sb1} \bar{A}}{(\bar{q}^2 + h_1^2)} \times$$

$$\left[\bar{q} \cos(h_1 \bar{d} - \bar{\Phi}_{sb1}) - h_1 \sin(h_1 \bar{d} - \bar{\Phi}_{sb1}) \right.$$

$$\left. + e^{-\bar{q}(D-\bar{d})} \left[h_1 \sin(h_1 D - \bar{\Phi}_{sb1}) - \bar{q} \cos(h_1 D - \bar{\Phi}_{sb1}) \right] \right]$$

$$P'_h(\sigma) = \sqrt{\frac{2}{\pi}} \frac{\varepsilon_3 - \varepsilon_1}{\varepsilon_{eh2} - \bar{\varepsilon}_{eh}} \frac{A_{sb2} \bar{A}}{(q_2^2 + \bar{h}^2)} \frac{\cos(h_2 d - \bar{\Phi}_{sb2})}{\cos(\bar{h}\bar{d} - \bar{\Phi}_b)} \times$$

$$\left[e^{-q_2(\bar{d}-d)} \left[\bar{h} \sin(\bar{h}\bar{d} - \bar{\Phi}_b) - q_2 \cos(\bar{h}\bar{d} - \bar{\Phi}_b) \right] \right.$$

$$\left. + q_2 \cos(\bar{h}d - \bar{\Phi}_b) - \bar{h} \sin(\bar{h}d - \bar{\Phi}_b) \right]$$

$$P_{he}(\rho) = \sqrt{\frac{2}{\pi}} \frac{\varepsilon_1 - \varepsilon_3}{\varepsilon_{eh1} - \bar{\varepsilon}_{eh}} \frac{A_{e1} \bar{A}}{(\bar{q}^2 + h_1^2)} \times$$

$$\left[\bar{q} \cos(h_1 \bar{d} - \bar{\Phi}_{e1}) - h_1 \sin(h_1 \bar{d} - \bar{\Phi}_{e1}) \right.$$

$$\left. + e^{-\bar{q}(D-\bar{d})} \left[h_1 \sin(h_1 D - \bar{\Phi}_{e1}) - \bar{q} \cos(h_1 D - \bar{\Phi}_{e1}) \right] \right]$$

$$P_{ho}(\rho) = \sqrt{\frac{2}{\pi}} \frac{\varepsilon_1 - \varepsilon_3}{\varepsilon_{eh1} - \bar{\varepsilon}_{eh}} \frac{A_{o1}\,\bar{A}}{(\bar{q}^2 + h_1^2)} \times$$

$$\left[h_1 \cos(h_1 \bar{d} - \bar{\phi}_{o1}) + \bar{q} \sin(h_1 \bar{d} - \bar{\phi}_{o1}) \right.$$

$$\left. - e^{-\bar{q}(D-\bar{d})} \left[h_1 \cos(h_1 D - \bar{\phi}_{o1}) + \bar{q} \sin(h_1 D - \bar{\phi}_{o1}) \right] \right]$$

$$P'_{he}(\rho) = \sqrt{\frac{2}{\pi}} \frac{\varepsilon_3 - \varepsilon_1}{\varepsilon_{eh2} - \bar{\varepsilon}_{eh}} A_{e2}\,\bar{A} \frac{\cos(h_2 d - \bar{\phi}_{e2})}{\cos(\alpha_{02}) \cos(\bar{h}\bar{d} - \bar{\phi}_b)} \times K$$

where

$$K = \frac{\sin(\rho_2(\bar{d}-d) - \bar{h}\bar{d} + \alpha_{02} + \bar{\phi}_b) + \sin(\bar{h}d - \alpha_{02} - \bar{\phi}_b)}{2\,(\rho_2 - \bar{h})}$$

$$+ \frac{\sin(\rho_2(\bar{d} - d) + \bar{h}\bar{d} + \alpha_{02} - \bar{\phi}_b) - \sin(\bar{h}d + \alpha_{02} - \bar{\phi}_b)}{2\,(\rho_2 + \bar{h})} \qquad ; \rho_2^2 \neq \bar{h}^2$$

$$K = \frac{\bar{d} - d}{2} \cos(\rho_2 d - \alpha_{02} - \bar{\phi}_b)$$

$$+ \frac{1}{4\rho_2} \left[\sin(\rho_2(2\bar{d} - d) + \alpha_{02} - \bar{\phi}_b) - \sin(\rho_2 d + \alpha_{02} - \bar{\phi}_b) \right] \qquad ; \rho_2^2 = \bar{h}^2$$

$$P'_{ho}(\rho) = \sqrt{\frac{2}{\pi}} \frac{\varepsilon_0 - \varepsilon_1}{\varepsilon_{eh2} - \bar{\varepsilon}_{eh}} A_{o2}\,\bar{A} \frac{\sin(h_2 d - \bar{\phi}_{o2})}{\sin(\alpha_{02}) \cos(\bar{h}\bar{d} - \bar{\phi}_b)} \times L$$

where

$$L = \frac{\cos(\bar{h}d - \alpha_{02} - \bar{\phi}_b) - \cos(\rho_2(\bar{d} - d) - \bar{h}\bar{d} + \alpha_{02} - \bar{\phi}_b)}{2\,(\rho_2 - \bar{h})}$$

$$+ \frac{\cos(\bar{h}d + \alpha_{02} - \bar{\phi}_b) - \cos(\rho_2(\bar{d} - d) + \bar{h}\bar{d} + \alpha_{02} - \bar{\phi}_b)}{2\,(\rho_2 + \bar{h})} \qquad ; \rho_2^2 \neq \bar{h}^2$$

$$L = \frac{\bar{d} - d}{2} \sin(-\rho_2 d + \alpha_{02} + \bar{\phi}_b)$$

$$- \frac{1}{4\rho_2} \left[\cos(\rho_2(2\bar{d} - d) + \alpha_{02} - \bar{\phi}_b) - \cos(\rho_2 d + \alpha_{02} - \bar{\phi}_b) \right] \qquad ; \rho_2^2 = \bar{h}^2$$

APPENDIX 4

CONSTRUCTION OF THE POLYNOMIAL $F_n(y)$

Beginning with the weight function $\overline{U}_{sh}^2(y)$, a set of polynomials $f_n(y)$ is constructed such that

$$\int_{-\infty}^{\infty} f_n(y)\, \overline{U}_{sh}^2(y)\, f_m(y)\, dy = \delta_{mn}$$

The set of the polynomials $F_n(y)$ is defined by

$$F_n(y) = f_n(y)\, \overline{U}_{sh}(y) \qquad \text{(A4.1)}$$

The polynomial is constructed using the Gram-Schmidt orthogonalisation procedure, where $f_0(y)$ is chosen to be unity so that

$$f_0(y) = 1$$

$$f_1(y) = \frac{y - < y,\ \overline{U}_{sh}^2(y) >}{\left[1 + < y,\ \overline{U}_{sh}^2 >^2 \right]^{\frac{1}{2}}}$$

$$f_2(y) = \frac{y^2 - < y^2,\ \overline{U}_{sh}^2(y)\, f_0(y) > f_0(y) - < y^2,\ \overline{U}_{sh}^2(y)\, f_1(y) > f_1(y)}{\left[1 + < y^2,\ \overline{U}_{sh}^2(y)\, f_0(y) >^2 + < y^2,\ \overline{U}_{sh}^2(y)\, f_1(y) >^2 \right]^2}$$

In general, for any n we have,

$$f_n(y) = \frac{y^n - \sum_{m=1}^{n} F_{n-m}^{(n)}\, f_{n-m}(y)}{\left[1 + \sum_{m=1}^{n} F_{n-m}^{(n)\,2} \right]^{\frac{1}{2}}} \qquad \text{(A4.2)}$$

where

$$F_m^{(n)} = \int_{-\infty}^{\infty} y^n\, \overline{U}_{sh}^2(y)\, f_m(y)\, dy \qquad \text{(A4.3)}$$

Equation (A4.2) and (A4.3) allow the entire set $f_n(y)$ to be generated from equation (A4.1).

We have a set of polynomial $F_n(y)$ defined by

$$F_n(y) = f_n(y)\,\overline{U}_{sh}(y)$$

i.e.

$$F_0(y) = f_0(y)\,\overline{U}_{sh}(y) = \overline{U}_{sh}(y)$$

$$F_1(y) = f_1(y)\,\overline{U}_{sh}(y) \ldots\ldots etc.$$

For a function H_y which is continuous, the expansion in terms of $F_n(y)$ is

$$H_y = H(y) = \sum_n h_n\,F_n(y)$$

where

$$h_n = \int_{-\infty}^{\infty} H(y)\,F_n(y)\,dy$$

$$= \frac{\int_{-\infty}^{\infty} H(y)\,y_n\,\overline{U}_{sh}(y)\,dy - \sum_{m=1}^{n} F_{n-m}^{(n)}\,h_{n-m}}{\left[1 + \sum_{m=1}^{n} F_{n-m}^{(n)2}\right]^{\frac{1}{2}}}$$

The coefficient $F_m^{(n)}$ is given by

$$F_m^{(n)} = \int_{-\infty}^{\infty} y^n\,\overline{U}_{sh}^2(y)\,f_m(y)\,dy$$

$$= \frac{\int_{-\infty}^{\infty} y^n\,\overline{U}_{sh}^2(y)\,y^m\,dy - \sum_{k=1}^{m} F_{m-k}^{(m)}\,F_{m-k}^{(n)}}{\left[1 + \sum_{k=1}^{m} F_{m-k}^{(m)2}\right]^{\frac{1}{2}}}$$

with

$$F_0^{(0)} = 1$$

$$F_m^{(n)} = \frac{\int_{-\infty}^{\infty} y^{m+n}\, \bar{U}_{sh}^2(y)\, dy - \sum_{k=1}^{m} F_{m-k}^{(m)} F_{m-k}^{(n)}}{\left[1 + \sum_{k=1}^{m} F_{m-k}^{(m)2} \right]^{\frac{1}{2}}}$$

In order to calculate $F_m^{(n)}$, we must first evaluate

$$\int_{-\infty}^{\infty} y^{m+n}\, \bar{U}_{sh}^2(y)\, dy = \bar{A}^2 \left[I_1(m+n) + \frac{1}{\cos^2(\bar{h}\bar{d} - \bar{\phi}_b)} I_2(m+n) + \frac{\cos^2(\bar{\phi}_b)}{\cos^2(\bar{h}\bar{d} - \bar{\phi}_b)} I_3(m+n) \right]$$

Therefore,

$$F_m^{(n)} = \left\{ \bar{A}^2 \left[I_1(m+n) + \frac{1}{\cos^2(\bar{h}\bar{d} - \bar{\phi}_b)} I_2(m+n) + \frac{\cos^2(\bar{\phi}_b)}{\cos^2(\bar{h}\bar{d} - \bar{\phi}_b)} I_3(m+n) \right] - \sum_{k=1}^{m} F_{m-k}^{(m)} F_{m-k}^{(n)} \right\} \times \left[1 + \sum_{k=1}^{m} F_{m-k}^{(m)2} \right]^{-\frac{1}{2}}$$

THE COEFFICIENTS $P_{hn}, P_{hn\mu}(\rho), P_{hn}(\sigma), P'_{hn}, P'_{hn\mu}(\rho)$ AND $P'_{hn}(\sigma)$ OF SECTION 3.232 (LSE)

$$P_{hn} = \int_{-\infty}^{\infty} \phi_{sh}(y)\, F_n(y)\, dy$$

$$= \left\{ A_1 \bar{A} \left[I_4(n,h) + \frac{I_5(n,h)}{\cos(h_1 D - \bar{\phi}_1)} + \frac{I_6(n,h)}{\cos(h_1 D - \bar{\phi}_1)\cos(\bar{h}\bar{d} - \bar{\phi}_b)} \right.\right.$$

$$\left.\left. + \frac{\cos(\bar{\phi}_1)\cos(\bar{\phi}_b)}{\cos(h_1 D - \bar{\phi}_1)\cos(\bar{h}\bar{d} - \bar{\phi}_b)} I_7(n,h) \right] - \sum_{m=1}^{n} F_{n-m}^{(n)} P_{hn-m} \right\} \times$$

$$\left[1 + \sum_{m=1}^{n} F_{n-m}^{(n)2} \right]^{-\frac{1}{2}}$$

$$P'_{hn} = \int_{-\infty}^{\infty} \psi_{sh}(y)\, F_n(y)\, dy$$

$$= \left\{ A_2 \bar{A} \left[I_8(n,h) + I_9(n,h) + \frac{I_{10}(n,h)}{\cos(h_2 d - \bar{\phi}_2)\cos(\bar{h}\bar{d} - \bar{\phi}_b)} \right.\right.$$

$$\left.\left. + \frac{\cos(\bar{\phi}_2)\cos(\bar{\phi}_b)}{\cos(h_2 d - \bar{\phi}_2)\cos(\bar{h}\bar{d} - \bar{\phi}_b)} I_{11}(n,h) \right] - \sum_{m=1}^{n} F_{n-m}^{(n)} P'_{hn-m} \right\} \times$$

$$\left[1 + \sum_{m=1}^{n} F_{n-m}^{(n)2} \right]^{-\frac{1}{2}}$$

$$P_{hn}(\sigma) = \int_{-\infty}^{\infty} \phi_h(y,\sigma)\, F_n(y)\, dy$$

$$= \left\{ \sqrt{\frac{2}{\pi}}\, \bar{A} \left[A_{sb1} \cos(h_1 D - \bar{\phi}_{sb1})\, I_{12}(n,h,\sigma_1) \right.\right.$$

$$+ A_{sb1}\, I_{13}(n,h,\sigma_1) + \frac{A_{sb1}}{\cos(\bar{\bar{h}}\bar{d} - \bar{\phi}_b)}\, I_{14}(n,h,\sigma_1)$$

$$\left.\left. + \frac{\cos(\bar{\phi}_b)}{\cos(\bar{\bar{h}}\bar{d} - \bar{\phi}_b)}\, I_{15}(n,h,\sigma_1) \right] - \sum_{m=1}^{n} F_{n-m}^{(n)}\, P_{hn-m}(\sigma) \right\} \times$$

$$\left[1 + \sum_{m=1}^{n} F_{n-m}^{(n)2} \right]^{-\frac{1}{2}}$$

$$P'_{hn}(\sigma) = \int_{-\infty}^{\infty} \psi_h(y,\sigma)\, F_n(y)\, dy$$

$$= \left\{ \sqrt{\frac{2}{\pi}}\, \bar{A} \left[A_{sb2} \cos(h_2 d - \bar{\phi}_{sb2})\, I_{16}(n,h,\sigma_2) \right.\right.$$

$$+ \frac{A_{sb2} \cos(h_2 d - \bar{\phi}_{sb2})}{\cos(\bar{\bar{h}}\bar{d} - \bar{\phi}_b)}\, I_{17}(n,h,\sigma_2) + \frac{A_{sb2}}{\cos(\bar{\bar{h}}\bar{d} - \bar{\phi}_b)}\, I_{18}(n,h,\sigma_2)$$

$$\left.\left. + \frac{\cos(\bar{\phi}_b)}{\cos(\bar{\bar{h}}\bar{d} - \bar{\phi}_b)}\, I_{19}(n,h,\sigma_2) \right] - \sum_{m=1}^{n} F_{n-m}^{(n)}\, P'_{hn-m}(\sigma) \right\} \times$$

$$\left[1 + \sum_{m=1}^{n} F_{n-m}^{(n)2} \right]^{-\frac{1}{2}}$$

$$P_{hne}(\rho) = \int_{-\infty}^{\infty} \phi_{he}(y,\rho)\, F_n(y)\, dy$$

$$= \left\{ \sqrt{\frac{2}{\pi}}\, \bar{A}\, A_{e1} \left[\frac{\cos(h_1 D - \bar{\Phi}_{e1})}{\cos(\alpha_{De1}} I_{20}(n,h,\rho_1) + I_{21}(n,h,\rho_1) \right.\right.$$

$$\left. + \frac{1}{\cos(\bar{h}\bar{d} - \bar{\Phi}_b)} I_{22}(n,h,\rho_1) + \frac{\cos(\bar{\Phi}_b)\cos(\bar{\Phi}_{e1})}{\cos(\bar{h}\bar{d} - \bar{\Phi}_b)\cos(\alpha_{0e1})} I_{23}(n,h,\rho_1) \right]$$

$$\left. - \sum_{m=1}^{n} F_{n-m}^{(n)}\, P_{hne-m}(\rho) \right\} \times \left[1 + \sum_{m=1}^{n} F_{n-m}^{(n)2} \right]^{-\frac{1}{2}}$$

$$P'_{hne}(\rho) = \int_{-\infty}^{\infty} \psi_{he}(y,\rho)\, F_n(y)\, dy$$

$$= \left\{ \sqrt{\frac{2}{\pi}}\, \bar{A}\, A_{e2} \left[\frac{\cos(h_2 d - \bar{\Phi}_{e2})}{\cos(\alpha_{De2})} I_{24}(n,h,\rho_2) \right.\right.$$

$$+ \frac{\cos(h_2 d - \bar{\Phi}_{e2})}{\cos(\bar{h}\bar{d} - \bar{\Phi}_b)\cos(\alpha_{De2})} I_{25}(n,h,\rho_2) + \frac{1}{\cos(\bar{h}\bar{d} - \bar{\Phi}_b)} I_{26}(n,h,\rho_2)$$

$$\left. + \frac{\cos(\bar{\Phi}_b)\cos(\bar{\Phi}_{e2})}{\cos(\bar{h}\bar{d} - \bar{\Phi}_b)\cos(\alpha_{0e2})} I_{27}(n,h,\rho_2) \right] - \sum_{m=1}^{n} F_{n-m}^{(n)}\, P'_{hne-m}(\rho) \left.\right\} \times$$

$$\left[1 + \sum_{m=1}^{n} F_{n-m}^{(n)2} \right]^{-\frac{1}{2}}$$

$$P_{hno}(\rho) = \int_{-\infty}^{\infty} \phi_{ho}(y,\rho)\, F_n(y)\, dy$$

$$= \left\{ \sqrt{\frac{2}{\pi}}\, \bar{A}\, A_{o1} \left[\frac{\sin(h_1 D - \bar{\Phi}_{o1})}{\sin(\alpha_{Do1})}\, I_{28}(n,h,\rho_1) + I_{29}(n,h,\rho_1) \right.\right.$$

$$\left.\left. + \frac{1}{\cos(\bar{h}\bar{d} - \bar{\Phi}_b)}\, I_{30}(n,h,\rho_1) + \frac{\cos(\bar{\Phi}_b)\sin(\bar{\Phi}_{o1})}{\cos(\bar{h}\bar{d} - \bar{\Phi}_b)\sin(\alpha_{0o1})}\, I_{31}(n,h,\rho_1) \right] \right.$$

$$\left. - \sum_{m=1}^{n} F_{n-m}^{(n)}\, P_{hno-m}(\rho) \right\} \times \left[1 + \sum_{m=1}^{n} F_{n-m}^{(n)2} \right]^{-\frac{1}{2}}$$

$$P'_{hno}(\rho) = \int_{-\infty}^{\infty} \psi_{ho}(y,\rho)\, F_n(y)\, dy$$

$$= \left\{ \sqrt{\frac{2}{\pi}}\, \bar{A}\, A_{o2} \left[\frac{\sin(h_2 d - \bar{\Phi}_{o2})}{\sin(\alpha_{Do2})}\, I_{32}(n,h,\rho 2) \right.\right.$$

$$+ \frac{\sin(h_2 d - \bar{\Phi}_{o2})}{\cos(\bar{h}\bar{d} - \bar{\Phi}_b)\sin(\alpha_{Do2})}\, I_{33}(n,h,\rho_2) + \frac{1}{\cos(\bar{h}\bar{d} - \bar{\Phi}_b)}\, I_{34}(n,h,\rho_2)$$

$$\left.\left. + \frac{\cos(\bar{\Phi}_b)\sin(\bar{\Phi}_{o2}}{\cos(\bar{h}\bar{d} - \bar{\Phi}_b)\sin(\alpha_{0o2})}\, I_{35}(n,h,\rho_2) \right] - \sum_{m=1}^{n} F_{n-m}^{(n)}\, P'_{hno-m}(\rho) \right\} \times$$

$$\left[1 + \sum_{m=1}^{n} F_{n-m}^{(n)2} \right]^{-\frac{1}{2}}$$

EXPRESSION FOR INTEGRALS I_1 to I_{35}

$$I_1(m+n) = \frac{(-1)^{m+n}}{2\,\bar{q}} \left[(D-\bar{d})^{m+n} + (m+n)! \sum_{k=1}^{m+n} \frac{(D-\bar{d})^{m+n-k}}{(-1)^k\,(m+n-k)!\,(2\,\bar{q})^k} \right]$$

$$I_2(m+n) = \frac{(-1)^{m+n}}{2} \left\{ \frac{D^{m+n+1} - (D-\bar{d})^{m+n+1}}{m+n+1} \right.$$

$$+ (m+n)! \sum_{k=0}^{m+n} \frac{1}{(-1)^k\,(2\,\bar{h})^{k+1}\,(m+n-k)!} \times$$

$$\left. \left[D^{m+n-k} \sin(2\bar{\phi}_b - \frac{k\pi}{2}) + (D-\bar{d})^{m+n-k} \sin(2\bar{h}\bar{d} - 2\bar{\phi}_b + \frac{k\pi}{2}) \right] \right\}$$

$$I_3(m+n) = \frac{(-1)^{m+n}}{2\,\bar{p}} \left[D^{m+n} + (m+n)! \sum_{k=1}^{m+n} \frac{D^{m+n-k}}{(2\,\bar{p})^k\,(m+n-k)!} \right]$$

$$I_4(n,h) = \frac{n!\,e^{-\bar{q}(D-\bar{d})}}{(q_1+\bar{q})^{n+1}}$$

$$I_5(n,h) = \frac{(-1)^n\,n!\,e^{-\bar{q}(D-\bar{d})}}{(\bar{q}^2+h_1^2)^{\frac{n+1}{2}}} \cos(h_1 D - \bar{\phi}_1 + (n+1)\theta)$$

$$- (-1)^n\,n! \sum_{k=1}^{n+1} \frac{(D-\bar{d})^{n-k+1}}{(n-k+1)!\,(\bar{q}^2+h_1^2)^{\frac{k}{2}}} \cos(h_1\bar{d} - \bar{\phi}_1 + k\theta)$$

where

$$\theta = \cos^{-1}\left(\frac{-\bar{q}}{\sqrt{\bar{q}^2+h_1^2}} \right)$$

$$I_6(n,h) = \frac{(-1)^n}{2} \left\{ D^n \left[\frac{\sin(\bar{\Phi}_1 - \bar{\Phi}_b)}{(h_1 - \bar{h})} + \frac{\sin(\bar{\Phi}_1 + \bar{\Phi}_b)}{(h_1 + \bar{h})} \right] \right.$$

$$+ (D - \bar{d})^n \left[\frac{\sin((h_1 - \bar{h})\bar{d} - \bar{\Phi}_1 + \bar{\Phi}_b)}{(h_1 - \bar{h})} + \frac{\sin((h_1 + \bar{h})\bar{d} - \bar{\Phi}_1 - \bar{\Phi}_b)}{(h_1 + \bar{h})} \right]$$

$$+ n! \sum_{k=0}^{n-1} \frac{(-1)^{-k}}{(n-1-k)!} \left\{ D^{n-1-k} \left[\frac{\cos(\bar{\Phi}_1 - \bar{\Phi}_b) - \frac{k\pi}{2})}{(h_1 - \bar{h})^{k+2}} \right. \right.$$

$$\left. + \frac{\cos(\bar{\Phi}_1 + \bar{\Phi}_b - \frac{k\pi}{2})}{(h_1 + \bar{h})^{k+2}} \right] - (D - \bar{d})^{n-1-k} \left[\frac{\cos((h_1 - \bar{h})\bar{d} - \bar{\Phi}_1 + \bar{\Phi}_b + \frac{k\pi}{2})}{(h_1 - \bar{h})^{k+2}} \right.$$

$$\left. \left. \left. + \frac{\cos((h_1 + \bar{h})\bar{d} - \bar{\Phi}_1 - \bar{\Phi}_b + \frac{k\pi}{2})}{(h_1 + \bar{h})^{k+2}} \right] \right\} \right\} \qquad ; h_1^2 \neq \bar{h}^2$$

$$I_6(n,h) = \frac{(-1)^n}{2} \left\{ \frac{(D - \bar{d})^n \sin(2h_1\bar{d} - \bar{\Phi}_1 - \bar{\Phi}_b) + D^n \sin(\bar{\Phi}_1 + \bar{\Phi}_b)}{2\,h_1} \right.$$

$$+ \left[D^{n+1} - (D - \bar{d})^{n+1} \right] \left[1 - \frac{n}{n+1} \right] \cos(\bar{\Phi}_1 - \bar{\Phi}_b)$$

$$+ n! \sum_{k=0}^{n-1} \frac{(-1)^{-k}}{(n-1-k)!\,(2\,h_1)^{k+2}} \left[D^{n-1-k} \cos(\bar{\Phi}_1 + \bar{\Phi}_b - \frac{k\pi}{2}) \right.$$

$$\left. \left. + (D - \bar{d})^{n-1-k} \cos(2h_1\bar{d} - \bar{\Phi}_1 - \bar{\Phi}_b + \frac{k\pi}{2}) \right] \right\} \qquad ; h_1^2 = \bar{h}^2$$

$$I_7(n,h) = \frac{(-1)^n D^n}{p_1 + \bar{p}} \left[1 + n! \sum_{k=1}^{n} \frac{1}{(n-k)!\,(p_1 + \bar{p})^k D^k} \right]$$

$$I_8(n,h) = (-1)^n (D - \bar{d})^n \frac{e^{-q_2(\bar{d}-d)}}{(q_2 + \bar{q})} \left[1 + n! \sum_{k=1}^{n} \frac{(-1)^{-k}}{(n-k)!\,(q_2 + \bar{q})^k (D - \bar{d})^k} \right]$$

$$I_9(n,h) = (-1)^n\, n! \sum_{k=1}^{n+1} \frac{1}{(n-k+1)!\,(q_2^2+\bar{h}^2)^{\frac{k}{2}}} \left\{ e^{-q_2(\bar{d}-d)}\,(D-\bar{d})^{n-k+1} \;\times \right.$$

$$\left. \cos(\bar{h}\bar{d}-\bar{\Phi}_b+k\theta) - (D-d)^{n-k+1}\cos(\bar{h}d-\bar{\Phi}_b+k\theta) \right\}$$

where

$$\theta = \cos^{-1}\left(\frac{-q_2}{\sqrt{(q_2^2+\bar{h}^2)}}\right)$$

$$I_{10}(n,h) = \frac{(-1)^n}{2}\left\{ D^n\left[\frac{\sin(\bar{\Phi}_2-\bar{\Phi}_b)}{(h_2-\bar{h})} + \frac{\sin(\bar{\Phi}_2+\bar{\Phi}_b)}{(h_2+\bar{h})}\right]\right.$$

$$+ (D-d)^n\left[\frac{\sin((h_2-\bar{h})d-\bar{\Phi}_2+\bar{\Phi}_b)}{(h_2-\bar{h})} + \frac{\sin((h_2+\bar{h})d-\bar{\Phi}_2-\bar{\Phi}_b)}{(h_2+\bar{h})}\right]$$

$$+ n!\sum_{k=0}^{n-1}\frac{(-1)^{-k}}{(n-1-k)!}\left\{ D^{n-1-k}\left[\frac{\cos(\bar{\Phi}_2-\bar{\Phi}_b)-\frac{k\pi}{2})}{(h_2-\bar{h})^{k+2}}\right.\right.$$

$$\left. + \frac{\cos(\bar{\Phi}_2+\bar{\Phi}_b-\frac{k\pi}{2})}{(h_2+\bar{h})^{k+2}}\right] - (D-d)^{n-1-k}\left[\frac{\cos((h_2-\bar{h})d-\bar{\Phi}_2+\bar{\Phi}_b+\frac{k\pi}{2})}{(h_2-\bar{h})^{k+2}}\right.$$

$$\left.\left. + \frac{\cos((h_2+\bar{h})d-\bar{\Phi}_2-\bar{\Phi}_b+\frac{k\pi}{2})}{(h_2+\bar{h})^{k+2}}\right]\right\}\right\} \qquad ; h_2^2 \neq \bar{h}^2$$

$$I_{10}(n,h) = \frac{(-1)^n}{2}\left\{ \frac{(D-d)^n \sin(2h_2 d - \bar{\phi}_2 - \bar{\phi}_b) + D^n \sin(\bar{\phi}_2 + \bar{\phi}_b)}{2h_2} \right.$$

$$+ \left[D^{n+1} - (D-d)^{n+1} \right] \left[1 - \frac{n}{n+1} \right] \cos(\bar{\phi}_2 - \bar{\phi}_b)$$

$$+ n! \sum_{k=0}^{n-1} \frac{(-1)^{-k}}{(n-1-k)!\,(2h_2)^{k+2}} \left[D^{n-1-k} \cos(\bar{\phi}_2 + \bar{\phi}_b - \frac{k\pi}{2}) \right.$$

$$\left. \left. - (D-d)^{n-1-k} \cos(2h_2 d - \bar{\phi}_2 - \bar{\phi}_b + \frac{k\pi}{2}) \right] \right\} \qquad ; h_2^2 = \bar{h}^2$$

$I_{11}(n,h) = I_7(n,h)$

with p_1 replaced by p_2.

$I_{12}(n,h,\sigma_1) = I_4(n,h)$; with parameters and wavenumbers appropriate for the substrate modes of inner slab guide.

$I_{13}(n,h,\sigma_1) = I_5(n,h)$; with parameters and wavenumbers appropriate for the substrate modes of inner slab guide.

$I_{14}(n,h,\sigma_1) = I_6(n,h)$; with parameters and wavenumbers appropriate for the substrate modes of inner slab guide.

$$I_{15}(n,h,\sigma_1) = (-1)^n\, n! \sum_{k=1}^{n+1} \frac{D^{n-k+1} \cos(\alpha_{sb1} - k\theta)}{(n-k+1)!\,(\sigma_1^2 + \bar{p}^2)^{\frac{k}{2}}}$$

with

$$\theta = \cos^{-1}\left(\frac{\bar{p}}{\sqrt{(\sigma_1^2 + \bar{p}^2)}} \right)$$

$I_{16}(n,h,\sigma_2) = I_8(n,h)$; with parameters and wavenumbers appropriate for the substrate modes of outer slab guide.

$I_{17}(n,h,\sigma_2) = I_9(n,h)$; with parameters and wavenumbers appropriate for the substrate modes of outer slab guide.

$I_{18}(n,h,\sigma_2) = I_{10}(n,h)$; with parameters and wavenumbers appropriate for the substrate modes of outer slab guide.

$I_{19}(n,h,\sigma_2) = I_{15}(n,h,\sigma_1)$; with parameters and wavenumbers appropriate for the substrate modes of outer slab guide.

$$I_{20}(n,h,\rho_1) = \frac{(-1)^{n+1}\, n!\, e^{-\bar{q}(D-\bar{d})}}{(\rho_1^2 + \bar{q}^2)^{\frac{n+1}{2}}} \cos(\alpha_{De1} + (n+1)\theta)$$

where

$$\theta = \cos^{-1}\left(\frac{-\bar{q}}{\sqrt{(\rho_1^2 + \bar{q}^2)}}\right)$$

$I_{21}(n,h,\rho_1) = I_5(n,h)$; with parameters and wavenumbers appropriate for the even air modes of inner slab guide.

$I_{22}(n,h,\rho_1) = I_6(n,h)$; with parameters and wavenumbers appropriate for the even air modes of inner slab guide.

$I_{23}(n,h,\rho_1) = I_{15}(n,h,\sigma_1)$; with parameters and wavenumbers appropriate for the even air modes of inner slab guide.

$$I_{24}(n,h,\rho_2) = (-1)^{n+1}\, n! \sum_{k=1}^{n+1} \frac{(D-\bar{d})^{n-k+1}}{(n-k+1)!\,(\rho_2^2+\bar{q}^2)^{\frac{k}{2}}} \cos(\rho_2(\bar{d}-d)+\alpha_{De2}+k\theta)$$

where

$$\theta = \cos^{-1}\left(\frac{-\bar{q}}{\sqrt{(\rho_2^2+\bar{q}^2)}}\right)$$

$$I_{25}(n,h,\rho_2) = \frac{(-1)^n}{2}\Bigg\{(D-\bar{d})^n \times$$

$$\left[\frac{\sin(\rho_2(\bar{d}-d)-\bar{h}\bar{d}+\alpha_{De2}+\bar{\phi}_b)}{(\rho_2-\bar{h})} + \frac{\sin(\rho_2(\bar{d}-d)+\bar{h}\bar{d}+\alpha_{De2}-\bar{\phi}_b)}{(\rho_2+\bar{h})}\right]$$

$$-(D-d)^n\left[\frac{\sin(\bar{h}d+\alpha_{De2}-\bar{\phi}_b)}{(\rho_2+\bar{h})} - \frac{\sin(\bar{h}d-\alpha_{De2}-\bar{\phi}_b)}{(\rho_2-\bar{h})}\right]$$

$$+n!\sum_{k=0}^{n-1}\frac{(-1)^{-k}}{(n-1-k)!}\Bigg\{(D-d)^{n-1-k}\times$$

$$\left[\frac{\cos(\bar{h}d-\alpha_{De2}-\bar{\phi}_b-\frac{k\pi}{2})}{(\rho_2-\bar{h})^{k+2}} + \frac{\cos(\bar{h}d+\alpha_{De2}-\bar{\phi}_b+\frac{k\pi}{2})}{(\rho_2+\bar{h})^{k+2}}\right]$$

$$-(D-\bar{d})^{n-1-k}\left[\frac{\cos(\rho_2(\bar{d}-d)-\bar{h}\bar{d}+\alpha_{De2}+\bar{\phi}_b+\frac{k\pi}{2})}{(\rho_2-\bar{h})^{k+2}}\right.$$

$$\left.+\left.\frac{\cos(\rho_2(\bar{d}-d)+\bar{h}\bar{d}+\alpha_{De2}-\bar{\phi}_b+\frac{k\pi}{2})}{(\rho_2+\bar{h})^{k+2}}\right]\right\}\Bigg\} \qquad ;\rho_2^2 \neq \bar{h}^2$$

$$I_{25}(n,h,\rho_2)=\frac{(-1)^n}{2}\left\{\left[(D-d)^{n+1}-(D-\bar{d})^{n+1}\right]\right.$$

$$\left[1-\frac{n}{n+1}\right]\cos(\rho_2 d-\alpha_{De2}-\bar{\phi}_b)$$

$$+\frac{(D-\bar{d})^n\sin(\rho_2(2\bar{d}-d)+\alpha_{De2}-\bar{\phi}_b)-(D-d)^n\sin(\rho_2 d+\alpha_{De2}-\bar{\phi}_b)}{2\rho_2}$$

$$+n!\sum_{k=0}^{n-1}\frac{(-1)^{-k}}{(n-1-k)!\,(2\rho_2)^{k+2}}\left[(D-d)^{n-1-k}\cos(\rho_2 d+\alpha_{De2}-\bar{\phi}_b+\frac{k\pi}{2})\right.$$

$$\left.\left.-(D-\bar{d})^{n-1-k}\cos(\rho_2(2\bar{d}-d)+\alpha_{De2}-\bar{\phi}_b+\frac{k\pi}{2})\right]\right\}\qquad;\rho_2^2=\bar{h}^2$$

$I_{26}(n,h,\rho_2)=I_{10}(n,h)$; with parameters and wavenumbers appropriate for the even air modes of outer slab guide.

$I_{27}(n,h,\rho_2)=I_{15}(n,h,\sigma_1)$; with parameters and wavenumbers appropriate for the even air modes of outer slab guide.

$$I_{28}(n,h,\rho_1)=\frac{(-1)^{n+1}\,n!\,e^{-\bar{q}(D-\bar{d})}}{(\rho_1^2+\bar{q}^2)^{\frac{n+1}{2}}}\sin((n+1)\theta+\alpha_{Do1})$$

where

$$\theta=\cos^{-1}\left(\frac{-\bar{q}}{\sqrt{(\rho_1^2+\bar{q}^2)}}\right)$$

$$I_{29}(n,h,\rho_1)=\frac{(-1)^n\,n!\,e^{-\bar{q}(D-\bar{d})}}{(h_1^2+\bar{q}^2)^{\frac{n+1}{2}}}\sin(h_1 D-\bar{\phi}_{o1}+(n+1)\theta)$$

$$-n!\sum_{k=1}^{n+1}\frac{(-1)^n\,(D-\bar{d})^{n-k+1}}{(n-k+1)!\,(\bar{q}^2+h_1^2)^{\frac{k}{2}}}\sin(h_1\bar{d}+k\theta-\bar{\phi}_{o1})$$

where

$$\theta = \cos^{-1}\left(\frac{-\bar{q}}{\sqrt{(\bar{q}^2 + h_1^2))}}\right)$$

$$I_{30}(n,h,\rho_1) = \frac{(-1)^n}{2}\left\{ D^n\left[\frac{\cos(\bar{\Phi}_{o1} - \bar{\Phi}_b)}{(h_1 - \bar{h})} + \frac{\cos(\bar{\Phi}_{o1} + \bar{\Phi}_b)}{(h_1 + \bar{h})}\right] - (D - \bar{d})^n \times \right.$$

$$\left[\frac{\cos((h_1 - \bar{h})\bar{d} - \bar{\Phi}_{o1} + \bar{\Phi}_b)}{(h_1 - \bar{h})} + \frac{\cos((h_1 + \bar{h})\bar{d} - \bar{\Phi}_{o1} - \bar{\Phi}_b)}{(h_1 + \bar{h})}\right]$$

$$-n!\sum_{k=0}^{n-1}\frac{(-1)^{-k}}{(n-1-k)!}\left\{(D - \bar{d})^{n-1-k}\left[\frac{\sin((h_1 - \bar{h})\bar{d} - \bar{\Phi}_{o1} + \bar{\Phi}_b + \frac{k\pi}{2})}{(h_1 - \bar{h})^{k+2}}\right.\right.$$

$$\left.+\frac{\sin((h_1 + \bar{h})\bar{d} - \bar{\Phi}_{o1} - \bar{\Phi}_b + \frac{k\pi}{2})}{(h_1 + \bar{h})^{k+2}}\right]$$

$$\left.\left. + D^{n-1-k}\left[\frac{\sin(\bar{\Phi}_{o1} - \bar{\Phi}_b - \frac{k\pi}{2})}{(h_1 - \bar{h})^{k+2}} + \frac{\sin(\bar{\Phi}_{o1} + \bar{\Phi}_b - \frac{k\pi}{2})}{(h_1 + \bar{h})^{k+2}}\right]\right\}\right\}$$

$$; h_1^2 \neq \bar{h}^2$$

$$I_{30}(n,h,\rho_1) = \frac{(-1)^n}{2}\left\{\left[D^{n+1} - (D - \bar{d})^{n+1}\right]\left[1 - \frac{n}{n+1}\right]\sin(\bar{\Phi}_b - \bar{\Phi}_{o1})\right.$$

$$+\frac{D^n\cos(\bar{\Phi}_{o1} + \bar{\Phi}_b) - (D - \bar{d})^n\cos(2h_1\bar{d} - \bar{\Phi}_{o1} - \bar{\Phi}_b)}{2h_1}$$

$$-n!\sum_{k=0}^{n-1}\frac{(-1)^{-k}}{(n-1-k)!\,(2h_1)^{k+2}}\left[(D - \bar{d})^{n-1-k}\sin(2h_1\bar{d} - \bar{\Phi}_{o1} - \bar{\Phi}_b + \frac{k\pi}{2})\right.$$

$$\left.\left. + D^{n-1-k}\sin(\bar{\Phi}_{o1} + \bar{\Phi}_b - \frac{k\pi}{2})\right]\right\} \qquad ; h_1^2 = \bar{h}^2$$

$$I_{31}(n,h,\rho_1) = n! \sum_{k=1}^{n+1} \frac{(-1)^n D^{n-k+1}}{(n-k+1)! \, (\bar{p}^2 + \sigma_1^2)^{\frac{k}{2}}} \sin(k\theta - \alpha_{0o1})$$

where

$$\theta = \cos^{-1}\left(\frac{\bar{p}}{\sqrt{(\bar{p}^2 + \sigma_1^2)}} \right)$$

$$I_{32}(n,h,\rho_2) = n! \sum_{k=1}^{n+1} \frac{(-1)^{n+1} (D-\bar{d})^{n-k+1}}{(n-k+1)! \, (\bar{q}^2 + \rho_2^2)^{\frac{k}{2}}} \sin(\rho_2(\bar{d}-d) + k\theta + \alpha_{Do2})$$

where

$$\theta = \cos^{-1}\left(\frac{-\bar{q}}{\sqrt{(\bar{q}^2 + \rho_2^2)}} \right)$$

$$I_{33}(n,h,\rho_2) = \frac{(-1)^n}{2} \left\{ (D-d)^n \left[\frac{\cos(\bar{h}d - \alpha_{Do2} - \bar{\phi}_b)}{(\rho_2 - \bar{h})} + \frac{\cos(\bar{h}d + \alpha_{Do2} - \bar{\phi}_b)}{(\rho_2 + \bar{h})} \right] \right.$$

$$- (D-\bar{d})^n \left[\frac{\cos(\rho_2(\bar{d}-d) - \bar{h}\bar{d} + \alpha_{Do2} + \bar{\phi}_b)}{(\rho_2 - \bar{h})} \right.$$

$$\left. + \frac{\cos(\rho_2(\bar{d}-d) + \bar{h}\bar{d} + \alpha_{Do2} - \bar{\phi}_b)}{(\rho_2 + \bar{h})} \right]$$

$$- n! \sum_{k=0}^{n-1} \frac{(-1)^{-k}}{(n-1-k)!} \left\{ (D-\bar{d})^{n-1-k} \left[\frac{\sin(\rho_2(\bar{d}-d) - \bar{h}\bar{d} + \alpha_{Do2} + \bar{\phi}_b + \frac{k\pi}{2})}{(\rho_2 - \bar{h})^{k+2}} \right. \right.$$

$$\left. \left. + \frac{\sin(\rho_2(\bar{d}-d) + \bar{h}\bar{d} + \alpha_{Do2} - \bar{\phi}_b + \frac{k\pi}{2})}{(\rho_2 + \bar{h})^{k+2}} \right] + (D-d)^{n-1-k} \times \right.$$

$$\times \left[\frac{\sin(\bar{h}d - \alpha_{Do2} - \bar{\phi}_b - \frac{k\pi}{2})}{(\rho_2 - \bar{h})^{k+2}} - \frac{\sin(\bar{h}d - \bar{\phi}_b + \alpha_{Do2} + \frac{k\pi}{2})}{(\rho_2 + \bar{h})^{k+2}} \right] \Bigg\} \Bigg\}$$

$$; \rho_2^2 \neq \bar{h}^2$$

$$I_{33}(n,h,\rho_2) = \frac{(-1)^n}{2} \left\{ \left[(D-d)^{n+1} - (D-\bar{d})^{n+1} \right] \left[1 - \frac{n}{n+1} \right] \sin(\alpha_{Do2} - \rho_2 d + \bar{\phi}_b) \right.$$

$$+ \frac{(D-d)^n \cos(\rho_2 d + \alpha_{Do2} - \bar{\phi}_b) - (D-\bar{d})^n \cos(\rho_2(2\bar{d} - d) + \alpha_{Do2} - \bar{\phi}_b)}{2\rho_2}$$

$$- n! \sum_{k=0}^{n-1} \frac{(-1)^{-k}}{(n-1-k)!\,(2\rho_2)^{k+2}} \times$$

$$\left[(D-\bar{d})^{n-k-1} \sin(\rho_2(2\bar{d} - d) + \alpha_{Do2} - \bar{\phi}_b + \frac{k\pi}{2}) \right.$$

$$\left. \left. - (D-d)^{n-k-1} \sin(\rho_2 d + \alpha_{Do2} - \bar{\phi}_b + \frac{k\pi}{2}) \right] \right\} \qquad ; \rho_2^2 = \bar{h}^2$$

$I_{34}(n,h,\rho_2) = I_{30}(n,h,\rho_1)$; with parameters and wavenumbers appropriate for the odd air modes of outer slab guide.

$I_{35}(n,h,\rho_2) = I_{32}(n,h,\rho_1)$ with parameters and wavenumbers appropriate for the odd air modes of outer slab guide.

APPENDIX 5

EXPRESSION FOR COEFFICIENTS $P_{se}, P'_{se}, P_e(\sigma), P'_e(\sigma), P_{e\mu}(\rho), P'_{e\mu}(\rho)$ OF SECTION 3.321 (LSM)

$$P_{se} = \int_{-\infty}^{\infty} \phi_{se}(y)\, E(y)\, dy$$

$$= A_1 \bar{A} \left[I_1 + \frac{I_2}{\varepsilon_1 \cos(h_1 D - \bar{\phi}_1)} + \frac{1}{\varepsilon_1 \cos(h_1 D - \bar{\phi}_1) \cos(\bar{h}\bar{d} - \bar{\phi}_b)} \frac{(\bar{d} - d)^{\alpha}}{(D - \bar{d})^{\alpha}} (I_3 + I_4) + \frac{\cos(\bar{\phi}_1) \cos(\bar{\phi}_b)}{\varepsilon_2 \cos(h_1 D - \bar{\phi}_1) \cos(\bar{h}\bar{d} - \bar{\phi}_b)} \frac{(\bar{d} - d)^{\alpha}}{(D - \bar{d})^{\alpha}} I_5 \right]$$

$$P'_{se} = \int_{-\infty}^{\infty} \psi_{se}(y)\, E(y)\, dy$$

$$= A_2 \bar{A} \left[I_6 + \frac{I_7}{\varepsilon_1} + \frac{1}{\varepsilon_1 \cos(\bar{h}\bar{d} - \bar{\phi}_b)} \frac{(\bar{d} - d)^{\alpha}}{(D - \bar{d})^{\alpha}} I_8 + \frac{1}{\varepsilon_1 \cos(h_2 d - \bar{\phi}_2) \cos(\bar{h}\bar{d} - \bar{\phi}_b)} \frac{(\bar{d} - d)^{\alpha}}{(D - \bar{d})^{\alpha}} I_9 + \frac{\cos(\bar{\phi}_2) \cos(\bar{\phi}_b)}{\varepsilon_2 \cos(h_2 d - \bar{\phi}_2) \cos(\bar{h}\bar{d} - \bar{\phi}_b)} \frac{(\bar{d} - d)^{\alpha}}{(D - \bar{d})^{\alpha}\, d^{\alpha}} I_{10} \right]$$

$$P_e(\sigma) = \int_{-\infty}^{\infty} \phi_e(y, \sigma)\, E(y)\, dy$$

$$= \sqrt{\frac{2\varepsilon_2}{\pi}}\, \bar{A} \left[A_{sb1} \cos(h_1 D - \bar{\phi}_{sb1})\, I_{11} + \frac{A_{sb1}}{\varepsilon_1} I_{12} + \frac{A_{sb1}}{\varepsilon_1 \cos(\bar{h}\bar{d} - \bar{\phi}_b)} \frac{(\bar{d} - d)^{\alpha}}{(D - \bar{d})^{\alpha}} (I_{13} + I_{14}) + \right.$$

$$+\frac{\cos(\bar{\phi}_b)}{\varepsilon_2\cos(\bar{h}\bar{d}-\bar{\phi}_b)}\frac{(\bar{d}-d)^{\alpha}}{(D-\bar{d})^{\alpha}d^{\alpha}}I_{15}\Bigg]$$

$$P'_e(\sigma)=\int_{-\infty}^{\infty}\psi_e(y,\sigma)\,E(y)\,dy$$

$$=\sqrt{\frac{2\,\varepsilon_2}{\pi}}\,\bar{A}\Bigg[A_{sb2}\cos(h_2d-\bar{\phi}_{sb2})\,I_{16}+\frac{A_{sb2}\cos(h_2d-\bar{\phi}_{sb2})}{\varepsilon_1}I_{17}$$

$$+\frac{A_{sb2}\cos(h_2d-\bar{\phi}_{sb2})}{\varepsilon_1\cos(\bar{h}\bar{d}-\bar{\phi}_b)}\frac{(\bar{d}-d)^{\alpha}}{(D-\bar{d})^{\alpha}}I_{18}+\frac{A_{sb2}}{\varepsilon_1\cos(\bar{h}\bar{d}-\bar{\phi}_b)}\frac{(\bar{d}-d)^{\alpha}}{(D-\bar{d})^{\alpha}}I_{19}$$

$$+\frac{\cos(\bar{\phi}_b)}{\varepsilon_2\cos(\bar{h}\bar{d}-\bar{\phi}_b)}\frac{(\bar{d}-d)^{\alpha}}{(D-\bar{d})^{\alpha}d^{\alpha}}I_{20}\Bigg]$$

$$P_{ee}(\rho)=\int_{-\infty}^{\infty}\phi_e(y,\rho)\,E(y)\,dy$$

$$=\sqrt{\frac{2}{\pi}}\,A_{e1}\,\bar{A}\Bigg[\frac{\cos(h_1D-\bar{\phi}_{e1})}{\cos(\alpha_{De1})}I_{21}+\frac{1}{\varepsilon_1}I_{22}$$

$$+\frac{1}{\varepsilon_1\cos(\bar{h}\bar{d}-\bar{\phi}_b)}\frac{(\bar{d}-d)^{\alpha}}{(D-\bar{d})^{\alpha}}(I_{23}+I_{24})$$

$$+\frac{\cos(\bar{\phi}_{e1})\cos(\bar{\phi}_b)}{\varepsilon_2\cos(\alpha_{0e1})\cos(\bar{h}\bar{d}-\bar{\phi}_b)}\frac{(\bar{d}-d)^{\alpha}}{(D-\bar{d})^{\alpha}d^{\alpha}}I_{25}\Bigg]$$

$$P'_{ee}(\rho)=\int_{-\infty}^{\infty}\psi_e(y,\rho)\,E(y)\,dy$$

$$=\sqrt{\frac{2}{\pi}}\,A_{e2}\,\bar{A}\Bigg[\frac{\cos(h_2d-\bar{\phi}_{e2})}{\cos(\alpha_{De2})}I_{26}+\frac{\cos(h_2d-\bar{\phi}_{e2})}{\varepsilon_1\cos(\alpha_{De2})}I_{27}$$

$$+\frac{\cos(h_2d-\bar{\phi}_{e2})}{\varepsilon_1\cos(\alpha_{De2})\cos(\bar{h}\bar{d}-\bar{\phi}_b)}\frac{(\bar{d}-d)^{\alpha}}{(D-\bar{d})^{\alpha}}I_{28}+\frac{1}{\varepsilon_1\cos(\bar{h}\bar{d}-\bar{\phi}_b)}\frac{(\bar{d}-d)^{\alpha}}{(D-\bar{d})^{\alpha}}I_{29}$$

$$+\frac{\cos(\bar{\phi}_{e2})\cos(\bar{\phi}_b)}{\varepsilon_2\cos(\alpha_{0e2})\cos(\bar{h}\bar{d}-\bar{\phi}_b)}\frac{(\bar{d}-d)^{\alpha}}{(D-\bar{d})^{\alpha}d^{\alpha}}I_{30}\Bigg]$$

$$P_{eo}(\rho) = \int_{-\infty}^{\infty} \phi_o(y,\rho)\, E(y)\, dy$$

$$= \sqrt{\frac{2}{\pi}}\, A_{o1}\, \bar{A} \left[\frac{\sin(h_1 D - \bar{\phi}_{o1})}{\sin(\alpha_{Do1})} I_{31} + \frac{1}{\varepsilon_1} I_{32} \right.$$

$$+ \frac{1}{\varepsilon_1 \cos(\bar{h}\bar{d} - \bar{\phi}_b)} \frac{(\bar{d}-d)^{\alpha}}{(D-\bar{d})^{\alpha}} (I_{33} + I_{34})$$

$$\left. + \frac{\sin(\bar{\phi}_{o1}) \cos(\bar{\phi}_b)}{\varepsilon_2 \sin(\alpha_{0o1}) \cos(\bar{h}\bar{d} - \bar{\phi}_b)} \frac{(\bar{d}-d)^{\alpha}}{(D-\bar{d})^{\alpha} d^{\alpha}} I_{35} \right]$$

$$P'_{eo}(\rho) = \int_{-\infty}^{\infty} \psi_o(y,\rho)\, E(y)\, dy$$

$$= \sqrt{\frac{2}{\pi}}\, A_{o2}\, \bar{A} \left[\frac{\sin(h_2 d - \bar{\phi}_{o2})}{\sin(\alpha_{Do2})} I_{36} + \frac{\sin(h_2 d - \bar{\phi}_{o2})}{\varepsilon_1 \sin(\alpha_{Do2})} I_{37} \right.$$

$$+ \frac{\sin(h_2 d - \bar{\phi}_{o2})}{\varepsilon_1 \sin(\alpha_{Do2}) \cos(\bar{h}\bar{d} - \bar{\phi}_b)} \frac{(\bar{d}-d)^{\alpha}}{(D-\bar{d})^{\alpha}} I_{38} + \frac{1}{\varepsilon_1 \cos(\bar{h}\bar{d} - \bar{\phi}_b)} \frac{(\bar{d}-d)^{\alpha}}{(D-\bar{d})^{\alpha}} I_{39}$$

$$\left. + \frac{\sin(\bar{\phi}_{o2}) \cos(\bar{\phi}_b)}{\varepsilon_2 \sin(\alpha_{0o2}) \cos(\bar{h}\bar{d} - \bar{\phi}_b)} \frac{(\bar{d}-d)^{\alpha}}{(D-\bar{d})^{\alpha} d^{\alpha}} I_{40} \right]$$

EXPRESSION FOR INTEGRALS I_1 to I_{40}

$$I_1 = \frac{e^{-\bar{q}(D-\bar{d})}\, \Gamma(1-\alpha)}{(q_1 + \bar{q})^{1-\alpha}}$$

$$I_2 = \frac{e^{-\bar{q}(D-\bar{d})}}{(\bar{q}^2 + h_1^2)^{\frac{1-\alpha}{2}}} \Gamma(1-\alpha) \cos(h_1 D - \bar{\phi}_1 - (1-\alpha)(\pi - \tan^{-1}(\frac{h_1}{\bar{q}})))$$

$$- \sum_{m=0}^{M-1} \frac{(-1)^m \Gamma(\alpha+m) \cos(h_1 \bar{d} - \bar{\phi}_1 - (m+1)(\pi - \tan^{-1}(\frac{h_1}{\bar{q}})))}{(D-\bar{d})^{m+\alpha} (\bar{q} + h_1^2)^{\frac{m+1}{2}} \Gamma(\alpha)}$$

$$I_3 = \frac{1}{2} \Gamma(1-\alpha) \left[\frac{\cos((h_1 + \bar{h})d - (\bar{\phi}_1 + \bar{\phi}_b) + (1-\alpha)\frac{\pi}{2})}{(h_1 + \bar{h})^{1-\alpha}} \right.$$

$$\left. + \frac{\cos((h_1 - \bar{h})d - (\bar{\phi}_1 - \bar{\phi}_b) + (1-\alpha)\frac{\pi}{2})}{(h_1 - \bar{h})^{1-\alpha}} \right]$$

$$- \frac{1}{2} \sum_{m=0}^{M-1} \frac{(-1)^m \Gamma(\alpha+m)}{\Gamma(\alpha)(\bar{d}-d)^{\alpha+m}} \left[\frac{\cos((h_1 + \bar{h})\bar{d} - (\bar{\phi}_1 + \bar{\phi}_b) + (m+1)\frac{\pi}{2})}{(h_1 + \bar{h})^{m+1}} \right.$$

$$\left. + \frac{\cos((h_1 - \bar{h})\bar{d} - (\bar{\phi}_1 - \bar{\phi}_b) + (m+1)\frac{\pi}{2})}{(h_1 - \bar{h})^{m+1}} \right]$$

$$I_4 = \frac{1}{2} \Gamma(1-\alpha) \left[\frac{\cos((h_1 + \bar{h})d - (\bar{\phi}_1 + \bar{\phi}_b) - (1-\alpha)\frac{\pi}{2})}{(h_1 + \bar{h})^{1-\alpha}} \right.$$

$$\left. + \frac{\cos((h_1 - \bar{h})d - (\bar{\phi}_1 - \bar{\phi}_b) - (1-\alpha)\frac{\pi}{2})}{(h_1 - \bar{h})^{1-\alpha}} \right] - \frac{1}{2} \sum_{m=0}^{M-1} \frac{(-1)^m \Gamma(\alpha+m)}{\Gamma(\alpha) d^{\alpha+m}}$$

$$\times \left[\frac{\cos(\bar{\phi}_1 + \bar{\phi}_b + (m+1)\frac{\pi}{2})}{(h_1 + \bar{h})^{m+1}} + \frac{\cos(\bar{\phi}_1 - \bar{\phi}_b + (m+1)\frac{\pi}{2})}{(h_1 - \bar{h})^{m+1}} \right]$$

$$I_5 = \frac{1}{p_1 + \bar{p}}$$

$$I_6 = \frac{\Gamma(1-\alpha)}{(q_2 + \bar{q})^{1-\alpha}} e^{-(q_2(D-d) + \bar{q}(D-\bar{d}))}$$

$$I_7 = e^{-q_2(D-d)}\, e^{-\bar{q}(D-\bar{d})} \sum_{k=0}^{\infty} \frac{(q_2 + \bar{q})^k\, (D-\bar{d})^{k+1-\alpha}}{k!\,(k+1-\alpha)}$$

$$I_8 = \frac{1}{(q_2^2 + \bar{h}^2)^{\frac{1-\alpha}{2}}} \Gamma(1-\alpha) \cos(\bar{h}d - \bar{\phi}_b + (1-\alpha)\tan^{-1}(\frac{\bar{h}}{q_2}))$$

$$- e^{-q_2(\bar{d}-d)} \sum_{m=0}^{M-1} \frac{(-1)^m\, \Gamma(\alpha+m) \cos(\bar{h}\bar{d} - \bar{\phi}_b + (m+1)\tan^{-1}(\frac{\bar{h}}{q_2}))}{(q_2^2 + \bar{h}^2)^{\frac{m+1}{2}}\, (\bar{d}-d)^{m+\alpha}\, \Gamma(\alpha)}$$

$I_9 = I_4$ and $I_{10} = I_5$; with parameters and wavenumbers appropriate for the surface mode of outer slab guide.

$I_{11} = I_1$, $I_{12} = I_2$, $I_{13} = I_3$, and $I_{14} = I_4$; with parameters and wavenumbers appropriate for the substrate modes of inner slab guide.

$$I_{15} = \frac{1}{\bar{p}^2 + \sigma_1^2} \left[\bar{p} \cos(\alpha_{sb1}) - \sigma_1 \sin(\alpha_{sb1}) \right]$$

$I_{16} = I_6$, $I_{17} = I_7$, $I_{18} = I_8$, $I_{19} = I_9$ and $I_{20} = I_{15}$; with parameters and wavenumbers appropriate for the substrate modes of outer slab guide.

$I_{22} = I_2$, $I_{23} = I_3$ and $I_{24} = I_4$; with parameters and wavenumbers appropriate for the even air modes of inner slab guide.

$$I_{25} = \frac{1}{\bar{p}^2 + \sigma_1^2} \left[\bar{p} \cos(\alpha_{0e1}) - \sigma_1 \cos(\alpha_{0e1}) \right]$$

$$I_{26} = \frac{e^{-\bar{q}(D-\bar{d})}}{(\rho_2^2 + \bar{q}^2)^{\frac{1-\alpha}{2}}} \Gamma(1-\alpha) \cos(\rho_2(D-d) + \alpha_{De2} + (1-\alpha)\tan^{-1}(\frac{\rho_2}{\bar{q}}))$$

$$I_{27} = \frac{e^{-\bar{q}(D-\bar{d})}}{(\bar{q}^2 + \rho_2^2)^{\frac{1-\alpha}{2}}} \Gamma(1-\alpha) \cos(\rho_2(D-d) + \alpha_{De2} - (1-\alpha)(\pi - \tan^{-1}(\frac{\rho_2}{\bar{q}}))$$

$$- \sum_{m=0}^{M-1} \frac{(-1)^m \Gamma(\alpha+m)}{(\bar{q}^2 + \rho_2^2)^{\frac{m+1}{2}} (D-\bar{d})^{m+\alpha} \Gamma(\alpha)} \cos(\rho_2(\bar{d}-d) + \alpha_{De2} - (m+1)(\pi - \tan^{-1}(\frac{\rho_2}{\bar{q}}))$$

$$I_{28} = \frac{1}{2}\Gamma(1-\alpha) \left[\frac{\cos(\bar{h}d - \bar{\phi}_b + \alpha_{De2} + (1-\alpha)\frac{\pi}{2})}{(\rho_2 + \bar{h})^{1-\alpha}} \right.$$

$$\left. + \frac{\cos(-\bar{h}d + \bar{\phi}_b + \alpha_{De2} + (1-\alpha)\frac{\pi}{2})}{(\rho_2 - \bar{h})^{1-\alpha}} \right.$$

$$- \frac{1}{2} \sum_{m=0}^{M-1} \frac{(-1)^m \Gamma(\alpha+m)}{(\bar{d}-d)^{\alpha+m} \Gamma(\alpha)} \left[\frac{\cos((\rho_2 + \bar{h})(\bar{d}-d) + (m+1)\frac{\pi}{2} + \bar{h}d + \alpha_{De2} - \bar{\phi}_b)}{(\rho_2 + \bar{h})^{m+1}} \right.$$

$$\left. \left. + \frac{\cos((\rho_2 - \bar{h})(\bar{d}-d) + (m+1)\frac{\pi}{2} - \bar{h}d + \alpha_{De2} + \bar{\phi}_b)}{(\rho_2 - \bar{h})^{m+1}} \right] \right]$$

$I_{29} = I_4$; with parameters and wavenumbers appropriate for the even air modes of outer slab guide.

$$I_{30} = \frac{1}{\bar{p}^2 + \sigma_2^2} \left[\bar{p} \cos(\alpha_{0e2}) - \sigma_2 \sin(\alpha_{0e2}) \right]$$

$$I_{31} = \frac{e^{-\bar{q}(D-\bar{d})}}{(\rho_1^2 + \bar{q}^2)^{\frac{1-\alpha}{2}}} \sin((1-\alpha)\tan^{-1}(\frac{\rho_1}{\bar{q}}) + \alpha_{Do1})$$

$$I_{32} = e^{-\bar{q}(D-\bar{d})}\,\Gamma(1-\alpha)\sin(h_1 D - \bar{\Phi}_{o1} - (1-\alpha)(\pi - \tan^{-1}(\frac{h_1}{\bar{q}}))$$

$$- \sum_{m=0}^{M-1} \frac{(-1)^m\,\Gamma(\alpha+m)}{(\bar{q}^2 + h_1^2)^{\frac{m+1}{2}}\,(D-\bar{d})^{m+\alpha}\,\Gamma(\alpha)} \sin(h_1\bar{d} - \bar{\Phi}_{o1} - (m+1)(\pi - \tan^{-1}(\frac{h_1}{\bar{q}}))$$

$$I_{33} = \frac{1}{2}\Gamma(1-\alpha)\left[\frac{\sin((h_1+\bar{h})d - (\bar{\Phi}_{o1}+\bar{\Phi}_b) + (1-\alpha)\frac{\pi}{2})}{(h_1+\bar{h})^{1-\alpha}}\right.$$

$$\left. + \frac{\sin((h_1-\bar{h})d - (\bar{\Phi}_{o1}-\bar{\Phi}_b) + (1-\alpha)\frac{\pi}{2})}{(h_1-\bar{h})^{1-\alpha}}\right]$$

$$- \sum_{m=0}^{M-1} \frac{(-1)^m\,\Gamma(\alpha+m)}{(\bar{d}-d)^{m+\alpha}\,\Gamma(\alpha)}\left[\frac{\sin((h_1+\bar{h})\bar{d} + (m+1)\frac{\pi}{2} - (\bar{\Phi}_{o1}+\bar{\Phi}_b))}{(h_1+\bar{h})^{m+1}}\right.$$

$$\left. + \frac{\sin((h_1-\bar{h})\bar{d} + (m+1)\frac{\pi}{2} - (\bar{\Phi}_{o1}-\bar{\Phi}_b))}{(h_1-\bar{h})^{m+1}}\right]$$

$$I_{34} = -\frac{\Gamma(1-\alpha)}{2}\left[\frac{\sin((h_1+\bar{h})d - (\bar{\Phi}_{o1}+\bar{\Phi}_b) - (1-\alpha)\frac{\pi}{2})}{(h_1+\bar{h})^{1-\alpha}}\right.$$

$$\left. + \frac{\sin((h_1-\bar{h})d - (\bar{\Phi}_{o1}-\bar{\Phi}_b) - (1-\alpha)\frac{\pi}{2})}{(h_1-\bar{h})^{1-\alpha}}\right]$$

$$- \frac{1}{2}\sum_{m=0}^{M-1} \frac{(-1)^m\,\Gamma(\alpha+m)}{d^{m+\alpha}\,\Gamma(\alpha)}\left[\frac{\sin((m+1)\frac{\pi}{2} + (\bar{\Phi}_{o1}+\bar{\Phi}_b))}{(h_1+\bar{h})^{m+1}}\right.$$

$$\left. + \frac{\sin((m+1)\frac{\pi}{2} + (\bar{\Phi}_{o1}-\bar{\Phi}_b))}{(h_1-\bar{h})^{m+1}}\right]$$

$$I_{35} = \frac{1}{\bar{p}^2 + \sigma_1^2} \left[\bar{p} \sin(\alpha_{0o1}) + \sigma_1 \sin(\alpha_{0o1}) \right]$$

$$I_{36} = \frac{e^{-\bar{q}(D-\bar{d})}}{(\rho_2^2 + \bar{q}^2)^{\frac{1-\alpha}{2}}} \Gamma(1-\alpha) \sin(\rho_2(D-d) + \alpha_{Do2} + (1-\alpha)\tan^{-1}(\frac{\rho_2}{\bar{q}}))$$

$$I_{37} = -\frac{e^{-\bar{q}(D-\bar{d})}}{(\bar{q}^2 + \rho_2^2)^{\frac{1-\alpha}{2}}} \Gamma(1-\alpha) \sin(\rho_2(D-d) + \alpha_{Do2} - (1-\alpha)(\pi - \tan^{-1}(\frac{\rho_2}{\bar{q}}))$$

$$+ \sum_{m=0}^{M-1} \frac{(-1)^m \Gamma(\alpha+m)}{(\bar{q}^2 + \rho_2^2)^{\frac{m+1}{2}} (D-\bar{d})^{m+\alpha} \Gamma(\alpha)} \times$$

$$\sin(\rho_2(\bar{d}-d) + \alpha_{Do2} - (m+1)(\pi - \tan_{-1}(\frac{\rho_2}{\bar{q}}))$$

$$I_{38} = \frac{1}{2}\Gamma(1-\alpha) \left[\frac{\sin(\bar{h}d - \bar{\phi}_b + \alpha_{Do2} + (1-\alpha)\frac{\pi}{2})}{(\rho_2 + \bar{h})^{1-\alpha}} \right.$$

$$\left. + \frac{\sin((1-\alpha)\frac{\pi}{2} - \bar{h}d + \alpha_{Do2} + \bar{\phi}_b)}{(\rho_2 - \bar{h})^{1-\alpha}} \right]$$

$$- \frac{1}{2} \sum_{m=0}^{M-1} \frac{(-1)^m \Gamma(\alpha+m)}{(\bar{d}-d)^{\alpha+m} \Gamma(\alpha)} \left[\frac{\sin((\rho_2 + \bar{h})(\bar{d}-d) + (m+1)\frac{\pi}{2} + \bar{h}d + \alpha_{Do2} - \bar{\phi}_b)}{(\rho_2 + \bar{h})^{m+1}} \right.$$

$$\left. + \frac{\sin((\rho_2 - \bar{h})(\bar{d}-d) + (m+1)\frac{\pi}{2} - \bar{h}d + \alpha_{Do2} + \bar{\phi}_b)}{(\rho_2 - \bar{h})^{m+1}} \right]$$

$I_{39} = I_{34}$; with parameters and wavenumbers appropriate for the odd air modes of outer slab guide.

$I_{40} = I_{35}$; with parameters and wavenumbers appropriate for the odd air modes of outer slab guide.